

Hydrmagmatic monogenetic volcanism in continental and oceanic island environments

Dario Pedrazzi



Aquesta tesi doctoral està subjecta a la llicència **Reconeixement- NoComercial – SenseObraDerivada 3.0. Espanya de Creative Commons.**

Esta tesis doctoral está sujeta a la licencia **Reconocimiento - NoComercial – SinObraDerivada 3.0. España de Creative Commons.**

This doctoral thesis is licensed under the **Creative Commons Attribution-NonCommercial-NoDerivs 3.0. Spain License.**

**HYDROMAGMATIC MONOGENETIC
VOLCANISM
IN CONTINENTAL AND OCEANIC ISLAND
ENVIRONMENTS**

Dario Pedrazzi

Department of Geodynamic and Geophysics
Universitat de Barcelona

Barcelona 2014



Universitat de Barcelona

Faculty of Geology

Department of Geodynamic and Geophysics

Doctorat en Ciències de la Terra



Institute of Earth Sciences Jaume Almera - CSIC

Department of Geophysics and Geohazards

**HYDROMAGMATIC MONOGENETIC
VOLCANISM
IN CONTINENTAL AND OCEANIC ISLAND
ENVIRONMENTS**

Dario Pedrazzi

PhD Thesis

Prof. Joan Martí Molist

Thesis Supervisor

Prof. Joan Manuel Vilaplana Fernández

Thesis Tutor

Barcelona 2014

"Per la stessa ragione del viaggio, viaggiare"

Acknowledgments

This thesis is the result of a hard work carried out with the help and assistance of different persons that I really would like to thank.

First of all I want to thank my PhD thesis supervisor Prof. Joan Martí for giving me the opportunity to realize this thesis and for teaching and supporting me during the last four years.

Thanks to the whole Group of Volcanology of the Jaume Almera Institute without whom this project would not have succeeded and in a special way to my friend and colleague Xevi for sharing friendship and hard work.

Thanks to Gerardo Aguirre for all that I could learn during our stay in Deception Island and to Leandro d'Elia for his help in the field and for the time spent together in Barcelona. I would also thank my colleagues at the University of Barcelona and Jaume Almera Institute for supporting and sharing their experiences with me. Thanks to the staff of the Parc Natural de la Zona Volcànica de la Garrotxa (Olot), Cabildo de Lanzarote and Casa de Los Volcanes and Cabildo de El Hierro for let me carry out these projects and helping during fieldwork.

Thanks to all the people that through their attitudes convinced me to move abroad arriving at Barcelona. A huge thanks goes to my friends for supporting me all the times I needed them, and of course to my family and especially to my parents who always encouraged me to travel and make new experience.

Last but not least a special thanks got to Antonella who endured and supported me during these last years spent in Barcelona.

Ringraziamenti

Questa tesi è il risultato di un duro lavoro portato a termine grazie all'aiuto di alcune persone che vorrei ringraziare sentitamente.

Prima di tutto grazie al Prof. Joan Martí per avermi dato l'opportunità di realizzare questa tesi di dottorato e per l'insegnamento e il sostegno in questi anni.

Grazie a tutto il Gruppo di Vulcanologia dell'Istituto Jaume Almera senza i quali questo progetto non avrebbe avuto successo e in modo speciale al mio amico e collega Xevi per aver condiviso amicizia e duro lavoro.

Grazie a Gerardo Aguirre per i suoi consigli durante il nostro lavoro a Deception Island e a Leandro d' Elia per il suo aiuto in campagna e per il tempo trascorso insieme a Barcellona.

Vorrei anche ricordare a tutte le persone presso l'Università di Barcellona e l'Istituto Jaume Almera che mi hanno sostenuto e hanno condiviso la loro esperienza con me. Grazie a tutti i membri del Parc Natural de la Zona volcànica de la Garrotxa (Olot), il Cabildo di Lanzarote e la Casa de Los Volcanes e il Cabildo de El Hierro per concederci l'opportunità di realizzare i nostri progetti e per l'aiuto durante il lavoro in campagna.

Grazie a tutte le persone che attraverso i loro atteggiamenti mi hanno convinto a trasferirmi all'estero arrivando a Barcellona. Un enorme ringraziamento va ai miei amici per avermi supportato e naturalmente, alla mia famiglia e in particolar modo ai miei genitori che mi hanno sempre incoraggiato a viaggiare e fare nuove esperienze .

Ultimo ma non meno importante un grazie speciale ad Antonella per avermi supportato e sopportato in questi ultimi anni a Barcellona.

Contents

ABSTRACT	1
RESUMEN	3
1. INTRODUCTION	4
1.1 Motivation	4
1.2 State of the art	4
1.3 Main objectives	6
1.4 Summary of the work	7
2. PHREATOMAGMATIC VOLCANISM IN HYDROGEOLOGICAL ENVIRONMENTS: LA CROSA DE SANT DALMAI MAAR (CATALAN VOLCANIC ZONE, NE SPAIN)	11
Abstract	12
2.1 Introduction	12
2.2 Geological setting	14
2.3 Methods	16
2.4 Characteristics of the pyroclastic succession	17
2.4.1 Facies analysis	18
Facies SDA: Large lithic ballistic deposits.....	18
Facies SDB: Clast supported deposits.....	19
Facies SDC: Scoriaceous clast-supported deposits.....	19
Facies SDD: Scoriaceous deposits.....	19
Facies SDE: Thinly bedded deposits.....	19
Facies SDF: Diffusely stratified deposits.	20
2.4.2 Stratigraphic units and facies associations	23
2.5 Grain size, modal variations and lithic distribution	25
2.5.1 Grain size and modal variations	25
2.5.2 Componentry analysis	26
2.6 Lithological and hydrogeological characteristics of the pre-volcanic substrate.	27
2.7 Discussion	30
2.8 Conclusion	36
References	36

3. STRATIGRAPHY, SEDIMENTOLOGY AND ERUPTIVE MECHANISMS IN THE TUFF CONE OF EL GOLFO (LANZAROTE, CANARY ISLANDS).....	43
Abstract.....	44
3.1 Introduction.....	44
3.2 Geological setting and general description of the tuff cone of El Golfo.....	46
3.3 Methods.....	50
3.4 Facies description.....	51
3.4.1 <i>Channel fill facies (A).....</i>	53
3.4.2 <i>Crudely stratified facies (B).....</i>	53
3.4.3 <i>Diffusely stratified facies (C).....</i>	53
3.4.4 <i>Planar stratified facies (D).....</i>	54
3.4.5 <i>Undulate ash bed facies (E).....</i>	54
3.4.6 <i>Dune facies (F).....</i>	54
3.4.7 <i>Antidune facies (G)</i>	55
3.4.8 <i>Accretionary lapilli facies (H).....</i>	55
3.5 Facies associations.....	57
3.6 Discussion.....	58
3.6.1 <i>Facies interpretation.....</i>	58
3.6.2 <i>Eruptive dynamics.....</i>	61
3.6.3 <i>Post-depositional processes.....</i>	65
3.6.4 <i>Hazard implications.....</i>	66
3.7 Conclusions.....	67
References.....	68
4. EXPLOSIVE FELSIC VOLCANISM ON EL HIERRO (CANARY ISLANDS).....	76
Abstract.....	77
4.1 Introduction.....	77
4.2 Geological setting.....	79
4.3 Methods.....	81
4.4 Stratigraphy.....	82
4.4.1 <i>Unit N1.....</i>	85
4.4.2 <i>Unit N2.....</i>	86
4.4.3 <i>Unit N3.....</i>	86

4.4.4 Unit N4.....	87
4.5 Isopach and Isopleth maps.....	87
4.6 Componentry characteristics and grain size distribution.....	88
4.7 Morphology of the juvenile material.....	91
4.8 Mineralogy.....	92
4.9 Discussion.....	93
4.9.1 Eruption and emplacement of the Malpaso Member.....	93
4.9.2 Age of the Malpaso Member and of the landslide at El Golfo.....	96
4.9.3 Volcanic Hazard Implications.....	99
4.10 Conclusion.....	100
References.....	101
5. THE 1970 ERUPTION ON DECEPTION ISLAND (ANTARCTICA): ERUPTIVE DYNAMICS AND IMPLICATION FOR VOLCANIC HAZARD.....	112
Abstract.....	113
5.1 Introduction.....	113
5.2 Geological setting and general characteristics of Deception Island.....	114
5.3 Methods.....	117
5.4 Characteristics of the 1970 craters.....	118
5.5 Characteristics of the pyroclastic succession.....	119
5.5.1 Eastern Craters.....	119
5.5.2 Western Craters.....	121
5.5.3 Distribution of ashfall deposits.....	124
5.5.4 Grain size, modal variation and clasts distribution.....	124
5.5.5 Componentry analysis.....	127
5.6 Discussion.....	128
5.7 Conclusions.....	132
References.....	133
6. SUMMARY OF RESULTS AND DISCUSSION.....	141
7. CONCLUSIONS.....	145
References.....	146
APPENDIX 1 CONTRIBUTION TO THE PAPERS	

**APPENDIX 2 PHREATOMAGMATIC VOLCANISM IN
HYDROGEOLOGICAL ENVIRONMENTS: LA CROSA DE SANT DALMAI
MAAR (CATALAN VOLCANIC ZONE, NE SPAIN)**

**APPENDIX 3 STRATIGRAPHY, SEDIMENTOLOGY AND ERUPTIVE
MECHANISMS IN THE TUFF CONE OF EL GOLFO (LANZAROTE,
CANARY ISLANDS)**

**APPENDIX 4 EXPLOSIVE FELSIC VOLCANISM ON EL HIERRO (CANARY
ISLANDS)**

Appendix 4.1 Proof of delivery of the paper: “*Explosive felsic volcanism on El Hierro (Canary Islands)*” in Bulletin of Volcanology

Appendix 4.2 Proof of delivery of the revised version of the accepted paper: “*Explosive felsic volcanism on El Hierro (Canary Islands)*” in Bulletin of Volcanology

**APPENDIX 5 THE 1970 ERUPTION ON DECEPTION ISLAND
(ANTARCTICA): ERUPTIVE DYNAMICS AND IMPLICATION FOR
VOLCANIC HAZARD**

Appendix 5.1 Proof of delivery of the paper: “*The 1970 eruption of Deception Island (Antarctica): eruptive dynamics and implication for volcanic hazard*” in Journal of the Geological Society

ABSTRACT

Monogenetic volcanism is characterized by a large diversity of eruptive styles, morphologies and deposits. Monogenetic landforms are the result of a complex merging of internal (magma composition, vesiculation) and external (geological setting, fracturation, hydrogeology, substrate stratigraphy, etc) parameters that govern the physics of the eruptions. Changes in these parameters may cause variations in the eruption style several times during the course of such short-lived volcanoes. Monogenetic volcanoes may form in any type of geological environment with scoria cones being the most common volcano type and hydrovolcanic tuff rings, tuff cones, and maars as the second in abundance. These small-volume volcanoes are generally the result of short-lived eruptions but the activity in a monogenetic volcanic field might exceed the total life of composite volcanoes.

The attention of this work was focused on the relation between monogenetic volcanic landforms and the external variables that influenced the dynamics of the eruptions (i.e. magmatism vs phreatomagmatism) through a multidisciplinary perspective, in marine and continental geological settings under which monogenetic volcanism may develop.

Different case studies representative of this type of activity and of these different environments have been considered. The first one corresponds to the La Crosa De Sant Dalmai volcano (Garrotxa Volcanic Field, southern sector of the Catalan Volcanic Zone), a roughly circular asymmetrical maar-diatreme volcano, which is one of the most characteristic volcanic edifices of this continental monogenetic volcanic field and the largest Quaternary volcanic crater on the Iberian Peninsula. This edifice is an example of monogenetic landform, mostly composed of phreatomagmatic deposits with subordinate Strombolian phases, constructed on a mixed basement made of hard Paleozoic granites and schists rocks and soft Plio-Quaternary deposits. Here, I reconstructed the hydrogeological conditions of the substrate and the implication for the eruptive dynamics. As a second case study, I carried out detailed stratigraphic and sedimentological studies of the succession of El Golfo tuff cone (Lanzarote, Canary Islands). The main objective of the work was to describe in detail the structure and association of facies of this edifice and use this information to infer changes in eruption style and depositional processes. Another type of eruption was studied in the same archipelago at El Hierro, an island essentially characterized by basaltic volcanism with

both Strombolian and Hawaiian activity. Here I reported the stratigraphic, lithological, sedimentological and petrographic characteristics of a felsic hydrovolcanic episode in order to discuss, transport/depositional mechanisms, dynamics, relative age and implications for hazard assessment on the island. Finally, the same type of methodology was applied at Deception Island (Southern Shetland Archipelago, Antarctica), determining the lithological and sedimentological characteristics, and clasts distribution (isopach and isopleth maps) of the eruption of 1970. This information was, then, used to determine depositional processes, eruption style and physical parameters (i.e. plume height, erupted volume, VEI) of the eruption in order to compare this episode with the previous 1967 episode, and to deduce their implications to conduct hazard assessment at the island.

Each work represents a diverse aspect of hydrovolcanism and the results obtained helped to better understand the eruptive behavior of this type of volcanoes, which is a fundamental task in order to understand the possible future hazards associated with this type of volcanism. The results obtained can be applied to monogenetic volcanic fields worldwide and are, therefore, useful to reconstruct the evolution of a certain volcanic fields, through the study of single monogenetic volcanoes, and to evaluate the possible volcanic hazards, as similar eruptions represent a serious threat, which is often underestimated. A more systematic study is, thus, needed in order to understand the role of shallow-level conditions in the formation of specific volcano types in such complex volcanic fields.

RESUMEN

El vulcanismo monogenético se caracteriza por una gran diversidad de estilos eruptivos, morfologías y depósitos. Los tipos de edificios que se forman son el resultado de una compleja combinación de parámetros que rigen la física de la erupción.

La atención de este trabajo se centra en la relación entre los edificios volcánicos monogenéticos y las variables externas que influyen en la dinámica de las erupciones (es decir, magmatismo vs freatomagmatismo) a través de un punto de vista multidisciplinar, en ambientes continentales y marinos en los que el vulcanismo puede desarrollar. Diferentes estudios, representativos de este tipo de actividad en diferentes entornos geográficos y geológicos, se han llevado a cabo. El primer ejemplo corresponde al volcán de La Crosa de Sant Dalmai (Campo Volcánico de La Garrotxa) donde se han reconstruido las condiciones hidrogeológicas del sustrato y la implicación para la dinámica eruptiva. Como segundo caso de estudio, se ha realizado una estratigrafía de detalle del cono de toba de El Golfo (Lanzarote, Islas Canarias), donde se han estudiado los mecanismos de emplazamiento de los depósitos para inferir cambios en la interacción magma/agua. Otro tipo de erupción se ha investigado en el mismo archipiélago, en la Isla de El Hierro, determinando las características físicas de un episodio félsico de origen hidrovulcánico ocurrido en una isla que se caracteriza esencialmente por el vulcanismo basáltico tanto Estromboliano como Hawaiano. Por último, este mismo tipo de metodología se ha aplicado a la Isla Decepción (archipiélago de las Shetland del Sur, Antártida), estableciendo los parámetros físicos de la erupción del 1970 con el fin de comparar este episodio con el evento anterior del 1967, y deducir sus consecuencias para llevar a cabo la evaluación de peligrosidad en la isla.

Los resultados obtenidos pueden ser aplicados a campos volcánicos monogenéticos en todo el mundo y, por tanto, son útiles para reconstruir la evolución de ciertos campos volcánicos, a través del estudio de volcanes monogenéticos individuales, para evaluar los posibles riesgos volcánicos, teniendo en cuenta como erupciones similares representan una grave amenaza, que es a menudo subestimada.

1. INTRODUCTION

1.1. Motivation

The complex dynamics of magma-water interaction determines the nature of explosive activity, characterized by variable energy outputs and different degrees of magmatic or hydromagmatic fragmentation (e.g., Wohletz and Sheridan, 1983; Houghton and Hackett, 1984; White and Houghton, 2000). Hydromagmatic eruptions are characterized by a more efficient conversion of thermal into mechanical energy involved in magma fragmentation compared to Hawaiian/Strombolian activity. This represents a greater threat because of the large diversity of eruptive styles and wider dispersal of the deposits.

Volcanic hazard, overall for long-term recurrence, is often underestimated for monogenetic volcanic fields with hydromagmatic episodes, particularly when there are no direct observations of the phenomena. This type of volcanism would be significantly impacting compared to the past, because of the increasing population and infrastructures even in remote areas. This is the reason why it is necessary to have a good knowledge of the past behaviour of monogenetic edifices in each volcanic field in order to understand the possible future hazards associated with this type of volcanism.

1.2 State of the art

Volcanic activity in terrestrial setting often results in the formation of volcanic fields rather than a single volcanic edifice (Connor and Conway, 2000; Walker, 2000). Monogenetic volcanic fields are those in which individual volcanoes (mainly basaltic) commonly form during single episodes of volcanic activity, without subsequent eruptions, while the whole volcanic field may be active for millions of year (Walker, 1993). Monogenetic volcanic fields commonly consist of large number of volcanic cluster and/or alignments that may reach the amount of hundreds of volcanoes (e.g., Connor 1987, 1990; Connor et al., 1992; Condit and Connor, 1996; Conway et al., 1998; Connor and Conway, 2000; Connor et al., 2000; Valentine et al., 2006). This type of volcanism is characterized by the large diversity of eruptive styles, morphologies and deposits that it may display despite the usual monotony in magma composition (Houghton et al., 1999; Connor and Conway, 2000; Parfitt, 2004; Valentine and Gregg, 2008).

Monogenetic volcanoes may form in any type of geological environment with scoria cones being the most common volcano type on land and hydrovolcanic tuff rings, tuff cones, and maars as second in abundance (Vespermann and Schmincke, 2000). These small-volume intracontinental volcanoes are generally the result of shortlived eruptions, determined by variables such as the exact nature of the magma and water involved, the proportions and properties of the interacting fluids, the lithology and mechanical properties of the rocks of the conduit wall, and vent geometry (Kokelaar, 1986; Sohn and Chough, 1989; Sohn, 1996; White, 1996; White and Houghton, 2000; White and Ross, 2011). Changes in these parameters might cause variations in the eruption style several times during the course of such short-lived volcanoes. This concept might help to understand the long-term evolution of a volcanic field in terms of internal (e.g., magma composition, vesiculation) vs external (geological setting, fracturation, presence of water) parameters.

These hydrovolcanic or hydromagmatic eruptions have only ever been observed or documented in a few occasions because of their short duration and occasional remote location. Recent events were recorded at Myojin, Japan (Morimoto, 1960), Surtsey, Iceland (Thorarinsson, 1965), Taal, Philippines (Moore et al., 1966), Capelinhos, Faial Island, Azores (Machado et al., 1962; Cole et al., 2001), Deception Island, Antarctica (Valenzuela et al., 1968), Ukinrek, Alaska (Kienle et al., 1980; Self et al., 1980), Karymskoye Lake, Kamchatka (Belousov and Belousova, 2001), Kavachi, Solomon Islands (Baker et al., 2002), Katla eruptions (Larsen et al., 2009; Larsen, 2010), Grimsvotn, Iceland (Jude-Eton et al., 2012) and Eyjafjallajokull, Iceland (Gudmundsson et al., 2012).

Studies on monogenetic volcanoes started in the late 1960s and beginning of 1970s, supported by the NASA for the lunar program. These researches were aimed at studying the morphological aspects of monogenetic volcanic landforms and their origin, in order to compare them with images of the surface of extraterrestrial bodies (e.g., the Moon) and to identify analogous landforms. Further studies were carried out in the 1970s and 1980s to understand the physics of magma/water interaction also defined (molten) fuel-coolant interaction (M)FCI (e.g., Sheridan and Wohletz, 1981, 1983; Wohletz and Sheridan, 1983; Heiken, 1985; Wohletz, 1986; Zimanoswki et al., 1986). An important step forward was made in the 1990s and 2000s through experimental volcanology, allowing to better understand magma-water interaction (e.g., Wohletz and Heiken, 1992; White, 1996; Buttner et al., 1999, 2002; Dellino et al., 2001; Dellino and

Liotino, 2002). Recent studies were aimed at understanding the sedimentological characteristics of hydrovolcanic edifices to interpret the evolution in terms of changing eruptive styles (e.g., Chough and Sohn, 1990; Sohn and Chough, 1989, 1992; Cole, 1991; Sohn, 1996; Druitt, 1998; Branney and Kokeelar, 2002; Dellino et al., 2004a,b; Brand and White, 2007). An increasing number of studies have been carried out in the last years, in order to investigate the evolution of tephra rings, maars-diatreme and tuff cones and their connection with structural and geophysical data on the tectonic environment in which they occur (e.g., Rout et al., 1993; Németh et al., 2001; Schulz et al., 2005; Auer et al., 2007; Carrasco Núñez et al., 2007; Cassidy et al., 2004; Giaccio et al., 2007; Solgevik et al., 2007; Sottili et al., 2009; Zanon et al., 2009; Wong and Larsen 2010; Ross et al., 2011; Bolós et al., 2012; Barde-Cabusson et al., 2013). This increasing trend in number of publications about monogenetic volcanism and hydromagmatic eruptions show the importance of understand the dynamics and mechanisms of eruption of single monogenetic landforms and the evolution of volcanic fields, due to the increasing hazard that this type volcanism is posing on a growing population all over the world.

1.3 Main objectives

The main objective of the present PhD thesis is, then, to focus on the relation between monogenetic volcanic landforms and the external variables that influenced the dynamics of the hydrovolcanic eruptions through a multidisciplinary perspective and in marine and continental volcanic fields under which these volcanoes have developed. The PhD thesis is divided into several parts where each one corresponds to a different scientific paper. Each work represents a different aspect of hydromagmatism with the final objective of developing a multidisciplinary investigation in different geological contexts and to apply the results obtained to the study of monogenetic volcanic fields worldwide. The methodology that was followed in this study was based mainly on field investigations, in order to obtain a detailed reconstruction of the stratigraphic sequences of the different hydromagmatic edifices. I also undertook laboratory studies, including grain-size analyses by dry sieving techniques and componentry studies, analysis on the morphologies and textural features, petrography, electron microprobe and SEM of juvenile clasts. This multidisciplinary approach is important in order to try to establish a general pattern to study the evolution of monogenetic volcanic fields and, consequently,

to evaluate the volcanic hazards and risks that this type of volcanism can pose for a growing populated area.

1.4 Summary of the work

Different case studies representative of the hydromagmatic activity in monogenetic volcanic fields developed in continental and ocean island environments were considered and studied in detail. The first one corresponds to the La Crosa De Sant Dalmai volcano (Garrotxa Volcanic Field, southern sector of the Catalan Volcanic Zone), one of the most characteristic volcanic edifices of this continental monogenetic volcanic field and the largest Quaternary volcanic crater on the Iberian Peninsula. Here, I reconstructed the hydrogeological conditions of the substrate and the implication for the eruptive dynamics. As a second case study, I carried out a detailed stratigraphy of El Golfo tuff cone (Lanzarote, Canary Islands), where I studied the mechanisms of emplacement of the deposits to infer changes in magma/water interaction. Another type of eruption was studied in the same archipelago at El Hierro Island, determining the physical characteristics of a felsic hydrovolcanic episode occurred on an island essentially characterized by basaltic volcanism with both Strombolian and Hawaiian activity. Finally, the same type of methodology was applied at Deception Island (Shetland Archipelago, Antarctica), determining the physical parameters of the eruption of 1970 in order to compare this episode with the previous 1967 episode, and to deduce their implications to conduct hazard assessment at the island.

The Catalan Volcanic Zone (CVZ) is one of the Quaternary alkaline volcanic provinces of the European rifts system and it is located at the NE of the Iberian Peninsula. The CVZ has been active during the last 12 Ma and volcanism with less than 0.5 Ma is located between the cities of Olot and Girona (Garrotxa Volcanic Field). One of the main characteristics of the CVZ is the different substrate on which these monogenetic volcanoes rest, with volcanic rocks lying on Tertiary sediments at the northern part, and on granites and schists of Palaeozoic age at the southern sector. The whole area comprises more than 50 monogenetic edifices with scoria cones, tephra rings and maar-diatreme volcanoes. Strombolian activity is often associated with phreatomagmatism, leading to the formation of complex eruptive successions. The main concentration of edifices is located in the northern sector (city of Olot) where the most representative volcanoes are Croscat and Santa Margarida, a phreatomagmatic/Strombolian complex, Can Tià and Cairat, which correspond to maar-

type constructions and Garrinada and Montsacopa with a similar sequence involving a Strombolian phase at the beginning and a phreatomagmatic one at the end. In the southern sector (close to the city of Girona) the most characteristic volcanoes are El Puig de Banya del Boc and El Clot de l'Omera that were originated during the same eruption. The former is characterized by magmatic and phreatomagmatic eruptive phases and the latter is a maar-type volcano. Another representative centre is El Puig d'Adri, produced by the superposition of two Strombolian cones and a tephra ring. The succession of deposits that form these volcanoes were analyzed and discussed, looking for the potential causes of such a wide diversity of eruptive styles.

One of the most representative edifices of the CVZ is La Crosa de Sant Dalmai, a roughly circular asymmetrical maar-diatreme volcano, which belongs to the Garrotxa Volcanic Field (GVF, 0.6–0.01 Ma, which includes the youngest volcanoes in the CVZ). The edifice is an example of monogenetic landform, mostly composed of phreatomagmatic deposits with subordinate Strombolian phases, constructed on a mixed basement made of hard Paleozoic granites and schists rocks and soft Plio-Quaternary deposits. Two different works were carried out in this area in order to understand the eruptive dynamics of this complex volcano. A detailed lithological and sedimentological analysis of the stratigraphic succession was performed, in order to determine how the magma/water interaction occurred during the eruption and the influence of the external parameter (i.e. stratigraphic, lithological and hydrological characteristics of the substrate). This area presents a complex hydrogeological substrate with high permeable alluvial and weathering materials of La Selva Basin and Paleozoic crystalline materials with structural heterogeneities (i.e. fractures, faults and joints). The heterogeneities and differences in these rocks' hydraulic properties and fracturing patterns influenced the way in which the magma/water interaction took place during the eruption and, consequently, the style of the eruption and the resulting deposits.

Monogenetic volcanoes may form in any type of geological environment and that is why two more surveys were carried out at Lanzarote and El Hierro Islands (Canary Archipelago, Spain) studying respectively a mafic edifice of littoral origin and a felsic hydromagmatic eruption developed at the interior of a volcanic ocean island. Lanzarote is the north easternmost island of the whole archipelago, and it represents the emergent part of the East Canary Ridge, a NNE–SSW linear volcanic structure. The island is characterized in the last stage of evolution mainly by aligned scoria cones and associated lava flows. Several hydrovolcanic monogenetic edifices are also located on

the island with the tuff cone of El Golfo being one of the most representatives. This volcanic edifice, sited on the western coast of Lanzarote Island, is aligned with other edifices of the same age, along a NEE–SWW oriented fracture, which represents the main structural trend of recent volcanism in this part of the island. The main objective of the work was to describe in detail the structure and association of the facies of this edifice and use this information to infer changes in eruption style and depositional processes and a detailed stratigraphic and sedimentological study of the succession of deposits was conducted. This type of volcanism is common in the coastal zones of Lanzarote and the other Canary Islands, representing a serious threat for the human population of the archipelago.

Volcanism at the Canary Islands is mostly associated with basanites, basalts, and trachybasalts with subordinate explosive felsic episodes responsible for the formation of large central volcanic complexes in Gran Canaria and Tenerife Islands. A new felsic deposit was discovered and studied at El Hierro Island, a complex basaltic shield volcano. The island is mainly characterised by effusive mafic volcanism with both Strombolian and Hawaiian activity and only subordinate felsic deposits mostly restricted to subvolcanic intrusions and a few lava flows of the oldest stage of the volcano. The 2011/2012 submarine eruption about 2 km off the southern coast of El Hierro revealed the presence of highly vesiculated lava balloons with low density aphyric white core of felsic composition, increasing the awareness of the possibility that more explosive eruption of felsic nature could occur on an island mainly characterized by less explosive mafic volcanism. The objective of this study was, then, to describe in detail a pumices deposit of hydromagmatic origin, named here as the Malpaso Member, reporting the stratigraphic, lithological, sedimentological and petrographic characteristics in order to discuss, transport/depositional mechanisms, dynamics, relative age and implications for hazard assessment on the island of El Hierro. This work provides a detailed stratigraphic and chronological framework for the area and also demonstrates that a future event with similar characteristics would have a serious impact on the population, infrastructures, and economy of the island of El Hierro.

The last survey was carried out at Deception Island (South Shetland Archipelago, Antarctic Peninsula group) where a hydromagmatic eruption took place in 1970. The eruption occurred in the northern sector of the island, leading to the formation of two groups of craters showing a different nature of the volcanic activity. The main objective was to describe in detail the stratigraphy of the deposits, the lithological and

sedimentological characteristics, and clasts distribution (isopach and isopleth maps). This information was, then, used to determine depositional processes, eruption style and physical parameters (i.e. plume height, erupted volume, VEI) of the eruptions. The 1970 eruption was undoubtedly the most violent recent volcanic activity on Deception Island and in a similar way the 1967 episode was characterized by submarine and land vents, with an analogous volume of erupted material and a similar dispersion of deposits. These episodes of the last century show how this type of activity is not uncommon at Deception Island having high possibility of further eruptions with similar characteristics.

2. PHREATOMAGMATIC VOLCANISM IN COMPLEX HYDROGEOLOGICAL ENVIRONMENTS: LA CROSA DE SANT DALMAI MAAR (CATALAN VOLCANIC ZONE, NE SPAIN)

Published in:

Geosphere

Authors of the paper:

Dario Pedrazzi, Institute of Earth Sciences Jaume Almera, ICTJA-CSIC, Group of Volcanology. SIMGEO (UB-CSIC) Lluís Solé i Sabarís s/n, 08028 Barcelona, Spain

Xavier Bolós, Institute of Earth Sciences Jaume Almera, ICTJA-CSIC, Group of Volcanology. SIMGEO (UB-CSIC) Lluís Solé i Sabarís s/n, 08028 Barcelona, Spain

Joan Martí, Institute of Earth Sciences Jaume Almera, ICTJA-CSIC, Group of Volcanology. SIMGEO (UB-CSIC) Lluís Solé i Sabarís s/n, 08028 Barcelona, Spain

The reference of this paper is:

Pedrazzi, D., Bolós, X. and Martí, J., 2014. Phreatomagmatic volcanism in complex hydrogeological environments: La Crosa de Sant Dalmai maar (Catalan Volcanic Zone, NE Spain). Geosphere.

Abstract

The volcano of La Crosa de Sant Dalmai is a roughly circular asymmetrical maar that forms part of the Catalan Volcanic Zone (Girona Province, NE Spain). The edifice is an example of a maar-diatreme volcano constructed on a mixed basement of hard Paleozoic granites and schists and soft Pliocene and Quaternary deposits. The heterogeneities and differences in these rocks' hydraulic properties and fracturing patterns influenced the way in which the magma-water interaction took place during the eruption and, consequently, the style of the eruption and the resulting deposits. The eruption of La Crosa de Sant Dalmai consisted of four consecutive eruptive phases characterized by alternating phreatomagmatic and magmatic fragmentation. The eruptive sequence and the variety of deposits—mainly fallout with subordinate surges—generated by this single eruption are a stark contrast to the compositional monotony of the magma, which thus highlights the role played by the geological and hydrological characteristics of the substrate in determining the eruptive style and associated hazards in this type of volcanism.

Keywords: Maar-diatreme, La Crosa de Sant Dalmai, Phreatomagmatism, Catalan Volcanic Zone, Hard-soft substrate

2.1 Introduction

Maar-diatreme volcanoes are typical products of phreatomagmatism (e.g., Fisher and Waters, 1970; Lorenz, 1973, 1974, 1986; Fisher and Schmincke, 1984). They represent one of the most interesting examples of the explosive excavation of geological substrate because the lithic components in the maar deposits are an excellent source of information that reveals much about the substrate and the depth of the explosions. These monogenetic volcanoes are created by comparatively low-volume and low-intensity eruptions, but this form of volcanism represents a localized, unpredictable volcanic hazard.

These volcanic explosions are caused by the interaction of magma with phreatic water, and their exact nature depends on the substrate and the proportions and extent to which magma and water interact (Wohletz and Sheridan, 1983; Houghton and Hackett, 1984; Kokelaar, 1986; White and Houghton, 2000; Mastin et al., 2004). The type of substrate controls the characteristics of the aquifer(s) in which the external water is stored (fracture-controlled vs. porous aquifers) and has an important influence on the

eruption dynamics and the characteristics of the resulting pyroclastic deposits. The substrate also affects the resulting overall shape of the volcano—for example, the diatreme and the posteruptive lacustrine architecture of the maar crater (Lorenz, 2003)—and gives rise to a wide range of maar types and maar processes (e.g., Tihany maar volcanic complex in Hungary [Németh et al., 2001]; Balaton Highland, Hungary [Auer et al., 2007]; Campo de Calatrava, Spain [Martín- Serrano et al., 2009]; Atexcac crater, eastern Mexico [Carrasco-Núñez et al., 2007]; Pali Aike volcanic field, Argentina [Ross et al., 2011]).

Maars commonly display evidence of complex eruptive dynamics and different phases during individual eruptive events that can include phreatic, phreatomagmatic, and magmatic episodes (e.g., Houghton et al., 1996; White and Houghton, 2000; Carrasco-Núñez et al., 2007; Németh et al., 2001).

The Catalan Volcanic Zone (Martí et al., 1992), one of the Quaternary volcanic regions related to the European rift system, exhibits a wide range of phreatomagmatic episodes that depend on the stratigraphic, structural, and hydrogeological characteristics of the subsoil below each volcano (Martí et al., 2011). Of these hydrovolcanic edifices, La Crosa de Sant Dalmai offers the most characteristic example of a maar structure in this volcanic field (Martí et al., 1986; Martí and Mallarach, 1987) and reveals how much the resulting volcanic edifice depends on the substrate (Bolós et al., 2012). La Crosa de Sant Dalmai represents, in fact, an example of an edifice emplaced in a mixed substrate. These types of edifices are so far less well documented (e.g., White, 1991; Sohn, 1996; Sohn and Park, 2005; Ross et al., 2011) compared to examples of maars emplaced in hard substrates (e.g., Lorenz, 1987; Lorenz and Zimanowski, 2008).

In order to determine how the magma-water interaction occurred during the eruption of La Crosa de Sant Dalmai and how it was influenced by the stratigraphic, lithological, and hydrological characteristics of the substrate, we performed a detailed lithological and sedimentological analysis of the stratigraphic succession of this volcano and interpreted it in terms of its eruption dynamics. In this paper, we describe the main characteristics of the deposits in La Crosa de Sant Dalmai and discuss the influence of the substrate on its eruption behavior. The results obtained here help to explain changes in the explosive behavior of a maar volcano emplaced in a mixed substrate with complex hydrogeological behavior and can be extrapolated to other phreatomagmatic volcanoes of similar characteristics.

2.2 Geological setting

The Catalan Volcanic Zone is situated in the NE Iberian Peninsula and is one of the Quaternary alkaline volcanic provinces that belong to the European Cenozoic rift system. The Catalan Volcanic Zone is mainly represented by alkali basalts and basanites and includes several distinct volcanic fields ranging in age from older than 12 Ma to early Holocene (Fig. 1; Martí et al., 1992). The volcanic activity in the Catalan Volcanic Zone is characterized by small scoria cones that were produced during short-lived monogenetic eruptions associated with widely dispersed fractures of short lateral extent. The total volume of extruded magma in each eruption was small (0.01–0.2 km³ dense rock equivalent [DRE]), suggesting that the amount of magma available to feed each eruption was also very limited. Strombolian and phreatomagmatic episodes alternated in most of these eruptions and gave rise to complex stratigraphic sequences displaying a wide range of pyroclastic deposits (Martí et al., 2011).

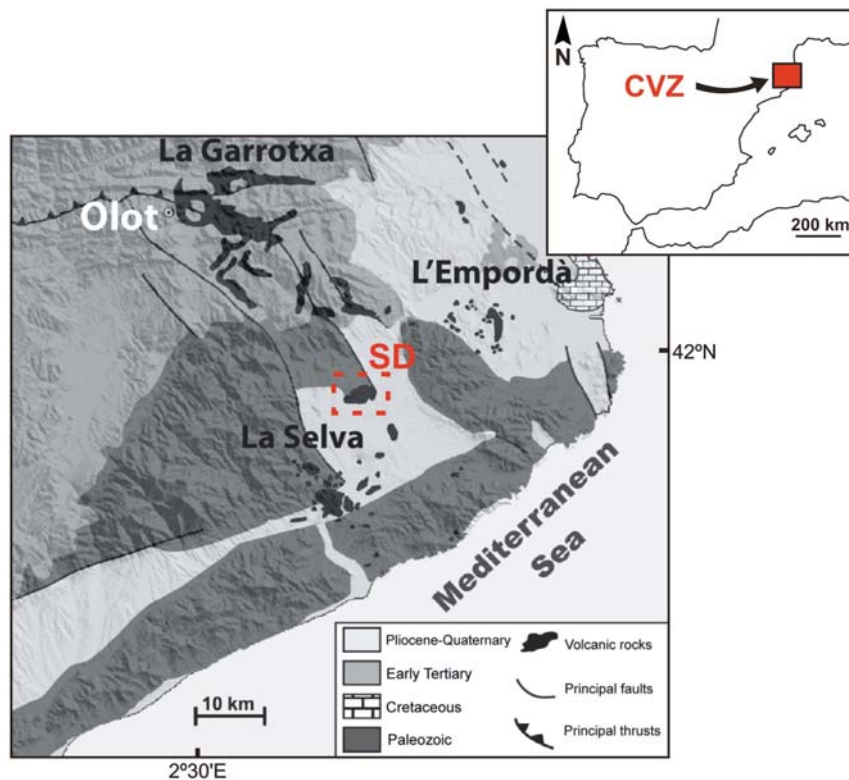


Fig. 1. Simplified geological map of the Catalan Volcanic Zone (CVZ) and its three subzones, La Selva (7.9–1.7 Ma), L'Empordà (12–8 Ma), and La Garrotxa (0.5–0.01 Ma) (modified from Guérin et al., 1986; Martí et al., 1992). Dashed red square and SD indicate La Crosa de Sant Dalmai location.

With a diameter of 1200 m, the maar of La Crosa de Sant Dalmai is the largest edifice in the Catalan Volcanic Zone. It belongs to the Garrotxa Volcanic Field (0.6–0.01 Ma), which includes the youngest volcanoes in the Catalan Volcanic Zone (Fig. 1).

This volcano is located at the northern border of La Selva graben, a Neogene tectonic depression bounded by ENE-WSW- and NW-SE-oriented normal fault systems that affect the Paleozoic basement, and it is infilled with Pliocene and Quaternary sediments (Fig. 1).

La Crosa de Sant Dalmai is an example of a maar-diatreme volcano consisting of a circular tephra ring, 30 m and 50 m high on its eastern and western sides, respectively. Volcanic deposits cover an area of 7 km², extending up to 4 km eastward but only a few hundred meters westward (Fig. 2).

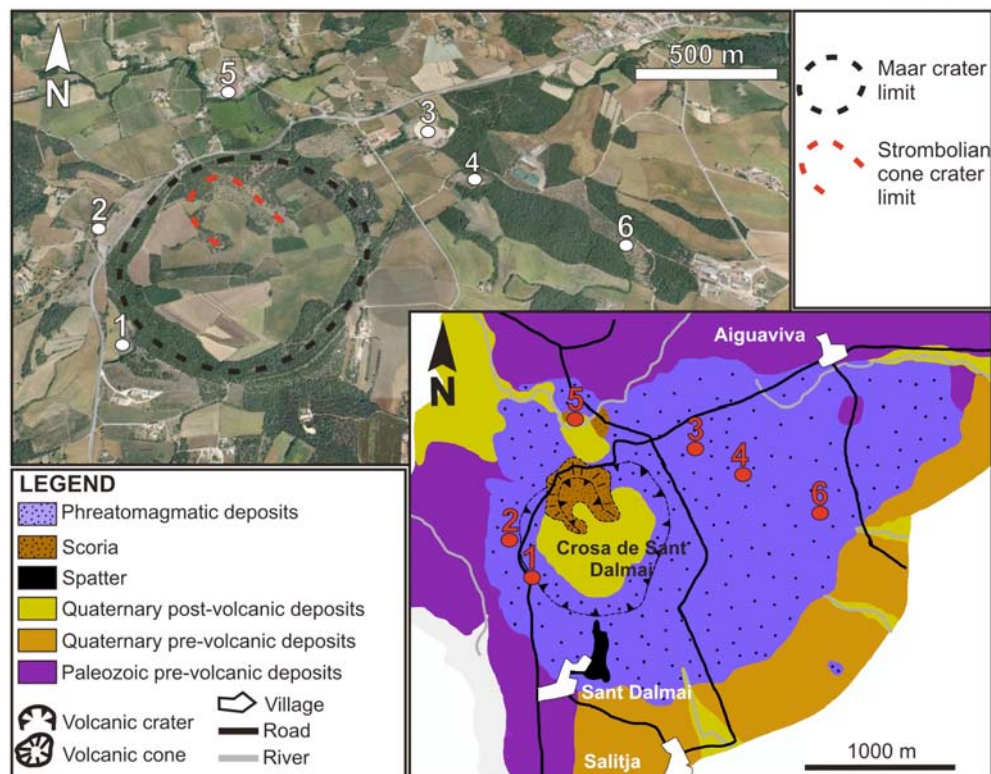


Fig. 2. Google Earth image and geological map of the volcano of La Crosa de Sant Dalmai (modified from Martí et al., 2011) showing the main crater and the inner scoria cone, as well as the extent of the phreatomagmatic deposits and the pre- and postvolcanic deposits. The studied outcrops are also shown (numbers).

Geophysical studies (Bolós et al., 2012) have found that La Crosa de Sant Dalmai developed on a NW-SE-oriented fault through which deep magmas were transported to the surface. This maar volcano is mostly composed of phreatomagmatic deposits with subordinate Strombolian phases. La Crosa de Sant Dalmai eruption ended with the formation of a scoria cone in the northern part of the main maar crater (Fig. 2). This small edifice emitted a basaltic lava flow that flowed southward and filled much of the maar crater (Bolós et al., 2012). Currently, postvolcanic lacustrine sediments cover this lava flow. The age of this volcano is not well constrained, but stratigraphic relations and

existing U-Th and C^{14} ages of the lava flow and post-eruptive sediments suggest that it dates from the end of the Quaternary age.

2.3 Methods

An important part of the research was carried out in the field in an area of ~ 10 km² surrounding the edifice of La Crosa de Sant Dalmai using as a reference the geological map produced by Bolós et al. (2012). In total, six stratigraphic sections were carefully studied. The stratigraphic criteria used to distinguish the different units forming the succession of volcanic deposits included color, nature and relative content of the components, and variations in grain size, texture, and sedimentary structures. Estimates of grain size were conducted partially in the field using a comparative grain size chart and then completed in the laboratory.

Grain-size analyses consisting of dry-sieving techniques and componentry analysis were performed by weighing/counting 47 representative samples of the identified units. Large boulders were not considered for sieving but were measured and considered as part of the stratigraphic column for comparison with other layers. Samples were sieved with a set of sieves with a mesh size ranging from -6ϕ to $+4\phi$ units (64 to 1/16 mm). Grain-size data were used to define the median diameter ($Md\phi$) and sorting ($\sigma\phi$) (Inman, 1952) to help discriminate between deposits emplaced by fall and flow mechanisms. Clast compositions were characterized immediately in the field by hand-sample observation and then confirmed in the laboratory using a binocular microscope and petrographic analysis. Component analysis was carried out on the -4ϕ , -3ϕ , -2ϕ fractions of the deposits. Clasts were separated into juvenile and accidental lithics classes belonging to the Paleozoic basement and La Selva infill succession. The main difference lies in the roundness and alteration of the clasts; nevertheless, this difference was not sufficient to discriminate between clasts in fractions smaller than -2ϕ . Maximum juvenile (scoria and cauliflower bombs) and lithic clast sizes were determined by measuring and averaging the long axes of 5–10 of the largest clasts in each bedset.

In order to establish a qualitative idea of the different degrees of vesiculation of the juvenile clasts, comparative petrographic and image analyses were carried out using a binocular microscope and ImageJ software (www.ImageJ.com).

Samples obtained from the lava flow and organic matter from a drill core made on the northeastern side of the maar crater (Bolós et al., 2012) were used for dating. A

prevolcanic organic sediment sample was sent for dating to the Beta Analytics Laboratory (UK). The analysis was performed through accelerator mass spectrometry (AMS) (radiocarbon.com/accelerator-mass-spectrometry.htm). The chemical procedure and mass spectrometry for lava samples are described in Sigmarsson et al. (1998).

2.4 Characteristics of the pyroclastic succession

In order to reconstruct the complete succession of deposits, we carried out a detailed characterization of six stratigraphic sections in which six different facies were identified (Fig. 3).

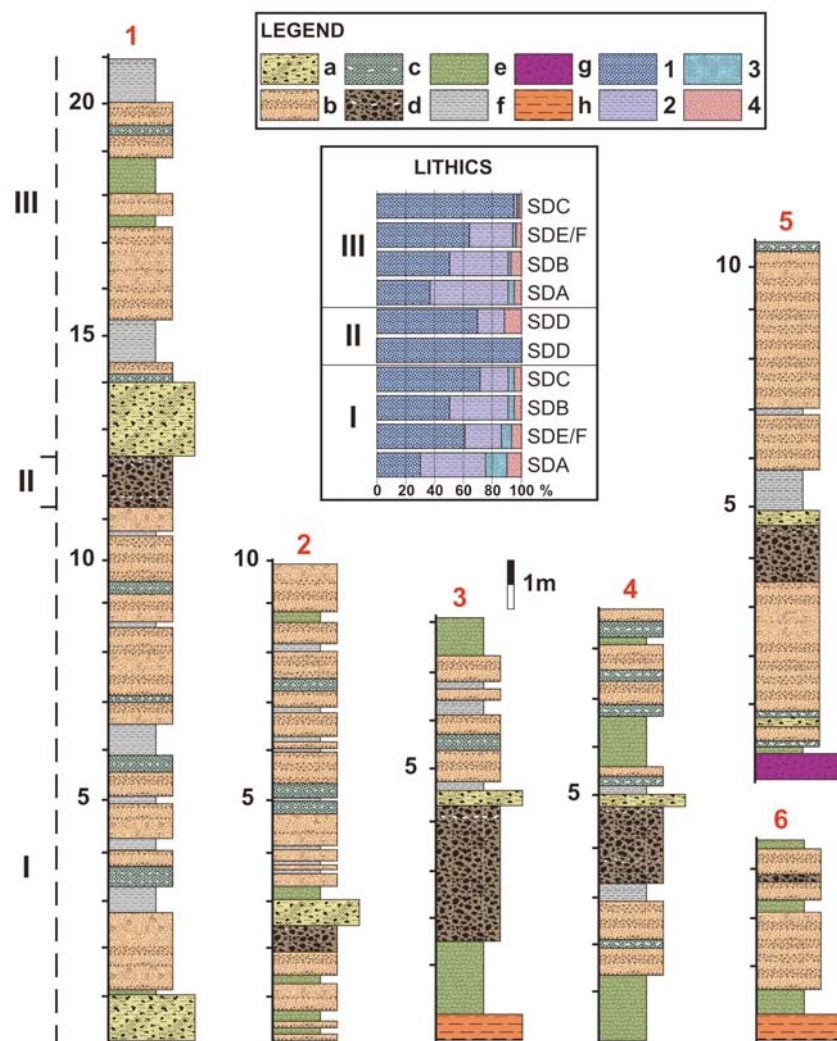


Fig. 3. Composite stratigraphic column of the deposits at La Crosa de Sant Dalmai showing the main facies: (a) facies SDA—large lithic ballistic deposits; (b) facies SDB—clast supported deposits; (c) facies SDC—scoriaceous clast-supported deposits; (d) facies SDD—scoriaceous deposits; (e) facies SDE—thinly bedded deposits; (f) facies SDF—diffusely stratified deposits; (g) Paleozoic basement; (h) Pliocene–Quaternary basement. Lithics contents in the various units are reported as well: (1) juvenile clasts; (2) Paleozoic lithic clasts; (3) Pliocene–Quaternary lithic clasts; (4) altered lithic clasts. Four lithofacies associations and four units are identified based on the depositional processes and resulting deposits. Unit IV corresponds to the product of the inner scoria cone shown in Figure 2.

The lateral correlation of individual beds was possible using stratigraphic markers (Fig. 3); the maximum thickness of the observed succession was ~20 m (column 1, Fig. 3).

2.4.1 Facies Analysis

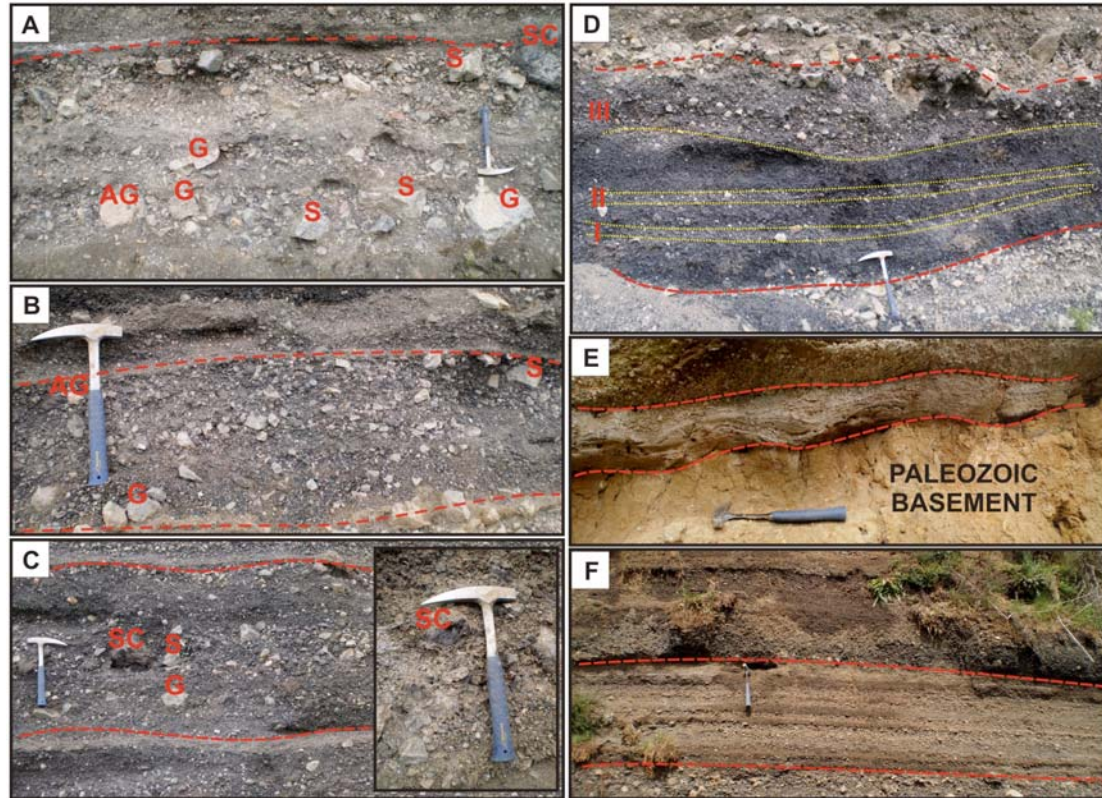


Fig. 4. Field photographs of the characteristic facies of the maar of La Crosa de Sant Dalmai: (A) Facies SDA: block- and lapilli-sized angular prevolcanic accidental lithic clasts (AG, G, and S) and poorly vesiculated scoriae (SC); (B) facies SDB: clast-supported, medium to well sorted, with coarse lapilli consisting of poorly vesiculated lithics (AG, G, and S); facies SDB resembles facies SDA closely but has a different percentage of lithics (up to 50%); (C) facies SDC: clast supported deposits with coarse lapilli consisting of vesiculated scoriae (SC) and subordinate lithics (G and S) in a mainly juvenile matrix with fine lapilli and coarse ash; (D) facies SDD: angular- to fluidally shaped, black-and-red, well-vesiculated bombs and lapilli scoriae, where I and II represent lithic rich levels (delimited by yellow dotted lines), and III represents the lithic-rich transitional upper part toward the following breccia deposit; (E) facies SDE: thinly bedded, poorly vesiculated fine scoria lapilli with subangular accidental lithics, where the bed surfaces show planar and low-angle cross-stratified laminations and basal erosional contact; and (F) facies SDF: poorly sorted deposits with coarse, poorly vesiculated scoria lapilli and accidental lithics, where the bed surfaces show a diffuse stratification. AG—altered granite, G—granite, S—schists, SC—scoriae. Dashed red lines represent the facies limit.

Facies SDA: Large Lithic Ballistic Deposits

This facies (Fig. 4A) has a maximum thickness of 200 cm (Fig. 3). It is clast supported and well sorted (e.g., samples SD1–1E, SD1–19E, SD2–1, SD3–2D; Fig. 5), with block- and lapilli sized angular prevolcanic accidental lithic clasts (up to 70%; Fig. 3), as well as poorly vesiculated scoria fragments (Fig. 6A) and a scarce interstitial matrix of juvenile coarse lapilli-sized to coarse ash-sized clasts and the same

prevolcanic accidental lithic clasts. The largest lithic clasts—up to 70–80 cm in diameter (Fig. 5)—are horizontally aligned and mainly correspond to granites and schists; they are subangular in shape, and some have partly or totally oxidized surfaces. Subordinate bombs of the same size are also present.

Facies SDB: Clast-Supported Deposits

The deposits of this facies (Fig. 4B) have a maximum thickness of ~300 cm (Fig. 3). They are clast supported and medium to well sorted (e.g., samples SD1–3CG, SD1–20, SD2–1B, SD2–5AB, SD2–7A, SD3–4G; Fig. 5), and they have coarse lapilli-sized fragments of poorly vesiculated scoriae (Fig. 6A) and granite and schist lithic clasts, with an interstitial matrix of lapilli and coarse ash fragments of the same composition. The largest clasts have a maximum size of 50 cm (Fig. 5). Facies SDB looks very similar to facies SDA (Fig. 4B), but it is characterized by a different percentage of nonvolcanic lithic clasts (up to 50%) compared to facies SDA (up to 70%; Fig. 3), and by poor stratification.

Facies SDC: Scoriaceous Clast-Supported Deposits

This facies (Fig. 4C) has a maximum thickness of 70 cm (Fig. 3). Its deposits are clast supported and moderately to well sorted (e.g., samples SD1–5AS, SD2–15BI; Fig. 5) and have vesiculated scoria (up to 70%; Fig. 3) the size of coarse lapilli (Fig. 6C), as well as granite and schist lithic clasts with a maximum size of 40 cm (Fig. 5) and an interstitial matrix mainly consisting of juvenile fine lapilli and coarse ash fragments. Impact structures are generally absent. These deposits are characterized by normal and reverse grading.

Facies SDD: Scoriaceous Deposits

This facies (Fig. 4D) occurs in the middle of the sequence, where it reaches a maximum thickness of 250 cm (Fig. 3) and also corresponds to the last episode of the eruption, which led to the formation of a Strombolian cone (Fig. 2). No deposits directly connected to the scoria cone located inside the crater were present in the studied sections. The facies mantles the topography and consists of black-and-red, well-vesiculated bombs and lapilli scoriae (Fig. 6D) covered by a subordinate fine lapilli and coarse ash matrix. These deposits are generally well sorted (e.g., samples SD1–18E, SD3–2AI; Fig. 5). A few accidental lithic (granites and schists) clasts with a maximum size of 10–15 cm are found at certain levels (Figs. 4D and 5).

Facies SDE: Thinly Bedded Deposits

This facies (Fig. 4E) consists of thinly bedded, poorly vesiculated scoria of fine lapilli size (Fig. 6E) with subangular accidental lithic clasts (up to 30%–40%; Fig. 3) having a maximum size of few centimeters. This deposit occurs overall at the bottom and top of the stratigraphic sequence with a maximum thickness of 50–70 cm (Fig. 3). The deposits are poorly sorted (e.g., samples SD1–2, SD3–1B; Fig. 5). The bed surfaces have planar and low-angle cross-stratified laminations and basal erosional contact (Fig. 4E).

Facies SDF: Diffusely Stratified Deposits

This facies (Fig. 4F) has a maximum thickness of 50 cm (Fig. 3) and consists of poorly sorted deposits (e.g., samples SD1–14, SD2–10; Fig. 5) with coarse, poorly vesiculated scoria lapilli (Fig. 6F) and accidental lithics (up to 30%–40%; Fig. 3) with a maximum size of 10 cm. The bed surfaces have diffuse stratification.

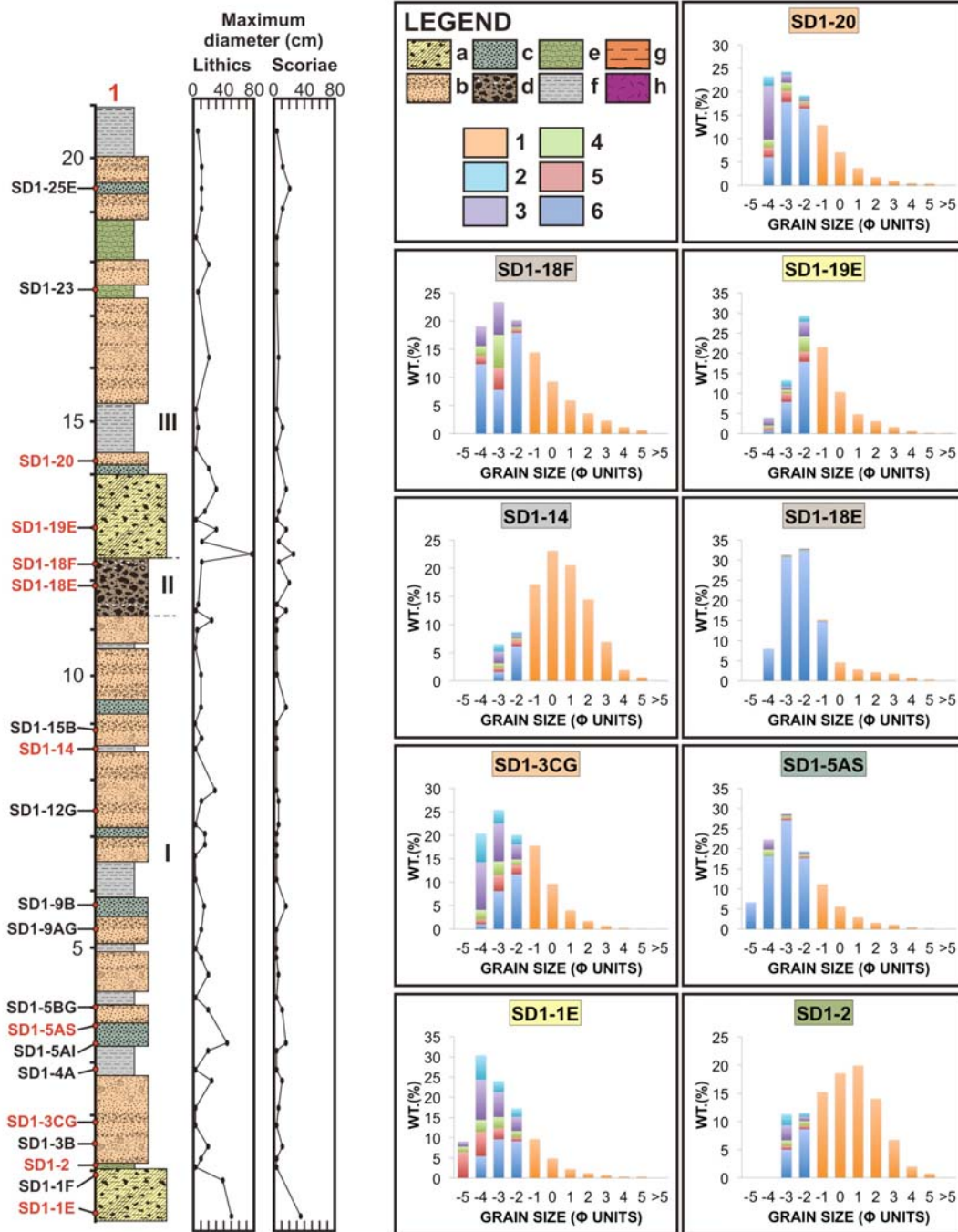


Fig. 5 (on this and following page). Composite stratigraphic column of the three main outcrops in La Crosa de Sant Dalmai. The lithics contents of the main samples are shown, and vertical variations in the maximum diameter of the lithic and scoria clasts are also indicated. (a) Facies SDA; (b) facies SDB; (c) facies SDC; (d) facies SDD; (e) facies SDE; (f) facies SDF, (g) Pliocene–Quaternary basement, (h) Paleozoic basement. 1) No componentry; (2) Pliocene and Quaternary lithic clasts; (3) metamorphic lithic clasts; (4) altered lithic clasts; (5) granite lithic clasts; (6) juvenile clasts.

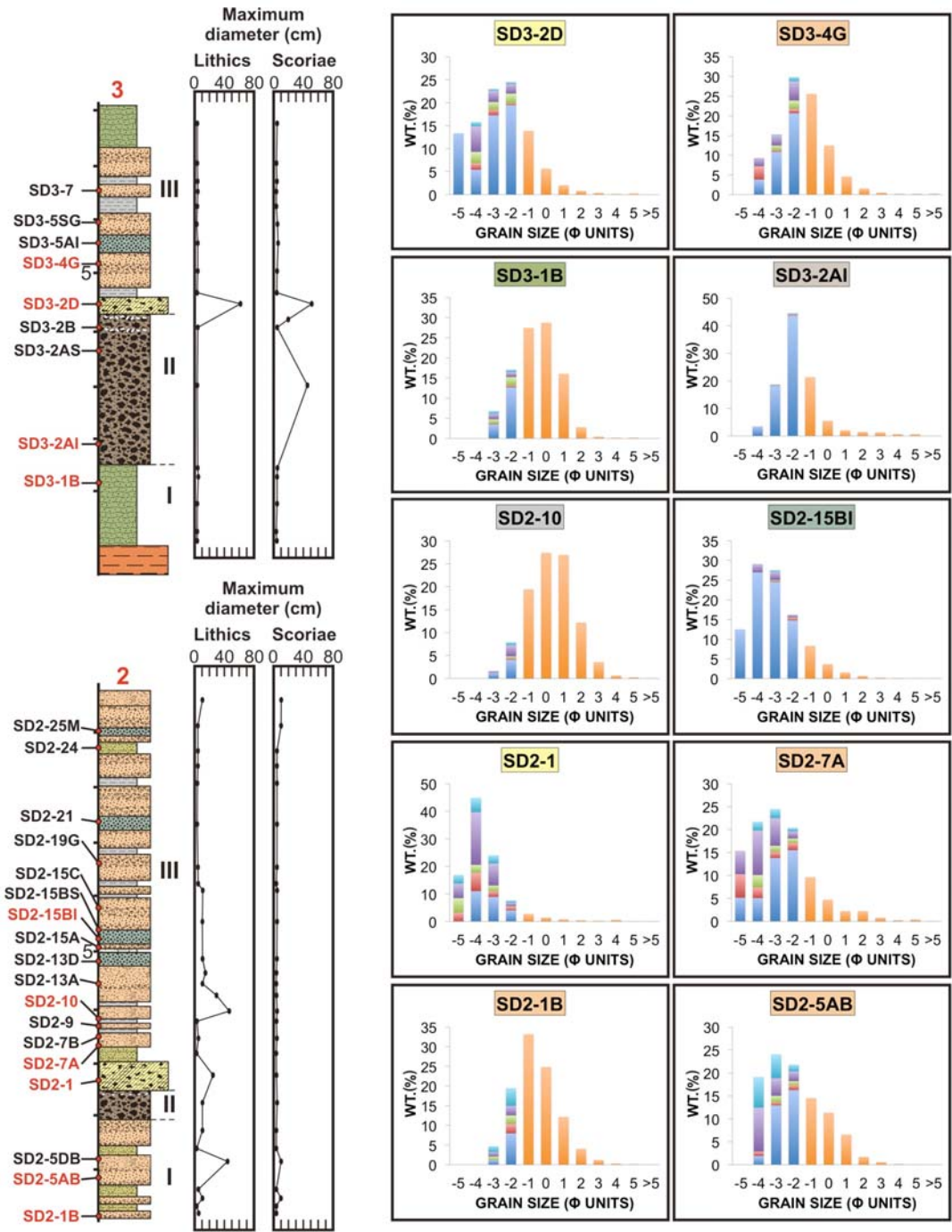


Fig. 5 (continued)

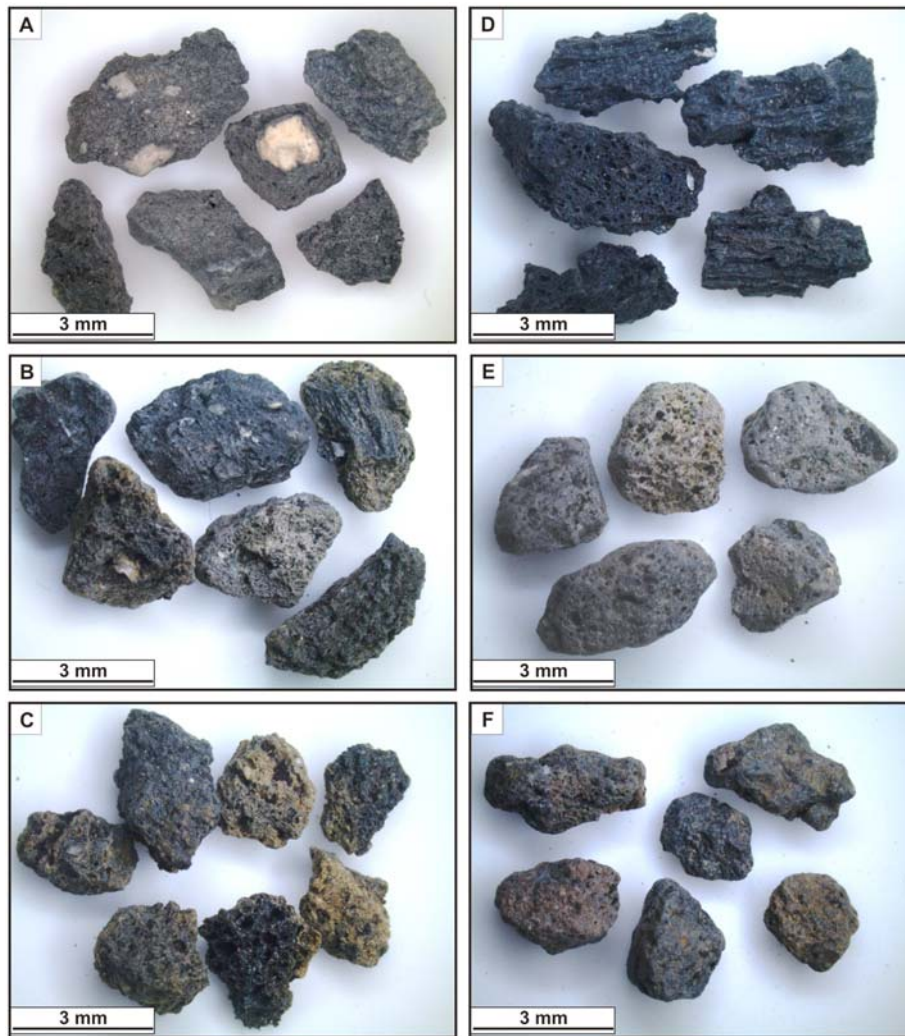


Fig. 6. Photographs comparing the juvenile fragments of different lithofacies: (A) facies SDA; (B) facies SDB; (C) facies SDC; (D) facies SDD; (E) facies SDE; and (F) facies SDF. Most of the samples are made of poorly vesiculated scoriae except that in D, which represents a pure Strombolian deposit (facies SDD).

2.4.2 Stratigraphic Units and Facies Associations

Four stratigraphic units (Figs. 2, 3, and 7) can be described from the study of the facies associations, each of which represents a successive stage in the construction of the volcano (Fig. 3). Unit I is represented by the lithofacies association I (facies SDA-SDB-SDC-SDE-SDF). Its thickness varies from 11 m in the western section (column 1, Fig. 3) to only 3 m in the east (column 6, Fig. 3). It is dominated by clast-supported deposits with relatively minor intercalated layers of lapilli-size material. The base of this unit is only visible in a few outcrops (columns 3, 5, and 6, Fig. 3), and it has thick layers of lithic-rich, fine lapilli (facies SDE) that correspond to the beginning of the eruption. On the eastern side, this initial deposit is overlain, in almost all the outcrops, by a series of thick deposits of coarse angular to subangular, lapilli-sized clasts (facies SDB) alternating with thin layers, just a few centimeters thick, of lapilli-sized clasts

(facies SDE and SDF). The following clast-supported, well-sorted deposit (facies SDA), with decimetric angular prevolcanic accidental lithic clasts, is a good stratigraphic marker found throughout almost all of these outcrops (Fig. 3). A monotonous sequence characterized by facies SDB, facies SDC, facies SDE, and facies SDF completes unit I. In the eastern section (column 3, Fig. 3), the sequence is characterized by thin, bedded deposits of fine and coarse lapilli-sized clasts (facies SDE).

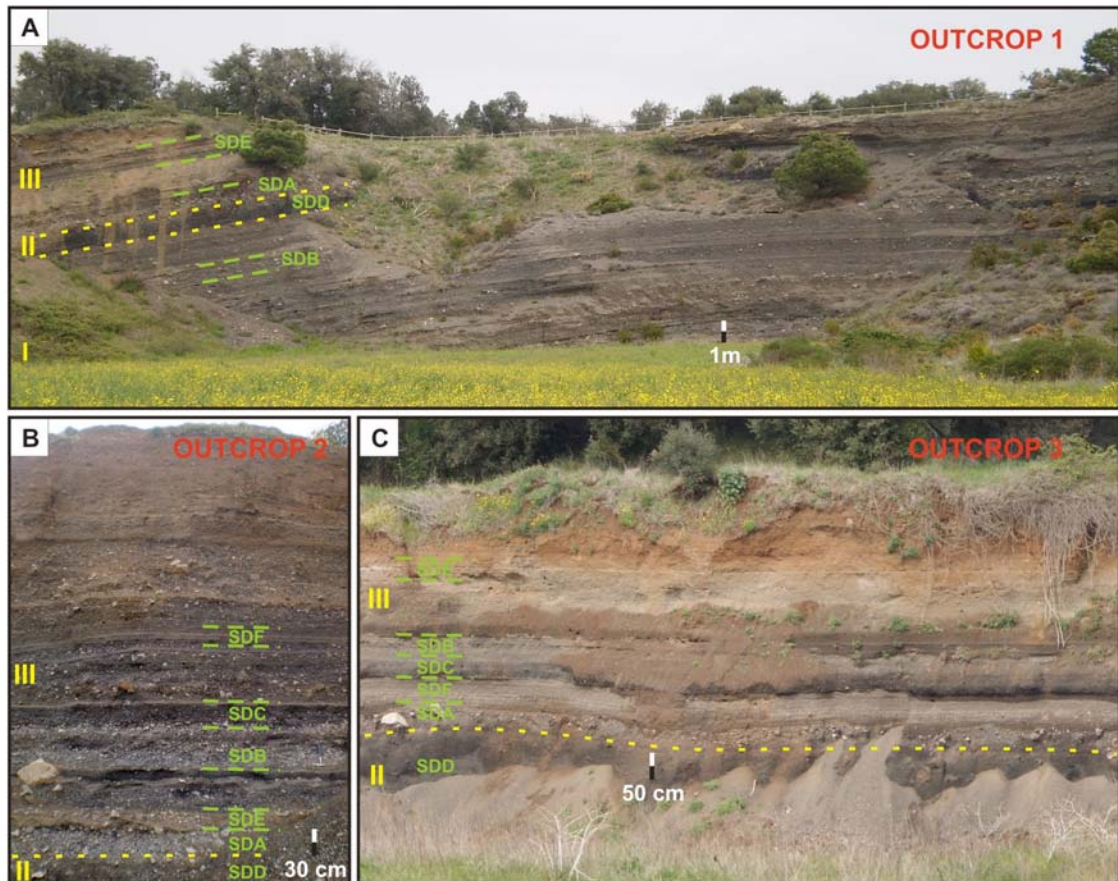


Fig. 7. The three main outcrops (1, 2, and 3) showing the main characteristics of the La Crosa de Sant Dalmai sequence. I, II, and III refer to the different units of the eruption, and the green letters represent the facies as shown in Figure 4.

Unit II (lithofacies association II, facies SDD) is represented by deposits that are almost 3 m thick in section 3 (Fig. 3) but that overall decrease to 1 m (column 1, Fig. 3) or less (column 2, Fig. 3). The unit is made up of highly vesiculated bombs and scoria lapilli with a certain percentage (up to 30%; Fig. 5) of accidental lithic clasts in certain levels. Unit III is somewhat similar to unit I, and it is composed of the lithofacies association III (facies SDASDB- SDC-SDE-SDF). All the stratigraphic logs (Figs. 3 and 7) have a similar pattern. Their thickness varies from 8 m to less than 1 m (Fig. 3). This unit begins with a breccia (facies SDA) that has the same grain size as unit I and large

blocks of accidental lithic clasts up to 70 cm (Fig. 5). The following deposits are dominated by thick, coarse layers of lapilli-sized breccia with accidental lithics up to 30 cm and non vesiculated (juvenile) scoria (facies SDB), and occasional deposits with more vesiculated juvenile scoriae (facies SDC), intercalated with a small proportion of thin fine lapilli layers with planar stratification (facies SDE). Unit IV corresponds to a small scoria cone with an associated lava flow formed inside the maar (lithofacies association IV-SDD).

No evidence of stratigraphic discontinuities was observed in the sequence, and in some cases, slightly diffused contacts were observed among the different facies (Fig. 4). Mantle derived nodules in the juvenile fragments are present in all of the units.

2.5 Grain size, modal variations and lithic distribution

2.5.1 Grain Size and Modal Variations

Vertical variations in the grain-size distribution and modal variations were analyzed by selecting representative samples from both the coarse- and fine-grained layers (Fig. 5). The maximum clast size is related to the energy conditions and efficiency of magma fragmentation, vent excavation, ejection, and emplacement. In the lowermost unit (unit I), fine layers dominate in the first part, with a general increase in grain size up to the first lithic-rich breccia. A general trend of alternating, well-sorted coarse lithic rich lapilli deposits and poorly sorted fine lapilli deposits characterizes the first unit. As shown in Figure 5, the largest blocks measure up to 50–70 cm. Unit II includes coarse juvenile fragment-rich layers. Unit III is similar to unit I and is dominated by coarse deposits, particularly in the lower half of the unit, and a grain size that gradually decreases toward its upper part. Both units show the same characteristics and can be distinguished by being above or below unit II, which is an important stratigraphic marker of the eruption. Although the distribution of large blocks is variable, units I and III clearly include the largest proportion of blocks of the whole sequence.

Based on the grain-size data, Inman parameters (Inman, 1952) of median diameter ($Md\phi$) and sorting ($\sigma\phi$) were obtained and plotted on frequency histograms (Fig. 8) in order to help discriminate between fall and surge deposits. Sorting ($\sigma\phi$) values for La Crosa de Sant Dalmai samples range between 1ϕ and 2.25ϕ , while the median diameter $Md\phi$ values generally range between -4.3ϕ and -0.2ϕ (Fig. 8).

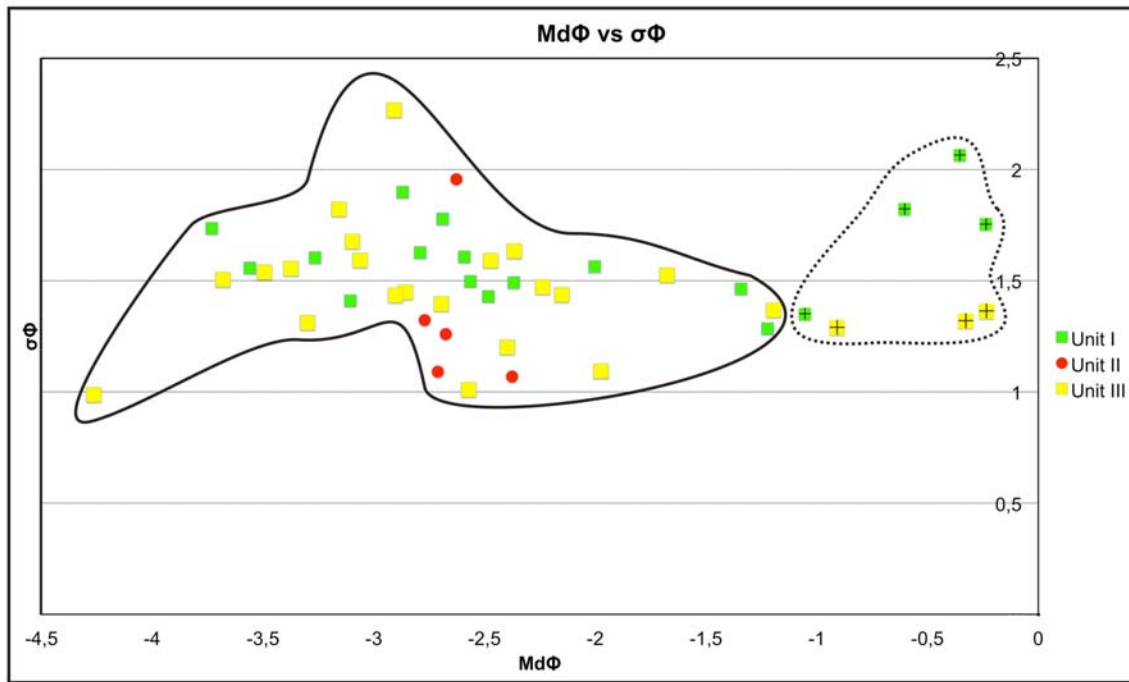


Fig. 8. Sorting ($\sigma\phi$) versus median diameter ($Md\phi$) plot of grain-size data from the fall and surge deposits. Dotted line defines samples from surge deposits, while continuous line shows samples from fall-out deposits.

2.5.2 Componentry Analysis

La Crosa de Sant Dalmai deposits consist of a mixture of juvenile scoria and accidental lithic clasts in differing proportions (Figs. 3 and 5 and the Supplemental Figure1). Juvenile fragments are fresh, black, dense or vesicular scoria with a basaltic composition. The lithic fragments found in the different beds throughout the succession include granite and schist from the Paleozoic basement, as well as the same type of fragments—but with a different grade of roundness—from the Pliocene–Quaternary sediments that fill La Selva depression. These latter fragments were formed by the erosion and reworking of the Paleozoic basement. Although the juvenile material is present at all stratigraphic levels, its distribution is variable (Figs. 3 and 5).

Small systematic variations in the occurrence of the lithic fragments can be seen in the stratigraphic succession. The lower part of unit I is characterized by a breccia deposit (e.g., sample SD1–1E; Fig. 5) with angular lithic fragments, mainly granites and schists (up to 40%), and Pliocene–Quaternary fragments (around 15%) with subordinate altered clasts (~10%). The whole of unit I is dominated by alternating coarse-grained deposits (e.g., samples SD1–3CG, SD2–1B, SD2–5AB; Fig. 5) that contain ~45%–50% juvenile lithic clast fragments (10% of Pliocene–Quaternary fragments, less than 5% of altered clasts, and around 40% of fragments from the Paleozoic basement), as well as

fine lapilli deposits (e.g., samples SD1–2, SD1–14, SD3–1B; Fig. 5) with lithic fragment contents of around 30%–40%. Only a few levels (e.g., sample SD1–5AS; Fig. 5) of unit I are dominated by juvenile material with lithic fragments reaching 20%–30% in abundance (with less than 5% of Pliocene–Quaternary lithics clasts). The highest proportion of juvenile clasts is found in unit II, where the accidental lithic fragments from the Paleozoic basement represent less than 1% (e.g., samples SD1–18E, SD3–2AI; Fig. 5). However, some levels in unit II show a notable increase in granite and schist fragments (up to 30%) and a very high content of altered clasts and metamorphic fragments with almost no Pliocene–Quaternary content (e.g., samples SD1–18F; Fig. 5). In unit III, the same trends as in unit I are present. The sequence starts with a lithic-rich breccia with a lithic content of 50%–60% (mainly from the Paleozoic basement; e.g., samples SD1–19E, SD2–1, SD3–2D; Fig. 5) and continues with the same alternating succession as in unit I, with a variable amount of lithic clasts (20%–40%), which mainly originate from the Paleozoic basement (e.g., samples SD1–20, SD2–7A, SD3–4G; Fig. 5) and with lesser amounts of Pliocene–Quaternary lithics (~5%). Unit IV is represented by a scoria cone (Fig. 2) largely made up of juvenile scoria fragments.

2.6 Lithological and hydrogeological characteristics of the prevolcanic substrate

The maar of La Crosa de Sant Dalmai is located on the northern border of La Selva Basin on the fault contact between the Paleozoic basement and the Pliocene–Quaternary sediments that fill the depression (Bolós et al., 2012). La Selva Basin covers an area of 565 km² and is located in NE Catalonia (Fig. 9). It has a graben structure (Pous et al., 1990) and is bounded on four sides by mountain ranges with greater relief, including the Guilleries range to the west, the Transversal range to the north, the massif of Gavarres to the east, and the Selva Marítima mountains to the south. This basin was created during the Neogene extensional period following the Alpine orogeny. Two main watersheds in the area correspond to the basins of the Santa Coloma and Onyar Rivers (Fig. 9). The Santa Coloma River Basin extends along the whole southwestern side of La Selva Basin and part of its headwaters are in the Montseny-Guilleries Mountains (Fig. 9). The Onyar River basin, on the other hand, occupies the northeastern side of the basin (Fig. 9) and has its headwaters in the Gavarres and Selva Marítima ranges. As proposed by Menció (2005) and Folch et al. (2011), three main hydrogeological units are present in La Selva Basin (Figs. 9 and 10): (1) alluvial materials, surface Neogene sedimentary layers, and highly porous and permeable weathered igneous rocks; (2)

layers of arkosic sands, gravels, and conglomerates with a low clay content and Neogene sediment alternating with layers of low-permeability clays and silt, which compose the main infilling in this basin (where the transmissivity and permeability of the Neogene sediments are both very low; except for the conglomerate-rich levels); and (3) crystalline materials (Paleozoic igneous and metamorphic rocks), which generally have low permeabilities but also have a set of structural heterogeneities (fractures, schistosity, presence of dikes and alteration) that act as zones of preferential flow.

As proposed by Menció et al. (2010) (Fig. 9), based on hydrochemical and isotopic data, the general model for underground flow requires a local flow system generated by the subsurface topography of the basin that is related to the main alluvial aquifers and more superficial Neogene layers. Furthermore, a regional flow system runs across La Selva Basin, and its recharge zone is located in the adjacent massifs (the Guillerias and Transversal ranges and, to a lesser extent, in the Gavarres and Selva Marítima ranges). Piezometric data proposed by Folch et al. (2011) indicate the presence in the La Selva area of unconfined aquifers less than 30 m deep and confined or semiconfined aquifers over 30 m deep. Furthermore, based on hydrochemical and isotopic data, the same authors proposed a lateral hydraulic connection between the range-front areas and the basin aquifers, which would indicate an effective recharge through fault zones and fracture networks within the basement. Similar behavior is also suggested to occur at the contact between the sedimentary infill of the basin and the basement, with the magnitude of the recharge depending on distinct geological features such as the hydraulic conductivity of the lowest Neogene sediments, the thickness of the weathered granite on top of the basement, and the fracture network. At the same time, hydraulic head data indicate a vertical connection between sedimentary aquifer levels at various depths, which allows distinct vertical connections between the Neogene sedimentary aquifer layers (Folch et al., 2011). Additionally, hydraulic head records indicate that the regional hydraulic head decline due to water withdrawal is recovered annually despite the rainfall regime. This behavior is attributable to the effective recharge from the aforementioned regional flow system (Menció, 2005).

In general, the distribution of the water table is consistent with the topography of the area. The western, eastern, and southeastern areas of La Selva Basin are characterized by a steep gradient (coinciding with the mountainous areas of Guillerias, Gavarres, and Selva Marítima), while in the central part of the basin, the distance

between the isopieces (equipotential curves representing the phreatic surfaces of the aquifer) grows, and the gradient decreases (Menció, 2005).

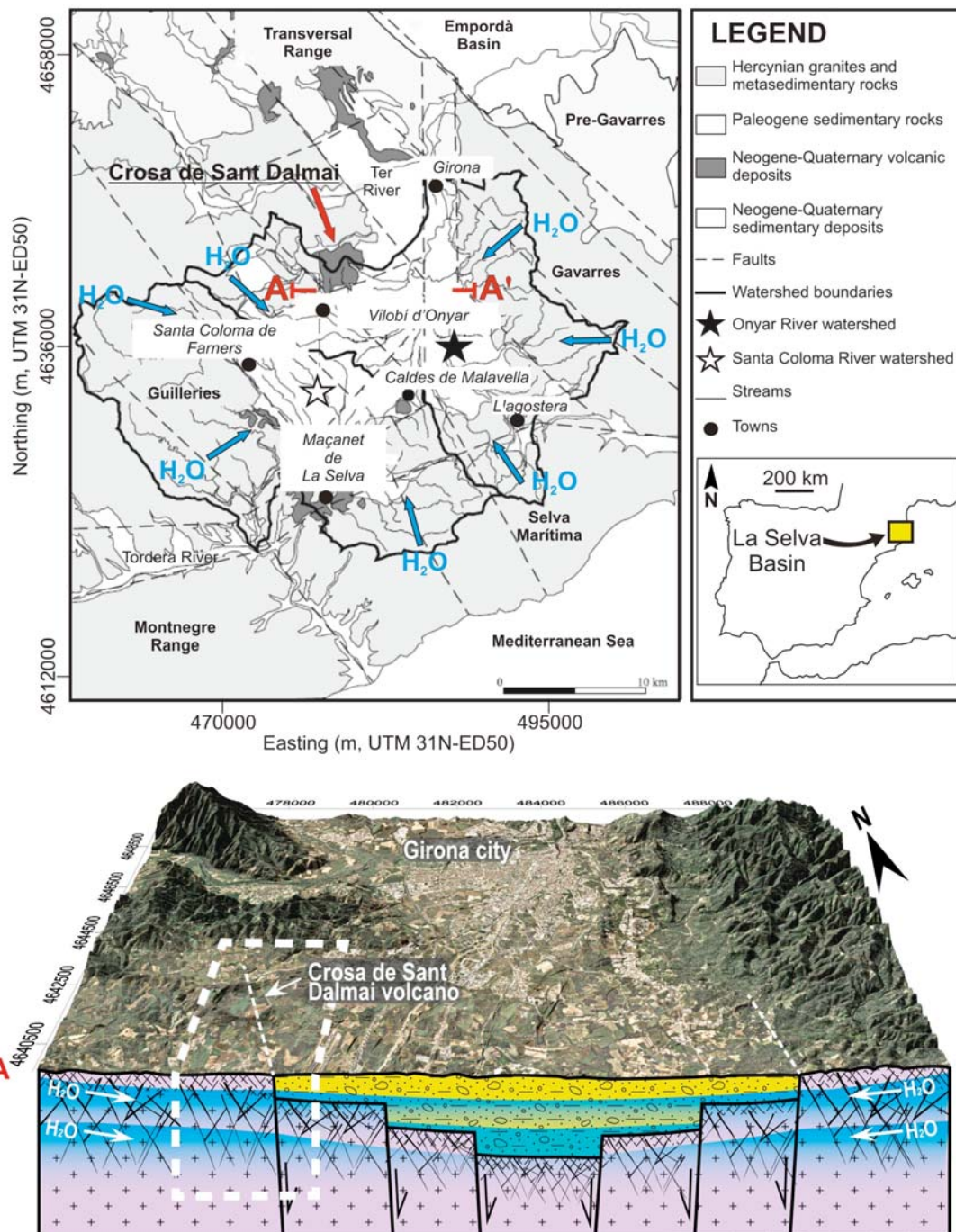


Fig. 9. Geographical and geological setting of La Selva Basin, with the watershed boundaries with the two main subbasins (Onyar and Santa Coloma Rivers) marked. Arrows indicate the recharging area of the basin (modified after Folch et al., 2011). The A-A' profile consists of a block diagram showing the general hydrogeological characteristics of the substrate below La Crosa de Sant Dalmai and La Selva depression and the infilling of the tectonic graben of La Selva Basin and the crystalline materials (igneous and metamorphic rocks). The orthophoto was provided by ICC (UTM 31N-ED50 Institut Cartogràfic de Catalunya, 2013, www.icc.cat).

2.7 Discussion

The eruption of La Crosa de Sant Dalmai included episodes that were clearly dominated by a magma-water interaction and magma-poor phases as shown by field evidence (Fig. 4), the abundance of lithic fragments (Figs. 3 and 5 and the Supplemental Figure [see the end of the chapter]), and the general low vesicularity of the juvenile fragments (Fig. 6). The lithological and depositional characteristics (Fig. 4) as well as the granulometrical analysis (Fig. 8) of the resulting deposits reveal that most were formed by fallout mechanisms of ballistic blocks and bombs impact sags, and subordinate pyroclastic surges. The characteristics of the lithofacies and lithofacies associations, as well as the results of the componentry analysis, provide the necessary clues for understanding the evolution of the eruption and the construction of the volcanic edifice.

The sequence starts with lithic-rich fine lapilli layers (facies SDE) deposited by pyroclastic surges, as suggested by the presence of cross laminations (Fig. 4E). This first episode corresponds to an initial phreatomagmatic phase during which the efficiency in the energy transfer from the magma to the phreatic water was optimal, as indicated by the characteristic high degree of fragmentation in the resulting deposit. At this stratigraphic level, it is very likely that the locus of the explosions was located between the weathered surface of the granite basement and the Quaternary deposits (stage I, Fig. 10), as shown by the relative abundance of Quaternary fragments compared to the rest of the sequence (Fig. 5). The characteristics of these initial deposits and their radial distribution reflect the presence of a base-surge-type explosion (Crowe and Fisher, 1973; Fisher and Waters, 1970; Druitt, 1998), as has occurred at the beginning of other phreatomagmatic eruptions (e.g., Atexcac crater [eastern Mexico], Carrasco-Núñez et al., 2007; Tihany [Hungary], Németh et al., 2001). The first episode was followed by the deposition of mainly lithic-rich fallout lapillized clast layers (e.g., samples SD2-1B, SD2-5AB; Fig. 5). As proposed by Carrasco-Núñez et al. (2007), the deposition of these layers could have been associated with the formation of an ephemeral eruptive column. This vent-opening episode was immediately followed by the formation of a thick breccia deposit (facies SDA), with abundant angular lithic clasts of block and lapilli size, derived from the mixed (Paleozoic and Pliocene-Quaternary) substrate rocks, and poorly vesiculated scoria fragments (Fig. 6A). This breccia corresponds to the main vent enlargement phase caused by a major influx of

phreatic water into the eruption conduit. The largest clasts, mainly granites and schists, are horizontally aligned and did not generate impact structures. Martí et al. (1986) suggested that this breccia originated from a very shallow explosion that generated ballistic trajectories with an important lateral component. Following this major explosive phase, a thick sequence formed the rest of unit I, dominated by poorly stratified, clast-supported deposits (facies SDB; Fig. 6B) alternating occasionally with deposits of more vesiculated scoriae (facies SDC; Fig. 6C) and diffusely stratified deposits of lapilli-sized clasts (facies SDF; Fig. 6F) and subordinate thinly bedded deposits (facies SDE; Fig. 6E).

We suggest that the whole of unit I derived from explosions occurring in the weathered granitic basement, which would have contained abundant water (stage I, Fig. 10). This idea is supported by the large proportion of basement derived granite and schist clasts in the beds that form this part of the succession (Fig. 5). Presumably, the rising magma would have occupied existing fractures in the granite and schist that would have probably filled with water. The lack of interaction with the first aquifer could be related to a high and rapid input of magma, as suggested by the presence of large mantle-derived nodules in the deposits, which would not have allowed the required energy transfer efficiency to permit magma-water interaction. Facies SDA, SDB, and SDC suggest fallout and ballistic emplacement (Fig. 8; see Németh et al., 2001). In particular, facies SDC includes some horizons of juvenile scoria lapilli with few prevolcanic lithic fragments (Fig. 5), probably indicating episodes involving less water recharge from the aquifer. Generally, these latter explosions did not have the same energy transfer efficiency during the magma-water interaction as during the first explosion, as shown by the abundance of breccia deposits. The stratified beds (facies SDE and SDF) could be interpreted as deposits originating from a high-concentration suspension with little tractional transport (e.g., Chough and Sohn, 1990).

These deposits, different than facies SDA–SDC, suggest other transport and depositional mechanisms, probably related to changes in the eruption dynamics caused by changes in the efficiency of the hydromagmatic fragmentation. The efficiency of hydromagmatic fragmentation and the corresponding eruption dynamics depend on the pressure differences between magma and water, the water-magma contact mode, and magma temperature and viscosity (Wohletz and Sheridan, 1983), as well as on the exact nature of the coolant (White, 1996). This implies that the eruption responsible for the

construction of La Crosa de San Dalmai maar was continuous but included several pulses in which different types of deposits were formed.

Unit II reflects an important change in the eruption dynamics (stage II, Fig. 10). It is made of well-vesiculated (Fig. 6D) scoria bombs and lapilli (facies SDD) with a few (less than 1%; Fig. 5) accidental lithic clasts in some levels. This facies is the result of fallout deposition from Hawaiian-style fire fountains. The fact that this scoria deposit appears in stratigraphic continuity (as suggested by the absence of erosional surfaces) with phreatomagmatic unit I and immediately precedes a new phreatomagmatic episode (Figs. 4D and 7) indicates that, at this stage, the water supply from the aquifer located between the altered granites and the Quaternary sediments (stage II, Fig. 10) was not sufficient to sustain the phreatomagmatic interaction with the ascending magma.

Due to the effect of hydromagmatic eruptions, a large amount of water is vaporized, causing a large and almost instantaneous withdrawal of groundwater from the aquifer. A lowering of the water table can be expected if hydromagmatic activity lasts over a period of several days (Lorenz, 1986). As suggested by Németh et al. (2001), in a porous media aquifer, with lateral heterogeneities, water might not flow fast enough to the vent area to maintain the phreatomagmatic character of the eruption, despite the abundance of groundwater in the rest of the aquifer. Thus, the conditions for a purely magmatic eruption might be reached, and Strombolian explosions may occur.

Unit III (stage III, Fig. 10) started with a new breccia episode (facies SDA) characterized by abundant large heterolithologic blocks (up to almost 1 m in diameter) originating from the Paleozoic basement, and poorly vesiculated juvenile scoria (Fig. 6) resulted from the intermittent fallout deposition (facies SDB and SBC) and the subordinate pyroclastic surges (facies SDE and SDF). The lithic fragment contents, which mostly correspond to Paleozoic basement clasts with lesser amounts of Pliocene–Quaternary clasts (Fig. 5), indicate that the locus of the explosions migrated downward.

A possible water transmissivity is thought to occur at the contact between the sedimentary infill of the basin and the basement, although it would depend on hydraulic conductivity of the lowest Neogene sediments, the thickness of the weathered granite on the top of the basement, and the fracture networks. As the eruption progressed, the fracture-controlled aquifer could have been disrupted by the initial shock wave, causing an increase of secondary permeability and further excavation of the maar crater. This might have led to a decrease of the lithostatic pressure and a progressive lowering of the position of the fragmentation level in the eruption conduit during the course of the

eruption (see Papale et al., 1998; Macedonio et al., 2005). This would have permitted a new phreatomagmatic episode when the magma interacted with a deeper aquifer located in the fractured Paleozoic basement, as indicated by the nature of the lithic fragments included in unit III.

A second line of evidence of the existence of a deeper aquifer was provided by Menció (2005) and Folch et al. (2011) with field data, where multilayer aquifers were recognized in the La Selva area. Furthermore, investigations carried out by Folch and Mas-Pla (2008) highlighted the relevance of fault geometry upon the flow system and the connection between the upper basin-fill formations and the Paleozoic basement. Moreover, the same authors explained how some deep wells located close to La Crosa de Sant Dalmai area showed a confined type of behavior according to structural characteristics, fault geometry, and scaling. This might suggest a similar behavior for La Crosa de Sant Dalmai, enhancing the hypothesis of multilayer aquifers acting at different depth.

The eruption ended with a Strombolian episode (unit IV) (stage IV, Fig. 10) focused in the interior of the maar crater, which gave rise to the formation of a small scoria cone (stage IVa, Fig. 10) and the emission of a lava flow (stage IVb, Fig. 10) that was subsequently covered by lacustrine deposits. The transition from wet to dry conditions might suggest a significant decrease in the volumetric water content in the deeper levels of the aquifer as well as a changing water supply that thus ensured that the eruption would continue in a pure Strombolian phase. As suggested by Németh et al. (2001), a fracture controlled aquifer might have a very strong seasonality, with an increasing or decreasing groundwater supply. Another hypothesis could suggest a magma conduit able to seal itself off from the surrounding aquifer, leading to a final purely magmatic phase.

The eruption sequence deduced for La Crosa de Sant Dalmai follows the generalized model proposed by Lorenz (1986). The proportion of lithic and juvenile fragments in the phreatomagmatic deposits and the presence of pure Strombolian phases in the middle and at the end of the eruption suggest that water supply was not constant. Even assuming that magma supply was not continuous, the changes observed in the eruption sequence and the resulting deposits are better explained by changes in the water supply. This variation in the amount of water interacting with the erupting magma could be due either to the intermittent recharge of the aquifer during the eruption or to the magma interacting with a heterogeneous aquifer (in which the levels had different

hydraulic characteristics) at different depths in the conduit. The first case would account for a relatively long eruption in which seasonal recharges of the aquifer could have induced this type of pulsating behavior. However, the eruption of La Crosa de Sant Dalmai seems to have occurred in a continuous fashion and over a short period of time, as is suggested by the absence of discontinuities in the stratigraphic sequence (Figs. 3 and 4). The intermittent magma-water interaction would thus seem to result from the interaction of the erupting magma with different aquifer levels located at different depths and with different hydrogeological properties, an explanation that matches the hydrogeological characteristics of the study area. Alluvial and weathering materials with high permeabilities composing the main infilling deposits of La Selva Basin would have allowed the first phreatomagmatic phase, while the crystalline materials characterized by structural heterogeneities, enhanced by the presence of a fault system connected to La Selva Basin, would explain the second phreatomagmatic phase. Similar to La Crosa de Sant Dalmai, the same types of stratigraphic successions can be observed in other edifices of the Catalan Volcanic Zone. Martí et al. (2011) explained the differences in the eruptive behavior of the Catalan Volcanic Zone as related to the occasional interaction of the ascending magma with groundwater rather than to changes in magma composition rheology or magma supply.

The succession of deposits that form La Crosa de Santa Dalmai has uniform stratigraphy all around the vent, albeit with smaller, thicker units and steeper angles in the west, and thinner units, gentler angles, and a broader distribution in the east, thereby suggesting a radial but asymmetrical distribution of the deposits (Fig. 2). This highlights the importance of differences in rock strength in mixed substrates, as already emphasized by Smith and Lorenz (1989), Sohn and Park (2005), and Auer et al. (2007) in other maar examples, which, in the case of La Crosa de Sant Dalmai (Bolós et al., 2012), made it easier for the phreatomagmatic explosions to excavate the eastern side where the soft Pliocene–Quaternary sediments were found. This is also suggested by the strong eastward horizontal component in the fallout deposits, which were probably influenced by this type of rheological contrast with the host rocks.

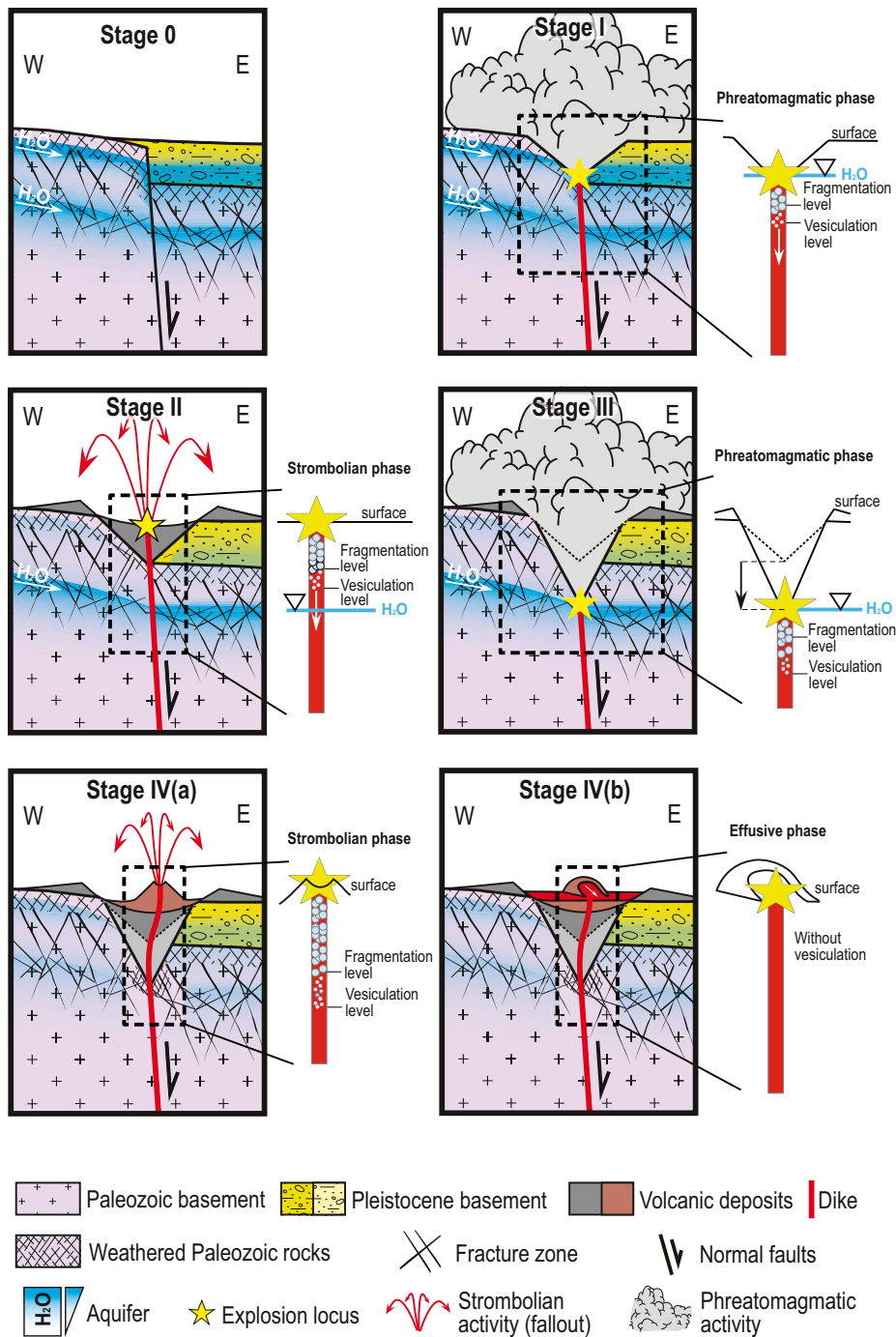


Fig. 10. Four stages of the evolution of La Crosa de Sant Dalmai edifice: Stage 0—formation of La Selva Basin with the associated aquifers; stage I—interaction of the ascending magma with the shallower Quaternary and Paleozoic altered granite aquifers; stage II—first magmatic phase, probably due to a general decreasing of the water content in the shallower aquifer; stage III—decrease in the fragmentation level in the conduit and a new phreatomagmatic episode in a deeper aquifer; stage IVa—pure Strombolian phase, with the rise and eruption of the magma and no interaction with the probably almost exhausted aquifer; stage IVb—emplacement of a lava flow inside the maar crater.

2.8 Conclusion

La Crosa de Sant Dalmai maar formed on the northern border of the Neogene La Selva Basin on a NW-SE-oriented normal fault that was probably used by deep magma to reach the surface. This maar volcano is an example of the way in which a tephra ring develops in a mixed setting characterized by a hard (Paleozoic granites and schists) and soft (Quaternary filling) basement with heterogeneities and differences in the hydrogeological structure of the area, and aquifer levels with different hydraulic properties and fracturing patterns. These differences clearly influenced the way in which the magmawater interaction occurred throughout the eruption and, consequently, the style of the eruption and the resulting deposits. The eruption at La Crosa de Sant Dalmai included four eruptive phases with alternating phreatomagmatic and magmatic fragmentation. As occurs in many other volcanoes in the same monogenetic field, the eruptive sequence and resulting deposits that formed La Crosa de Sant Dalmai contrast with the compositional monotony of the magma, thereby emphasizing the role played by the geological characteristics of the substrate in determining the eruptive style and associated hazards in this type of volcanism.

Acknowledgments

This study was partially funded by the grant CROSAND and the European Commission (FT7 Theme: ENV.2011.1.3.3-1; grant 282759: “VUELCO”). We would like to thank Lluís Motjé (Consortium of La Crosa de Sant Dalmai: management of field geology in La Crosa volcanic area) for his logistical support during the field work. We are also grateful to Llorenç Planagumà and Leandro d’Elia for their help with the field work and Guillem Serra for his contribution to the discussion of this paper. We are also grateful to Editor Tim Wawrzyniec, Associate Editor Dave Hirsch, and Pete Stelling and an anonymous reviewer for their constructive reviews of this manuscript. English text was corrected by Michael Lockwood.

References

Auer, A., Martin, U. and Németh, K., 2007. The Fekete-hegy (Balaton Highland Hungary) “soft-substrate” and “hard-substrate” maar volcanoes in an aligned volcanic complex – Implications for vent geometry, subsurface stratigraphy and the

palaeoenvironmental setting. *Journal of Volcanology and Geothermal Research*, 159(1–3): 225-245.

Bolós, X., Barde-Cabusson, S., Pedrazzi, D., Martí, J., Casas, A., Himi, M. and Lovera, R., 2012. Investigation of the inner structure of La Crosa de Sant Dalmai maar (Catalan Volcanic Zone, Spain). *Journal of Volcanology and Geothermal Research*, 247–248(0): 37-48.

Carrasco-Núñez, G., Ort, M.H. and Romero, C., 2007. Evolution and hydrological conditions of a maar volcano (Atexcac crater, Eastern Mexico). *Journal of Volcanology and Geothermal Research*, 159(1–3): 179-197.

Chough, S.K. and Sohn, Y.K., 1990. Depositional mechanics and sequences of base surges, Songaksan tuff ring, Cheju Island, Korea. *Sedimentology* 37(6): 1115–1135.

Crowe, B.M. and Fisher, R.V., 1973. Sedimentary Structures in Base-Surge Deposits with Special Reference to Cross-Bedding, Ubehebe Craters, Death Valley, California. *Geological Society of America Bulletin*, 84(2): 663-682.

Druitt, T.H., 1998. Pyroclastic density currents. In: Gilbert, J.S., Sparks, R.S.J. (Eds.), *The Physics of Explosive Volcanic Eruptions*. Geological Society, Spec. Publ. , 145: 145-182.

Fisher, R. and Waters, A., 1970. Base surge bed forms in maar volcanoes. *American Journal of Science*, 268 (2): 157-180.

Fisher, R.V. and Schmincke, H.U., 1984. *Pyroclastic Rocks*. Springer-Verlag Inc, Berlin. 474 pp.

Folch, A. and Mas-Pla, J., 2008. Hydrogeological interactions between fault zones and alluvial aquifers in regional flow systems. *Hydrological Processes*, 22(17): 3476-3487.

Folch, A., Menció, A., Puig, R., Soler, A. and Mas-Pla, J., 2011. Groundwater development effects on different scale hydrogeological systems using head, hydrochemical and isotopic data and implications for water resources management: The Selva basin (NE Spain). *Journal of Hydrology*, 403(1–2): 83-102.

Guérin, G., Benhamou, G. and Mallarach, J.M., 1986. Un exemple de fusió parcial en medi continental. *El vulcanisme quaternari de Catalunya*. *Vitrina*, 1: 20–26.

- Houghton, B.F. and Hackett, W.R., 1984. Strombolian and phreatomagmatic deposits of Ohakune craters, Ruapehu, New Zealand: A complex interaction between external water and rising basaltic magma. *Journal of Volcanology and Geothermal Research*, 21(3–4): 207-231.
- Houghton, B.F., Wilson, C.J.N., Rosenberg, M.D., Smith, I.E.M. and Parker, R.J., 1996. Mixed deposits of complex magmatic and phreatomagmatic volcanism: an example from Crater Hill, Auckland, New Zealand. *Bulletin of Volcanology*, 58(1): 59-66.
- Inman, D., 1952. Measures for describing the size distribution of sediments. *Journal of Sedimentary Petrology*, 22(125–145).
- Kokelaar, P., 1986. Magma-water interactions in subaqueous and emergent basaltic volcanism. *Bulletin of Volcanology*, 48: 275-289.
- Lorenz, V., 1973. On the formation of maars. *Bulletin Volcanologique*, 37(2): 183-204.
- Lorenz, V., 1974a. Studies of the Surtsey tephra deposits. *Surtsey Res. Prog. Rep.* , 7: 72–79.
- Lorenz, V., 1986. On the growth of maars and diatremes and its relevance to the formation of tuff rings. *Bulletin of Volcanology*, 48(5): 265-274.
- Lorenz, V., 1987. Phreatomagmatism and its relevance. *Chemical Geology*, 62(1–2): 149-156.
- Lorenz, V., 2003. Maar-diatreme volcanoes, their formation, and their setting in hard-rock or soft-rock environments. *GeoLines (Prague)*, 15: 72–83.
- Lorenz, V. and Zimanowski, B., 2008. Volcanology of the West Eifel Maars and Its Relevance to the Understanding of Kimberlite Pipes: Field Trip for 9th IKC Held in Frankfurt Am Main, Germany. University of Würzburg, Physical Volcanological Laboratory.
- Macedonio, G., Neri, A., Martí, J. and Folch, A., 2005. Temporal evolution of flow conditions in sustained magmatic explosive eruptions. *Journal of Volcanology and Geothermal Research*, 143(1–3): 153-172.

Martí, J. and Mallarach, J.M., 1987. Erupciones hidromagmáticas en el volcanismo cuaternario de Olot. *Estudios Geológicos*, 43: 31–40.

Martí, J., Mitjavila, J., Roca, E. and Aparicio, A., 1992. Cenozoic magmatism of the Valencia trough (western Mediterranean): relationship between structural evolution and volcanism. *Tectonophysics*, 203: 145-165.

Martí, J., Ortiz, R., Claudin, F. and Mallarach, J.M., 1986. Mecanismos eruptivos del volcán de la Closa de Sant Dalmai (Prov. Gerona). *Anales de Física*, Vol. 82, special series B: 143–153.

Martí, J., Planagumà, L., Geyer, A., Canal, E. and Pedrazzi, D., 2011. Complex interaction between Strombolian and phreatomagmatic eruptions in the Quaternary monogenetic volcanism of the Catalan Volcanic Zone (NE of Spain). *Journal of Volcanology and Geothermal Research*, 201(1–4): 178-193.

Martín-Serrano, A., Vegas, J., García-Cortés, A., Galán, L., Gallardo-Millán, J.L., Martín-Alfageme, S., Rubio, F.M., Ibarra, P.I., Granda, A., Pérez-González, A. and García-Lobón, J.L., 2009. Morphotectonic setting of maar lakes in the Campo de Calatrava Volcanic Field (Central Spain, SW Europe). *Sedimentary Geology*, 222(1–2): 52-63.

Mastin, L.G., Christiansen, R.L., Thornber, C., Lowenstern, J. and Beeson, M., 2004. What makes hydromagmatic eruptions violent? Some insights from the Keanakāko'i Ash, Kīlauea Volcano, Hawai'i. *Journal of Volcanology and Geothermal Research*, 137(1–3): 15-31.

Menció, A., 2005. Anàlisi multidisciplinària de l'estat de l'aigua a la depressió de la Selva. Phd Thesis Universitat Autònoma De Barcelona.

Menció, A., Folch, A. and Mas-Pla, J., 2010. Analyzing Hydrological Sustainability Through Water Balance. *Environmental Management*, 45(5): 1175-1190.

Németh, K., Martin, U. and Harangi, S., 2001. Miocene phreatomagmatic volcanism at Tihany (Pannonian Basin, Hungary). *Journal of Volcanology and Geothermal Research*, 111(1–4): 111-135.

Papale, P., Neri, A. and Macedonio, G., 1998. The role of magma composition and water content in explosive eruptions: 1. Conduit ascent dynamics. *Journal of Volcanology and Geothermal Research*, 87(1–4): 75-93.

Pous i Fàbregas, J., Solé Sugrañes, L. and Badiella, P., 1990. Estudio geoelectrico de la depresión de la Selva (Girona). *Acta Geologica Hispanica*, 25(4): 261-269.

Ross, P.-S., Delpit, S., Haller, M.J., Németh, K. and Corbella, H., 2011. Influence of the substrate on maar–diatreme volcanoes — An example of a mixed setting from the Pali Aike volcanic field, Argentina. *Journal of Volcanology and Geothermal Research*, 201(1–4): 253-271.

Sigmarrsson, O., Carn, S. and Carracedo, J.C., 1998. Systematics of U-series nuclides in primitive lavas from the 1730–36 eruption on Lanzarote, Canary Islands, and implications for the role of garnet pyroxenites during oceanic basalt formations. *Earth and Planetary Science Letters*, 162(1–4): 137-151.

Smith, C.B. and Lorenz, V., 1989. Volcanology of the Ellendale lamproite pipes, Western Australia. In: Ross, J. (Ed.), *Kimberlites and Related Rocks*: Geological Society of Australia, Special publication, 14: pp. 505–519.

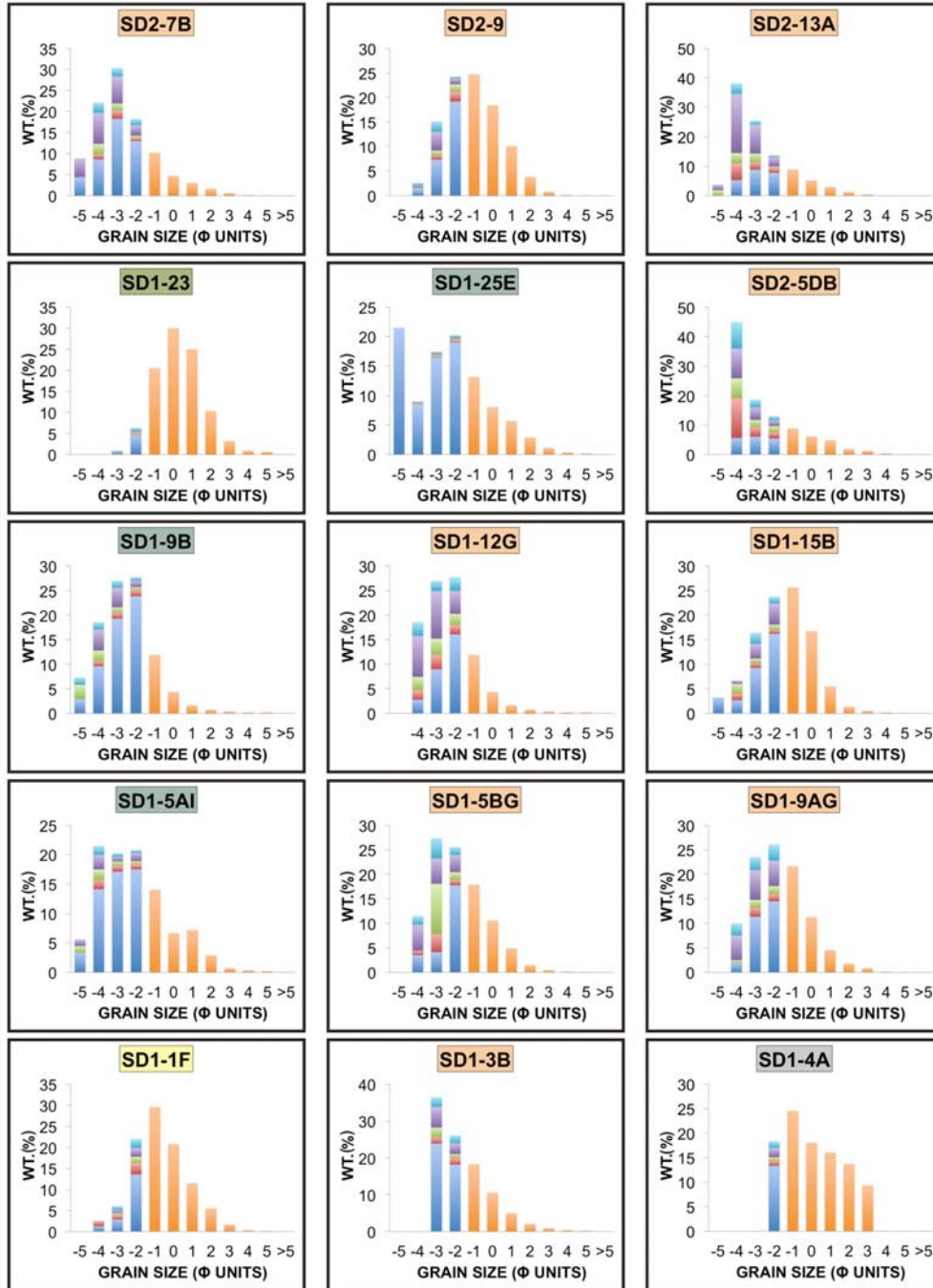
Sohn, Y.K., 1996. Hydrovolcanic processes forming basaltic tuff rings and cones on Jeju Island, Korea. *Geological Society of America Bulletin*, 108: 1199-1211.

Sohn, Y.K. and Park, K.H., 2005. Composite tuff ring/cone complexes in Jeju Island, Korea: possible consequences of substrate collapse and vent migration. *Journal of Volcanology and Geothermal Research*, 141(1–2): 157-175.

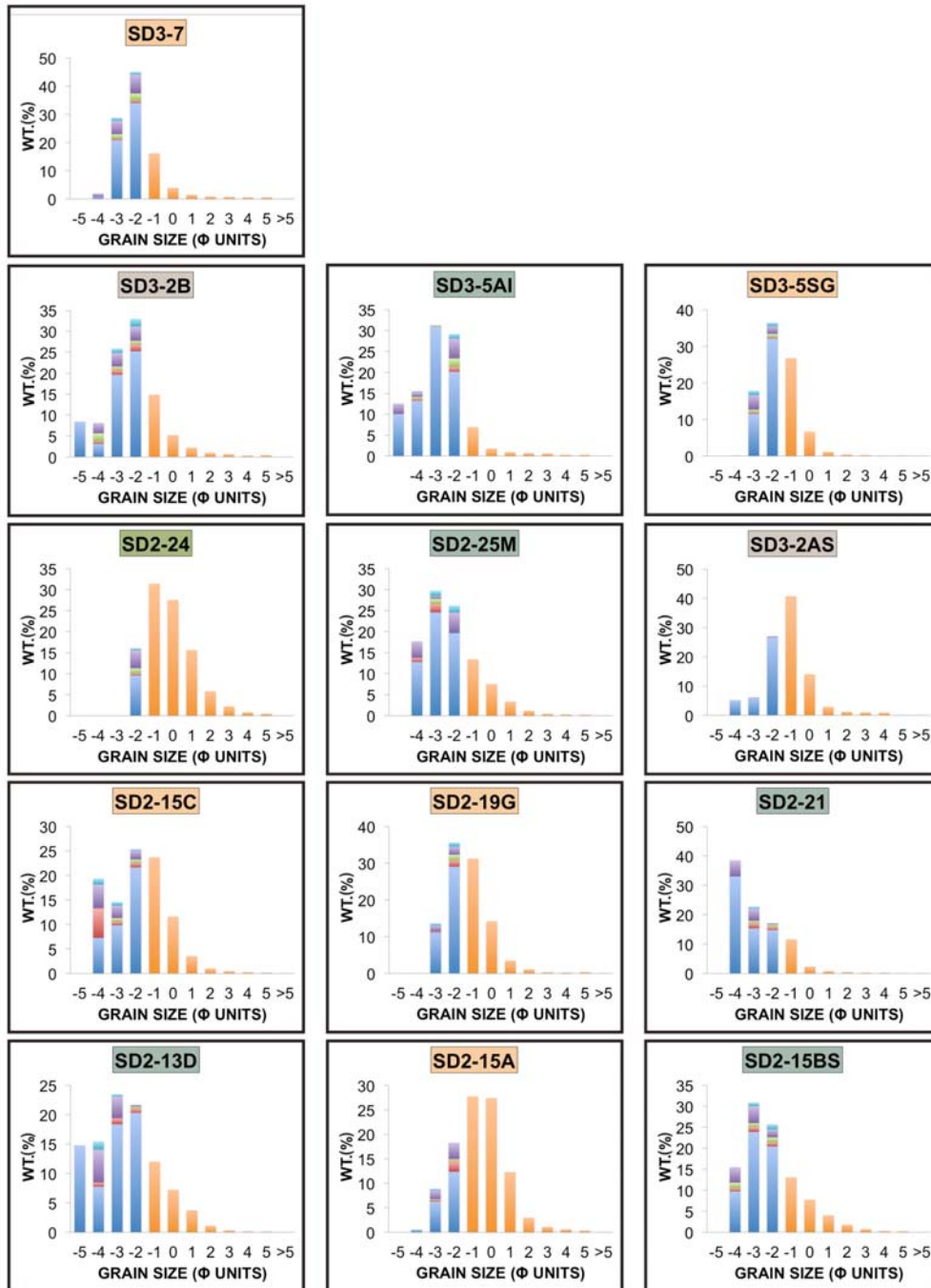
White, J.D.L., 1991. Maar-diatreme phreatomagmatism at Hopi Buttes, Navajo Nation (Arizona), USA. *Bulletin of Volcanology*, 53(4): 239-258.

White, J.D.L. and Houghton, B., 2000. Surtseyan and related phreatomagmatic eruptions. In: Sigurdsson, H., Houghton, B.F., McNutt, S.R., Rymer H., Stix J. (Editors), *Encyclopedia of Volcanoes*. Academic Press, San Diego: 495-511.

Wohletz, K.H. and Sheridan, M.F., 1983. Hydrovolcanic explosions; II, Evolution of basaltic tuff rings and tuff cones. *American Journal of Science*, 283(5): 385-413.



Supplemental Figure. Lithics content of additional samples from the composite stratigraphic columns shown in Figure 5.



Supplemental Figure (continued)

3. STRATIGRAPHY, SEDIMENTOLOGY AND ERUPTIVE MECHANISMS IN THE TUFF CONE OF EL GOLFO (LANZAROTE, CANARY ISLANDS)

Published in:

Bulletin of Volcanology

Authors of the paper:

Dario Pedrazzi, Institute of Earth Sciences Jaume Almera, ICTJA-CSIC, Group of Volcanology. SIMGEO (UB-CSIC) Lluís Solé i Sabarís s/n, 08028 Barcelona, Spain

Joan Martí, Institute of Earth Sciences Jaume Almera, ICTJA-CSIC, Group of Volcanology. SIMGEO (UB-CSIC) Lluís Solé i Sabarís s/n, 08028 Barcelona, Spain

Adelina Geyer, Institute of Earth Sciences Jaume Almera, ICTJA-CSIC, Group of Volcanology. SIMGEO (UB-CSIC) Lluís Solé i Sabarís s/n, 08028 Barcelona, Spain

The reference of this paper is:

Pedrazzi, D., Martí, J. and Geyer, A., 2013. Stratigraphy, sedimentology and eruptive mechanisms in the tuff cone of El Golfo (Lanzarote, Canary Islands). *Bulletin of Volcanology*, 75(7): 1-17.

Abstract

The tuff cone of El Golfo on the western coast of Lanzarote (Canary Islands) is a typical hydrovolcanic edifice. Along with other edifices of the same age, it was constructed along a fracture oriented NEE–SWW that coincides with the main structural trend of recent volcanism in this part of the island. We conducted a detailed stratigraphic study of the succession of deposits present in this tuff cone and here interpret them in light of the depositional processes and eruptive dynamics that we were able to infer. The eruptive sequence is represented by a succession of pyroclastic deposits, most of which were emplaced by flow, plus a number of air-fall deposits and ballistic blocks and bombs. We distinguished five different eruptive/depositional stages on the basis of differences in inferred current flow regimes and fragmentation efficiencies represented by the resulting deposits; the different stages may be related to variations in the explosive energy. Eight lithofacies were identified based on sedimentary discontinuities, grain size, components, variations in primary laminations and bedforms. The volcanic edifice was constructed very rapidly around the vent, and this is inferred to have controlled the amount of water that was able to enter the eruption conduit. The sedimentological characteristics of the deposits and the nature and distribution of palagonitic alteration suggest that most of the pyroclastic succession in El Golfo was deposited in a subaerial environment. This type of hydrovolcanic explosive activity is common in the coastal zones of Lanzarote and the other Canary Islands and is one of the main potential hazards that could threaten the human population of this archipelago. Detailed studies of these hydrovolcanic eruptions such as the one we present here can help volcanologists understand the hazards that this type of eruption can generate and provide essential information for undertaking risk assessment in similar volcanic environments.

Keywords: El Golfo, Lanzarote, Canary Islands, Tuff cone, Hydrovolcanism, Facies analysis

3.1 Introduction

Hydrovolcanism is a volcanic phenomenon in which magma or magmatic heat interacts with an external source of water (Macdonald, 1972; Sheridan and Wohletz, 1981). Typically, it takes place in deep or shallow submarine, littoral, lacustrine, phreatic or subglacial environments. Common volcanic landforms produced by

hydrovolcanic eruptions include tuff cones, tuff rings and maar-diatreme volcanoes. Varieties of landforms are attributable to differences in eruption intensities, in styles of explosions and in depositional processes (Sheridan and Wohletz, 1983). These differences are determined by variables such as the exact nature of the magma and water involved, the proportions and properties of the interacting fluids, the lithology and mechanical properties of the rocks of the conduit wall, and vent geometry (Kokelaar, 1986; Sohn and Chough, 1989; Sohn, 1996; White, 1996; White and Houghton, 2000; White and Ross, 2011). Also of importance is the geometry of the water-to-magma interface. Due in some cases to their short duration and often remote location, these hydrovolcanic eruptions have only ever been observed or documented on a few occasions in places such as Myojin, Japan (Morimoto, 1960), Surtsey, Iceland (Thorarinsson, 1965), Taal, Philippines (Moore et al., 1966), Capelinhos, Faial Island, Azores (Machado et al., 1962; Cole et al., 2001), Ukinrek, Alaska (Kienle et al., 1980; Self et al., 1980), Karymskoye Lake, Kamchatka (Belousov and Belousova, 2001), Kavachi, Solomon Islands (Baker et al., 2002), Katla eruptions (Larsen et al., 2009; Larsen, 2010), Grimsvotn, Iceland (Jude-Eton et al., 2012; IMO/IES websites, Iceland) and Eyjafjallajokull, Iceland (Gudmundsson et al., 2012).

Hydrovolcanic eruptions are common in coastal environments where erupting magma is prone to interact with seawater in either subaquatic or subaerial settings depending on the location of the eruption conduit and vent (Sheridan and Wohletz, 1983). Water may gain access to magma either in the subsurface as groundwater or at the surface, and water entry is controlled largely by the exact nature of the rocks enveloping the vent site and eruption-related. Near-shore and shallow subaqueous activity may generate high-intensity explosions characterised by ballistic blocks, ash fall and pyroclastic density currents that can represent a hazard for nearby population centres. This is a threat above all on volcanic islands where basaltic magmas, which can erupt relatively passively under magmatic conditions, may become highly explosive when interacting with seawater in coastal environments (Moore et al., 1966; Waters and Fisher, 1971; Sumner, 1998; Cole et al., 2001; Baker et al., 2002; Sohn et al., 2003; Cronin et al., 2006; Clark et al., 2009; Németh and Cronin, 2009, 2011).

Although examples of basaltic hydrovolcanic eruptions can be found on all the Canary Islands in the form of maars and tuff cones and rings, very few have ever been studied in detail. Published studies include those of include Montaña Amarilla, Montaña Escachada and Caldera del Rei on Tenerife (De La Nuez et al., 1993), Bandama on

Gran Canaria (Araña et al., 1988), La Palma's 1949 eruption (White and Schmincke, 1999) and Montaña Los Erales on Tenerife (Clark et al., 2009). Canarian hydrovolcanic events include both inland phreatomagmatic eruptions generated by erupting magmas interacting with groundwater and surtseyan eruptions caused by the interaction of magma with water in coastal or shallow offshore settings.

In the present paper, we study the tuff cone of El Golfo, located on the west coast of Lanzarote and a very typical of Canarian hydrovolcanic coastal edifice (Fig. 1). Our main objective was to describe in detail the structure and association of the facies in an archetypal tuff cone and use this information to infer changes in eruption style and depositional processes applicable to tuff cones worldwide. In the case of El Golfo, eruption of the basaltic magma was modified by interaction with seawater, and the eruptive sequence is characterised by a simple pyroclastic succession. In order to identify and characterise the different eruptive phases and pulses that constructed El Golfo, we here (1) describe the stratigraphy of the succession of deposits, (2) analyse their lithological and sedimentological characteristics, and (3) interpret these deposits in terms of the depositional regime and the efficiency of the magma fragmentation, which in turn are used to infer changes in the eruption dynamics and the degree of the magma-to-water interaction (Wohletz and Sheridan, 1983). Finally, we discuss the implications for human settlements on Lanzarote of the hazards that are inherent in this type of eruption.

3.2 Geological setting and general description of the tuff cone of El Golfo

The Canary Islands are a group of seven large islands and several islets that form a 450-km-long archipelago located 100 km off the northwest coast of Africa (Fig. 1). They were constructed by volcanic and tectonic activities that started at around 60 Ma ago and continue to the present day (Robertson and Stillman, 1979; Le Bas et al., 1986; Marinoni and Pasquarè, 1994; Marinoni and Gudmundsson, 2000).

Lanzarote is the north easternmost of the Canary Islands (Fig. 1). It represents the emergent part of the East Canary Ridge, a NNE–SSW linear volcanic structure located on typical oceanic crust that is at least 11 km thick (Banda et al., 1981). The shallow basement of the island is probably about 4–5 km thick (Banda et al., 1981) and is composed of sedimentary (quartzite and shales), plutonic (basic and ultrabasic) and subvolcanic rocks (basaltic and trachytic dikes). The erupted magma contains an abundance of quartzite and sandstone xenoliths (Araña and Carracedo, 1978). Although

the island's lavas are almost all basaltic, there are small outcrops of massive trachytes in the oldest parts of the island (NW and SE).

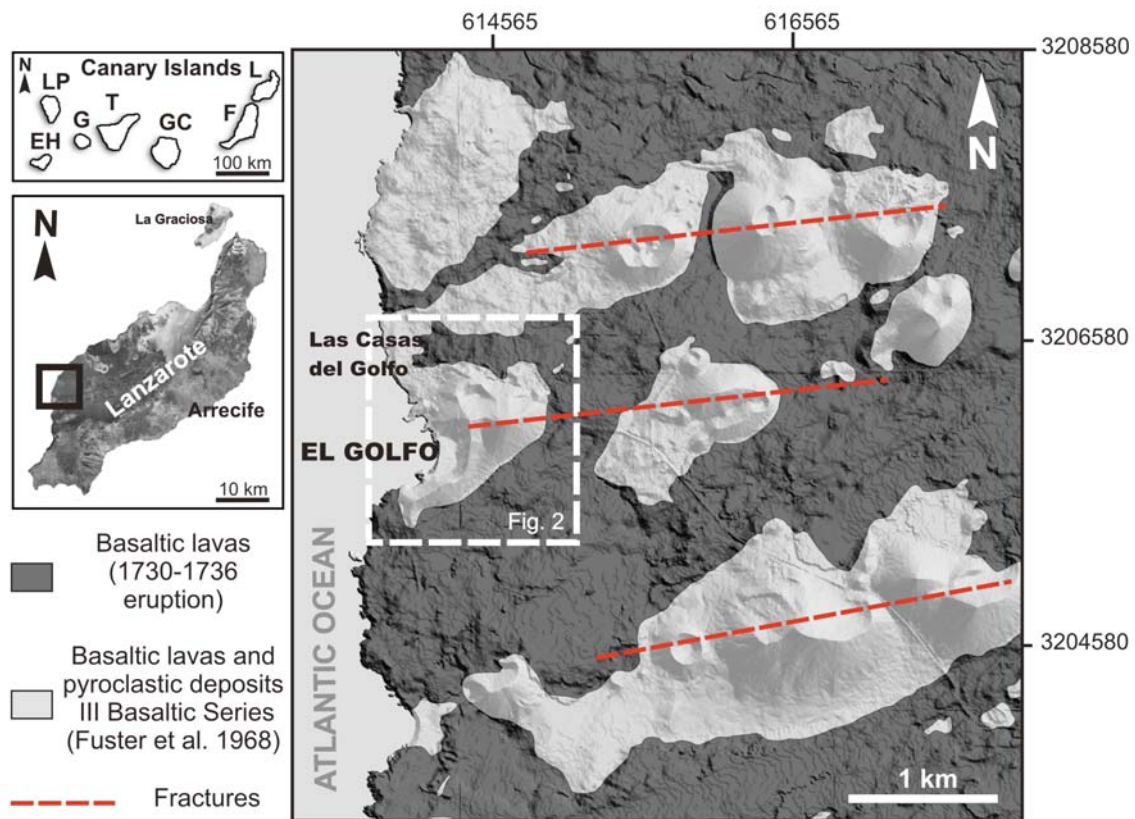


Fig. 1 Location and simplified geological map of the study area: EH El Hierro, F Fuerteventura, G Gomera, GC Gran Canaria, L Lanzarote, LP La Palma, T Tenerife.

The volcanic stratigraphy of Lanzarote was first classified by Fuster et al. (1968) as having four eruptive series: (I) a tableland with basalts dated at 6–12 Ma (Miocene–Pliocene); (II–III) Quaternary volcanism dated at 1 Ma and separated from stage I by an erosional unconformity; and (IV) recent volcanism including the 1730–1736 eruption, the largest eruption in modern times on the Canary Islands.

Marinoni and Pasquarè (1994) divided the geological evolution of the emergent part of Lanzarote into two principal construction stages named the ‘Pre-erosional or Shield stage’ and the ‘Post-erosional or Differentiated stage’. The main volcanostratigraphic units of the former stage are exposed locally on the west coast of the island and correspond to scoriaceous lavas of basaltic composition and subordinate trachytic intrusions, scoria and tuff cones, as well as lavas of basaltic composition. The post-erosional Quaternary stage is characterised mainly by aligned scoria cones and associated lava flows.

The volcanic edifice of El Golfo, located on the western coast of Lanzarote (Fig. 1), reaches 60 m a.s.l. and has a basal diameter of approximately 1 km, which gives it an aspect ratio of about 0.05. The volcanic edifice has been partially destroyed by marine erosion, and only its eastern part remains intact. The age of this volcano is not well known, but it is assumed to be a product of recent volcanism on the island (since 2 Ma) (Abdel-Monem et al., 1972).

A simplified geological map of El Golfo is given in Fig. 2. Its deposits are covered by the lavas that were generated by the 1730–1736 event. El Golfo, together with other edifices of the same age, forms a linear vent system running NEE–SWW that coincides with the main orientation of recent volcanism in this part of the island (Marinoni and Pasquarè, 1994), whose products, today eroded by wave action, partially cover the area of El Golfo.

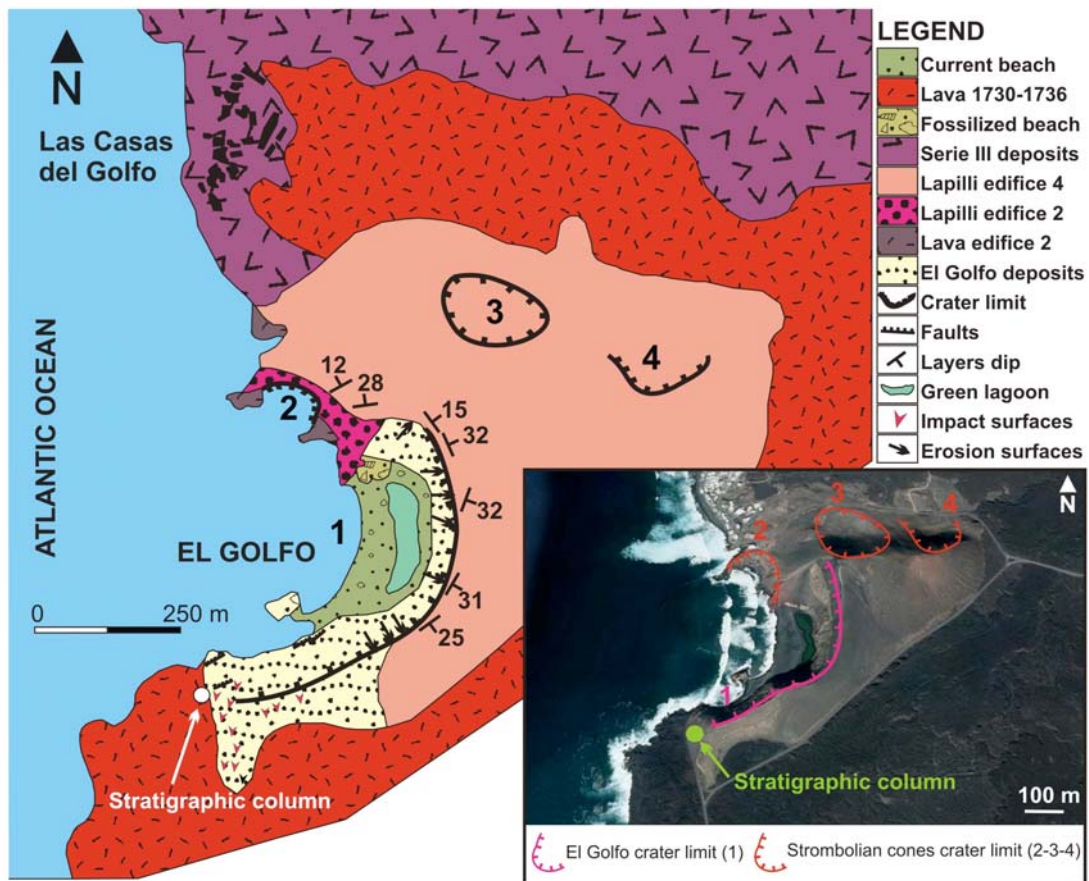


Fig. 2 Geological map of the tuff cone of El Golfo (modified from Martí and Colombo, 1990) from a Google Earth image of the volcanic edifice showing the main crater (1), the three subsequent craters (2–3–4) located to the north of the volcanic edifice, and the location of the studied stratigraphic sequence.

The tuff cone consists entirely of a succession of pyroclastic deposits with different lithological and sedimentological characteristics. The composition of its

juvenile fragments is homogeneous which are of poorly evolved intraplate alkali basalt that does not vary through the whole eruptive sequence (Martí and Colombo, 1990). The pyroclasts are rich in olivine and pyroxene phenocrysts, which are enclosed within the glassy groundmasses of the pyroclasts. A number of lapilli are highly vesicular (>70 % vesicles) and have a very low density (<1 g/cm³); nevertheless, their mineralogical and chemical compositions do not differ from those of the other, denser, juvenile pyroclasts. Dunite and gabbro xenoliths ranging in size from 5–30 cm are common (Fig. 3).

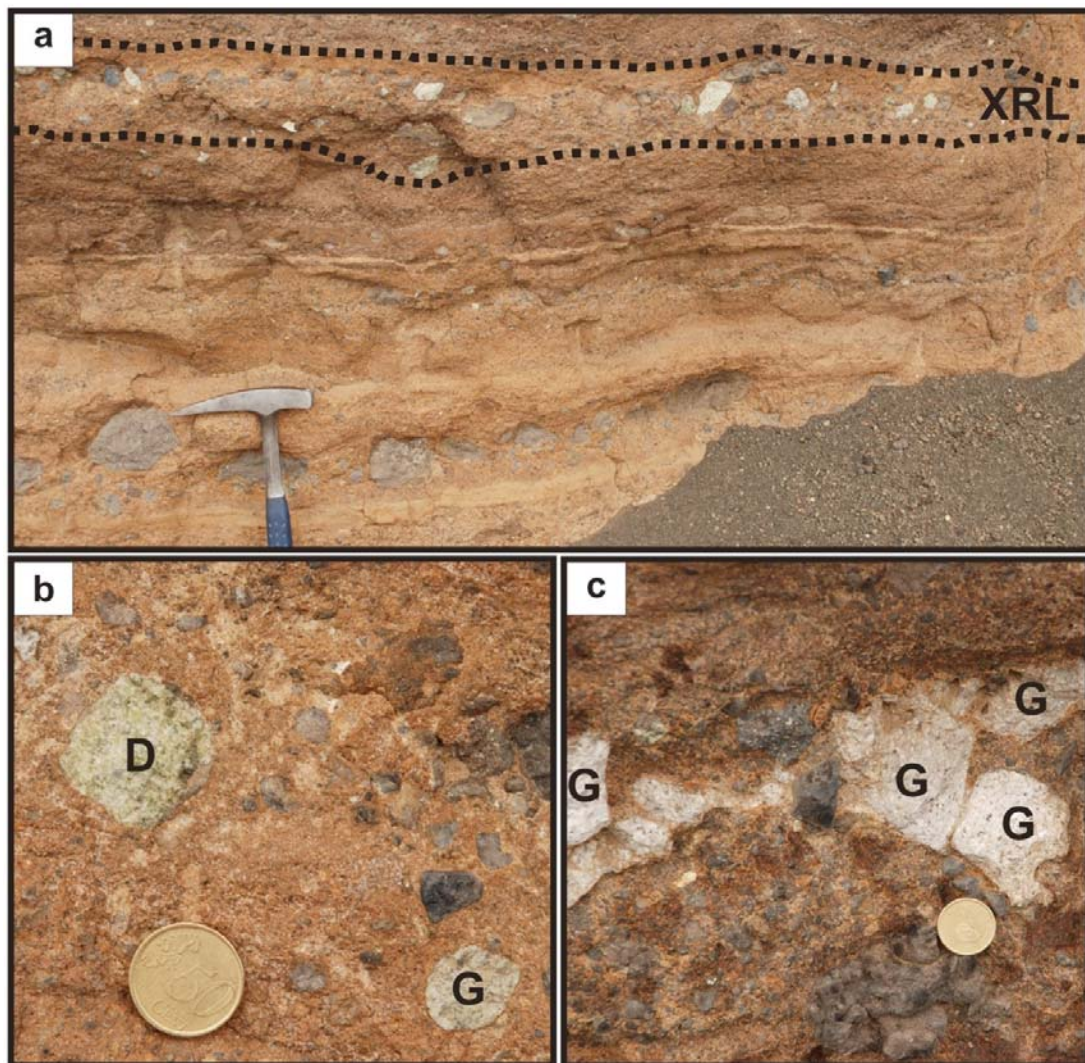


Fig. 3 Field photographs of: a detail of the deposits in which the levels with gabbro and dunite xenoliths are visible (XRL); b detail of dunite (D) and gabbro (G) xenoliths; c detail of gabbro (G) xenoliths.

An irregularly distributed palagonitic alteration of the juvenile vitric fragments, which were devitrified and transformed into smectites, zeolites (mainly phillipsite) and Fe

oxides, is another distinctive feature of the deposits on El Golfo (Martí and Colombo, 1990) (Fig. 4).

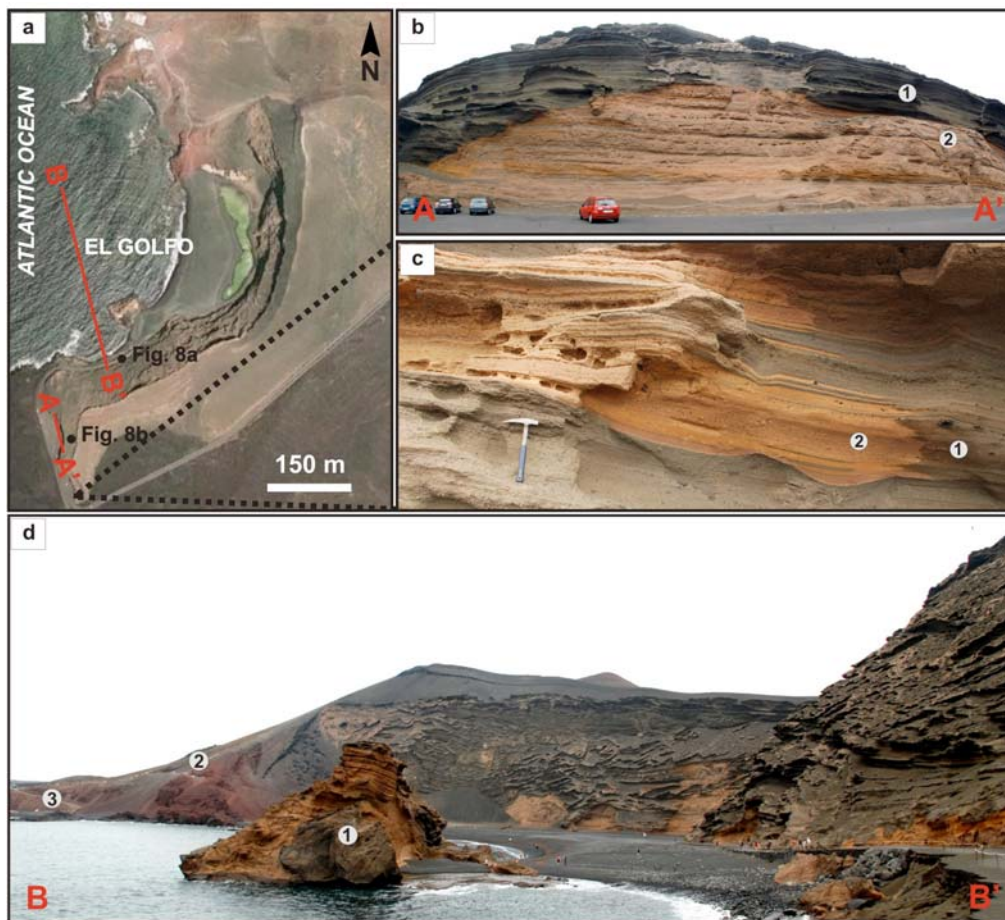


Fig. 4 a Google Earth image of the volcanic edifice of El Golfo; b field photographs of a NNW–SSE cross-section of the deposit sequence at El Golfo (A–A’); c detail of the deposits, where both the non-altered deposits (1) and the palagonitised deposits (2) are visible. Note the irregularity of the limit between the altered and non-altered zones that is independent of the current topographical surface; d field photograph of El Golfo showing (1) the fallen block of the tuff cone in the presentday beach and (2 and 3) the Strombolian deposits (posterior to the emplacement of the tuff cone) located to the northeast (B–B’).

3.3 Methods

The research we present here is above all the result of new fieldwork. An investigation was carried out in order to establish the relationships between the different volcanic edifices present in an area 2 km² around El Golfo. Relative ages were determined on the basis of stratigraphic correlations. Detailed field measurements of the succession were then conducted on the main outcrop located in the southern part of the edifice (Fig. 2). Unfortunately, access to the other parts of the cone for close observation is impossible. Our studies included bed-by-bed thickness measurements of the deposits and facies analysis. Deposits were divided into lithofacies (Table 1) based

on different criteria (see below) and following the facies model and nomenclature proposed by Chough and Sohn (1990) and Solgevik et al. (2007).

Table 1 Lithofacies and lithofacies association			
Units	Lithofacies associations	Lithofacies	Interpretation
I	G1	B E	High rate of direct suspension sedimentation that alternate with tractional deposition (depending on the deposition rate)
II	G2	D E	Upper flow-regime bedforms
III	G3	A C E	A Erosive initial phase with a following depositional stage C-E Deposition of turbulent pyroclastic surges fluctuating in velocity and particle concentration with episodes of high shear stress
IV	G4	A D G H	A Eroding current with erosive surfaces with larger size than G3 D-G-H Multiple pyroclastic surges with "wet" hydromagmatic explosion
V	G5	D E F G H	Continuous changing conditions of the surge with possible moderate amount of liquid water

Tab. 1 Letters indicate the different lithofacies: A channel-fill facies, B massive crudely stratified facies, C diffusely stratified facies, D stratified facies, E undulate ash-bed facies, F dune facies, G antidune facies and H accretionary lapilli facies.

Due to the postdepositional palagonitisation that affects an important part of the sequence, it was not possible to obtain samples for mechanical sieving in the laboratory. Therefore, grain size determinations for the >64 mm fraction were performed partially in the field using grain size comparators. The grain size of clasts smaller than 64 mm was determined from thin sections using image analysis techniques (e.g., ImageJ software). The grain size classification is modified after Chough and Sohn (1990) due to field conditions and comprises ash <2 mm, fine lapilli = 2–8 mm; medium lapilli = 8–32 mm and coarse lapilli = 32–64 mm. Bed thickness is based on Ingram(1954): lamina (<1 cm); very thin bed (1–3 cm), thin bed (3–10 cm), medium bed (10–30 cm), thick bed (30–100 cm) or very thick bed (>100 cm). Scanning electron microscopy data for juvenile particles were taken from Martí and Colombo (1990).

3.4 Facies description

The tuff cone of El Golfo stands at sea level and has a well-exposed 45-m-thick stratigraphic section that exhibits differences in the size and shape of the clasts, in the levels of alteration and in the depositional features. We grouped the cone's deposits into eight facies and facies associations based on the following criteria: (1) sedimentary discontinuities such as erosion surfaces, (2) variations in grain size and percentage of volcanic bombs and (3) variations in primary bedforms. Erosion surfaces constitute the main discontinuity between deposits but only affect specific levels, the rest of the stratigraphic column being depositionally continuous (Fig. 5).

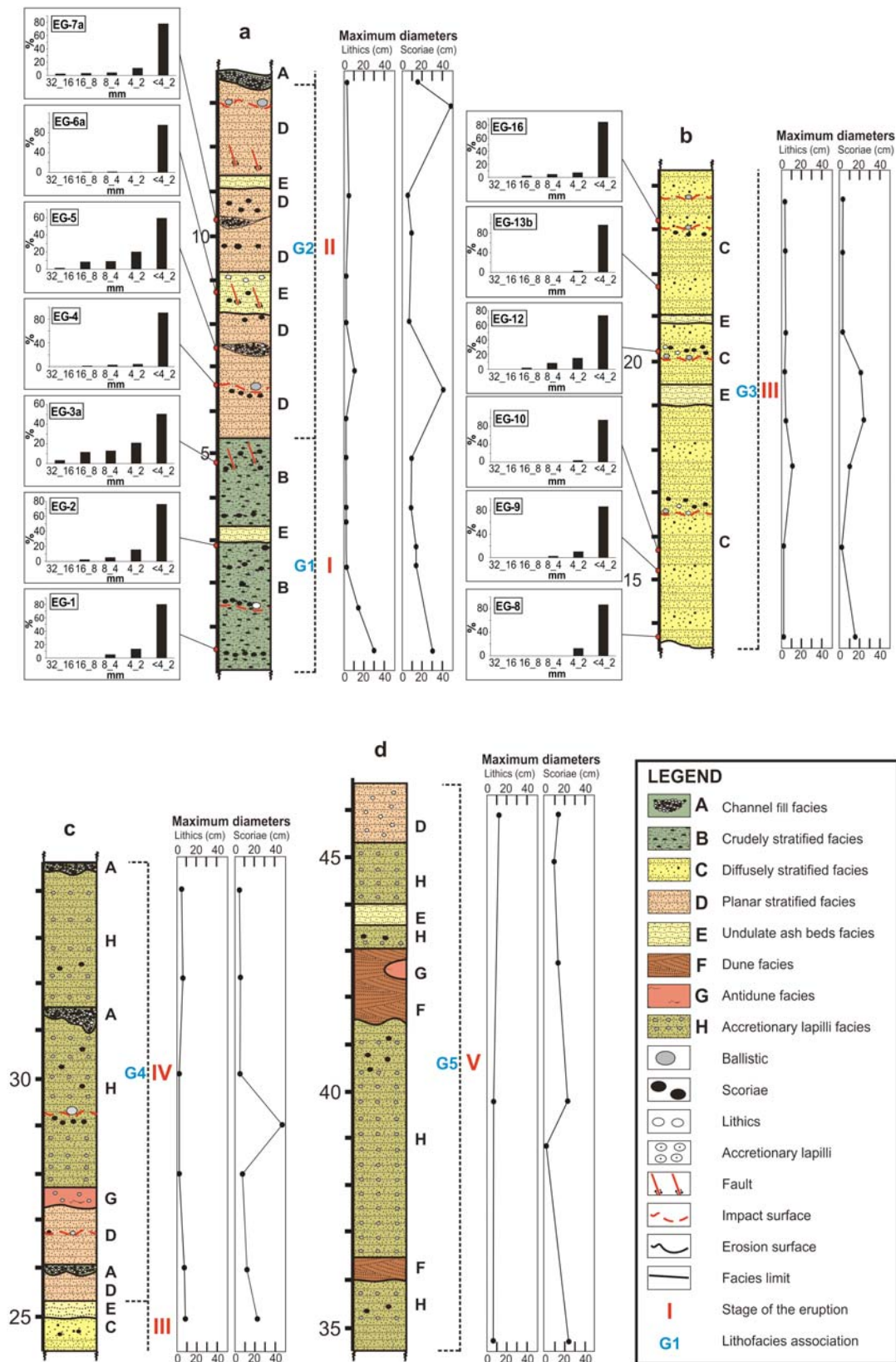


Fig. 5 Composite stratigraphic column of the deposits at El Golfo showing the main facies: a channel fill facies, b crudely stratified facies, c diffusely stratified facies, d planar stratified facies, e undulate ash-bed facies, f dune facies, g antidune facies and h accretionary lapilli facies. Five stages (I–V) are identified based on the depositional processes and resulting deposits. Vertical variations in grain size and the maximum diameter of lithics and scoriae clasts are also indicated.

3.4.1 Channel fill facies (A)

This facies consists predominantly of thin structureless beds of juvenile and lithic clasts (Fig. 6a). Juvenile ash and medium lapilli fragments are rounded, dense and non-vesicular. Juvenile vesicular ballistic fragments (up to 3 cm) occur on specific levels. Angular lithic fragments of lavas and xenoliths (up to 3 cm) can be found alongside accretionary lapilli of 1 cm. The average size of matrix grains is about 2 mm. The coarsest lithic fragments tend to be concentrated in the lowest part of the deposits. This facies is present mainly as fillings of depressions and occurs as lenses (maximum depth of 0.5 m and width of 0.4 m) (Fig. 7a–c) or in V- or U-shaped channels (depth of 1.5 m with a maximum width of 2 m) (Fig. 7d). The bedding planes are marked by sharp variation in grain size. Individual beds are generally ungraded and have irregular and erosive boundaries.

3.4.2 Crudely stratified facies (B)

This facies has a maximum thickness of 3 m (Fig. 5) with crude thin to medium beds (Fig. 6b). It consists of clast supported layers, with subrounded, poorly vesicular juvenile coarse-to-medium lapilli with ballistic ejecta (up to 30 cm) in a matrix of fine lapilli and coarse ash (EG1; EG2; EG3A; Fig. 5). The fragment population in this facies is dominantly juvenile. However, many of the ballistic blocks are accidental basaltic fragments. The crude layering in this facies is defined by the presence of thick-bedded packets containing several indistinct and discontinuous boundaries with about 10–30 cm vertical spacing. Overall, the sequences are laterally continuous with single beds pinching and swelling laterally, and grading that varies vertically from normal to reverse.

3.4.3 Diffusely stratified facies (C)

This facies has a maximum thickness of 5 m (range, 1–5 m) (Fig. 5) and consists of alternating ash and lapilli beds (Fig. 6c). The juvenile fine lapilli are rounded and non-vesicular. The matrix is palagonitised basaltic ash with crystal fragments of olivine and clinopyroxene. In a few levels (often in the middle of the deposits), there is a significant increase in the number of bombs and blocks (plutonic xenoliths). Bombs can be up to 35 cm in size, while blocks are no larger than 20 cm. This facies is characterised by a visually obvious separation between layers. It consists of laterally continuous beds where, on the one hand, poorly sorted fine, lapilli-rich massive layers with a coarse ash matrix (EG9; EG13B; EG16; Fig. 5) and thicknesses ranging from a

few centimetres to several decimetres thick alternate with, on the other hand, a coarse ash matrix and well-sorted ash-rich layers (EG8; EG10: Fig. 5) with thin laminations.

3.4.4 Planar stratified facies (D)

This facies is represented by a set of up to 2-m-thick homogeneous planar (Fig. 5) and laterally continuous multiple layers moderately sorted with bedding planes plus internal planar laminations (Fig. 6d). Juvenile fine lapilli are commonly subangular and non-vesicular. The coarse fraction (up to 10 cm) consists of lava fragments and poorly vesicular juvenile ballistic scoria bombs, with somewhat fewer xenolith fragments (max 3–5 cm). The matrix is made up of palagonitised basaltic ash with crystal fragments of olivine and clinopyroxene. Planar lamination is locally visible in the less palagonitised layers; otherwise, the matrix appears generally to be massive due to textural modification by alteration. Typically, the contact below each bed is well-defined and non-erosive. Ballistic fragments up to 50 cm can be found. Individual beds are thin (1–5 cm) and vary from fine lapilli-rich beds to ash and exhibit good sorting with both normal and reverse grading. Some levels are characterised by poorly sorted deposits (EG5; EG7a: Fig. 5) with coarse and medium lapilli in a matrix of fine lapilli and coarse ash that fill in the small depressions. Despite resembling a diffusely stratified facies, this planar stratified facies is distinguished by the presence of continuous lateral planar bedding with constant moderately sorted layers of 2–3 cm and better sorting of each bed.

3.4.5 Undulate ash bed facies (E)

This facies, with a maximum detected thickness of just a few decimetres (Fig. 5), is represented by laterally continuous, well-sorted ash beds alternating with fine lapilli beds (EG6a: Fig. 5), which have undulate laminations and pinch-and-swell structures (Fig. 6e). Crests can be up to 5 cm in height and wavelengths vary from 5 to 10 cm. Some beds display brittle rupture due to the impact of ballistic ejecta.

3.4.6 Dune facies (F)

This facies is only present in the upper part of the succession at El Golfo. It has a maximum thickness of 1.5 m (Fig. 5) and forms large dunes (Fig. 6f). These can be up to 40 cm in height, and their wavelengths vary from 1.5 to 2 m. Individual thin beds are generally moderately sorted, structureless or reversely graded. The coarse fraction consists of juvenile medium lapilli, accretionary lapilli up to 1 cm and accidental lithic

fragments (up to 4 cm) that are basaltic in nature with a matrix of coarse ash. The laminae are defined by a clast-supported fabric from which all fine material has disappeared. In front of these structures, the foresets (maximum length 50 cm) are well-preserved and exhibit clear sigmoidal geometry. Both the top and bottom set laminations are still observable, the latter asymptotic to the basal bedding plane (Fig. 6f). These dunes are similar to the ones described as Type A by Cole (1991).

3.4.7 *Antidune facies (G)*

This facies, with a maximum thickness of a few decimetres (Fig. 5), consists of small bedforms with stoss sides preserved (Fig. 6g). These deposits are generally moderately sorted with individual beds alternating between juvenile fine lapilli-rich and ash-rich and loose accretionary lapilli with a maximum size of 1 cm. Crests are up to 15 cm in height with a wavelength of 40 cm (Fig. 5).

3.4.8 *Accretionary lapilli facies (H)*

This facies is only found in the upper part of the sequence, where it has a maximum thickness of 5 m (Fig. 5) and represents a level of mainly accretionary lapilli (Fig. 6h). Although present in small amounts in other facies, the accretionary lapilli are mostly concentrated in this level. They commonly contain cores of juvenile coarse ash and fine lapilli with coarser clasts up to about 3 cm in size and are defined as rim type (Schumacher and Schmincke, 1991, 1995). Deposits are usually moderately sorted, showing planar and laterally continuous beds with internal lamination. Individual plane beds are 5 cm thick and alternate between fine lapilli-rich and ash-rich layers.

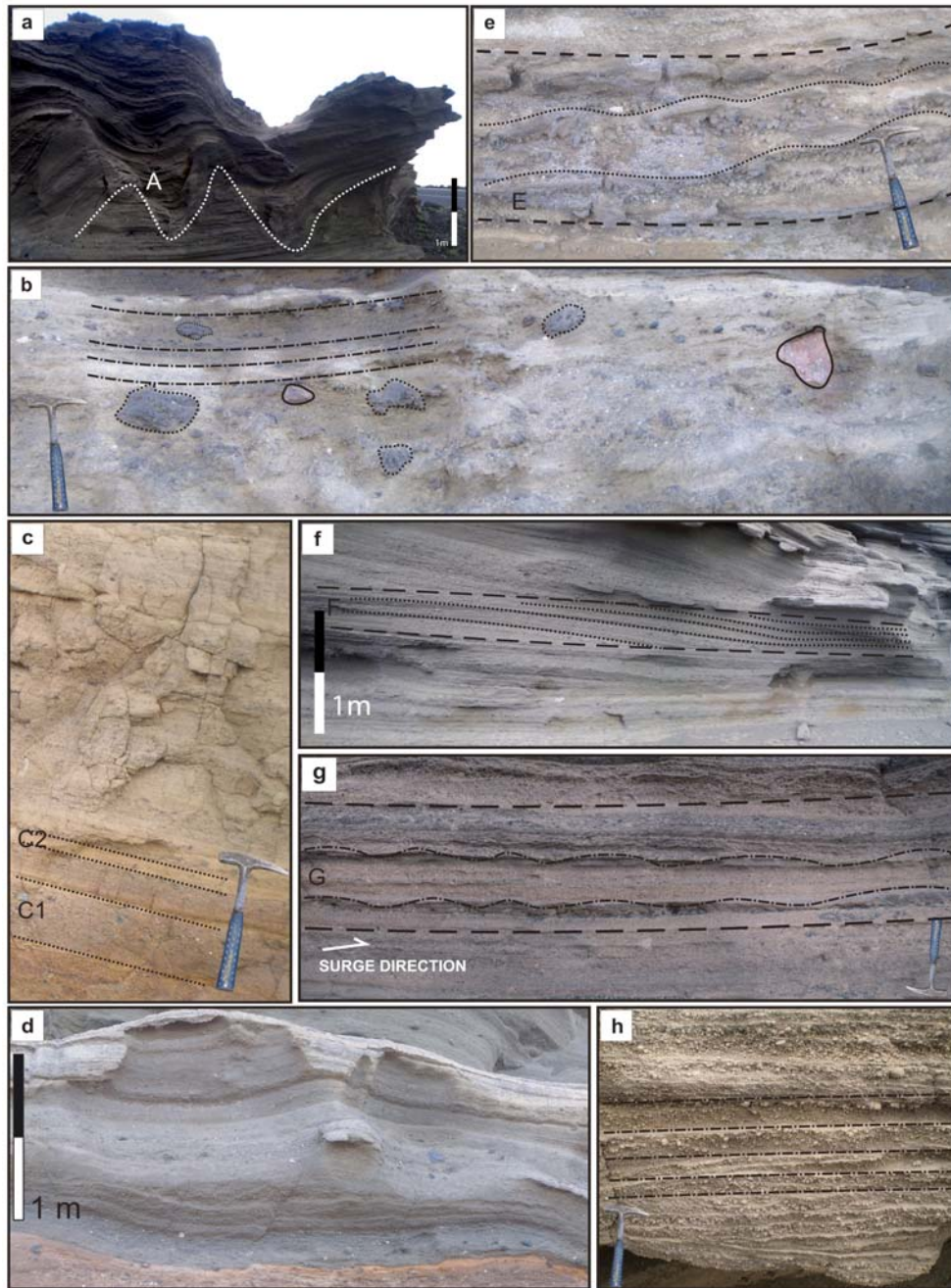


Fig. 6 Field photographs of the characteristic facies at the tuff cone of El Golfo: a channel-fill facies made of heterogeneous bedded ash and lapilli. Individual beds are generally ungraded with irregular and erosive boundaries. The dashed white line indicates the erosion surface; b massive crudely stratified facies including a thin- to medium-bedded, massive to crudely stratified unit (dotted-dashed line). It is also possible to distinguish the ballistic clasts corresponding to accidental basaltic fragments (continuous line) and bombs (dotted line); c diffusely stratified facies with continuous beds (C1) of poorly sorted lapilli-rich layers alternating with (C2) lapilli-poor layers with a yellow ashmatrix; d planar stratified facies composed of planar and laterally continuous beds with internal stratification. This facies can be distinguished from the diffusely stratified facies because this has continuous lateral planar bedding with constant moderately sorted layers 2–3 cm and better sorting in each bed; e undulate ash-bed facies consisting of laterally continuous, well-sorted ash and lapilli beds with pinch-and-swell structures and undulate laminations (dotted line); f dune facies with crests up to 40 cm and sets with foresets dipping downstream migrating downstream (dotted line); g antidune facies with crest (dotted-dash line) up to 40 cm height with a wavelength of 15 cm; h accretionary lapilli facies commonly containing cores of coarse ash and fine lapilli. Individual plane-beds (dotted-dash line) alternate from fine lapilli-rich to ash-rich layers.

3.5 Facies associations

We distinguished five lithofacies associations between the base and the top of the succession at El Golfo (Fig. 5, Table 1). As we explain below (see “Discussion”), these facies associations can be correlated to the different stages in the eruption that constructed the volcanic edifice on the basis of, on the one hand, the physical appearance of the deposits that make up the succession and, on the other, the differences in the inferred fragmentation, transportation and deposition mechanisms.

The first lithofacies association (G1) (stage I; Fig. 5) is represented by deposits exposed at sea level, mainly correspond to crudely stratified facies alternating with a small proportion of undulate ash-bed facies. Both of these facies are clearly characterised by juvenile clasts with accidental basaltic ballistic fragments, as well as notable differences in the distribution of the grain size of the deposits (Fig. 5). This lithofacies association represents the lowest part of the volcanic sequence at El Golfo (Fig. 5). The second lithofacies association (G2) (stage II; Fig. 5) exhibits a gradual transition from the previous stage and has planar stratified facies with minor undulate ash-bed facies. These deposits are finergrained, planar and laterally continuous with episodes with undulate beds. Both facies are characterised by impact lithics of basalt. The following lithofacies association (G3) (stage III; Fig. 5) is characterised by an abrupt change, and deposits are present mainly as fillings of depressions and as lenses (channel-fill facies). As the construction of the edifice progressed, deposits became progressively more poorly sorted: Massive lapilli-rich facies alternate with deposits characterised by well-sorted lapilli-poor, thinly bedded, internally stratified (diffuse stratified deposits) and, to a lesser extent, undulate facies. Accidental fragments (basaltic and xenoliths) characterise specific levels of the lithofacies (Fig. 5). This lithofacies association corresponds to the mid-part of the volcanic sequence. The next facies association (G4) (stage IV; Fig. 5) is characterised by a transitional change to planar stratified facies, accretionary lapilli and antidune facies, all followed by abundant lenses and V- and U-shaped channels associated with larger-sized channel-fill facies than those in G3. The final stage (G5) (stage V; Fig. 5) produced dunes and antidunes and accretionary lapilli, along with undulate and planar stratified facies. This lithofacies association is the uppermost in the depositional sequence and reveals an important change in the bedforms: dunes and antidunes predominate, with a decrease in the average grain size of the matrix from fine lapilli/coarse ash to coarse-fine ash.

3.6 Discussion

3.6.1 Facies interpretation

Based on the stratigraphic and geological features discussed in this study, the volcano of El Golfo is revealed as a tuff cone constructed close to the shoreline mainly by deposition from pyroclastic surges and emplacement of minor ballistic blocks and bombs. The interpretation of the lithofacies and the lithofacies associations identified in this study provides the necessary clues for understanding the eruption, transport and depositional mechanisms involved in the construction of the volcanic edifice of El Golfo. A channel-fill facies (A) consists of beds confined to channels formed by an eroding current with an erosive initial phase followed by a depositional stage. Massive muddy ash and lapilli lenses (Fig. 6a) can be interpreted as volcanoclastic water-logged gravity currents (Cas and Wright, 1987) based on the observed clearly defined boundaries and massive fine ash appearance. These geometries are in fact replaced in the lower part of the facies by massive deposits (Fig. 7a). In some cases, it is possible to infer that a two-stage process filled these channels (Fig. 7b–c): first of all, erosion by a passing current generated the V-shaped geometries that were subsequently coated by a thin veneer of fine ash deposited presumably by an ash-rich current through the channels (Fisher, 1977; Verwoerd and Chevallier, 1987); secondly, the channels were completely filled in by the materials transported the later pyroclastic surges. In other cases such as the U- and V-shaped rills (Fig. 7d), the erosive surfaces are larger and were probably formed by surface runoff from flows after the deposition of the pyroclastic material. Erosional features in surge deposits are well documented (e.g., Moore, 1967; Fisher, 1977; Kieffer and Sturtevant, 1986). As proposed in Wohletz (1998), the two-phase flow behaviour of a surge is influenced by topographic variability and implies particle deposition in cases of subsonic surges or erosion in supersonic surges.

As suggested by Valentine (1987), for any given stratified flow encountering an obstacle, there will be a level (streamline) above which all fluid has sufficient energy to surpass the obstacle and below which all fluid either is stopped (blocked) or simply moves around the obstacle with no upward motion. This critical level is referred to as the ‘dividing streamline’. An increasing Rouse number, that is, the ratio of particle settling velocity to the scale of turbulence (Middleton and Southard, 1978), due possibly to the confinement of the surge, causes lower parts to become dense enough to assume

the characteristics of a pyroclastic flow. This leads to the deposition of the characteristic facies observed at El Golfo, where the deposits tend to have a massive fine ash appearance, and the coarsest lithics tend to be found in the lowest part of the deposits.

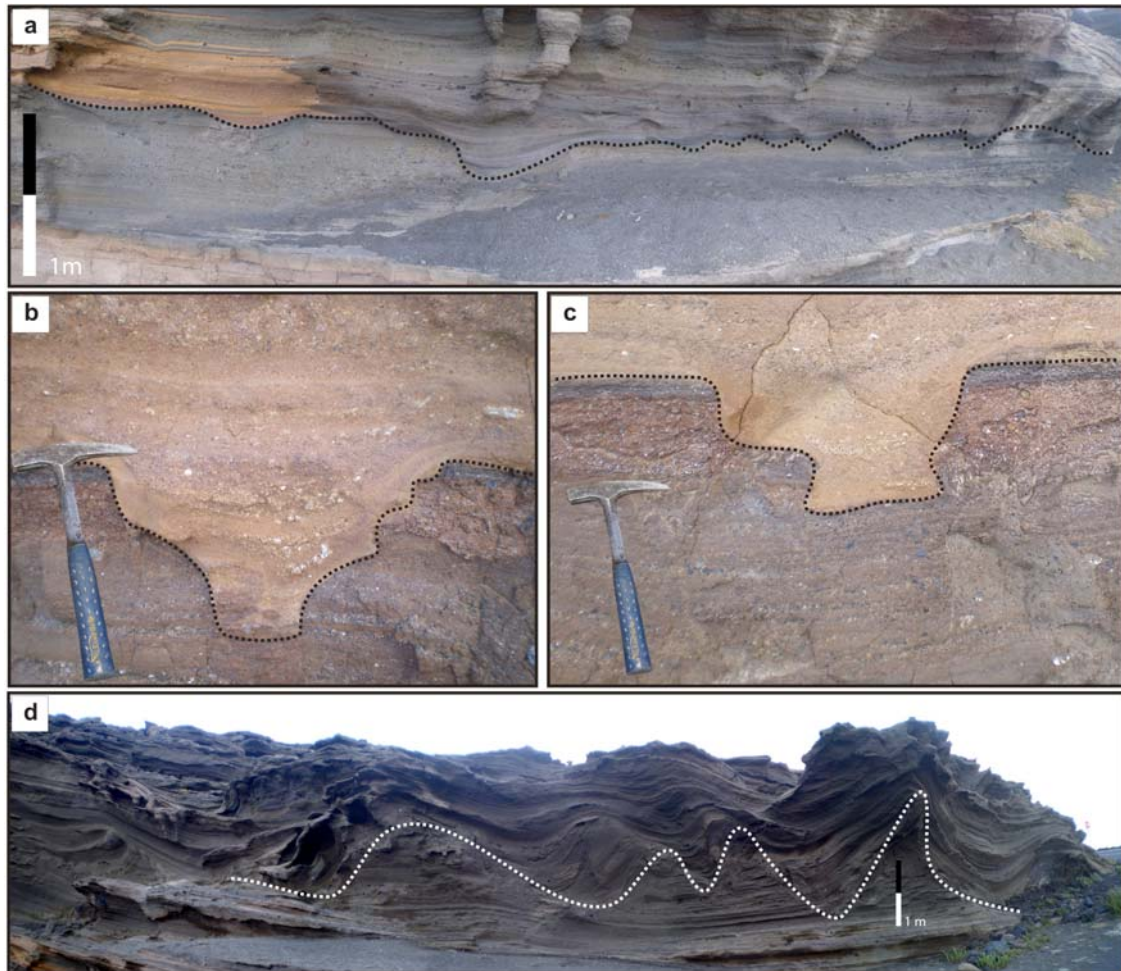


Fig. 7 Field details of channel-fill facies: a V-shaped geometry (dotted line) and crudely stratified replenishment of the erosion cavities excavated in plane beds by pyroclastic surge deposits; b c channels filled in two stages: First, the flow generated the V-shaped geometries (dotted line) that were subsequently coated by the massive dense flows that circulated through the channels. Finally, the materials transported by the latter pyroclastic surges replenished the cavities; d U- and V-shaped rill geometries (white dotted line). The erosive surfaces have larger geometries and are thought to have been formed by surface runoff from flows after the deposition of the pyroclastic material.

As suggested by Solgevik et al. (2007) for the Capelas tuff cone (Sao Miguel Island, Azores), crudely stratified facies (B) (Fig. 6b) might be the result of a rapid emplacement from a high concentration boundary layer with weak tractional transport. Alternatively (in the case of more pronounced tractional transport), this facies might be interpreted as deposits from a traction carpet in a highly concentrated boundary layer. The presence of blocks and bombs is indicative of ballistically emplaced ejecta.

The diffusely stratified facies (C) is characterised by a visible difference in grain size and sorting between the lapilli and ash-rich layers (Fig. 6c) and could be interpreted as the result of either an unsteady pyroclastic surge or multiple, closely spaced events (Dellino et al. 2004a). Poorly sorted, lapilli-rich, massive layers with crude associated stratification might be the result of rapid deposition from suspension with little traction, whereas well-sorted lapilli-poor layers with thin internal laminations could be indicative of a relatively slow deposition rate resulting in grain segregation (Arnott and Hand, 1989).

In the planar stratified facies (D), it is difficult to discriminate the depositional mechanisms due to a lack of outcrops. Planar lamination, sometimes visible in the less palagonitised layers (Fig. 6d), could suggest that the facies was the product of a pyroclastic surge in which a single couplet consisting of fine lapilli and ash-grade beds was formed by a single surge (Sohn and Chough, 1989; Dellino et al., 2004a, b).

The undulate ash beds (E) can be interpreted as pyroclastic surge deposits primarily on the basis of the low-angle cross lamination. The existence of these structures (Fig. 6e) may be the result of variations in the flow regime (Valentine and Fisher, 2000) and in particle concentration (Sohn and Chough, 1989; Sohn, 1996). Given the relationship between flow regimes and resulting bedforms (Cas and Wright, 1987), low-angle undulate ash-beds with weak stratification could be interpreted as the result of a low-flow regime, thereby indicating a decreasing velocity of the flow or lower to transitional regime produced by a relatively low concentration pyroclastic surge.

Aside from undulate ash-beds, the dune facies (F) (Fig. 6f) are classified as lower-flow-regime bedforms (Cas and Wright, 1987). Fisher and Schmincke (1984) argued that sand-wave migration direction is controlled by velocity and flow regime, and a similar situation was proposed by Druitt (1992) for the May, 1980, Mount St. Helens basalt deposits: regressive sandwaves (antidunes) formed where the blast was accelerating and progressive sand waves (dunes) where it was decelerating.

The antidune facies (G) (Fig. 6g) occurs where there is supercritical flow (Cas and Wright, 1987). The presence of accretionary lapilli might indicate that the corresponding pyroclastic surges were wet (i.e. they consisted of three-phase flows with gas, particles and liquid water), as suggested by Lorenz (1974a, 1974b), Walker (1984) and Sohn and Chough (1992).

Accretionary lapilli facies (H) (Fig. 6h) commonly forming steam-rich hydrovolcanic eruption columns (Self and Sparks, 1978) or in convecting pyroclastic surge clouds when solid particles pick up sticky wet ash (Waite and Dzurisin, 1981). During the lateral spreading of surges, particles form core agglomerate due to accidental collisions and when the binding forces of liquid bridges from condensed moisture exceed the grain-dispersive forces (Schumacher and Schmincke, 1995).

The depositional characteristics of the pyroclastic surge deposits at El Golfo and the absence of secondary reworking by seawaves suggest that the emplacement of the deposits and the construction of the cone occurred in a subaerial environment. In addition, the irregular distribution of palagonitic alteration indicate that, given the depositional characteristics of the deposits, the palagonitisation was produced in a subaerial environment, as suggested by Martí and Colombo (1990).

Most of the pyroclastic deposits in the edifice consist of a fine-grained matrix embedding coarse scoria, lithic fragments and volcanic bombs and blocks (emplaced ballistically) (Figs. 6 and 8), which suggests that the transportation process of this pyroclastic material was not able to develop any proper grain-sorting process. The lack of clear fallout deposits is a remarkable feature of the succession at El Golfo. This, together with lithological and depositional features such as ripples, dunes, antidunes and tabular forms, as well as the circular distribution of deposits, indicates that most pyroclastic deposits formed from turbulent, highly dilute pyroclastic surges (see Druitt, 1998; Freundt and Bursik, 1998; Huppert, 1998; Branney and Kokelaar, 2002) expanding radially from the eruptive vent. In fact, variations in vertical facies are usually related to variable rates of energy release occurring during an ongoing eruption (Sohn and Chough, 1989). The apparent lack of fallout deposits may be interpreted either as a direct consequence of the eruption dynamics (i.e. absence of fallout mechanisms in proximal areas) or of their erosion and assimilation by the pyroclastic surges.

3.6.2 Eruptive dynamics

Along with accretionary lapilli and accidental lithics, particles with morphology and textures related to hydromagmatic fragmentation (block-like shapes, low vesicularity, presence of adhered dust, tephra size and superficial chemical alteration) (Martí and Colombo, 1990) dominate the deposits found in the tuff cone of El Golfo. The dynamics of hydrovolcanism are controlled by the complex thermodynamics of

magma–water interaction, which determines the nature of explosive activity, and are characterised by variable energy outputs and different degrees of magmatic or hydromagmatic fragmentation (Wohletz and Sheridan, 1983; Houghton and Hackett, 1984; Kokelaar, 1986; White and Houghton, 2000; Mastin et al., 2004). Depending on the extent of the magma–water interaction and the modes of transport and deposition, hydrovolcanic deposits show remarkable variability in between-layer and within layer. The efficiency of hydromagmatic fragmentation and the corresponding eruption dynamics are controlled by magma viscosity, temperature, the pressure differences between magma and water, and the water/magma contact mode (supply rate of magma and the external water; Wohletz and Sheridan, 1983), as well as by the exact nature of the coolant (White, 1996).

The lithological and stratigraphic variations shown by the deposits at El Golfo (Fig. 5) suggest that the different transport and depositional mechanisms that characterize them were a product of changes in the eruption dynamics caused by changes in the efficiency of the hydromagmatic fragmentation. This implies that the eruption responsible for the construction of this tuff cone was continuous but had several pulses in which different types of deposits were formed. According to the resulting facies associations described above and their interpretation in light of the mechanisms of fragmentation, transportation and deposition, we are able to distinguish five stages or pulses in the eruption of this volcano (Table 1).

The first stage (I) is represented by the lithofacies association G1 (Fig. 5, Table 1), which consists of deposits characterised by the effects of the high rate of direct suspension sedimentation that alternate with tractional deposition (depending on the deposition rate). The general aspect of this lithofacies, characterised by poor sorting with coarse-grained tephra (coarse lapilli) alternating with beds of coarse ash, along with large clasts and blocks up to 30 cm in diameter, reflects in general high-energy transport with changes in the rate of deposition. The trajectories of the ballistic impacts indicate north-to-south transportation. The large amount of accidental basaltic lithic clasts can be interpreted as a ventopening episode that occurred during the initial stages of the subsurface hydrovolcanic explosions.

The second stage (II) corresponds predominantly to the emplacement of multiple pyroclastic surges with subordinate undulate ash-beds (lithofacies association G2) (Fig. 5, Table 1). The resulting deposits show characteristic planar bedding, which may be considered as an upper flow-regime bedform. Higher fragmentation efficiency is

suggested by the abundance of ash matrix in these deposits. This suggests an increase in the energy of the explosions, probably associated with greater efficiency in the energy transfer during the hydromagmatic process. Similar deposits can be observed at Surtsey, Capelinhos and Capelas (Waters and Fisher, 1971; Kokelaar, 1983, 1986; Solgevik et al., 2007). The presence of a number of ballistic blocks up to 50 cm in diameter (Fig. 5) suggest episodes of higher explosive energy.

The third stage (III) of the eruption is reflected in the succession of deposits in the lithofacies association G3 (Fig. 5, Tab. 1), which represents a further change in the transportation and depositional conditions. This stage consists of beds confined to channels formed by an eroding current with an initial erosive phase followed by a depositional stage. The rest of the unit is interpreted as resulting from the deposition of turbulent pyroclastic surges with fluctuating velocity and particle concentration, as well as episodes of high shear stress leading to the formation of undulate deposits. These deposits are similar to the ones described in Solgevik et al. (2007) and Cole et al. (2001). These features—by comparison with those of the previous stage—indicate that this stage was characterised by higher energy transport related to episodes of higher explosive energy, which also generated bomb- and block-rich (up to 35 cm in diameter) horizons.

Stage four (IV) can be correlated with wet explosions (lithofacies association G4) (Fig. 5, Tab. 1) in which a remobilisation of material occurred due to an excess of water (e.g., Sohn and Chough, 1992). Individual explosions could also have produced water-charged tephra jets that landed on the flanks of the growing cone and acted as a source of ready to- move free water. The U-shaped channels might also be the result of topographic variability with particle deposition or erosion. The presence of antidunes, planar stratified and accretionary lapilli suggest a complex emplacement of pyroclastic density currents with continuous changes in transportation and depositional conditions. The presence in smaller proportions of bedforms with ripple-type geometries and slopes in the opposite direction to the propagation direction of the main pyroclastic surges (i.e. antidunes) suggests an important increase in the energy of the flow (Fisher and Schmincke 1984), whilst the dunes represent lower-flow-regime bedforms.

Stage five (V) corresponds to the lithofacies association G5 (Fig. 5, Tab. 1) and is characterised by deposits containing large dunes, accretionary lapilli, antidunes, and undulate and planar stratified facies. The duration of the pyroclastic surges that caused their deposition was probably very short, and there is no evidence that during flow

emplacement the materials of the bedform were eroded and adapted to the new flow conditions. The lack of fine material, probably elutriated during the transport process, in the cross-bedded levels, indicates that the flows generating these dunes were gas supported. However, the presence of a facies with accretionary lapilli in the deposits of this last stage suggests that occasionally there was a moderate amount of liquid water (or moisture) in the surges and/or eruption clouds from which they formed (e.g., Fisher and Schmincke, 1984; Heiken and Wohletz, 1985). As a surge moves laterally away from the vent, it loses heat, solids and momentum, resulting in a decreasing wavelength and amplitude of the cross-stratified surge deposits as the distance from the vent increases (e.g., Waters and Fisher, 1971; Wohletz and Sheridan, 1979; Sohn and Chough, 1989). The loss of heat results in the condensation of steam, which explains the increase in wet features. The amount of water might thus be related to the dynamics of the flow rather than the changing eruption conditions. This hypothesis was first proposed by Wohletz and Sheridan (1983).

In summary, the diversity of emplacement mechanisms inferred and grain size distributions observed in the stratigraphic sequence indicates that the eruptive and emplacement mechanisms were not constant during the eruptive episode that generated the tuff cone of El Golfo. A general increase in the explosive energy can be seen as one moves upwards in the pyroclastic succession, indicating possibly that there was a trend towards an optimum magma/water ratio in the second half of the eruption, which would have led to an increase in the energy-exchange efficiency and, consequently, in the magma fragmentation. This is illustrated by the progressive increase in the degree of fragmentation (i.e. decrease in grain size) and in the energy of the resulting pyroclastic surges, which was probably related to a progressive reduction in the amount of sea water entering the vent as the volcanic edifice was being built. However, there is no evidence of any Strombolian phase during the eruption, which would seem to imply that to the west the tuff cone remained open to the sea during the whole eruption sequence, even at its end when the eastern side of the edifice had reached around 60 m a.s.l. This might probably due to the continuous partial collapse of part of the edifice. The absence of any significant volume of lithic clasts derived from the substrate (e.g., fragments of older lavas or fossil beaches) suggests that the eruption did not excavate deeply into the substrate, and so we can assume that the magma– water interaction occurred mostly at a very shallow depth or even at sea level and can discard the idea that water could have been drawn into the conduit from a subsurface aquifer.

3.6.3 Post-depositional processes

The irregular geometry of the different alteration zones suggests that some primary causes for the palagonitisation should have existed. This process may be almost contemporaneous to tuff deposition (e.g., Capelas, Capelinhos and Sao Roque tuff cones in Azores, Solgevik et al., 2007; Cole et al., 2001; Zanon et al., 2009; Sinker Butte Volcano in USA, Brand and White, 2007). The fact that the materials that are in contact with the highest topographic surface are the least altered indicates that, during the late depositional stages, the pyroclastic materials retained a small amount of steam shortly after being deposited. By contrast, the materials located in the lower half of the sequence are more altered, which implies that at the moment of deposition they retained a greater proportion of water as steam. In these lower sections, the steam remained trapped for longer, which may be related to the fact that the accumulation of materials occurred very rapidly and thus prevented the steam from escaping. Thus, once covered by the successive pyroclastic surges, the deposits would have acted as an aquatard that could explain the different degree of alteration between the upper and lower parts of the sequence at El Golfo, despite the lack of any clear (eruptive) separation.

The presence of interstitial water in the lower part of the sequence of deposits is also shown by the existence of tephra slips that affected the whole wall and which are associated with circular compaction faults (Fig. 8).

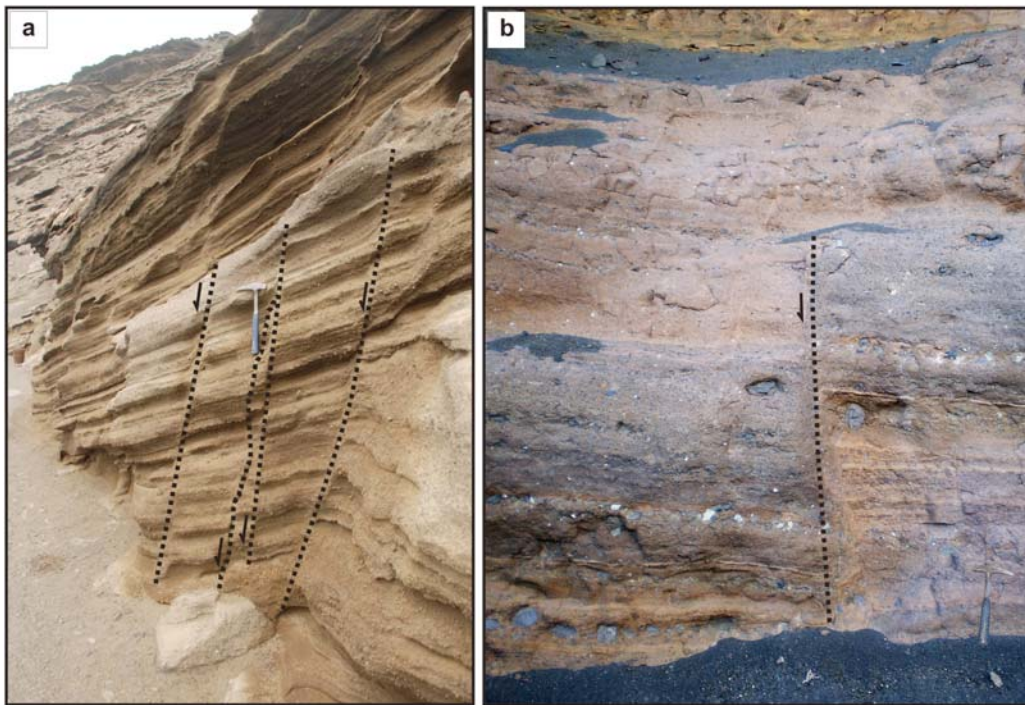


Fig. 8 Field photographs showing examples of subvertical settlement faults existing around the edifice.

The palagonitisation induced high secondary resistance in the tuff, resulting in a stress response that changed from pseudo-plastic to pseudobrittle in behaviour. As a consequence, the response to this oriented stress was the formation of fractures and an immediate failure. During these slides, the entire block behaved as a single rigid unit (but sufficiently plastic). It is important to note that the downdropped section in front of El Golfo (Fig. 4d) exhibits the same type of alteration as the rest of the edifice but with the addition of a chaotic structure due to the slumping process. This suggests that the main landslide occurred once the palagonitization processes had already started. However, as has been demonstrated in the case of the Surtsey eruption (Kokelaar, 1983; Moore, 1985), it is possible that slumps occurred during the construction of the volcanic edifice and that the material displaced towards the vent was re-ejected during subsequent explosions.

3.6.4 Hazard implications

El Golfo is a good example of a tuff cone demonstrating how a single eruption may produce a complex sequence of eruption styles and depositional processes. Nonetheless, an examination of this volcano sheds light on a number of important implications for hazard assessment when considered within the framework of the fissural volcanism present in the Canary Islands. After the construction and partial erosion of its edifice, another eruptive episode took place in the northern section of El Golfo (Fig. 2). Three craters were formed, and lavas and Strombolian pyroclasts were emitted (Fig. 4d). Despite not occurring during the same eruptive episode, the formation of these new edifices can be linked to the same NEE–SWW fracture system that originated the tuff cone at El Golfo. We can see here how a fissure-dominated system in which scoria and/or lava spatter cones form long chains exhibits very different styles of eruptions at the extremities of the fissure. Subaerial conditions changing to shallow submarine conditions allowed for the development of a hydrovolcanic landform in the area. Sea-level changes during the long time in which the overall fissure system was active (as shown by the presence of fossil beaches) may have led to the construction of a complex set of volcano types in this lowland area with contrasting eruption styles and, consequently, a variety of associated hazards. While a small lava spatter eruption may be manageable, a full tuff cone or maar eruption would cause havoc on a local scale and would have very different repercussions in terms of its potential hazards. Furthermore, the pyroclastic deposits at El Golfo are very rich in xenoliths, and the existence of these

plutonic enclaves in the basalts of Lanzarote would seem to suggest that on occasions a rapid ascent of magma to the surface occurs. On Lanzarote and the other Canary Islands, this type of longlived fissure-dominated volcanism incorporating contrasting eruption styles is not uncommon and should be studied in more detail as a means of conducting appropriate hazard assessment for this area.

3.7 Conclusions

The tuff cone at El Golfo is an example of a coastal volcanic edifice caused by simple hydrovolcanic activity without any evidence of Strombolian phases. Interaction of water with magma, mostly at sea level, dominated the whole eruptive process. The lithological and stratigraphic features present in the deposits at El Golfo suggest that most were formed by deposition from turbulent pyroclastic surges. These characteristics, together with the type and distribution of the palagonitic alteration that affects part of the materials and the absence of hyaloclastites, suggest that they were emplaced in a subaerial environment. The growth of the tuff cone can be divided roughly into five stages on the basis of the resulting deposits and different corresponding eruption mechanisms inferred. A continuous change in the transport/depositional system is revealed, with a possible progressive increase in the energy transfer efficiency from magma to water and, consequently, in the eruption explosivity and in the degree of fragmentation. This volcano forms part of a long-lived fissural system that reaches down to the coastal plains, along which several monogenetic cones showing a large diversity of eruptive styles have formed. It reminds us that eruption dynamics and associated hazards may differ considerably within the same volcanic system if external variables (e.g., the availability of water) change.

Acknowledgements

This research was partially funded by CTM2009-05919-E/ANT. The authors are grateful to the Cabildo of Lanzarote and the National Park of Timanfaya for giving permission to undertake this research, and to Orlando Hernandez (Casa de Los Volcanes-Cabildo de Lanzarote) for his assistance with the logistics. We are also grateful to the Editor James White, the Associated Editor Thorvaldur Thordarson and the reviewers Danilo Palladino, Karoly Németh and Christopher Hamilton for their constructive reviews of this manuscript.

References

- Abdel-Monem, A., Watkins, N.D. and Gast, P.W., 1972. Potassium-argon ages, volcanic stratigraphy, and geomagnetic polarity history of the Canary Islands; Tenerife, La Palma and Hierro. *American Journal of Science*, 272(9): 805-825.
- Araña, V. and Carracedo, J., 1978. *Cañarían Volcanoes: Gran Canaria*. Editorial Rueda, Madrid: 1-175.
- Araña, V., Hansen, A. and Martí, J., 1988. La caldera y el Pico de Vandama (Gran Canaria). *Boletín Geológico y Minero*, T. XCIX-I 47-58.
- Arnott, R.W.C. and Hand, B.M., 1989. Bedforms, primary structures and grain fabric in the presence of suspended sediment rain. *Journal of Sedimentary Petrology*, 59: 1062-1069.
- Baker, E., Massoth, G., de Ronde, C., Lupton, J. and McInnes, B., 2002. Observations and sampling of an ongoing subsurface eruption of Kavachi volcano, Solomon Islands. *Geology*, 30(11): 975-978.
- Banda, E., Danobeitia, J.J., Surinach, E. and Ansorge, J., 1981. Features of crustal structure under the Canary Islands. *Earth and Planetary Science Letters*, 55(1): 11-24.
- Belousov, A. and Belousova, M., 2001. Eruptive process, effects and deposits of the 1996 and the ancient basaltic phreatomagmatic eruptions in Karymskoye lake, Kamchatka, Russia. *Spec. Publs int. Ass. Sediment.*, 30: 35-60.
- Brand, B.D. and White, C.M., 2007. Origin and stratigraphy of phreatomagmatic deposits at the Pleistocene Sinker Butte Volcano, Western Snake River Plain, Idaho. *Journal of Volcanology and Geothermal Research*, 160(3-4): 319-339.
- Branney, M.J. and Kokelaar, P., 2002. Pyroclastic density currents and the sedimentation of ignimbrites. *Geological Society of London Memoirs*, 150 pp.
- Cas, R.A.F. and Wright, J.V., 1987. *Volcanic successions, modern and ancient. A geological approach to processes products and successions*. 528 pp.
- Chough, S.K. and Sohn, Y.K., 1990. Depositional mechanics and sequences of base surges, Songaksan tuff ring, Cheju Island, Korea. *Sedimentology* 37(6): 1115-1135.

- Clarke, H., Troll, V.R. and Carracedo, J.C., 2009. Phreatomagmatic to Strombolian eruptive activity of basaltic cinder cones: Montaña Los Erales, Tenerife, Canary Islands. *Journal of Volcanology and Geothermal Research*, 180(2–4): 225-245.
- Cole, P., Guest, J., Duncan, A. and Pacheco, J., 2001. Capelinhos 1957–1958, Faial, Azores: deposits formed by an emergent surtseyan eruption. *Bulletin of Volcanology*, 63(2): 204-220.
- Cole, P.D., 1991. Migration direction of sand-wave structures in pyroclastic-surge deposits; implications for depositional processes. *Geology* 19(11): 1108-1111.
- Cronin, S.J., Bonte-Graptin, M. and Nemeth, K., 2006. Samoa technical report - Review of volcanic hazard maps for Savai'i and Upolu.
- De La Nuez, J., Alonso, J., Quesada, M. and Macu, M., 1993 Edificios hidromagmáticos costeros de Tenerife (Islas Canarias) *Rev Soc Geol España* 6 (1-2): 47-59.
- Dellino, P., Isaia, R., La Volpe, L. and Orsi, G., 2004a. Interaction between particles transported by fallout and surge in the deposits of the Agnano-Monte Spina eruption (Campi Flegrei, Southern Italy). *Journal of Volcanology and Geothermal Research*, 133(1-4): 193-210.
- Dellino, P., Isaia, R. and Veneruso, M., 2004b. Turbulent boundary layer shear flows as an approximation of base surges at Campi Flegrei (Southern Italy). *Journal of Volcanology and Geothermal Research*, 133(1-4): 211-228.
- Druitt, T.H., 1992. Emplacement of the 18 May 1980 lateral blast deposit ENE of Mount St. Helens, Washington. *Bulletin of Volcanology*, 54(7): 554-572.
- Druitt, T.H., 1998. Pyroclastic density currents. In: Gilbert, J.S., Sparks, R.S.J. (Eds.), *The Physics of Explosive Volcanic Eruptions*. Geological Society, Spec. Publ. , 145: 145-182.
- Fisher, R.V., 1977. Erosion by volcanic base-surge density currents: U-shaped channels. *Geological Society of America Bulletin*, 88(9): 1287-1297.
- Fisher, R.V. and Schmincke, H.U., 1984. *Pyroclastic Rocks*. Springer–Verlag Inc, Berlin. 474 pp.

Freundt, A. and Bursik, M., 1998. Pyroclastic flow transport mechanisms. In: Freundt, A., Rosi, M. (Eds.), *From Magma to Tephra, Modeling Physical Processes of Explosive Volcanic Eruptions*, 4(Elsevier Science, Amsterdam): 173–231.

Fuster, J.M., Cendro, A., Gastesi, P., Ibarróla, E. and Ruiz, J.L., 1968. *Geología y volcanología de las islas Canarias: Tenerife*. Instituto 'Lucas Mallada', CSIC, Madrid: 218 pp.

Gudmundsson, M.T., Thordarson, T., Höskuldsson, Á., Larsen, G., Björnsson, H., Prata, F.J., Oddsson, B., Magnússon, E., Högnadóttir, T., Petersen, G.N., Hayward, C.L., Stevenson, J.A. and Jónsdóttir, I., 2012. Ash generation and distribution from the April–May 2010 eruption of Eyjafjallajökull, Iceland. *Sci. Rep.*, 2.

Heiken, G. and Wohletz, K., 1985. *Volcanic ash*. University of California Press, Berkeley. 246 pp.

Houghton, B.F. and Hackett, W.R., 1984. Strombolian and phreatomagmatic deposits of Ohakune craters, Ruapehu, New Zealand: A complex interaction between external water and rising basaltic magma. *Journal of Volcanology and Geothermal Research*, 21(3–4): 207–231.

Huppert, H.E., 1998 Quantitative modelling of granular suspension flows. *Phil. Trans. R. Soc. Lond.*, 356: 2471–2496.

(IMO), Icelandic Meteorological Office. <http://en.vedur.is/earthquakes-and-volcanism/articles/nr/1884>.

Ingram, R.L., 1954. Terminology for the thickness of stratification and parting units in sedimentary rocks. *Geological Society of America Bulletin*, 65(9): 937–938.

Jude-Eton, T.C., Thordarson, T., Gudmundsson, M.T. and Oddsson, B., 2012. Dynamics, stratigraphy and proximal dispersal of supraglacial tephra during the ice-confined 2004 eruption at Grímsvötn Volcano, Iceland. *Bulletin of Volcanology*, 74(5): 1057–1082.

Kieffer, S. and Sturtevant, B., 1986. Erosional furrows formed during the lateral blast at Mount St. Helens, May 18, 1980: indicators of longitudinal vortices in the boundary layer. *Abstr. Intl. Volcanol. Cong. New Zealand*, 53.

- Kienle, J., Kyle, P.R., Self, S., Motyka, R.J. and Lorenz, V., 1980. Ukinrek Maars, Alaska, I. April 1977 eruption sequence, petrology and tectonic setting. *Journal of Volcanology and Geothermal Research*, 7(1–2): 11-37.
- Kokelaar, B.P., 1983. The mechanism of Surtseyan volcanism. *Journal of the Geological Society*, 140(6): 939-944.
- Kokelaar, P., 1986. Magma-water interactions in subaqueous and emergent basaltic volcanism. *Bulletin of Volcanology*, 48: 275-289.
- Larsen, G., 2010. 3 Katla: Tephrochronology and Eruption History. In: J.K. Anders Schomacker and H.K. Kurt (Editors), *Developments in Quaternary Sciences*. Elsevier, pp. 23-49.
- Larsen, G., Guðmundsson, M.T. and Sigmarsson, O., 2009 Katla. In: Sólnes, J. et al. (Eds), *Náttúruvá á Íslandi-Tekist á við náttúruöflin í 1100 ár*. Eldgosavá. Viðlagatrygging Íslands, Reykjavík.
- Le Bas, M.J., Rex, D.C. and Stillman, C.J., 1986. The early magmatic chronology of Fuerteventura, Canary Islands. *Geological Magazine*, 123: 287-298.
- Lorenz, V., 1974a. Studies of the Surtsey tephra deposits. *Surtsey Res. Prog. Rep.* , 7: 72–79.
- Lorenz, V., 1974b. Vesiculated tuffs and associated features. *Sedimentology* 21: 273–291.
- Macdonald, G.A., 1972. *Volcanoes*. Prentice-Hall, Inc., N.J.: 510 pp.
- Machado, F., Parsons, W.H., Richards, A.F. and Mulford, J.W., 1962. Capelinhos Eruption of Fayal Volcano, Azores, 1957-1958. *J. Geophys. Res.*, 67(9): 3519-3529.
- Marinoni, L.B. and Gudmundsson, A., 2000. Dykes, faults and palaeostresses in the Teno and Anaga massifs of Tenerife (Canary Islands). *Journal of Volcanology and Geothermal Research*, 103(1-4): 83-103.
- Marinoni, L.B. and Pasquarè, G., 1994. Tectonic evolution of the emergent part of a volcanic ocean island: Lanzarote, Canary Islands. *Tectonophysics*, 239(1-4): 111-137.

- Martí, J. and Colombo, F., 1990. Estratigrafía, sedimentología y mecanismos eruptivos del edificio hidromagmático de El Golfo (Lanzarote). *Boletín Geológico y Minero*, 101(4): 560-579.
- Mastin, L.G., Christiansen, R.L., Thornber, C., Lowenstern, J. and Beeson, M., 2004. What makes hydromagmatic eruptions violent? Some insights from the Keanakāko'i Ash, Kīlauea Volcano, Hawai'i. *Journal of Volcanology and Geothermal Research*, 137(1-3): 15-31.
- Middleton, G. and Southard, J., 1978. Mechanics of sediment movement. *Soc Econ Paleontol Mineral Short Course 3, Eastern Section*: pp 6.37-36.41.
- Moore, J., 1967. Base surge in recent volcanic eruptions. *Bulletin of Volcanology*, 30(1): 337-363.
- Moore, J.G., 1985. Structures and eruptive mechanisms at Surtsey Volcano, Iceland. *Geology magazine*, 122(6): 649-661.
- Moore, J.G., Nakamura, K. and Alcaraz, A., 1966. The 1965 Eruption of Taal Volcano. *Science*, 151(3713): 955-960.
- Morimoto, R., 1960. Submarine eruption of the Myōjin reef. *Bulletin of Volcanology*, 23(1): 151-160.
- Németh, K. and Cronin, S.J., 2009. Volcanic structures and oral traditions of volcanism of Western Samoa (SW Pacific) and their implications for hazard education. *Journal of Volcanology and Geothermal Research*, 186(3-4): 223-237.
- Németh, K. and Cronin, S.J., 2011. Drivers of explosivity and elevated hazard in basaltic fissure eruptions: The 1913 eruption of Ambrym Volcano, Vanuatu (SW-Pacific). *Journal of Volcanology and Geothermal Research*, 201(1-4): 194-209.
- Robertson, A.H.F. and Stillman, C.J., 1979. Late Mesozoic sedimentary rocks of Fuerteventura, Canary Islands: Implications for West African continental margin evolution. *Journal of the Geological Society*, 136(1): 47-60.
- Schumacher, R. and Schmincke, H.-U., 1991. Internal structure and occurrence of accretionary lapilli — a case study at Laacher See Volcano. *Bulletin of Volcanology*, 53(8): 612-634.

- Schumacher, R. and Schmincke, H.U., 1995. Models for the origin of accretionary lapilli. *Bulletin of Volcanology*, 56(8): 626-639.
- Self, S., Kienle, J. and Huot, J.-P., 1980. Ukinrek Maars, Alaska, II. Deposits and formation of the 1977 craters. *Journal of Volcanology and Geothermal Research*, 7(1-2): 39-65.
- Self, S. and Sparks, R.S.J., 1978. Characteristics of widespread pyroclastic deposits formed by the interaction of silicic magma and water. *Bulletin Volcanologique*, 41(3): 196-212.
- Sheridan, M.F. and Wohletz, K.H., 1981. Hydrovolcanic explosions: the systematics of water-pyroclast equilibration. *Science*, 212: 1387-1389.
- Sheridan, M.F. and Wohletz, K.H., 1983. Hydrovolcanism: Basic considerations and review. *Journal of Volcanology and Geothermal Research*, 17(1-4): 1-29.
- Sohn, Y.K., 1996. Hydrovolcanic processes forming basaltic tuff rings and cones on Jeju Island, Korea. *Geological Society of America Bulletin*, 108: 1199-1211.
- Sohn, Y.K. and Chough, S.K., 1989. Depositional processes of the Suwolbong tuff ring, Cheju Island (Korea). *Sedimentology*, 36(5): 837-855.
- Sohn, Y.K. and Chough, S.K., 1992. The Ilchulbong tuff cone, Cheju Island, South Korea: depositional processes and evolution of an emergent, Surtseyan-type tuff cone. *Sedimentology* 39: 523-544.
- Sohn, Y.K., Park, J.B., Khim, B.K., Park, K.H. and Koh, G.W., 2003. Stratigraphy, petrochemistry and Quaternary depositional record of the Songaksan tuff ring, Jeju Island, Korea. *Journal of Volcanology and Geothermal Research*, 119(1-4): 1-20.
- Solvevik, H., Mattsson, H.B. and Hermelin, O., 2007. Growth of an emergent tuff cone: Fragmentation and depositional processes recorded in the Capelas tuff cone, São Miguel, Azores. *Journal of Volcanology and Geothermal Research*, 159(1): 246-266.
- Sumner, J.M., 1998. Formation of clastogenic lava flows during fissure eruption and scoria cone collapse: the 1986 eruption of Izu-Oshima Volcano, eastern Japan. *Bulletin of Volcanology*, 60(3): 195-212.

- Thorarinsson, S., 1965. The Surtsey Eruption: course of events and development of the new island. Surtsey Research Progress Report, 1: 51-55.
- Valentine, G.A., 1987. Stratified flow in pyroclastic surges. *Bulletin of Volcanology*, 49(4): 616-630.
- Valentine, G.A. and Fisher, R.V., 2000. Pyroclastic surges and blasts. In: Sigurdsson, H., Houghton, B.F., McNutt, S.R., Rymer, H., Stix, J. (Eds.), *Encyclopedia of Volcanoes*. Academic Press: 571–580.
- Verwoerd, W.J. and Chevallier, L., 1987. Contrasting types of surtseyan tuff cones on Marion and Prince Edward islands, southwest Indian Ocean. *Bulletin of Volcanology*, 49(1): 399-413.
- Waite, R.B. and Dzurisin, D., 1981. Devastating pyroclastic density flow and attendant air fall of May 18-Stratigraphy and sedimentology deposits. In: *The 1980 Eruptions of Mount St. Helens, Washington* (Ed. by P.W. Lipman & D.R. Mullineaux), *Pap. US Geol. Surv.*, 1250 439-458.
- Walker, G.P.L., 1984. Characteristics of dune-bedded pyroclastic surge bedsets. *Journal of Volcanology and Geothermal Research*, 20(3–4): 281-296.
- Waters, A.C. and Fisher, R.V., 1971. Base Surges and Their Deposits: Capelinhos and Taal Volcanoes. *J. Geophys. Res.*, 76(23): 5596-5614.
- White, J.D.L., 1996. Impure coolants and interaction dynamics of phreatomagmatic eruptions. *Journal of Volcanology and Geothermal Research*, 74(3–4): 155-170.
- White, J.D.L. and Houghton, B., 2000. Surtseyan and related phreatomagmatic eruptions. In: Sigurdsson, H., Houghton, B.F., McNutt, S.R., Rymer H., Stix J. (Editors), *Encyclopedia of Volcanoes*. Academic Press, San Diego: 495-511.
- White, J.D.L. and Ross, P.S., 2011. Maar-diatreme volcanoes: A review. *Journal of Volcanology and Geothermal Research*, 201(1–4): 1-29.
- White, J.D.L. and Schmincke, H.-U., 1999. Phreatomagmatic eruptive and depositional processes during the 1949 eruption on La Palma (Canary Islands). *Journal of Volcanology and Geothermal Research*, 94(1–4): 283-304.

Wohletz, H., 1998. Pyroclastic surges and compressible two-phase flow. In: From magma to tephra: Modelling physical processes of explosive volcanic eruptions Edited by: Freundt, A and Rosi, M Elsevier, Amsterdam.

Wohletz, K.H. and Sheridan, M.F., 1979. A model of pyroclastic surge. In: Chapin, C.E., Elston, W.E. (Eds.), Geol. Soc. Am. Spec. Pap., 180: 177–194.

Wohletz, K.H. and Sheridan, M.F., 1983. Hydrovolcanic explosions; II, Evolution of basaltic tuff rings and tuff cones. *American Journal of Science*, 283(5): 385-413.

Zanon, V., Pacheco, J. and Pimentel, A., 2009. Growth and evolution of an emergent tuff cone: Considerations from structural geology, geomorphology and facies analysis of São Roque volcano, São Miguel (Azores). *Journal of Volcanology and Geothermal Research*, 180(2–4): 277-291.

4. EXPLOSIVE FELSIC VOLCANISM ON EL HIERRO (CANARY ISLANDS)

Submitted to:

Bulletin of Volcanology

Authors of the paper:

Dario Pedrazzi, Institute of Earth Sciences Jaume Almera, ICTJA-CSIC, Group of Volcanology. SIMGEO (UB-CSIC) Lluís Solé i Sabarís s/n, 08028 Barcelona, Spain

Laura Becerril, Institute of Earth Sciences Jaume Almera, ICTJA-CSIC, Group of Volcanology. SIMGEO (UB-CSIC) Lluís Solé i Sabarís s/n, 08028 Barcelona, Spain

Instituto Geológico y Minero de España (IGME) c/ Alonso Alvarado,
43-2010 A 35003-Las Palmas de Gran Canaria, Spain.

Joan Martí, Institute of Earth Sciences Jaume Almera, ICTJA-CSIC, Group of Volcanology. SIMGEO (UB-CSIC) Lluís Solé i Sabarís s/n, 08028 Barcelona, Spain

Stavros Meletlidis, Centro Geofísico de Canarias, IGN, Santa Cruz de Tenerife, Spain

Inés Galindo, Instituto Geológico y Minero de España (IGME) c/ Alonso Alvarado, 43-2010 A 35003-Las Palmas de Gran Canaria, Spain.

The reference of this paper is:

Pedrazzi, D., Becerril, L., Martí, J., Meletlidis, S. and Galindo, I., Submitted. Explosive felsic volcanism on El Hierro (Canary Islands). Bulletin of Volcanology.

Abstract

The Canary Islands consist of a number of complex basaltic shield edifices whose submerged portion is much more voluminous than the emerged islands. Like so many other oceanic volcanic islands, the presence of explosive felsic volcanism is not a common feature in this archipelago and has only been reported from the central islands of Gran Canaria and Tenerife, where it has been responsible for the formation of large central volcanic complexes. On the other Canary Islands, the presence of felsic rocks is mostly restricted to subvolcanic intrusions and a few lava flows, generally associated with the oldest parts of the islands. In this paper we present a detailed stratigraphic, lithological, and sedimentological study of a significant trachytic pumice deposit on the island of El Hierro, referred here as the Malpaso Member, which represents the only explosive episode of felsic composition found on the Canary Islands (apart from those on Gran Canaria and Tenerife). Four different subunits were identified on the basis of their lithological and granulometrical characteristics. The products of the eruption correspond to a single eruptive event and cover an area of about 13 km². This work provides a detailed stratigraphic and chronological framework for El Hierro Island and demonstrates the importance of an explosive eruption within an environment in which effusive basaltic activity predominates. Bearing in mind the style and the spatial extent of the Malpaso eruption, a future event with similar characteristics would have a serious impact on the population, infrastructures, and economy of the island of El Hierro.

Keywords: El Hierro, Canary Islands, phreatomagmatism, explosive volcanism, volcanic hazard

4.1 Introduction

The island of El Hierro (Canary Archipelago) is a typically complex basaltic shield volcano characterised by mainly effusive volcanism that exhibits both Strombolian and Hawaiian activity. Most of the rocks that form the subaerial succession on El Hierro are of basic composition and include, above all, basanites, basalts, and trachybasalts (Pellicer, 1975; Ballcels and Gómez, 1997; Carracedo et al., 2001). Although the presence of subordinate trachytic compositions on El Hierro has been reported by previous studies (Pellicer, 1975; Pellicer, 1977; Fuster et al., 1993; Ballcels and Gómez, 1997; Carracedo et al., 2001), its relevance in the volcanological evolution of this island has never been discussed in detail, probably because these rocks are

volumetrically subordinate to the island's mafic rocks. Felsic rocks appear as dikes and lava flows associated with the older parts of the island, where minor pumice deposits interbedded with basanitic lavas occur, above all in the upper part of the stratigraphic sequence that forms the shield edifice of El Golfo. These felsic deposits have been interpreted as normal products of the basaltic differentiation that occurs in this type of volcanic system (Carracedo et al., 2001). Radiometric ages ranging from 8.13 ± 0.06 to 3.95 ± 0.07 ka have been determined for these pumice deposits (Pellicer, 1977; Pérez-Torrado et al., 2011).

The submarine eruption that lasted from early October 2011 to the end of February 2012 about 2 km off the southern coast of El Hierro increased awareness of the possibility that felsic (i.e. more explosive) eruptions could occur on an island that is mostly characterised by mafic (i.e. less explosive) volcanism. Although this eruption mostly extruded basanitic magmas in the form of lava flows and pyroclastic fragments (Martí et al. 2013, a, b), the first observed products corresponded to lava balloons of highly vesiculated, low density aphyric white core, surrounded by a thin, highly vesiculated basanitic carapace. The white component was identified as being the result of the remobilization of a small volume of stagnant rhyolitic melt formed as the result of the incorporation of approximately 10 % quartz-rich sediment into a late differentiate magma of trachytic composition by a gas-rich basanitic melt (Meletlidis et al., 2012; Sigmarsson et al., 2013).

The fact that felsic episodes have occurred in Holocene times is significant for hazard assessment given that this island has just entered into a period of renewed activity; likewise, these episodes are particularly relevant since an explosive episode could represent a major threat to the island. In the recent geological record of El Hierro only one explosive felsic episode of trachytic composition – which would have produced pumice-rich deposits and whose characteristics are unknown – has ever been reported by previous studies (Pellicer, 1977; Balcells and Gómez, 1997; Carracedo et al., 2001; Pérez-Torrado et al., 2011).

In this study we describe a detailed stratigraphic, lithological, and sedimentological study of these pumice deposits, which we name here as the Malpaso Member. We present the field descriptions and the petrographic and granulometric data of these felsic deposits and discuss their relative age, transport/depositional mechanisms, the corresponding eruption dynamics, and implications for hazard assessment on the island of El Hierro.

4.2 Geological setting

Located 100 km off the east coast of Africa, the Canary Archipelago is composed of seven major volcanic islands and a number of smaller islets and has a total surface area of almost 500 km² (Fig. 1).

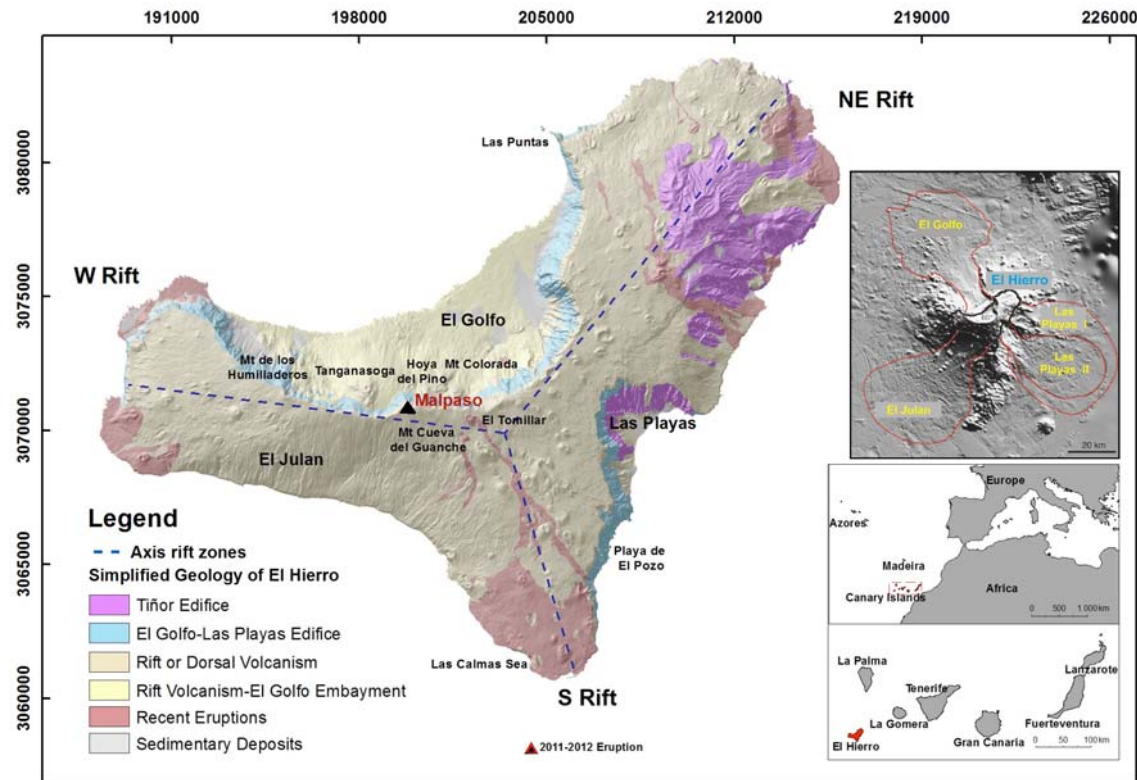


Fig. 1 Location and simplified geological map of El Hierro.

The islands are Neogene in age (Schmincke, 1982; Araña and Ortiz, 1991) and their subaerial activity began around 24 Ma (Robertson and Stillman, 1979; Le Bas et al. 1986; Marinoni and Pasquarè, 1994; Marinoni and Gudmundsson, 2000). El Hierro is the southwesternmost and smallest island in the archipelago, with an area of 269 km². It has an estimated total edifice volume (subaerial and submarine) of 5,500 km³ and rises about 5,500 m from its submarine base at a depth of 4,000 m (Schmincke, 1990). The highest point on the island is Malpaso (1,501 m a.s.l.).

With its oldest subaerial deposits dated at 1.12 Ma, this island is considered to be the youngest in the Canary Archipelago (Guillou et al., 1996, Fuster et al., 1993), Carracedo (1996) and Carracedo et al. (1998) have cited El Hierro as a classic case of a triple-armed rift system (Fig. 1) inasmuch as it is the result of three main volcanic cycles corresponding to the construction and partial destruction of successive volcanic

edifices (Guillou et al., 1996; Balcells and Gómez, 1997). The first edifice corresponds to the Tiñor volcano (1.12–0.88 Ma), the second to El Golfo-Las Playas edifice (545–176 ka) and the third to the island’s rift or dorsal volcanism (158 ka–Present time) (Fig. 1). During the island’s growth at least five debris avalanches occurred (Masson, 1996; Urgeles et al., 1996, 1997; Carracedo et al., 1999, 2001; Masson et al., 2002; Longpré et al., 2011) that notably changed its morphology. The ages of these debris avalanches range from <880 ka and 545–176 ka for the first at Tiñor and Las Playas I, and was followed by landslides at Las Playas II (176–145 ka) and El Julan (>158 ka), located at SE and at SW of the island respectively (Fig. 1). The most recent landslide corresponds to El Golfo, whose age has been recently proposed more precisely as between 87–39 ka (Longpré et al., 2011) (Fig. 1). The latest eruption took place on the submarine south rift in the sea off Las Calmas (Fig. 1) and lasted from 10 October 2011 to the end of February 2012 (Martí et al., 2013).

The geology of the island is characterised by effusive magmatic eruptions of basic composition, mainly Hawaiian-Strombolian in nature, fed by subvertical dykes (Becerril et al., 2013), combined with a number of hydromagmatic episodes (Becerril, 2009). In general the island’s eruptions have been monotonous in composition and mainly basanitic in nature (Pellicer, 1977; Carracedo et al., 2001). An example of one of the few types of felsic deposits that have been described from the island are the trachytic lava flows near Las Puntas dated by Guillou et al. (1996) at an age of 176 ka. Other trachytic lava flows are present in the east of the island, above all close to Playa del Pozo and on the uppermost part of the cliff of Las Playas (Ballcells and Gómez, 1997). Pellicer (1977) remarked on the presence of trachytic pyroclastic deposits around Malpaso (Fig. 1), which were dated by ^{14}C at an age of 6.74 ± 0.15 ka and attributed to an explosive eruption subsequent to the construction of the Tanganasoga edifice (Fig. 1). Balcells and Gómez (1997) described these deposits as laminated “surge-type” trachytic materials originating during a previous eruption of Tanganasoga. Carracedo et al. (2001) interpreted these deposits as volcanic differentiates from the terminal stages of activity of the volcano of El Golfo (176 ka) prior to the establishment of the Rift volcanism. More recently, Pérez Torrado et al. (2011) obtained ^{14}C ages ranging from 8.13 ± 0.06 to 3.95 ± 0.07 ka for charcoal located in a paleosol under these deposits and suggested that their emplacement was coeval to the construction of Tanganasoga inside the landslide depression of El Golfo.

4.3 Methods

A preliminary study and interpretation of 1:5,000-scale orthophotos was carried out to obtain a complete overview of the area, to identify possible outcrops of interest, and to discriminate the different morphologies occurring in the field. In order to understand the general geological framework of the area and to define the characteristics and extent of the deposits, we undertook extensive field mapping at 1:5,000 scale in an area covering about 13 km². The stratigraphic criteria used to distinguish different units included primarily sedimentary structures and the apparent component content (juvenile and lithic fragments), as well as characteristics such as grading, colour, and sorting. Nomenclature used in the text for bed thickness, grain size, and sorting of the pyroclastic deposits follows the one proposed by Sohn and Chough (1989).

In all, 152 stratigraphic sections were measured and used to document the geometry of the deposits and their component proportions (Online Resource 1). Maximum clast sizes and thickness of the units were measured to create isopleth and isopach maps; sections with eroded tops were not considered for calculations. All data were managed and processed using the software ARCGIS 10.0 by ESRI and Surfer 7. To obtain volumetric data from the maps we used Kriging interpolation technique by Surfer 7.

The geographical coordinates of relevant locations, as well as the stratigraphic sections and sampling points, were recorded using a portable GPS to a precision of about 3 m (additional data are given in Online Resource 1). The reference zone used was the UTM projection Datum: D_WGS_1984, zone 27–28N.

Binocular and electron microscopes were used to determine the main petrographic and textural characteristics of the juvenile components. As well, pumice particles ~125µm diameter from each unit were analysed with the scanning electron microscope (SEM, QUANTA 200-FEI) at the University of Barcelona (UB) to discriminate the magmatic-phreatomagmatic mechanism of the eruption. In addition petrographic analyses were carried out in order to identify the mineralogy and general composition of the studied deposits.

The most representative levels of each stratigraphic unit were sampled and analysed (11 samples in total) for grain-size distribution and componentry. Grain-size analysis was performed by dry sieving at 1Φ (phi) with sieves with aperture sizes

ranging from 32 to 1/32 mm (-5Φ to 5Φ). The weight percentages of the sieved fractions were calculated and then plotted as cumulative curves to give grain-size distribution and the Inman parameters (median grain size, $Md\Phi$ and the Inman sorting coefficient, $\sigma\Phi$). The proportion of juveniles from -5Φ to 0Φ was defined by hand picking and from 0Φ to 5Φ using a binocular microscope and image analysis techniques (e.g. ImageJ software).

4.4 Stratigraphy

The studied deposits (Malpaso Member) form a succession of pyroclastic units of variable thickness ranging from 3 to 81 cm and are exposed around the area of Malpaso (1,500 m a.s.l.) (Figs. 2–3), the highest point on the island of El Hierro.

These deposits overlie unconformably previous massive-to-stratified Strombolian scoria fall deposits and lava flows originated from the uppermost part of the edifice of El Golfo (Carracedo et al., 2001). They are discontinuously covered by younger lava flows and by later deposits from the volcano Tanganasoga and other nearby vents, all of which are constructed inside the embayment of El Golfo (Fig. 2).

Well-developed paleosols have formed at the base and top of the studied sequence, indicating that a significant period of time elapsed between its deposition and previous and posterior eruptive events.

Figure 2 shows the stratigraphic correlation among 8 synthetic stratigraphic columns constructed around the whole area. In the central sector of the study area, close to Malpaso (Column 1 and 2; Fig. 2), the Malpaso Member lies above a paleosol developed on older mafic Strombolian deposits, and consists of a lithic-rich pumice deposit directly overlain by the Tanganasoga deposits (Column 8; Fig. 2). Beyond the headwall of the landslide at El Golfo, on the northern flank of El Hierro, the Malpaso Member could not be identified. In the eastern area (Column 3,4,5, Fig. 2) a series of Strombolian deposits – including material from Montaña Cueva del Guanche, probably corresponding to the vents located inside the embayment of El Golfo (e.g. Hoya del Pino and Montaña Colorada) (Fig. 2) – and a lava flow originating from El Tomillar, overlie the Malpaso Member. The southern sector is mainly covered by lava flows and subordinate Strombolian deposits (Column 6 and 7, Fig. 2). The western side of the area shows a similar sequence with Strombolian deposits of magmatic and hydromagmatic origin covering the Malpaso Member (Column 8, Fig. 2).

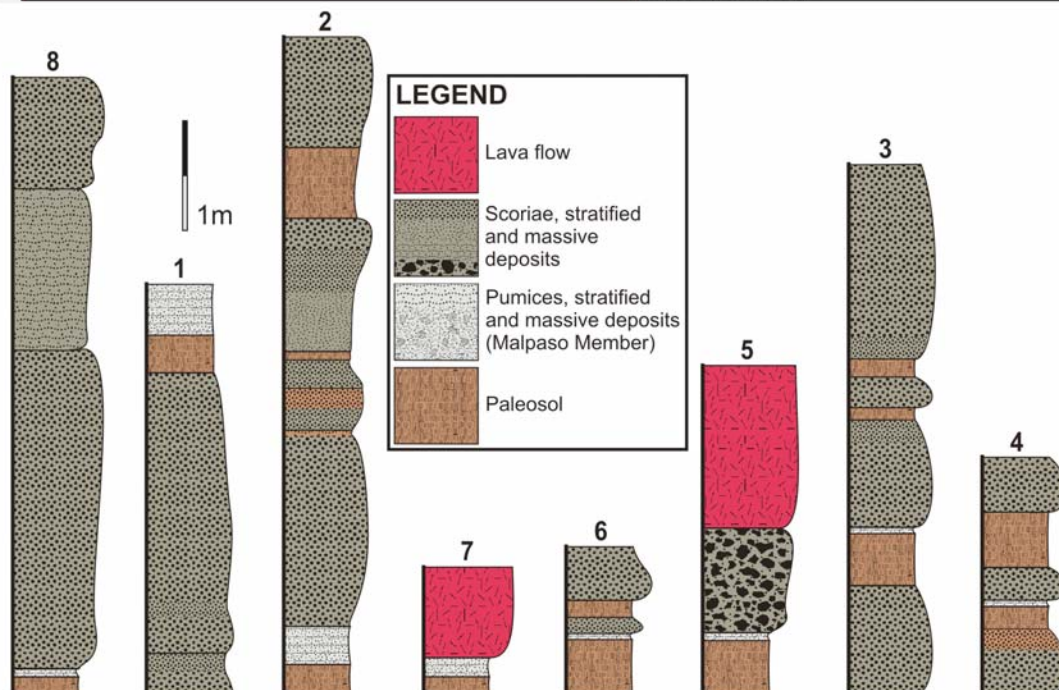
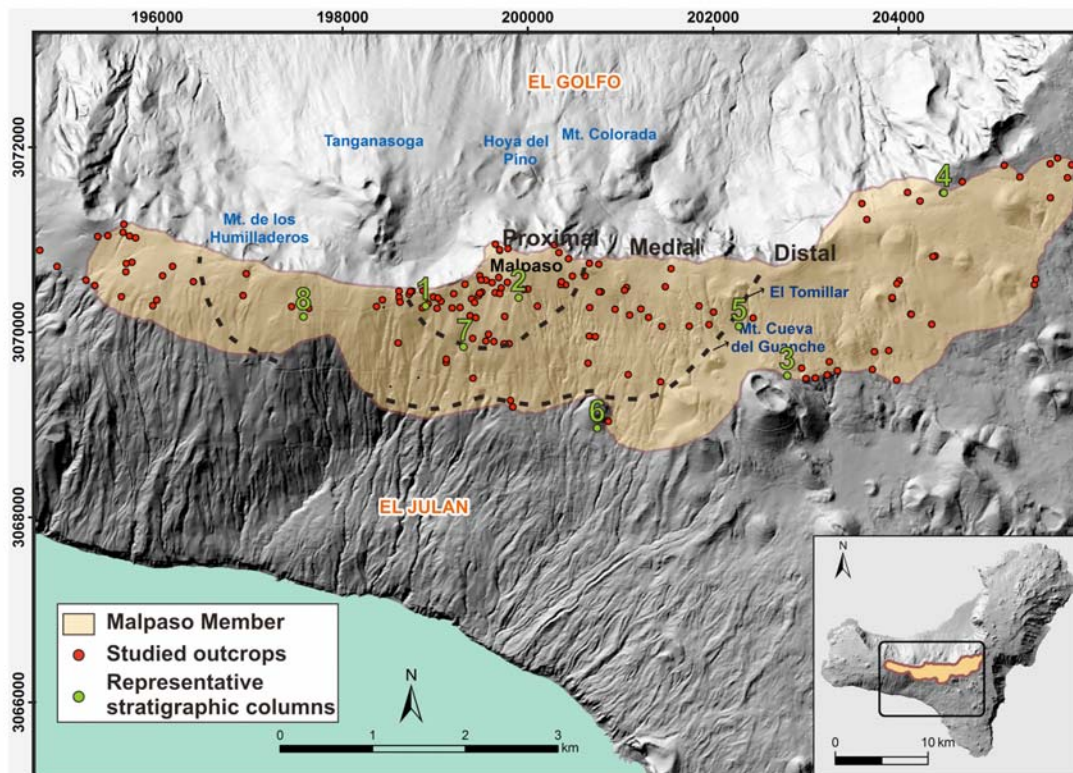


Fig. 2 Aerial distribution of the Malpaso Member deposits, with all the studied outcrops indicated. Selected stratigraphic columns showing the field relationships between the Malpaso Member and the older and younger deposits are shown as well.

The Malpaso Member consists of different units (Fig. 3) with no field evidence of any temporal hiatus. These units cover the whole of the terrain in the Malpaso area (Fig. 2) and tend to thicken in depressions and valleys. Investigated in 152 outcrops (Fig. 2), these deposits extend mostly in a southeastern direction, reaching a maximum

distance of ≥ 2.5 km from the peak of Malpaso (Fig. 2). Simplified stratigraphic sections from 11 key localities are shown in Figure. 3.

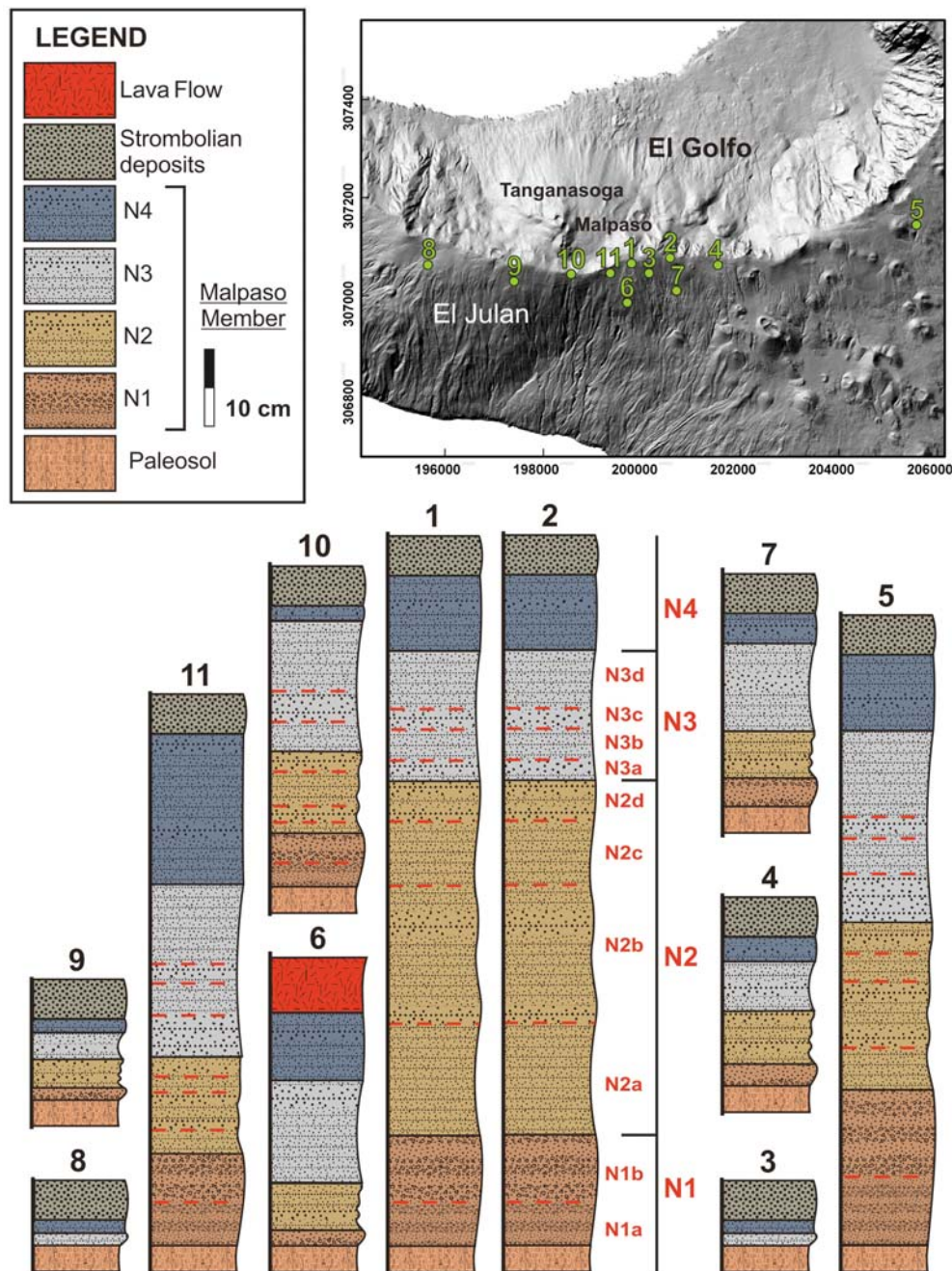


Fig. 3 Detailed stratigraphic sections of the Malpaso Member and its different units and subunits. See text for further details.

The area was divided into proximal (0-1 km), medial (1-2.5 km) and distal zones (≥ 2.5 km) based on thickness and grain size characteristics of the deposit (Fig. 2). The maximum observed thickness of the entire succession lie in the range 40–81 cm at Malpaso and 3–5 cm in the most distal outcrops (≥ 2.5 km). Some apparently anomalously thick values occur inside some channels and depressions. We divided the

Malpaso Member into four units (from base to top: N1, N2, N3, N4) in terms of their lithological and sedimentological characteristics (Fig. 3 and 4) that can be recognised throughout almost all of the area covered by these deposits.

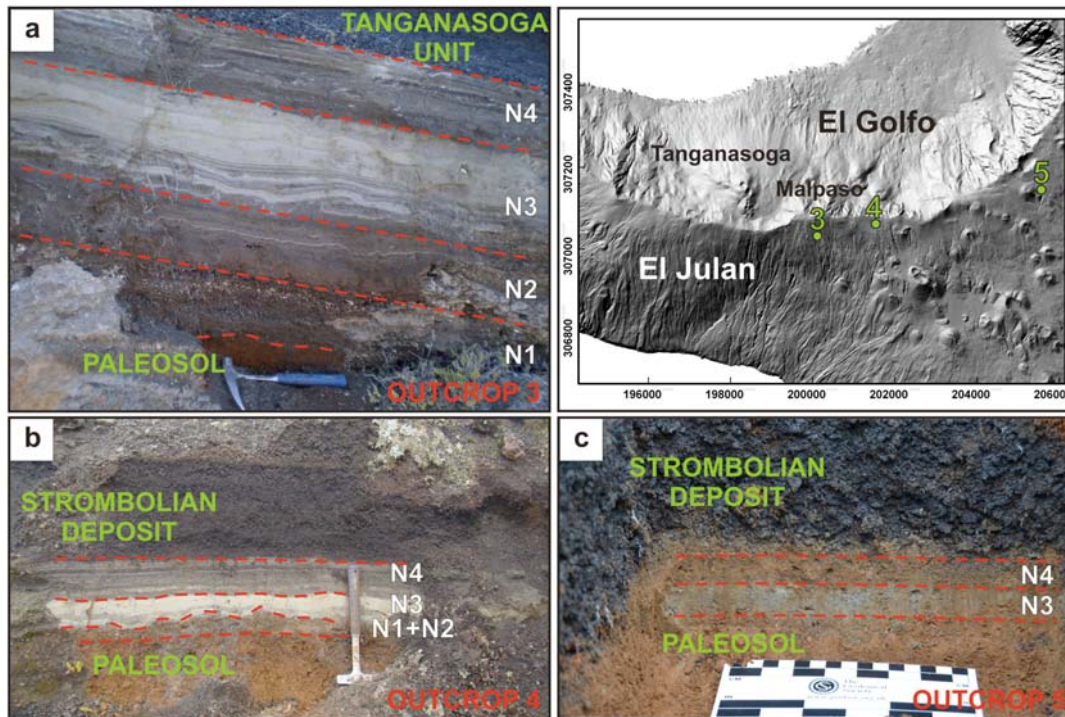


Fig. 4 Field photographs of the Malpaso Member deposits at (a) proximal, (b) medial, and (c) distal outcrops.

4.4.1 Unit N1

This unit is up to 21-cm thick (Figs. 3 and 4) and is composed mainly of well-sorted, clast-supported, pumice thin lapilli beds alternating with matrix-supported, poorly stratified thin beds of fine lapilli/ash with well-defined boundaries (Fig. 4). The pumice is light grey in colour and has small vesicles (millimetric to submillimetric in size) and lithic clasts consisting mainly of lava fragments. The base of Unit N1 is erosive as observed by the interaction with the underlying topography (Fig. 4a,b). Unit N1 rests directly on a paleosol that, according to radiocarbon ages given by Pellicer (1977) and Pérez Torrado et al. (2011), was dated as 6.74 ± 0.15 ka BC or 8.1 ± 0.06 ka BP, respectively. To the north, south, and east N1 thins out rapidly to just a few centimetres.

Two subunits are distinguishable: N1a and N1b (Fig. 3). N1a at Malpaso reaches a maximum thickness of 8–10 cm and has alternated centimetric clasts supported pumice lapilli (< 1 cm) very thin beds and ash-rich 1–2-cm beds. Lava lithic fragments

reach up to 2 cm in size. N1b is similar but shows a remarkable increase in the size of pumices, which reach up to 10 cm in diameter. N1 is similar in the proximal zone (0-1 km) than in the medial zone (1-2.5 km) (Figs. 2, 3 and 4b) and the distinction between the two subunits is unclear; at greater distances (≥ 2.5 km; Fig. 2) the subunits are thinner and finer-grained making almost impossible to separate them (Fig. 4c).

4.4.2 Unit N2

This unit has a maximum thickness of about 20 cm (Fig. 3). It consists of poorly stratified, dark-brown, matrix-supported thin ash beds with some interbedded very thin beds that are up to 5-mm thick of lapilli-rich poorly vesiculated pumices (Fig. 4a), which contain lava lithic clasts of the same size. At proximal exposures (0-1 km; Fig. 3) it is possible to differentiate four sub-levels (N2a, N2b, N2c, and N2d). N2a is made up of 1–2-mm thick ash-rich laminae that progressively increase in grain size and merge into the up-to-5-mm thick lapilli-rich beds that form N2b. The same pattern is repeated for sub-levels N2c and N2d. Lithic fragments reach a maximum size of 5 mm in the lapilli-rich layers. At more distal exposures (Figs. 2 and 4b), it becomes harder to distinguish the different sub-levels, which progressively fade away (Fig. 4c) until they disappear completely.

4.4.3 Unit N3

Within the area around Malpaso (Fig. 2), Unit N3 shows an apparent massive aspect but it is predominantly composed of stratified thin ash beds with a maximum total thickness of 25 cm (Figs. 3 and 4). Minor fine-grained lapilli beds up to 5-cm thick are interbedded with individual very thin ash beds in its lower part. Loose lava lithic clasts are also recognisable. N3 is lighter in colour than N2 and there is a clear contrast at the contact zone (Fig. 4a). Four sub-levels, N3a, N3b, N3c, and N3d, are identifiable in the proximal outcrops (0-1 km; Fig. 2) although in the outermost distal zone (≥ 2.5 km; Fig. 2) the various sub-levels disappear and become a single fine-grained very thin (2–3 cm) massive bed (Fig. 4c). N3a consists of lithic-poor finely stratified ash-rich beds with subordinate cross-bedded undulate millimetric very thin lapilli-rich beds with loose millimetric lava lithic clasts; N3b is more massive, lithic-poor, homogeneous, and ash-rich, although with a few coarse-grained interbedded horizons; N3c and N3d follow the same pattern with a general decrease in grain size from lapilli to ash-rich beds. In intermediate zones (1-2.5 km; Fig. 2) N3 is perfectly visible with the same characteristics (Fig. 4b) as in the proximal outcrops although tends to be massive (Fig.

4c) with poor evidence of cross-bedded structures in the most distal outcrops (≥ 2.5 km.; Fig. 2).

4.4.4 Unit N4

This unit is up to 20-cm thick (Fig. 3) in the proximal outcrops (0-1 km; Fig. 2) and is composed of ash and lithic-rich lapilli thin beds. Abundant lithic clasts from older lava flows, millimetric to centimetric in size, are found throughout the entire unit and give it a characteristic gray-black colour (Fig. 4a). Some loose, white-coloured beds (like unit N3 in appearance) are also present. N4 is either normally or reversely graded with coarse- and fine-grained stratifications. At intermediate distances (1-2.5 km; Fig. 2) N4 is still perfectly recognisable because it has the same characteristics as in the proximal outcrops (Fig. 4b); nevertheless, in most distal exposures (≥ 2.5 km; Fig. 3) it is 1–2-cm thick before it becomes a massive layer (Fig. 4c).

4.5 Isopach and Isopleth maps

Isopach and isopleth maps of the Malpaso Member (Fig. 5) were obtained from the field data.

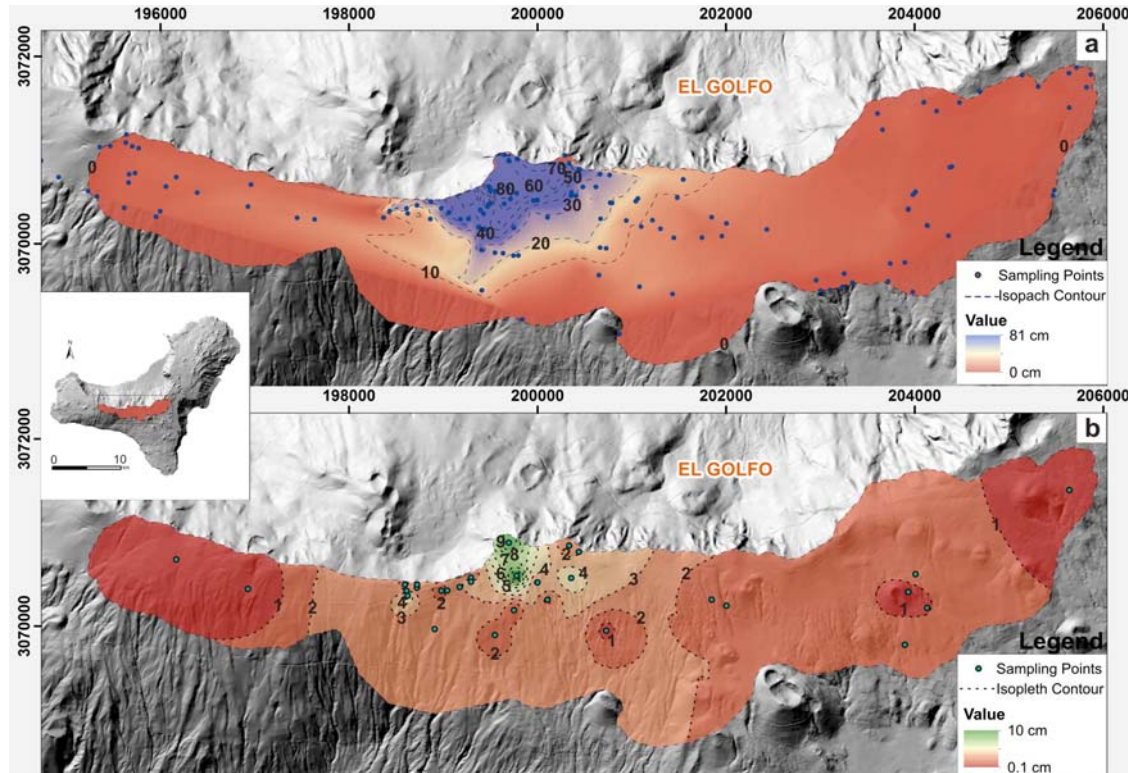


Fig. 5 a) Isopach map showing the variations in thickness of the Malpaso Member; b) Isopleth map of the distribution of the average maximum pumice-clast diameter (cm) in level N1 in the Malpaso Member.

The isopach map was computed using 134 sections that illustrate that the thickness of the deposit changes sharply over short distances. This map enabled us to calculate the area of the deposit at 13 km² with a volume of about 1.81·10⁶ m³ using kriging with Surfer 7. The isopleth map was based on 30 measurements of the five largest pumice clasts in level N1 in the study area. The largest pumice clast, 10 cm in diameter, was found in the Malpaso area. The pumice diameter represented on the isopleth map ranges from <1 cm to the maximum diameter measured.

4.6 Componentry characteristics and grain size distribution

The vertical variations in grain size distribution and componentry of individual beds are described in Figure 6 and Figure 7. They show median grain size (Md Φ ,) and sorting ($\sigma\Phi$) parameters, as well as a comparison between F1 (wt% <1 mm diameter) and F2 (wt% <1/16 mm diameter). Juvenile pumice fragments, free crystals, and accidental lithic fragments (mostly derived from older lava flows) can be distinguished in each class size. Modal components are unevenly distributed among the various grain-size fractions and the different subunits. Although all the samples belonging to N1 have the same component distribution with crystals and lithic fragments increasing in percentage in the 1 Φ –5 Φ size range, the pumice component typically has a wider range of sizes (Fig. 6). The total amount of juvenile fragments (pumices and free crystals) ranges from 60% (N1BF) to a maximum of 75% (N1BG). N2 samples are not significantly different and the percentage of juvenile fragments is around 70%. As in the N1 subunits, this same trend is noticeable in N2 and crystals and lithic fragments increase in proportion in the greatest Φ size range. Compared to the previous units, Unit N3 is significantly different. Sample N3A taken from the lowest part of the unit exhibits the same trend as in previous units, with a c. 65% content of juvenile fragments. However, this content increases in the upper part of the unit as the obvious change in colour from dark-gray to light-gray occurs; on the other hand, samples N3C and N3D have juvenile fragment content of around 90% and of free crystals of about 25%. The contact with the following unit (N4) is marked by a clear change in colour from light grey to dark brown. This variation in color may be due to an increase in lithic clasts with total values of 55–60% with a constant percentage throughout almost all of the range in grain sizes.

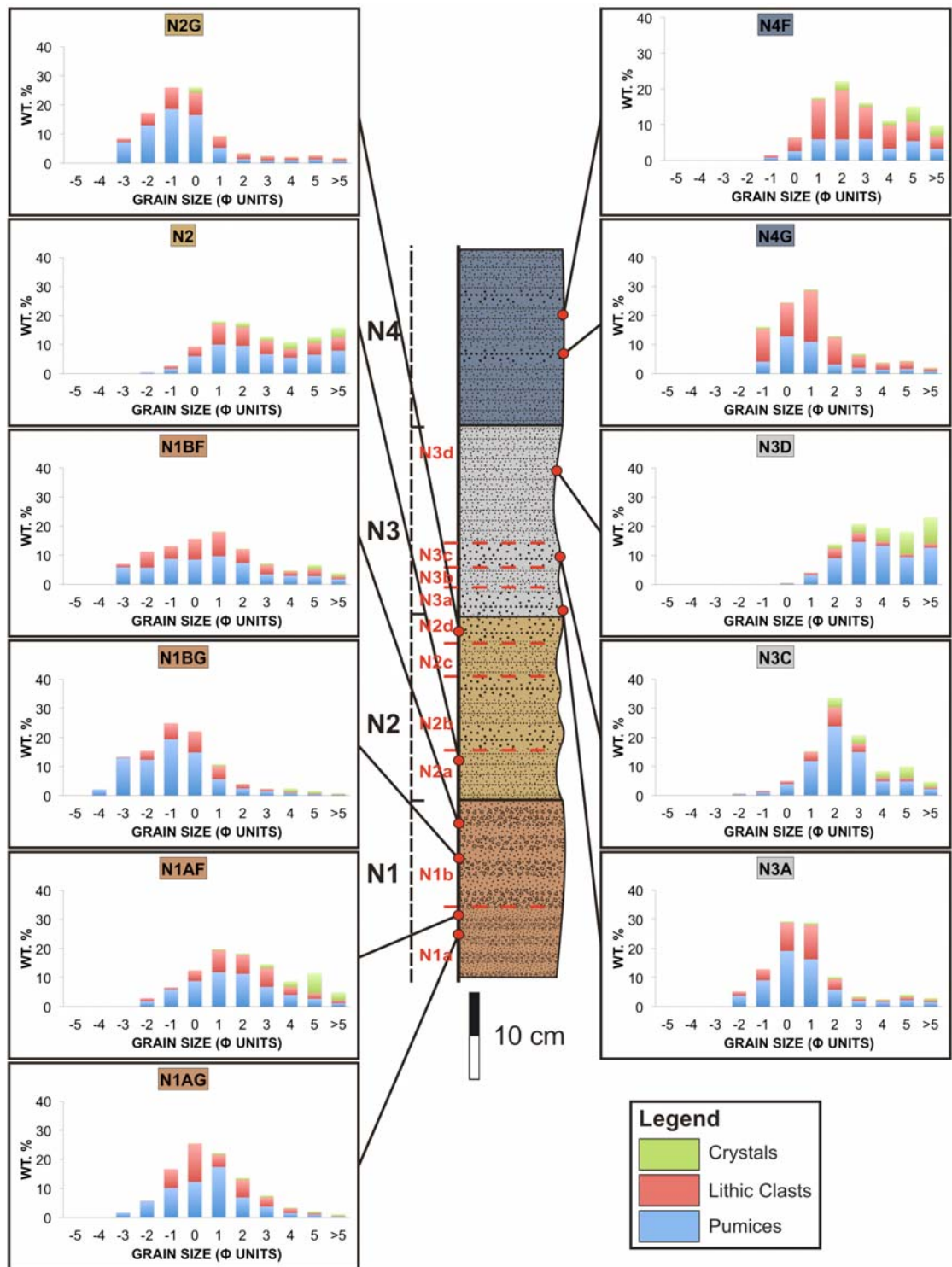


Fig. 6 Grain-size distribution and modal composition of representative samples from the Malpas Member. N1: pumice lapilli layers alternating with poorly stratified ash layers; N2: ash layers with loose pumice-lapilli-rich layers; N3: massive poorly stratified ash beds with interbedded lapilli layers; N4: ash and pumice-rich lapilli layers with abundant lava lithic clasts. The different sublevels (e.g. N1a) are indicated.

In terms of grain size distribution, the two subunits (N1A and N1B) that conform the basal unit (N1) of the Malpas Member are characterised by an alternation

of ash and lapilli layers and a general increase in grain size in the lapilli layers towards the upper part of the unit (Fig. 6).

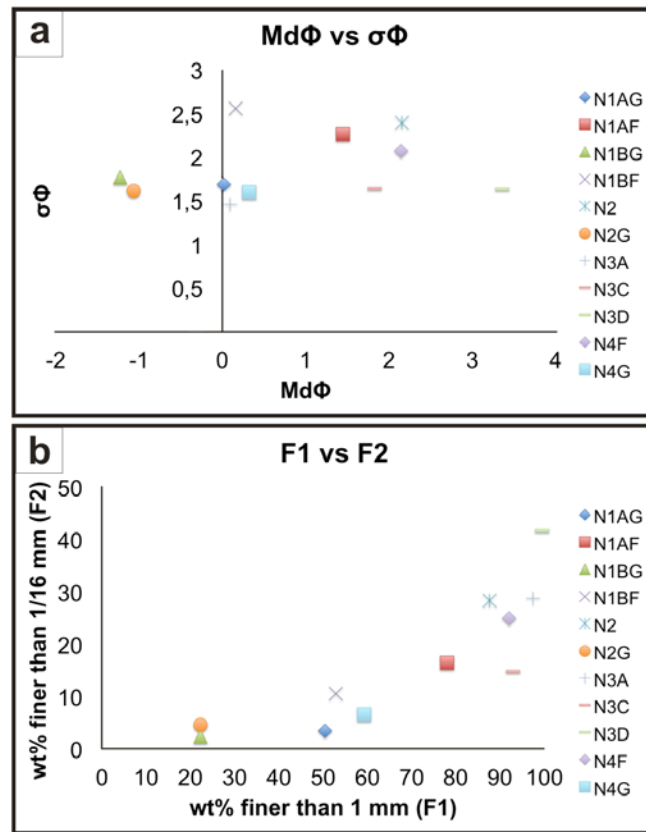


Fig. 7 a) graphic standard deviation versus median diameter; b) F2 (wt% < 1 mm diameter) versus F1 (wt% < 1/16 mm diameter).

Both subunits are characterised by well-sorted unimodal (N1AG and N1BG) and poorly sorted polymodal (N1AF and N1BF) samples with $\sigma\Phi$ values ranging from 1.68 to 2.55 (Fig. 7a). N1AG and N1BG are characterised respectively by 3% and 2% of fine ash (<63 μm). N1AF and N1BF show an increase in the amount of fine ash with 16% and 11% in weight, respectively (Fig. 7b). Two representative samples (N2 and N2G) from Unit N2 with similar characteristics as those from Unit N1 layers were analysed: N2 is a polymodal poorly sorted fine-ash-poor sample ($\sigma\Phi=2.39$), with 28% by weight of fine ash, whereas N2G is well sorted, unimodal with $\sigma\Phi=1.61$ and 4.6% of fine ash. The N3 subunit is the most distinguishable unit in the field due to its peculiar white/grey colour. Three representative samples were considered for grain size analysis: N3A from the first subunit and N3C and N3D from the second (Fig. 7). N3A and N3C are well-sorted, lapilli-ash samples with $\sigma\Phi$ values in the range 1.46–1.63 (Fig. 7a). N3D is a well-sorted sample mainly made up of ash with $\sigma\Phi$ values reaching 1.63 (Fig. 7a). N3D is richer in fine ash (41%) than subunit N3A (28%) and N3C (14%) (Fig. 7b). Unit N4

is mainly made up of ash, although some lapilli-rich horizons can also be found toward its upper part. As observed in Figure 7a,b, N4F is a polymodal, poorly sorted ($\sigma\Phi=2.06$) ash-rich layer with 25% by weight of fine ash, while N4G is a unimodal, well-sorted ($\sigma\Phi=1.59$) lapilli-rich layer with 6.5% of fine ash.

4.7 Morphology of the juvenile material

The morphology of juvenile clasts $\sim 125 \mu\text{m}$ in diameter was examined with the electron microscope (SEM) in order to discriminate between purely magmatic and phreatomagmatic fragmentation processes during the Malpas Member formation.

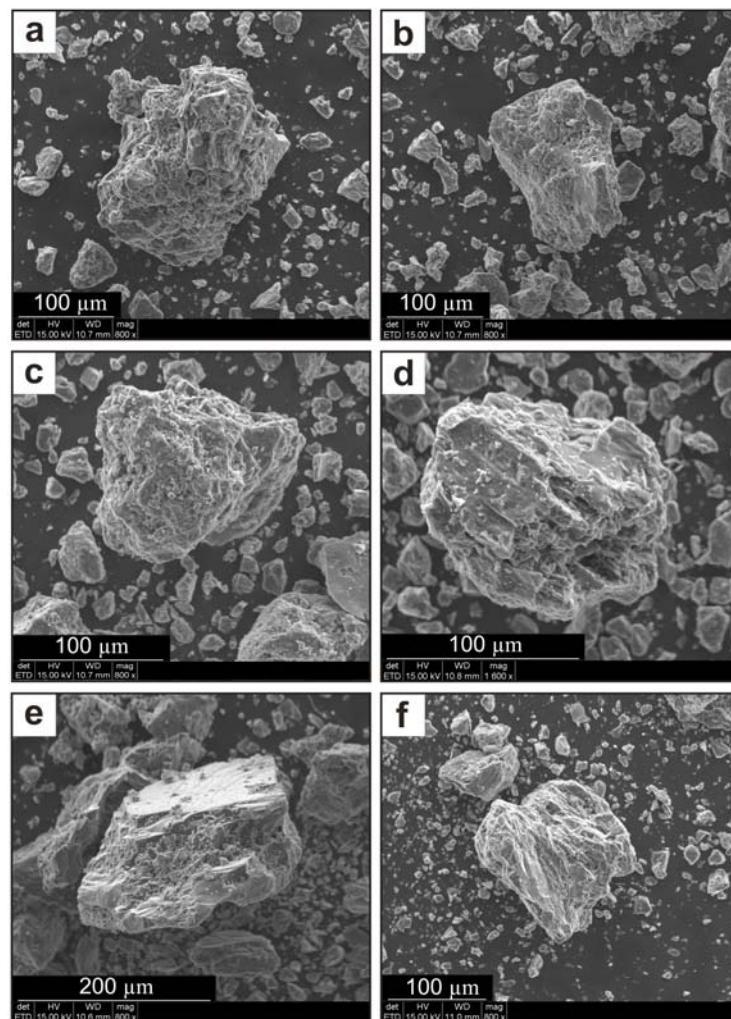


Fig. 8 Scanning electron microscope (SEM) images of pumice from Units 2, 3 and 4. Clasts show little abrasion due to transport. Several examples of the most typical morphological features are shown. (a-b): poorly vesiculated particles from Unit N2 with mainly blocky morphologies; (c-d): poorly vesiculated clasts from Unit N3 with tiny adhering particles and elongate vesicles; (e-f): dense and poorly vesiculated grains with blocky morphology, quenching crack structures and stepped textures.

Texturally, individual particles in levels N2–N4 are subangular with spherical forms tending to have blocky and stepped morphologies with poor or no vesicularity

(Figs. 8). Fine particles (<32 μm) commonly adhere to larger surface fragments as dust (Fig. 8c). Another characteristic feature of these particles is the presence of quenching cracks (Fig. 8e).

Knowledge of certain morphological and textural features of the particles can help to resolve whether the eruption mechanisms were purely magmatic or hydromagmatic due to magma-water interaction. In particular, blocky shapes, low vesicularities and glass shards, although not unique to, are characteristic of eruptions in which water intervenes (Wohletz, 1983; Heiken and Wohletz, 1985). Another common feature of hydrovolcanic eruptions is the presence of micron-sized dust particles adhering to the fragment surfaces and aggregate multicomponent particles (Wohletz, 1983; Heiken and Wohletz, 1985).

4.8 Mineralogy

Juvenile components have identical mineralogy that suggests a trachiphonolitic composition throughout the whole Malpaso Member but there are variations in texture between units.

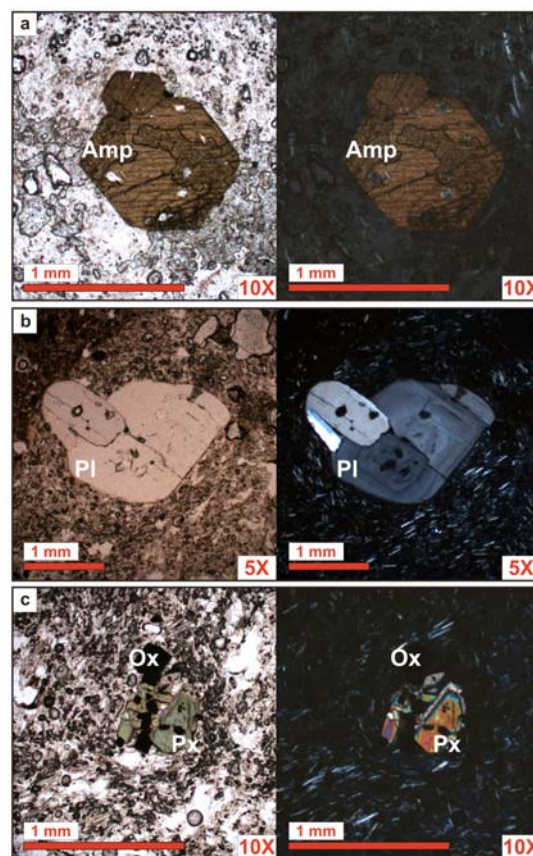


Fig. 9 Petrographic composition of juvenile samples from the eruption: a) Amphibole, b) Plagioclase, c) Pyroxene and oxide.

Pumice fragments are porphyritic, with 25–30% of phenocrysts in volume that are surrounded by a glassy groundmass with a variable amount of vesicles of different sizes ($6 < 0.05$ mm) and forms (elongated and spherical). The mineral assemblage consists of euhedral-to-subhedral plagioclase, amphiboles and, to a lesser extent, clinopyroxene (Fig. 9). The same phases were also found in the groundmass, along with oxides and glass. The maximum size of the phenocrysts is 2.5 mm (plagioclase) and 2 mm (amphiboles).

4.9 Discussion

4.9.1 Eruption and emplacement of the Malpaso Member

The Malpaso Member covers an area of approximately 13 km² (Fig. 2), almost 5% of the total area of El Hierro Island. Calculations of the volume of the exposed deposit is about $1.81 \cdot 10^6$ m³. However, its original extent and volume was significantly larger since most of the original deposits have been removed by subsequent erosion, in particular during the landslide at El Golfo. The stratigraphic relationships and distribution of the Malpaso Member demonstrate that it was emplaced before this landslide occurred (87-39 Ka; Longpré et al., 2011) as it is clearly barren by this sector collapse. Consequently, the mapped distribution of the Member does not represent its original extent. Despite these practical limitations, variations in distribution and thickness can still be observed suggesting an emplacement direction spreading radially from the vent.

The stratigraphic, lithological, and sedimentological characteristics of the Malpaso Member suggest that it corresponds to the products of a single eruptive event with several pulses of PDCs (Pyroclastic Density Currents) generation.

The presence of subrounded/rounded pumice clasts, as well as lateral variations in thickness and sedimentary features such as undulate deposits, tendency to fill channels of the pre-eruptive surface on outcrop scale, and the poor sorting and polymodality of grain size curves, might be indicative of a lateral flow component of transport. The very low aspect ratio and regular thickness decaying with distance are consistent with an origin from a dilute, turbulent pyroclastic density current. Furthermore, thinning and fining of the deposits from proximal to distal locations indicate a base surge in which concentration decreased down-current (Sohn and Chough, 1989; Dellino et al., 2004a,b).

Grain-size data [median diameter ($Md\Phi$) and sorting ($\sigma\Phi$); Fig. 7a] and the F1 vs. F2 diagram of Walker (1983) (Fig. 7b) support the idea that the Malpaso Member was formed by PDCs currents although some grain size histograms seem describing fallout deposits (N1AG, N1BG, N2G, N4G; Fig. 7a). These samples refer to the thin coarse-grained layers observed throughout the sequence but field evidence such as rounding of pumice, and lateral changes of texture and thickness on local scale, allow the distinction from fall deposits. Furthermore, a granulometrical shift toward finer values from an increasing distance from the vent is observed for the same deposit, in accordance with the sequential fragmentation/transportation model of grain-size distribution of Wohletz et al. (1989). This is due to a selective transportation mechanism related to turbulent suspensions.

The four recognized units (N1, N2, N3, N4) marked different phases of the eruption and can be interpreted in terms of changing of eruptive dynamics and of the transport and depositional systems.

Unit N1 is characterized by an alternation of centimetre beds of well sorted fines-poor pumice lapilli and poorly sorted ash layers. This unit is characterised by a visible difference in grain size and sorting between the lapilli and ash-rich layers (Fig. 3 and 4) and could be interpreted as the result of either an unsteady pyroclastic surge or multiple, closely spaced events (Dellino et al., 2004a). These types of deposits resemble the type 1a deposit described in Palladino and Simei (2002). Deposition from dilute, turbulent suspensions commonly produces normally graded beds or ungraded beds for high depositional rates. Prolonged, unsteady currents may also produce multiple graded deposits by progressive aggradation (Branney and Kokelaar, 1992). These deposits, thus, might be the result of sedimentation from a turbulent and low concentrated unsteady current with direct suspension sedimentation. As proposed by Fisher (1966), deposition occurs progressively during the passage of the current.

Unit N2 shows similar characteristics respect to N1, but it is made of matrix-supported thin ash beds with interbedded very thin beds of fine pumice lapilli. Lapilli-poor layers with thin internal laminations could be indicative of a relatively slow deposition rate resulting in grain segregation, whereas lapilli-rich layers with crude associated stratification might be the result of rapid deposition from suspension with little traction (Arnott and Hand, 1989).

Unit N3 looks massive but it is characterized by stratified thin ash beds and minor fine-grained lapilli beds. This unit can be interpreted as pyroclastic surge deposits

based on plane parallel and low-angle cross laminations. The lower part of Unit N3 is characterized by minor fine-grained lapilli interbedded with individual very thin ash beds, which might reflect the presence of a turbulent and unsteady current with deposition, under a tractive regime passing to a slower sedimentation rate as reflected by the presence of the finer-grained beds. Some ash layers have variations in lateral thickness, as well as in cross-bedding and undulating structures. The existence of these structures may be the result of variations in the flow regime (Valentine and Fisher, 2000) and in particle concentration (Sohn and Chough, 1989; Sohn, 1996).

Unit N4 is composed of ash and lithic-rich lapilli thin beds where each alternation between coarse and fine-grained layers could be interpreted as deposits emplaced from a single surge (see Sohn and Chough, 1989; Dellino et al., 2004). These alternating fine and coarse grained beds might be the result of deposition under a tractive regime. As proposed by Valentine (1987) a turbulent pyroclastic current tends to develop stratification by particle sizes and densities to form a more concentrated dispersion towards the base.

Pyroclastic density currents (PDCs) might be associated with either magmatic or phreatomagmatic fragmentation (e.g. Cas and Wright, 1987; Carey, 1991; Branney and Kokelaar, 2002). The lithological and stratigraphic variations shown by the Malpaso Member units imply that the eruption responsible for the emplacement of these deposits was continuous but had several pulses.

Based on field evidences (thinly laminated, fine- and coarse-grained beds) (Fig. 4), grain size and componentry of deposits (fine-grained, negatively skewed grain size distribution, high lithic content; see Self and Sparks, 1978; Barberi et al., 1989) (Fig. 6) and textural features of the juvenile fragments (shape of the fragments; presence of quenching cracks and fine adhering dust on particle surfaces; see Heiken and Wohletz, 1985; Buttner et al., 1999; Buttner et al., 2002) (Fig. 8), it is possible to assume that magma/water interaction played a major role in the dynamics of the eruption.

The absence, in general, of any fall deposits at the base of each unit, rules out the possibility of a column collapse and supports the idea that most of the studied deposits were formed directly from base surges radially expanding from the vent during vulcanian-type explosions with no rise of any sustained convective column.

The N1 (Figs. 3 and 4) with a total amount of lithic clasts (35–40%) (Fig. 6) – consisting of lava fragments – suggests that significant erosion of the conduit might have occurred during the first phase of the eruption. Within the N2 unit (Figs. 3 and 4)

layers are more massive and fine-grained, reflecting a better efficiency in the magma-water interaction with an increase in the energy of the explosions (e.g. Wohletz, 1986). Magma/water interaction is supported by the occurrence of accidental lithics (30%) (Fig. 6) and textural surfaces of juvenile fragments (Fig. 8). The transition from N2 to N3 seems gradual, although the evident change to a lighter grey colour in N3 (Fig. 4) reveals a rapid decrease in lithics of around 10% (Fig. 6). The lithological features of the deposits in N3 (extremely fine grained tephra) suggest efficient fragmentation of the magma although the presence of only a few accidental lithics hint at the secondary role played by magma/water interaction during this phase of the eruption. Furthermore, the absence of fall deposit at the base of N3 beds rules out the possibility of a gravitational collapse from a sustained column. This type of deposits might be associated with sharp increases in magma discharge and/or changes in upper conduit-crater geometries as observed in the case of Mt. Pinatubo (Hoblitt et al., 1996), Greenish eruption of Somma-Vesuvius (Cioni et al., 2003a), Montserrat (Formenti et al., 2003), or Pollena (Sulpizio et al., 2005).

Hydromagmatic activity characterised the final phase of the eruption. A clearly defined limit marks the change from N3 to N4 and a rapid change in the overall aspect of the deposit (Fig. 4). The lithology (lava lithics up to 55–60%) (Fig. 6), bedding characteristics (ash layers, generally with lapilli-rich horizons toward the upper part of the unit) (Fig. 4) and textural characteristics (Fig. 8) of N4 reflecting the great efficiency of the magma-water interaction (e.g. Wohletz, 1986).

As proposed by Sulpizio et al. (2005), the presence of lithic-enriched layers might not be indicative of magma/water interaction, but it might reflect the clearing of the conduit and restoration of the pristine magma discharge conditions. In such cases, density of the erupting mixture increases due to incorporation of large amounts of cold and heavy lithics. However, we can exclude this possibility because the lithic-enriched layers are associated with textural, stratigraphic and grain-size features suggesting that magma/water interaction exerted the main control on magma fragmentation during the eruption.

4.9.2 Age of the Malpaso Member and of the landslide at El Golfo

The authors who have mentioned the presence of the trachytic pumice deposit on El Hierro have offered contrasting explanations for its origin, significance, and age. Pellicer (1977) attributed this deposit to an explosive eruption subsequent to the

Tanganasoga eruption (dated at 6.74 ± 0.15 ka), whilst Balcells and Gómez (1997) described this deposit as a laminated “surge-type” deposit originating during an eruption that predates Tanganasoga. Carracedo et al. (2001) assumed that this deposit represents later evolutionary stages of the El Golfo volcano construction, thereby interpreting it as a pre-El Golfo sector collapse dated around 176 ka. Finally, Pérez Torrado et al. (2011) dated a paleosol at the base of the pumice deposit at 8.13 ± 0.06 ka attributing the overlying deposit to Tanganasoga.

Given the new stratigraphy described in this paper, the dates hitherto ascribed to this deposit and their interpretations do not match the stratigraphic position of the Malpaso Member. Bearing in mind that Tanganasoga and other vents (e.g Hoya del Pino, Montaña Colorada) postdate the landslide of El Golfo, and that their deposits cover the pumice products, no stratigraphic evidence exists to support the idea that the Malpaso Member was associated with Tanganasoga or to any subsequent eruption. Therefore, stratigraphically speaking, the Malpaso Member must belong to the final episodes in the construction of the composite El Golfo volcano, as has been suggested by Carracedo et al. (2001). However, between the deposition of the Malpaso Member and the deposits on Tanganasoga there is no paleosol that could indicate any significant time lapse between the two events. This implies that the eruption of the Malpaso Member, the landslide of El Golfo and the eruption (and construction) of Tanganasoga occurred sequentially in a relatively short period of time. Furthermore, it is also possible that the eruption of the Malpaso Member was the impulse behind the landslide of El Golfo. The construction of Tanganasoga could correspond to a volumetrically significant post-collapse eruptive episode that was triggered by the decompression of the deep magmatic system caused by the massive removal of part of El Golfo. This matches well with the model proposed by Manconi et al. (2009) and similar successions of events that have occurred after the formation of volcanic landslides on other oceanic volcanic islands (Lipman et al., 1990; Presley et al., 1997; Hildenbrand et al., 2004).

These stratigraphic constraints also generate an inconsistency with published data regarding the date of the landslide at El Golfo. Using radio-isotopic dating this event has been established as occurring between 134 ± 4 and 21 ± 3 ka (Guillou et al., 1996; Széreméta et al., 1999; Carracedo et al., 1999, 2001); on the other hand, marine geological studies, primarily concerned with the age of turbidite deposits associated with the massive landslide avalanche, give a younger age of 17–13 ka (Masson, 1996; Urgelés et al., 1997; Masson et al., 2002). A more recent study using new radio-isotopic

data from pre- and post-landslide materials from El Golfo valley dates the event at between 87 ± 8 and 39 ± 13 ka (Longpré et al., 2011). However, if the emplacement of the Malpaso Member took place between 8.13 ± 0.06 and 3.95 ± 0.07 ka – as suggested by Pérez-Torrado et al. (2011) – and given that it clearly predates the formation of the landslide on El Golfo (as demonstrated in this study), the age of this destructive event must be at least the same as that of the Malpaso Member or younger. Thus, either the age attributed to the landslide by the above-quoted authors is mistaken or the age of the Malpaso Member (Pérez Torrado et al., 2011) is wrong. We only found charcoal samples in the paleosol near Malpaso (same location of previous ^{14}C dates) and found no evidence of any charcoal in the paleosol in distal parts of the deposits. This finding, coupled with the facts that in proximal and intermediate areas the Malpaso member is overlain by several pyroclastic deposits of local eruptions, and that these deposits are separated by well-developed paleosols (e.g. Column 2 and Column 3; Figs. 2 and Fig. 10), suggesting that between these eruptions occur long periods of repose that once thought between the emplacement of the Malpaso Member and the present day.

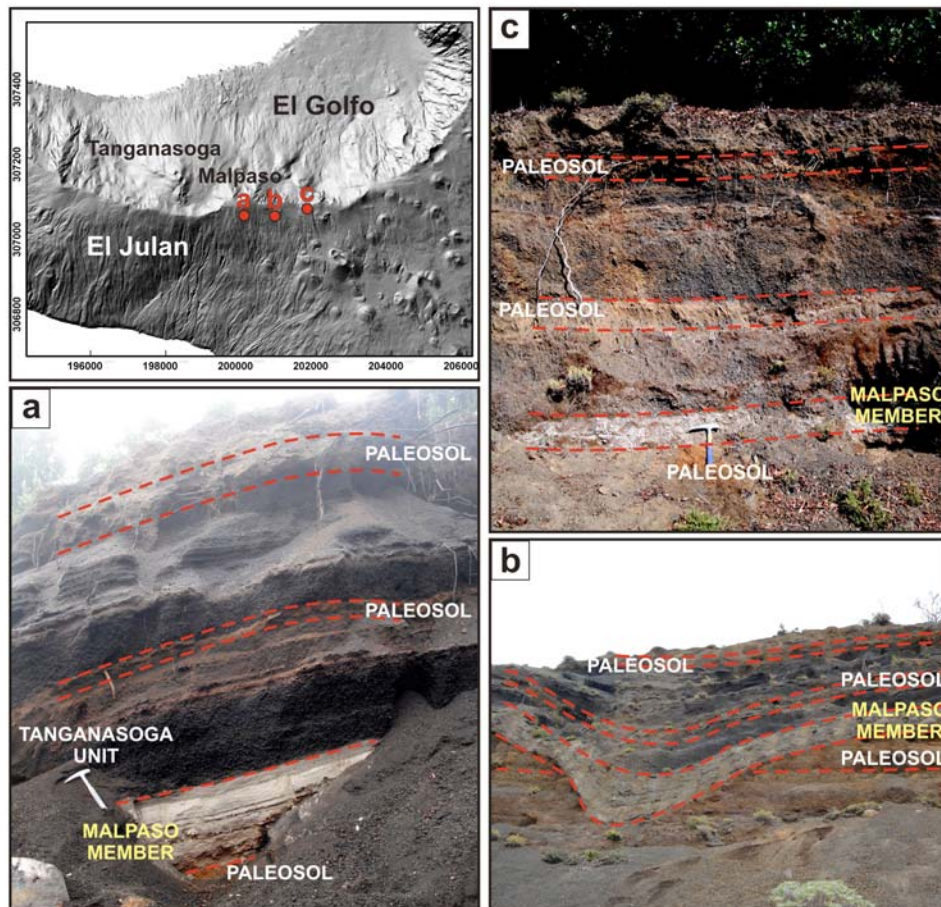


Fig. 10 Pyroclastic deposits corresponding to local Strombolian eruptions and to the studied eruption close to Malpaso but separated by well-developed paleosols.

In addition, morphological characteristics of the paleosol, where the charcoal dated by Pérez Torrado et al. (2011) was found, indicate that it is an Andosol (Padrón, 1993). The formation of this type of soils requires between several tens of thousands to hundreds of thousands of years (~150 ka) in areas as Hawaii (Torn et al., 1997). If we assume that El Hierro has similar climatic characteristics as Hawaii (mild temperatures, although lower rainfall rates) we can think that the paleosol formation required more than few thousand years. This leads us to conclude that the ages obtained by Pérez Torrado et al. (2001) are too young and that the charcoal they used may correspond to charcoal from younger plant roots growing on Malpaso or to younger deposits.

The distribution of the pumice deposits (in particular the isopach map), variations in lateral grain-size, and the isopleth map (Fig. 5a, b) suggest that the position now occupied by Tanganasoga is the most suitable location for the vent of the Malpaso Member. This would be consistent with the distribution of all the products from El Golfo in the area and with the location of Tangansoga itself, and would provide a site for the main vent of El Golfo and its eruptive activity in the area.

4.9.3 Volcanic Hazard Implications

The style and magnitude of this type of eruption is clearly of great importance in assessing the potential volcanic hazard on El Hierro. The presence of similar compositions in the erupted products during the recent 2011–2012 eruption raises the question as to whether this felsic magma represents an assimilated product from a previous eruption or whether it represents a juvenile component (i.e. differentiated product) from the last eruption. Needless to say, the most important question to answer is whether or not El Hierro's magmas have the potential to generate a large volume of eruptable felsic magma. The sequence of unrest episodes following this very recent eruption, characterized by heightened seismicity mostly located at a depth of about 20–25 km and significant surface deformation that has already accumulated more than 25 cm of total vertical uplift (www.ign.es), suggests that fresh magma has continued to accumulate below the surface of the island.

These petrological issues are beyond the scope of this paper but nevertheless still should be investigated in detail. From the results obtained we can see that an eruption of similar characteristics to that of the Malpaso Member does not require a large amount of eruptable magma and that its associated hazards are much greater than those related to

the mafic volcanism that has characterised most of the recent eruptions on El Hierro. The results of our study show that the pumice deposits reached a radial distance of at least 3 km from the hypothetical vent site (Fig. 3) and it seems likely that the pyroclastic density currents that produced these deposits could have travelled much further. The degree of hazard depends on the location of the vent and the topography of the surrounding area, as well as the initial energy in the flow. Our data suggest that the vent area of the Malpaso Member eruption was located in a similar position to that currently occupied by Tanganasoga, probably due to the position of the main feeding system from the previous El Golfo volcano. However, the characteristics of the 2011–2012 eruption and of the preceding episode of unrest (Martí et al., 2013) suggest that the position of future vents (i.e. current volcanic susceptibility; see Becerril et al., 2013) is not controlled by the same stress configuration as during the construction of El Golfo and Tanganasoga. This introduces additional uncertainty into the evaluation of hazards on El Hierro and thus is an indication that both long- and short-term hazard assessment on the island should take into account possible scenarios related to the eruption of felsic magmas.

4.10 Conclusion

In this study we conducted a detailed stratigraphic, lithological, and sedimentological study of a trachytic pumice deposit, named here as the Malpaso Member. This deposit originated from a base-surge-type explosive eruption with a subsequent radial emplacement of dilute PDC currents from the vent that would have been located in a similar position to the volcano of Tanganasoga. The low vesicularity of juvenile fragments and the morphological characteristics of the fine particles, as well as the high proportion of lithic fragments and the ash-rich nature of the deposit, suggest that magma/water interaction controlled the dynamics of the eruption.

In the light of the new stratigraphy described in this paper and previously available data, we thus conclude that the Malpaso Member was not associated with the eruption of Tanganasoga or any subsequent eruption and instead corresponds to the final episodes in the construction of the composite volcano of El Golfo.

The presence of similar compositions in the erupted products of the recent 2011–2012 eruption indicate that the magmas from El Hierro could have the potential for producing a large volume of eruptable felsic magma, a finding that obliges both long-

and short-term hazard assessment to take into account possible scenarios that include the eruption on El Hierro of felsic magmas.

Acknowledgments

This research was partially funded by the MINECO grant CGL2011-16144-E and the European Commission (FT7 Theme: ENV.2011.1.3.3-1; Grant 282759: "VUELCO"). The authors are grateful to the Cabildo of El Hierro for permission to undertake this research and, above all, to the Consejo Insular de Aguas de El Hierro for its support and to Orlando Hernandez, Xavier Bolós, Daniele Giordano, Jose Morales de Francisco, and Llorenç Planagumà for their assistance in the field as well as Olaya García for some contributions to the paper. We are also grateful to the Associated Editor Thorvaldur Thordarson, to the reviewer Roberto Sulpizio and the two anonymous reviewers for their constructive reviews of this manuscript. The English text was corrected by Michael Lockwood.

References

- Araña, V. and Ortiz, R., 1991. The Canary Islands: Tectonics, Magmatism and Geodynamic Framework. In: A.B. Kampunzu and R.T. Lubala (Editors), *Magmatism in Extensional Structural Settings*. Springer Berlin Heidelberg, pp. 209-249.
- Arnott, R.W.C. and Hand, B.M., 1989. Bedforms, primary structures and grain fabric in the presence of suspended sediment rain. *Journal of Sedimentary Petrology*, 59: 1062-1069.
- Balcells, R. and Gomez, J.A., 1997a. Memorias y mapas geológicos del Plan MAGNA a escala 1:25.000 de las Hojas correspondientes a la isla de El Hierro. Hoja de Frontera, Instituto Geológico y Minero de España, Spain.
- Balcells, R. and Gomez, J.A., 1997b. Memorias y mapas geológicos del Plan MAGNA a escala 1:25.000 de las Hojas correspondientes a la isla de El Hierro. Hoja de Sabinosa, Instituto Geológico y Minero de España, Spain.
- Barberi, F., Cioni, R., Rosi, M., Santacroce, R., Sbrana, A. and Vecci, R., 1989. Magmatic and phreatomagmatic phases in explosive eruptions of Vesuvius as deduced by grain-size and component analysis of the pyroclastic deposits. *Journal of Volcanology and Geothermal Research*, 38(3–4): 287-307.

Becerril, L., 2009. Approach to volcanic hazard and its effects in coastal areas of the Canary Islands. Master's thesis, Universidad de Las Palmas de Gran Canaria, Spain.

Becerril, L., Cappello, A., Galindo, I., Neri, M. and Del Negro, C., 2013. Spatial probability distribution of future volcanic eruptions at El Hierro Island (Canary Islands, Spain). *Journal of Volcanology and Geothermal Research*, 257(0): 21-30.

Branney, M. and Kokelaar, P., 1992. A reappraisal of ignimbrite emplacement: progressive aggradation and changes from particulate to non-particulate flow during emplacement of high-grade ignimbrite. *Bulletin of Volcanology*, 54(6): 504-520.

Branney, M.J. and Kokelaar, P., 2002. Pyroclastic density currents and the sedimentation of ignimbrites. *Geological Society of London Memoirs*, 150 pp.

Büttner, R., Dellino, P., La Volpe, L., Lorenz, V. and Zimanowski, B., 2002. Thermohydraulic explosions in phreatomagmatic eruptions as evidenced by the comparison between pyroclasts and products from Molten Fuel Coolant Interaction experiments. *Journal of Geophysical Research: Solid Earth*, 107(B11): 2277.

Büttner, R., Dellino, P. and Zimanowski, B., 1999. Identifying modes of magma/water interaction from the surface features of ash particles. *Nature* 401: 688-690.

Carey, S.N., 1991. Transport and deposition of tephra by pyroclastic flows and surges. In: R.V. Fisher and G.A. Smith (Editors), *Sedimentation in volcanic setting*. Society of Economic Paleontologists and Mineralogists, Special publications, pp. 39-57.

Carracedo, J.C., 1996. Morphological and structural evolution of the western Canary Islands: hotspot-induced three-armed rifts or regional tectonic trends? *Journal of Volcanology and Geothermal Research*, 72(1-2): 151-162.

Carracedo, J.C., Day, S., Guillou, H., Rodríguez Badiola, E., Canas, J.A. and Pérez Torrado, F.J., 1998. Hotspot volcanism close to a passive continental margin: the Canary Islands. *Geological Magazine*, 135(05): 591-604.

Carracedo, J.C., Day, S.J., Guillou, H. and Pérez Torrado, F.J., 1999. Giant Quaternary landslides in the evolution of La Palma and El Hierro, Canary Islands. *Journal of Volcanology and Geothermal Research*, 94(1-4): 169-190.

Carracedo, J.C., Rodríguez Badiola, E., Guillou, H., de La Nuez, H.J. and Pérez Torrado, F.J., 2001. Geology and volcanology of the western Canaries: La Palma and El Hierro. *Estudios Geológicos* 57: 171–295.

Cas, R.A.F. and Wright, J.V., 1987. Volcanic successions, modern and ancient. *MA geological approach to processes products and successions*. 528 pp.

Cioni, R., Sulpizio, R. and Garruccio, N., 2003a. Variability of the eruption dynamics during a Subplinian event: the Greenish Pumice eruption of Somma–Vesuvius (Italy). *Journal of Volcanology and Geothermal Research*, 124(1–2): 89-114.

Dellino, P., Isaia, R., La Volpe, L. and Orsi, G., 2004a. Interaction between particles transported by fallout and surge in the deposits of the Agnano-Monte Spina eruption (Campi Flegrei, Southern Italy). *Journal of Volcanology and Geothermal Research*, 133(1-4): 193-210.

Dellino, P., Isaia, R. and Veneruso, M., 2004b. Turbulent boundary layer shear flows as an approximation of base surges at Campi Flegrei (Southern Italy). *Journal of Volcanology and Geothermal Research*, 133(1-4): 211-228.

Fisher, R.V., 1966. Mechanism of deposition from pyroclastic flows. *American Journal of Science*, 264(5): 350-363.

Formenti, Y., Druitt, T.H. and Kelfoun, K., 2003. Characterisation of the 1997 Vulcanian explosions of Soufrière Hills Volcano, Montserrat, by video analysis. *Bulletin of Volcanology*, 65(8): 587-605.

Fuster, J.M., 1993. Geochronología de la Isla de El Hierro (Islas Canarias). *Bol. R. Soc. Esp. Hist. Nat (Sec. Geol)*, 88((1-4)): 85-97.

Guillou, H., Carracedo, J.C., Torrado, F.P. and Badiola, E.R., 1996. K-Ar ages and magnetic stratigraphy of a hotspot-induced, fast grown oceanic island: El Hierro, Canary Islands. *Journal of Volcanology and Geothermal Research*, 73(1–2): 141-155.

Heiken, G. and Wohletz, K., 1985. Volcanic ash. University of California Press, Berkeley. 246 pp.

- Hildenbrand, A., Gillot, P.-Y. and Le Roy, I., 2004. Volcano-tectonic and geochemical evolution of an oceanic intra-plate volcano: Tahiti-Nui (French Polynesia). *Earth and Planetary Science Letters*, 217(3–4): 349-365.
- Hoblitt, R., Wolfe, E., Scott, W., Couchman, M., Pallister, J. and Javier, D., 1996. The preclimatic eruptions of Mount Pinatubo, June 1991. In: Newhall CG, Punongbayan RS (eds) *Fire and mud: eruptions and lahars of mount Pinatubo, Philippines*. Philippines Institute of Volcanology and Seismology, Quezon 766 City and University of Washington Press, Seattle and London: pp 457–511.
- Le Bas, M.J., Rex, D.C. and Stillman, C.J., 1986. The early magmatic chronology of Fuerteventura, Canary Islands. *Geological Magazine*, 123: 287-298.
- Lipman, P., Rhodes, J.M. and Dalrymple, G., 1990. The Ninole Basalt — Implications for the structural evolution of Mauna Loa volcano, Hawaii. *Bulletin of Volcanology*, 53(1): 1-19.
- Longpré, M.-A., Chadwick, J.P., Wijbrans, J. and Iping, R., 2011. Age of the El Golfo debris avalanche, El Hierro (Canary Islands): New constraints from laser and furnace $^{40}\text{Ar}/^{39}\text{Ar}$ dating. *Journal of Volcanology and Geothermal Research*, 203(1–2): 76-80.
- Manconi, A., Longpré, M.-A., Walter, T.R., Troll, V.R. and Hansteen, T.H., 2009. The effects of flank collapses on volcano plumbing systems. *Geology*, 37(12): 1099-1102.
- Marinoni, L.B. and Gudmundsson, A., 2000. Dykes, faults and palaeostresses in the Teno and Anaga massifs of Tenerife (Canary Islands). *Journal of Volcanology and Geothermal Research*, 103(1-4): 83-103.
- Marinoni, L.B. and Pasquarè, G., 1994. Tectonic evolution of the emergent part of a volcanic ocean island: Lanzarote, Canary Islands. *Tectonophysics*, 239(1-4): 111-137.
- Martí, J., Castro, A., Rodríguez, C., Costa, F., Carrasquilla, S., Pedreira, R. and Bolos, X., 2013. Correlation of Magma Evolution and Geophysical Monitoring during the 2011–2012 El Hierro (Canary Islands) Submarine Eruption. *Journal of Petrology*, 54(7): 1349-1373.
- Martí, J., Pinel, V., López, C., Geyer, A., Abella, R., Tárraga, M., Blanco, M.J., Castro, A. and Rodríguez, C., 2013. Causes and mechanisms of the 2011–2012 El Hierro

(Canary Islands) submarine eruption. *Journal of Geophysical Research: Solid Earth*, 118(3): 823-839.

Masson, D.G., 1996. Catastrophic collapse of the volcanic island of Hierro 15 ka ago and the history of landslides in the Canary Islands. *Geology* 24: 231-234.

Masson, D.G., Watts, A.B., Gee, M.J.R., Urgeles, R., Mitchell, N.C., Le Bas, T.P. and Canals, M., 2002. Slope failures on the flanks of the western Canary Islands. *Earth-Science Reviews*, 57(1–2): 1-35.

Meletlidis, S., Di Roberto, A., Pompilio, M., Bertagnini, A., Iribarren, I., Felpeto, A., Torres, P.A. and D'Oriano, C., 2012. Xenopumices from the 2011–2012 submarine eruption of El Hierro (Canary Islands, Spain): Constraints on the plumbing system and magma ascent. *Geophysical Research Letters*, 39(17): L17302.

Padrón Padrón, P., 1993. Estudio edafoambiental de la isla de El Hierro, Tesis Doctoral inédita. Departamento de Edafología y Geología. Universidad de La Laguna. 285 p.+ mapas.

Palladino, D.M. and Simei, S., 2002. Three types of pyroclastic currents and their deposits: examples from the Vulcini Volcanoes, Italy. *Journal of Volcanology and Geothermal Research*, 116(1–2): 97-118.

Pellicer, M.J., 1975. Estudio vulcanológico, petrológico y geoquímico de la isla de El Hierro (Archipiélago Canario). Tesis Doctoral. Facultad de Ciencias Geológicas. Universidad Complutense de Madrid: 179 pp.

Pellicer, M.J., 1977. Estudio vulcanológico de la Isla de El Hierro, Islas Canarias. *Estudios Geológicos*, 33: 181-197.

Perez-Torrado, F.J., Rodríguez-Gonzalez, A., Carracedo, J.C., Fernández-Turiel, J.L., Guillou, H., Hansen, A. and Rodríguez Badiola, E., 2011. Edades C-14 Del Rift ONO de El Hierro (Islas Canarias). In: *El Cuaternario en España y Áreas Afines, Avances en 2011* (Turu, V. & Constante, A., eds.), Asociación Española para el Estudio del Cuaternario (AEQUA), Andorra 101-104.

Presley, T.K., Sinton, J.M. and Pringle, M., 1997. Postshield volcanism and catastrophic mass wasting of the Waiaanae Volcano, Oahu, Hawaii. *Bulletin of Volcanology*, 58(8): 597-616.

Robertson, A.H.F. and Stillman, C.J., 1979. Late Mesozoic sedimentary rocks of Fuerteventura, Canary Islands: Implications for West African continental margin evolution. *Journal of the Geological Society*, 136(1): 47-60.

Schmincke, H.-U., 1982. Volcanic and Chemical Evolution of the Canary Islands. In: U. Rad, K. Hinz, M. Sarnthein and E. Seibold (Editors), *Geology of the Northwest African Continental Margin*. Springer Berlin Heidelberg, pp. 273-306.

Schmincke, H.U., 1990. *Geology and Geological Field Guide of Gran Canaria*. Pluto Press, Kiel. 212 pp.

Self, S. and Sparks, R.S.J., 1978. Characteristics of widespread pyroclastic deposits formed by the interaction of silicic magma and water. *Bulletin Volcanologique*, 41(3): 196-212.

Sigmarsson, O., Laporte, D., Carpentier, M., Devouard, B., Devidal, J.-L. and Marti, J., 2013. Formation of U-depleted rhyolite from a basanite at El Hierro, Canary Islands. *Contributions to Mineralogy and Petrology*, 165(3): 601-622.

Sohn, Y.K., 1996. Hydrovolcanic processes forming basaltic tuff rings and cones on Jeju Island, Korea. *Geological Society of America Bulletin*, 108: 1199-1211.

Sohn, Y.K. and Chough, S.K., 1989. Depositional processes of the Suwolbong tuff ring, Cheju Island (Korea). *Sedimentology*, 36(5): 837-855.

Sulpizio, R., Mele, D., Dellino, P. and Volpe, L., 2005. A complex, Subplinian-type eruption from low-viscosity, phonolitic to tephri-phonolitic magma: the AD 472 (Pollena) eruption of Somma-Vesuvius, Italy. *Bulletin of Volcanology*, 67(8): 743-767.

Székéméta, N., Laj, C., Guillou, H., Kissel, C., Mazaud, A. and Carracedo, J.-C., 1999. Geomagnetic paleosecular variation in the Brunhes period, from the island of El Hierro (Canary Islands). *Earth and Planetary Science Letters*, 165(3-4): 241-253.

- Torn, M.S., Trumbore, S.E., Chadwick, O.A., Vitousek, P.M. and Hendricks, D.M., 1997. Mineral control of soil organic carbon storage and turnover. *Nature*, 389(6647): 170-173.
- Urgeles, R., Canals, M., Baraza, J. and Alonso, B., 1996. The submarine “El Golfo” debris avalanche and the Canary debris flow, West Hierro Island: the last major slides in the Canary archipelago. *Geogaceta*, 20: 390–393.
- Urgeles, R., Canals, M., Baraza, J., Alonso, B. and Masson, D.G., 1997. The most recent megaslides on the Canary Islands: the El Golfo Debris Avalanche and the Canary Debris Flow, west El Hierro Island. *J. Geophys. Res.* , 102: 20305-20323.
- Valentine, G.A., 1987. Stratified flow in pyroclastic surges. *Bulletin of Volcanology*, 49(4): 616-630.
- Valentine, G.A. and Fisher, R.V., 2000. Pyroclastic surges and blasts. In: Sigurdsson, H., Houghton, B.F., McNutt, S.R., Rymer, H., Stix, J. (Eds.), *Encyclopedia of Volcanoes*. Academic Press: 571–580.
- Walker, G.P.L., 1983. Ignimbrite types and ignimbrite problems. *Journal of Volcanology and Geothermal Research*, 17(1–4): 65-88.
- Wohletz, K., 1986. Explosive magma-water interactions: Thermodynamics, explosion mechanisms, and field studies. *Bulletin of Volcanology*, 48(5): 245-264.
- Wohletz, K.H. and Sheridan, M.F., 1983. Hydrovolcanic explosions; II, Evolution of basaltic tuff rings and tuff cones. *American Journal of Science*, 283(5): 385-413.
- Wohletz, K.H., Sheridan, M.F. and Brown, W.K., 1989. Particle size distributions and the sequential fragmentation/transport theory applied to volcanic ash. *Journal of Geophysical Research: Solid Earth*, 94(B11): 15703-15721.

Studied outcrop Number	Coordinates (UTM)		Thickness (cm)
	X	Y	
1	201065	3070484	22
2	200791	3070436	27
3	200408	3070513	45
4	199997	3070466	61
5	199063	3070334	21
6	199696	3070885	60
7	199712	3070479	81
8	199549	3070564	30
9	199686	3070592	61
10	200000	3070467	65
11	199503	3070433	67
12	199469	3070396	53
13	199482	3070425	55
14	199956	3070461	68
15	201043	3070455	19
16	200770	3070438	19
17	200357	3070513	53
18	200361	3070546	62
19	199779	3070540	73
20	199785	3070903	70
21	199696	3070891	55
22	199484	3070609	69
23	199495	3070564	62
24	199647	3070427	26,7
25	200336	3070861	55
26	200439	3070793	75,5
27	200664	3070744	39,5
28	200765	3070734	32
29	200619	3070607	29,5
30	200482	3070606	45
31	201219	3070252	12
32	201304	3070160	10
33	201446	3070064	7,5
34	201743	3070065	7
35	201432	3069465	9
36	201083	3069542	7,5
37	200651	3069666	3
38	199409	3069503	21,5
39	194840	3031098	0
40	199393	3070361	54
41	199183	3070261	42
42	199020	3070259	0
43	198862	3070265	8

44	198924	3070308	0
45	199425	3070321	44
46	199375	3070179	46
47	199438	3070157	58
48	199750	3070170	61
49	200104	3070282	29
50	200668	3070267	23
51	199438	3070157	31
52	200942	3070247	21
53	201546	3070687	9
54	201546	3070687	15
55	201956	3070083	3
56	201100	3070185	10,5
57	200728	3069953	20
58	200663	3069959	21
59	199797	3069876	23
60	199744	3069873	25
61	199634	3069900	25
62	199547	3069905	38
63	199406	3069933	14
64	199270	3070267	40
65	201483	3070491	10
66	199614	3070536	0
67	199322	3070517	62
68	198720	3070410	24
69	198610	3070378	21
70	198870	3070450	30
71	204689	3071626	0
72	204476	3071507	0
73	204233	3071417	2,5
74	203659	3071217	1
75	203606	3071390	2
76	204098	3071510	1
77	201848	3070283	5
78	202005	3070218	5
79	202432	3070153	5
80	203933	3070365	3
81	204132	3070195	4
82	203897	3069802	3
83	203741	3069790	3
84	203254	3069681	3
85	202955	3069612	2
86	204397	3070823	1
87	204373	3070817	1
88	204009	3070555	2
89	203984	3070525	1

90	203934	3070374	2
91	204138	3070195	1
92	204359	3070085	1
93	205467	3070514	0
94	205483	3070573	0
95	205311	3071677	0
96	205640	3071454	2
97	198367	3070279	0
98	198431	3070350	0
99	198622	3070325	32
100	198980	3070379	32
101	199032	3070370	31
102	199200	3070415	25
103	199698	3070417	22
104	198751	3070444	31
105	198733	3070441	0
106	198609	3070445	26
107	198609	3070445	0
108	196927	3070397	6
109	197450	3070277	5
110	198445	3070268	20
111	198601	3069885	10
112	199576	3069976	16
113	199119	3069674	0
114	199120	3069708	0
115	199814	3069263	30
116	196167	3070712	3
117	195768	3071020	2
118	195701	3071041	1
119	195632	3071079	0
120	195468	3071043	0
121	195357	3071033	0
122	195640	3071167	0
123	196960	3070632	3
124	197635	3070261	7
125	196389	3070546	2
126	196058	3070611	2
127	195729	3070755	2
128	195666	3070742	2
129	195662	3070653	2
130	195996	3070349	2
131	195952	3070287	2
132	195614	3070383	2
133	195327	3070504	0
134	195232	3070563	0
135	194920	3070711	0

136	194733	3070887	0
137	199839	3069194	0
138	200870	3069036	0
139	203002	3069499	0
140	203104	3069505	0
141	203231	3069538	0
142	203340	3069585	0
143	203719	3069598	0
144	203980	3069485	0
145	205141	3071803	0
146	205637	3071820	0,5
147	205718	3071881	0
148	205823	3071670	0
149	205870	3071808	0
150	206077	3071549	0
151	200289	3070943	0
152	199650	3070950	0

Online Resource 1 Geographical coordinates of relevant locations, as well as stratigraphic sections and sampling points

5. THE 1970 ERUPTION ON DECEPTION ISLAND (ANTARCTICA): ERUPTIVE DYNAMICS AND IMPLICATION FOR VOLCANIC HAZARD

Submitted to:

Journal of the Geological Society

Authors of the paper:

Dario Pedrazzi, Institute of Earth Sciences Jaume Almera, ICTJA-CSIC, Group of Volcanology. SIMGEO (UB-CSIC) Lluís Solé i Sabarís s/n, 08028 Barcelona, Spain

Gerardo Aguirre Díaz, Centro de Geociencias, Universidad Nacional Autónoma de México, Campus Juriquilla, Querétaro, Qro. 76230, Mexico

Stefania Bartolini, Institute of Earth Sciences Jaume Almera, ICTJA-CSIC, Group of Volcanology. SIMGEO (UB-CSIC) Lluís Solé i Sabarís s/n, 08028 Barcelona, Spain

Joan Martí, Institute of Earth Sciences Jaume Almera, ICTJA-CSIC, Group of Volcanology. SIMGEO (UB-CSIC) Lluís Solé i Sabarís s/n, 08028 Barcelona, Spain

Adelina Geyer, Institute of Earth Sciences Jaume Almera, ICTJA-CSIC, Group of Volcanology. SIMGEO (UB-CSIC) Lluís Solé i Sabarís s/n, 08028 Barcelona, Spain

The reference of this paper is:

Pedrazzi, D., Aguirre-Diaz, G., Bartolini, S., Martí, J. and Geyer, A., Submitted. The 1970 eruption on Deception Island (Antarctica): eruptive dynamics and implication for volcanic hazard. Journal of the geological society.

Abstract

In 1970, a hydrovolcanic eruption took place in the northern part of Deception Island (South Shetland Archipelago, Antarctic Peninsula group). The eruption occurred in the same general area as the 1967 eruption, but with new, more widely distributed vents. Two groups of craters were formed as a result of the 1970 eruption, which suggests that different active fissures and eruptive dynamics were operating during the same eruption. One group consists of maar-like craters, while the other group is made of conical shape edifices. The 1970 eruption can be classified as a VEI 3 eruption, with mainly phreatomagmatic episodes that generated a bulk volume of about 0.1 km³ of pyroclastic material and an eruptive column of up to 10 km in height, from which fallout deposits have been recognized at a distance of more than 100 km to the northeast. The 1970 eruption was similar to that of 1967 and conjointly these two events show how eruption dynamics can be controlled by the physical characteristics of the vents (e.g. the uppermost part of the volcano's substrate and the width and orientation of the eruptive fissure) and by changing magma/water interaction, which together generate different eruptive phases and associated volcanic hazards.

Keywords: Deception Island, South Shetland Archipelago, Antarctica, phreatomagmatism, 1970 eruption, volcanic hazard

5.1 Introduction

Hydrovolcanic eruptions are common in coastal environments where erupting magma may interact with seawater in either subaquatic or subaerial settings depending on the location of the eruption conduit and vent (Sheridan and Wohletz, 1983). Near-shore and shallow subaqueous activity may generate high-intensity explosions characterised by ballistic blocks, ash-fall and pyroclastic density currents, which, in contrast with the lesser impact typically associated with magmatic eruptions of the same size, may severely affect surrounding areas.

The 1970 eruption on Deception Island, whose over 20 recognised eruptions during the past two centuries make it the most active volcano in the South Shetland Archipelago (Antarctic Peninsula group), is an excellent example of a monogenetic hydrovolcanic eruption in a coastal environment (e.g. Sheridan and Wohletz, 1983). This eruption took place in the northern part of the Deception caldera and gave rise to the formation of several vents and cones that differ significantly in the shape of their

craters (Baker and McReath, 1971, 1975). Several preliminary accounts of the 1970 eruption that include a general description in Baker and McReath (1975) have already been published (e.g. Baker and McReath, 1971; Gonzalez Ferran et al., 1971; Shultz, 1972). However, a detailed description of the succession of deposits, as well as an accurate reconstruction of the eruptive activity, is still lacking.

In this paper we describe in detail the stratigraphy, lithology and sedimentology of the deposits of the 1970 eruption and use this information to infer the eruption dynamics and transport and depositional processes. We then compare these data with those from the 1967 eruption and analyse the potential hazard implications of this type of eruptive activity on Deception Island, which is becoming one of the main tourist attractions on the Antarctica.

5.2 Geological setting and general characteristics of Deception Island

Deception Island is the southernmost island in the South Shetland Archipelago and is located at the southwestern end of the Bransfield Strait. It consists of a young (<1.4 Ma) back-arc basin (Fig. 1a), which was formed as a consequence of the Phoenix plate subduction under the Antarctic plate during the upper Mesozoic–Cenozoic interval (Dalziel 1984). The Bransfield basin, <60-km wide and 500-km long, separates the South Shetland Islands from the Antarctic Peninsula (Fig. 1b) and has a characteristic graben structure, with tilted blocks and rotational faults developed under a regime of continental extension (Jeffers and Anderson, 1990; Gràcia et al., 1996; Vuan et al., 2005).

Deception Island consists of a <0.75-Ma (Valencio et al., 1979; Smellie, 1988) horseshoe-shaped volcanic edifice, with a below-sea-level diameter of 25 km (Smellie, 1988; Barclay et al., 2009) and an above-sea-level diameter of around 13 km (Fig. 1c). A sea-flooded depression known as Port Foster occupies the central part of the island (Smellie, 2001; Marti et al., 2013). Several periods of contrasting styles of volcanic activity can be distinguished (Smellie et al., 2002). Over 20 eruptions have been identified over the past two centuries (Roobol, 1980; Pallàs et al., 2001; Smellie et al., 2002), the most recent of which occurred in 1967, 1969 and 1970 (see: Orheim, 1971c; Baker et al., 1975; Roobol, 1980; Smellie, 2002).

The construction of this composite volcanic complex, which rises up to 540 m a.s.l. at Mount Pond and 460 m at Mount Kirkwood (Fig. 1c), was truncated by the formation of a central caldera (Port Foster) resulting from an explosive eruption of

basaltic-to-andesitic magmas, mostly as pyroclastic density currents with a total bulk volume in the order of 90 km³ (Martí et al., 2013).

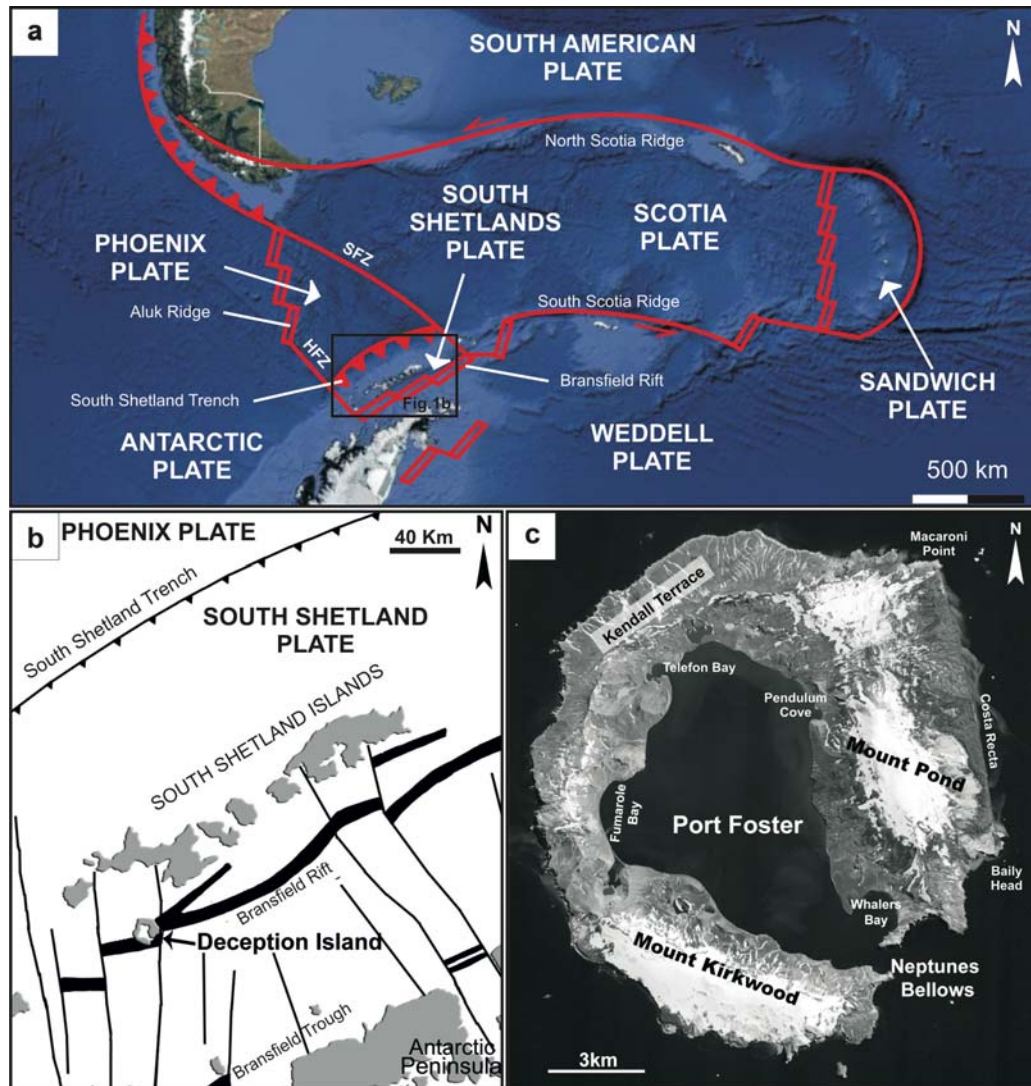


Fig. 1. (a) Simplified regional tectonic map and location of the South Shetland Islands Archipelago (modified from Ibañez et al., 2003). HFZ- Hero Fracture Zone, SFZ- Shetland Fracture Zone; (b) South Shetland Islands Archipelago and location of Deception Island (modified from Grad et al., 1992); (c) Orthophotomap of Deception Island (http://lagc.uca.es/web_lagc/orto.jpg).

The basement of the island is not exposed but probably corresponds to Cretaceous–Tertiary consolidated sedimentary and volcanic rocks and/or unconsolidated and poorly consolidated pre-Quaternary marine sediments deposited on the submerged South Shetland Islands platform (Ashcroft, 1972; Grad et al., 1992; Smellie, 2001). The pre-caldera units (BSF-Fig. 2) correspond mostly to volcanic shield deposits, in which different eruptive cycles and vents can be distinguished (Smellie, 2001). Most of these units correspond to lava flows and Strombolian deposits, as well as to palagonitised hyaloclastitic breccias. The shield-related units are overlaid unconformably by a thick

sequence of massive ignimbrites and minor pyroclastic surge deposits of basaltic-to-andesitic composition, which represent the syn-caldera deposits (Martí et al., 2013) (OCTF-Fig. 2). This succession is overlaid unconformably by discontinuous sequences of post-caldera deposits originating from different vents (PCD-Fig. 2), most located inside or around the caldera depression itself (Smellie, 2001).

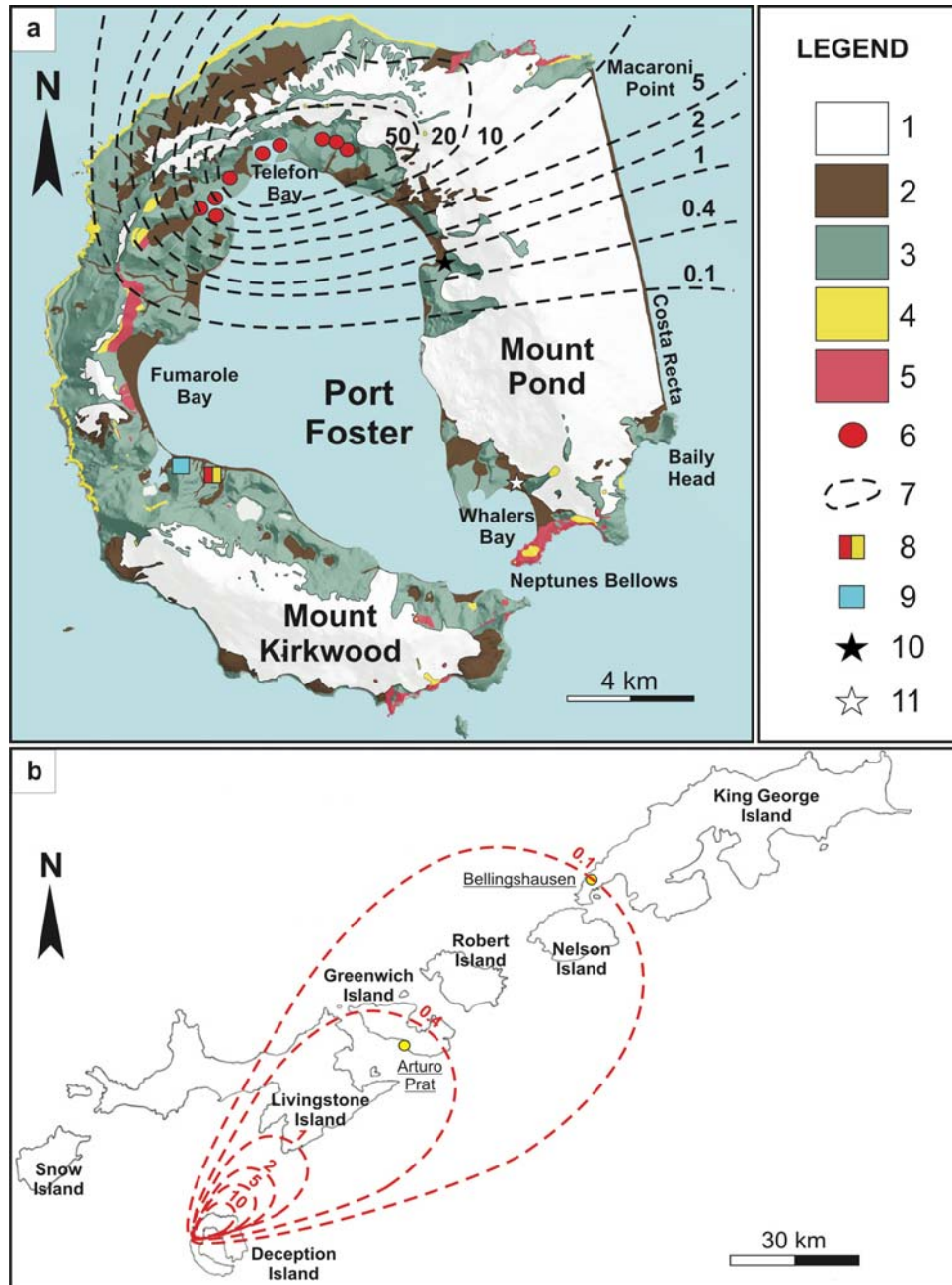


Fig. 2. (a) Simplified geological map of Deception Island (modified from Martí et al., 2013) showing the isopachs (black dashed lines) in cm of the 1967 eruption (modified from Baker and McReath, 1975); (b) Isopachs (red dashed lines) in cm of the 1970 eruption in the Shetlands Archipelago (modified from Baker and McReath, 1975). 1-Permanent ice, 2-alluvium, moraine, beach and undifferentiated deposits, 3-(PCD) Post-Caldera Deposits, 4-(OCTF) Outer Coast Tuff Formation, 5-(BSF) Basaltic Shield Formation, 6-Sites of 1970 eruption, 7-isopachs of 1970 eruption, 8-Spanish Base, 9-Argentinian Base, 10-abandoned Chilean Base, 11-abandoned British base.

5.3 Methods

A photointerpretation of ortophotos at a scale of 1:5,000 was necessary to identify the potentially most interesting outcrops in the area. Fieldwork was conducted during the austral summer of 2012–2013 in an area of about 5 km² around the cones of the 1970 and 1967 eruptions. A total of six detailed stratigraphic logs were established but due to the difficult access to some zones, it was not possible to cover the whole of the area covered by the deposits from these eruptions. Nevertheless, these stratigraphic logs are representative of the resulting successions of deposits.

The geometry and lithology of the deposits were documented in each outcrop following lithostratigraphic and stratigraphic criteria; the colour, nature and relative content of components, grain size variations, texture and sedimentary structures were analysed. Maximum clasts (scoriae and lithics) of each identified layer were established based on the geometric mean average of the three axes of the five largest clasts sampled from a horizontal area of 0.5 m².

All data were managed using Surfer 7 and an open-source Geographic Information System (GIS) framework (QGIS, www.qgis.org). The location of relevant sites and the position of the stratigraphic logs were recorded using a portable GPS with a precision of about 3 m. The reference zone used was the UTM projection Datum: D_WGS_1984, zone 20 South.

Grain-size analyses employing dry-sieving techniques and componentry analysis were performed by weighing/counting 42 representative samples. Samples were sieved at 1 ϕ using sieves with mesh sizes in the range 32–1/32 mm (-5 ϕ to 5 ϕ). Clast compositions were initially characterised in the field via hand-sample observations and then later in the laboratory under a binocular microscope. Component analysis was carried out on the -5 ϕ -4 ϕ , -3 ϕ , -2 ϕ and -1 ϕ fractions of the deposits. Clasts were separated into juvenile and accidental lithics, the latter belonging to the island basement and to the syn- and post-caldera phase. Further analysis of the samples finer than -1 ϕ is not provided here since the original content and grain size distribution of the fine fraction are significantly affected by the sieving process itself.

The physical parameters of the eruption were obtained: the erupted volume was calculated with an isopach map using Pyle's method (1989), while the plume height was determined by applying the method described by Carey and Sparks (1986) to an isopleth map of clasts.

5.4 Characteristics of the 1970 craters

The 1970 craters are located in the northern part of Deception Island, between Goddard Hill and Cross Hill, at the foot of the caldera wall and close to the beach (Fig. 3a). At least 13 vents from this eruption were identified and can be separated into two main groups – the eastern and western – based on the location and shape of the craters. The former group is located at the foot of Goddard Hill and consists of seven conical shape edifices (a-g; Fig. 3b) that are aligned roughly in a NW-SW direction (Fig. 3b).

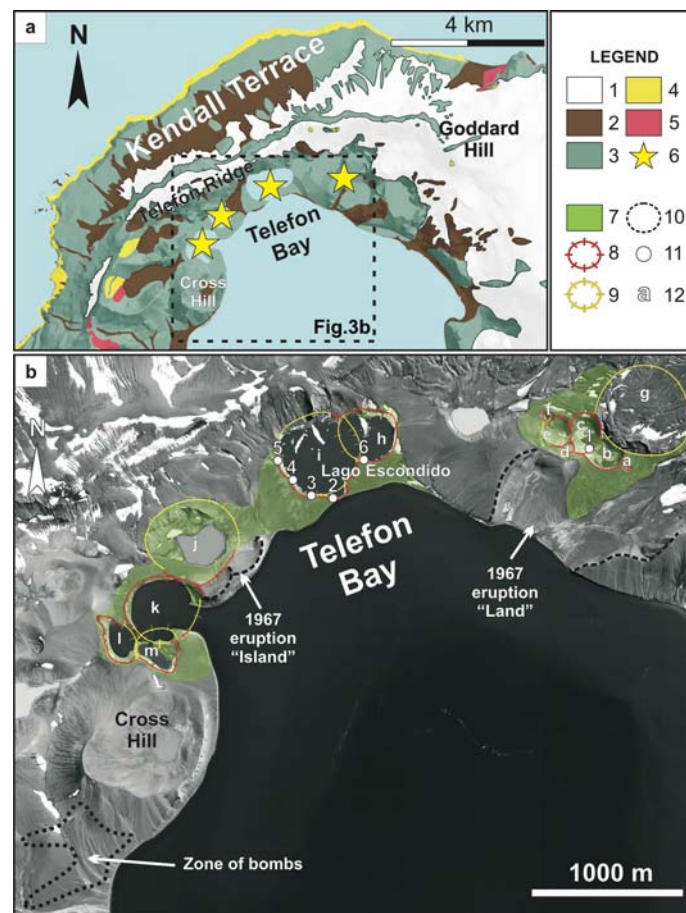


Fig. 3. (a) Geological map of the northern part of Deception Island (modified from Martí et al., 2013); (b) orthophotomap of the same area showing the extent of the proximal deposits, as well as an anomalous zone of bombs probably indicating a hidden vent south of Cross Hill. 1-Permanent ice, 2-alluvium, moraine, beach and undifferentiated deposits, 3-(PCD) post-caldera deposits, 4-(OCTF) Outer Coast Tuff Formation, 5-(BSF) Basaltic Shield Formation, 6-locus of the eruption, 7-extent of the proximal deposits, 8-crater rims, 9-inferred crater rims, 10-1967 eruption crater rims, 11-crater numbers, 12- Sites of stratigraphic logs.

These steep-sided craters reach a maximum depth of 60 m. Crater g, described by Baker and McReath (1975), has been eroded away by the island's glacier. The western group, with maar-like shapes, is located at the foot of the exposed part of the caldera wall (Fig. 3b); its craters have almost vertical sides and rims that only reach about 15 m above sea

level. The first crater (h,i; Fig. 3b) is a composite structure consisting of two major craters whose southernmost points are connected to Telefon Bay by a narrow, around 10-m-wide isthmus. The second crater (j; Fig. 3b), a depression located in the northwestern part of the complex originating from the 1967 eruption, is partially filled by a lake and seems to represent the remains of another eruptive centre. The last three craters (k–m; Fig. 3b) are connected to each other by narrow channels and to Port Foster by a 150-m-wide channel located in the eastern part. As reported by Baker & McReath (1975), the isolated area of relatively large bombs with no traces of a source crater that lies south of Cross Hill (Fig. 3b) might indicate another eruptive vent, supposedly located near the shore.

5.5 Characteristics of the pyroclastic succession

We carried out a detailed characterisation of six stratigraphic logs in order to reconstruct the succession of deposits. Although limited exposure only allowed us to obtain one representative stratigraphic log from the Eastern Craters (1; Fig. 4), five stratigraphic logs were obtained from the Western Craters (Lago Escondido Edifice) (2–6; Fig. 4).

5.5.1 Eastern Craters

Stratigraphic log 1 has a total thickness of about 40 m with a visible unconformity in the middle (Figs. 4 and 5a,b), which marks the important change between the two parts of the succession (22–41 m). The base of the succession is not exposed (Figs. 4 and 5e). The first part of the stratigraphic log (0–1 m) shows a continuous change from laminated poorly sorted vesiculated, fine-to-coarse lapilli-sized clasts with accidental lithics (syn-caldera ignimbrites and lava flows) that suddenly change to a massive, poorly sorted, lithic-rich breccia deposit (1–4 m) with poorly vesiculated bombs (Fig. 4). The succession continues from 4–11 m with a sequence of bomb-rich deposits (Figs. 4 and 5c), alternating with massive, poorly sorted, lithic-rich deposits (Figs. 4 and 5d). The next deposit is about 0.5 m thick, has an erosive base, and is made up of coarse lapilli and bombs with a peculiar yellow colour. The rest of the first half of the succession (11–22 m) consists of thick, massive, poorly sorted, lithic-rich (lava and ignimbrite clasts) breccia deposits without any visible depositional structures (Fig. 4). A marked unconformity indicates a change in the type of deposits in the second half of the succession (Figs. 4 and 5a,b), which is characterised by a

continuous alternation of thick, coarse well sorted lapilli-sized breccia layers with accidental lithics and non-vesiculated (juvenile) scoria and fine and coarse lapilli layers with planar stratification (Fig. 4).

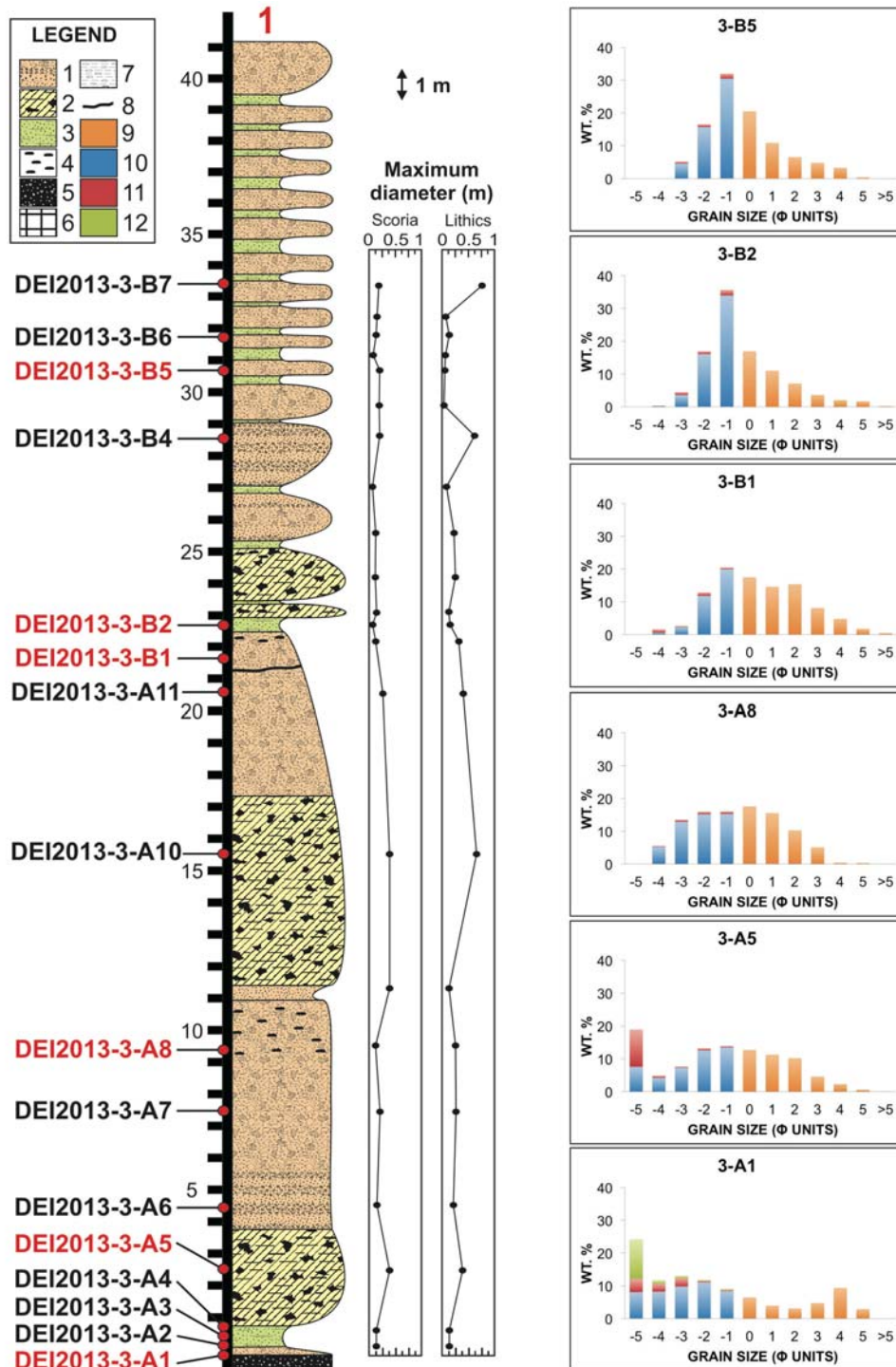


Fig. 4. Composite stratigraphic logs of the deposits and componentry analysis of the most representative samples. Stratigraphic log 1 refers to the Eastern Craters, whilst stratigraphic logs 2-6 are located around Lago Escondido. Vertical variations in grain size and the maximum diameter of lithic and scoria clasts are also indicated. 1: Massive, poorly sorted, lithic-rich breccia, 2: massive, poorly sorted, lithic-rich breccia with large lithic ballistic ejecta, 3: pyroclastic surge deposits, 4: scoriae, 5: debris deposits, 6: ice, 7: beach deposits, 8: unconformity, 9: no componentry, 10: juveniles, 11: lava, 12: yellow tuff.

5.5.2 Western Craters

Stratigraphic logs 2–6 were taken around the crater of Lago Escondido, the easternmost edifice of the Western Craters (h,i Figs. 3b and 5f).

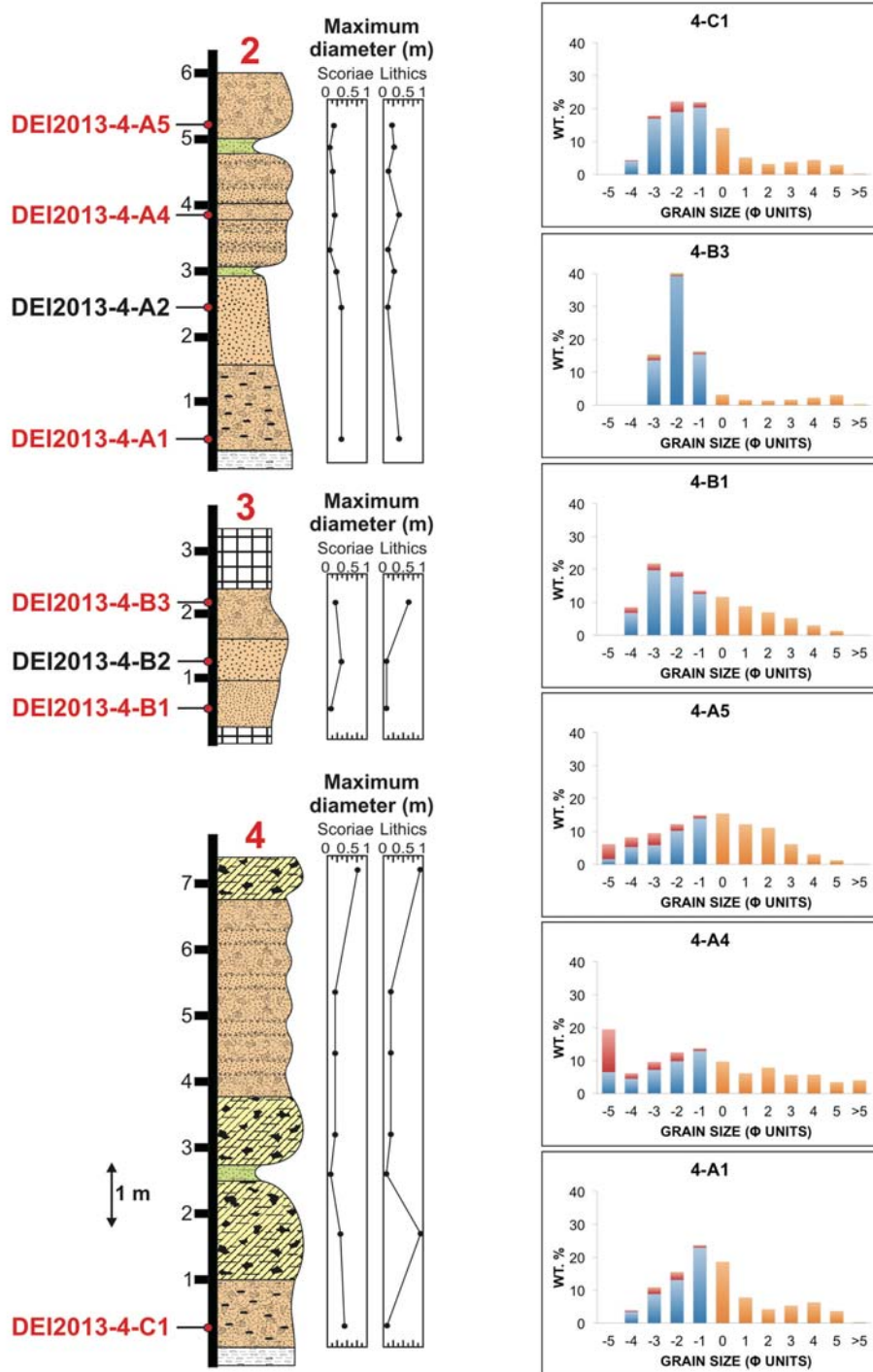


Fig. 4. Continue

All stratigraphic logs show a similar succession, mainly characterised by thick, massive, poorly sorted, lithic-rich (ignimbrites and lava clasts) breccia with some levels of poorly

sorted coarse lapilli with weak lamination (Figs. 4 and 5g,h). The thickness of the sequence varies from about 6 m in stratigraphic log 2 to less than 15 m in stratigraphic log 6 (Fig. 4). A little stratification can be identified in some of the deposits (stratigraphic log 2; Fig. 4), as well as enrichment by scoria bombs (Fig. 5i). A general increase in the content of lithic clasts and grain size is observed in the uppermost deposits (Figs. 4 and 5j).

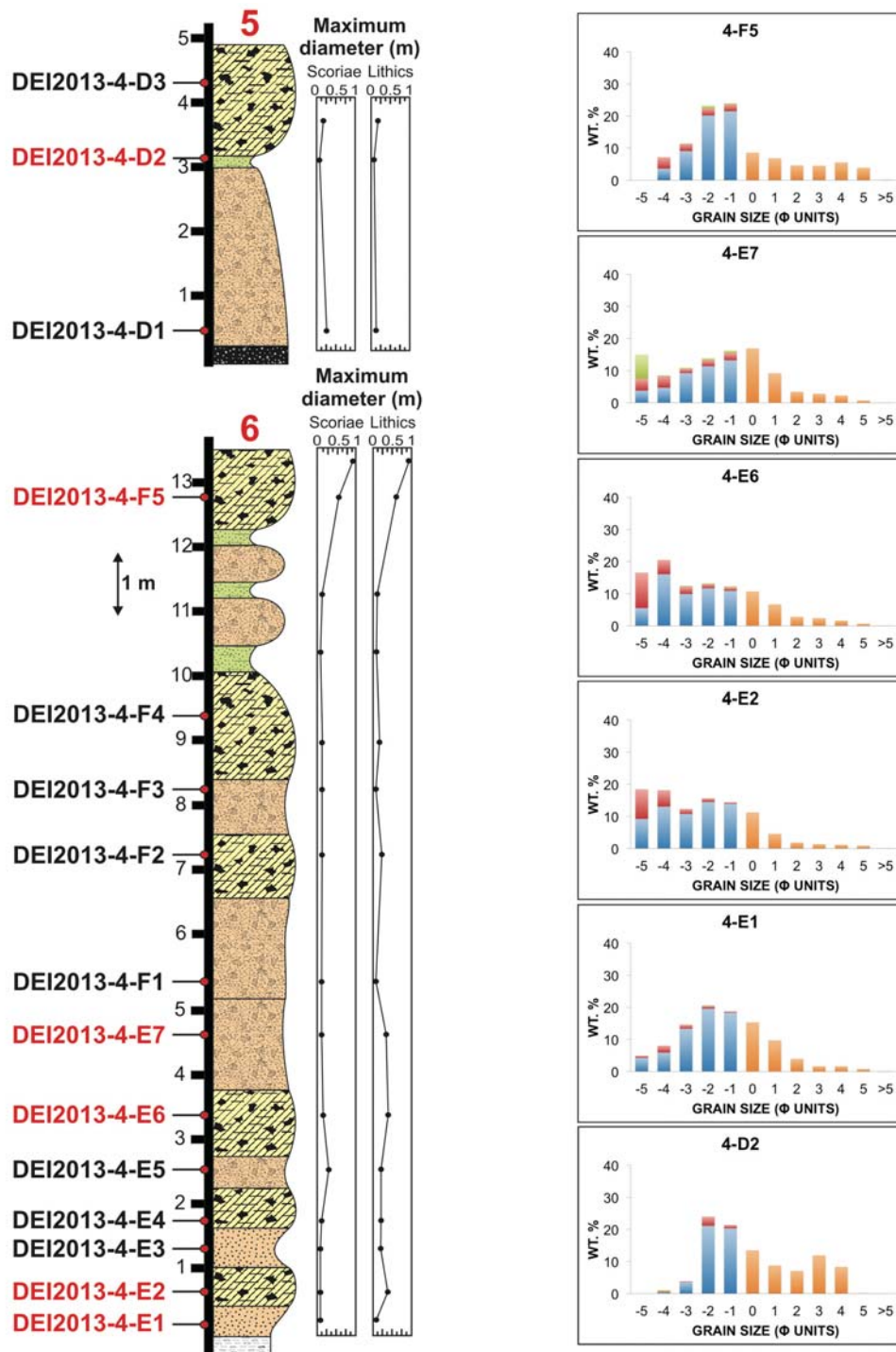


Fig. 4. Continue

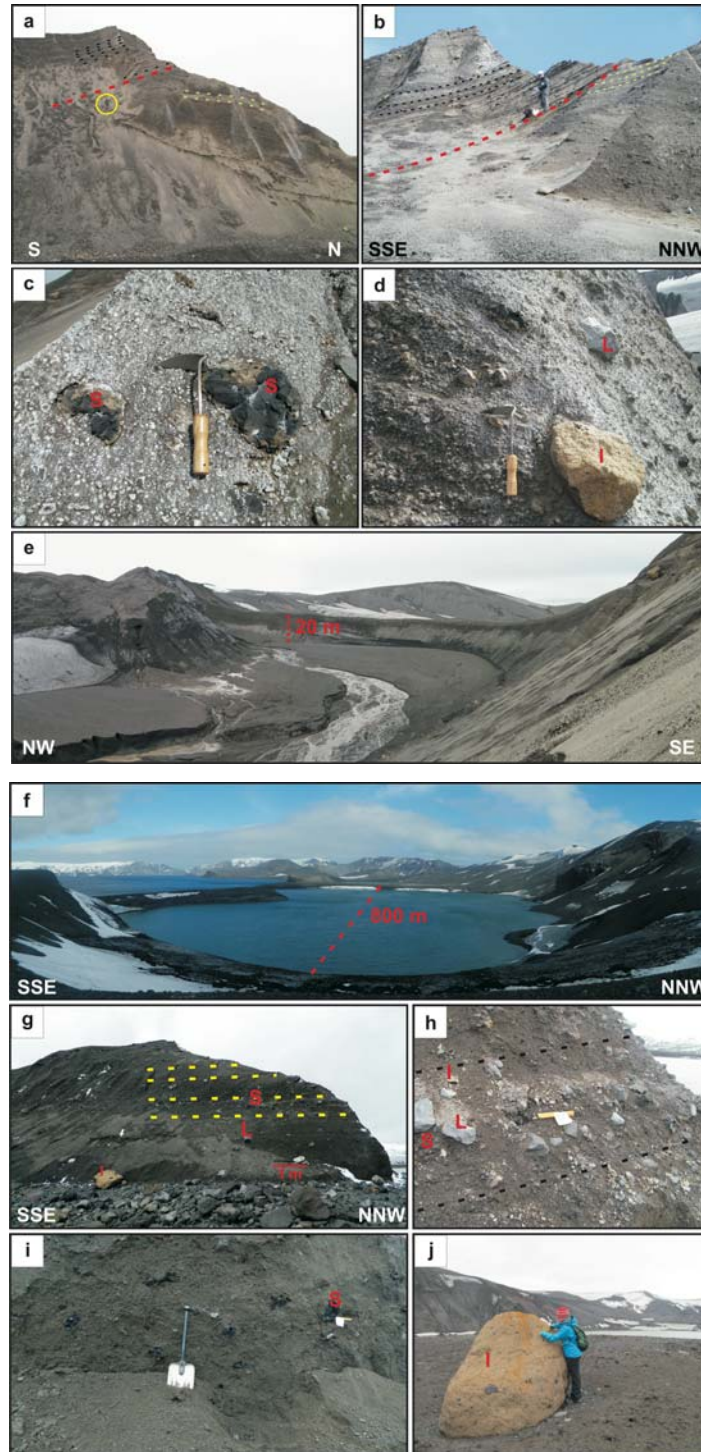


Fig. 5. Field photographs of the main stratigraphic logs: (a) general view of outcrop 1 showing the unconformity (dashed red line) in its highest part. Green and black dashed lines indicate, respectively, the dip of the layers below and above the unconformity. Yellow circle indicates the person used as a scale; (b) detailed view of outcrop 1. The lower part is characterized mainly by massive deposits, whilst the upper part above the unconformity (dashed red line) is constituted by alternating (black dashed lines) of thick, coarse, lapilli-sized breccia layers and fine and coarse lapilli layers with planar stratification; (c) example of bomb-enriched deposits; (d) typical massive lithic-rich deposit; the scraper is about 15-cm long; (e) general view of the inner part of the easternmost crater with a height of about 20 m in the background; (f) general view of Lago Escondido; (g) typical outcrop consisting mainly of massive, unbedded and subordinate fine lapilli deposits; the shovel is about 1-m long; (h) detail of a massive deposits; the stick is 10-cm long; (i) bomb-rich deposit; (j) example of lithic close to Lago Escondido Craters. L=lava, I=ignimbrite, S=scoria.

5.5.3 *Distribution of ash-fall deposits*

All vents were located in the northern part of the island and the ejecta were mostly carried northwards. Ash-fall was restricted to the northern sector of the island between the central part of Kendall Terrace and Pendulum Cove (Fig. 2a). No evidence of ash was found on Mont Kirkwood. A considerable amount of the ash fell beyond Deception Island, as shown in Figure 2b. Approximately 4 mm of fine ash fell on Arturo Prat station, Greenwich Island, and about 1 mm on Bellingshausen station, King George Island (Baker and McReath, 1975). As shown in Figure 2b, variations in thickness and distribution are consistent with a northeastward pattern of isopachs that extends along the axis of the South Shetland Islands under the influence of a southwesterly wind, which carried part of the material into the Bransfield Strait (Baker and McReath, 1971, 1975).

5.5.4 *Grain size, modal variation and clast distribution*

Vertical variations in the grain size distribution and modal variations were analysed by selecting representative samples from both the coarse- and fine-grained layers (Fig. 4 and Supp. Material). The vertical variation of maximum clast sizes (bombs and blocks) is shown in Figure 4. At stratigraphic log 1 there is a dominance of coarse deposits in the lower part with a general decrease in grain size throughout the succession. The Median Diameter ($Md\phi$) values of all samples range from -2.9 to -0.15, while Sorting ($\sigma\phi$) values range from 1.08 to 3.76 (Fig. 6a). Deposits from the lowest part of the succession are poorly sorted compared to the deposits from the upper part, which are generally finer grained. Skewness ($\alpha\phi$) varies from 0.27 to -0.75 (Fig. 6d). In the general trend of the lithic clast distribution (Fig. 4), the lowest part of the succession has the largest proportion of blocks, which can measure up to 60 cm.

Stratigraphic logs 2–6 have similar successions. A dominance of coarse deposits is observable in all the stratigraphic logs, with just an occasional slight decrease in grain size corresponding to coarse and fine lapilli layers. The Median Diameter ($Md\phi$) values of the all samples range from -3.11 to -0.018, while Sorting ($\sigma\phi$) values range from 1.75 to 3.52 (Fig. 6a); the deposits are generally poorly sorted. Skewness ($\alpha\phi$) varies from 0.34 to -1.96 (Fig. 6d). Maximum clast size reaches 60 cm except in the upper part of the succession, where a general increase of up to several decimetres is observed (Fig. 4).

Median Diameter and Sorting were used to compare the deposits with the diagrams proposed by Walker (1971) (Fig. 6b) and Houghton et al. (2000) (Fig. 6c). The former demonstrates how most of the deposits fell inside the fallout and surge fields, while the latter show deposits that are scattered over the phreatomagmatic and the magmatic/phreatomagmatic fields. The final two diagrams (Figs. 6d,e) illustrate the grain size distribution of the samples shown in Figure 4 and highlight the fact that the most representative classes range from 0ϕ to -3ϕ .

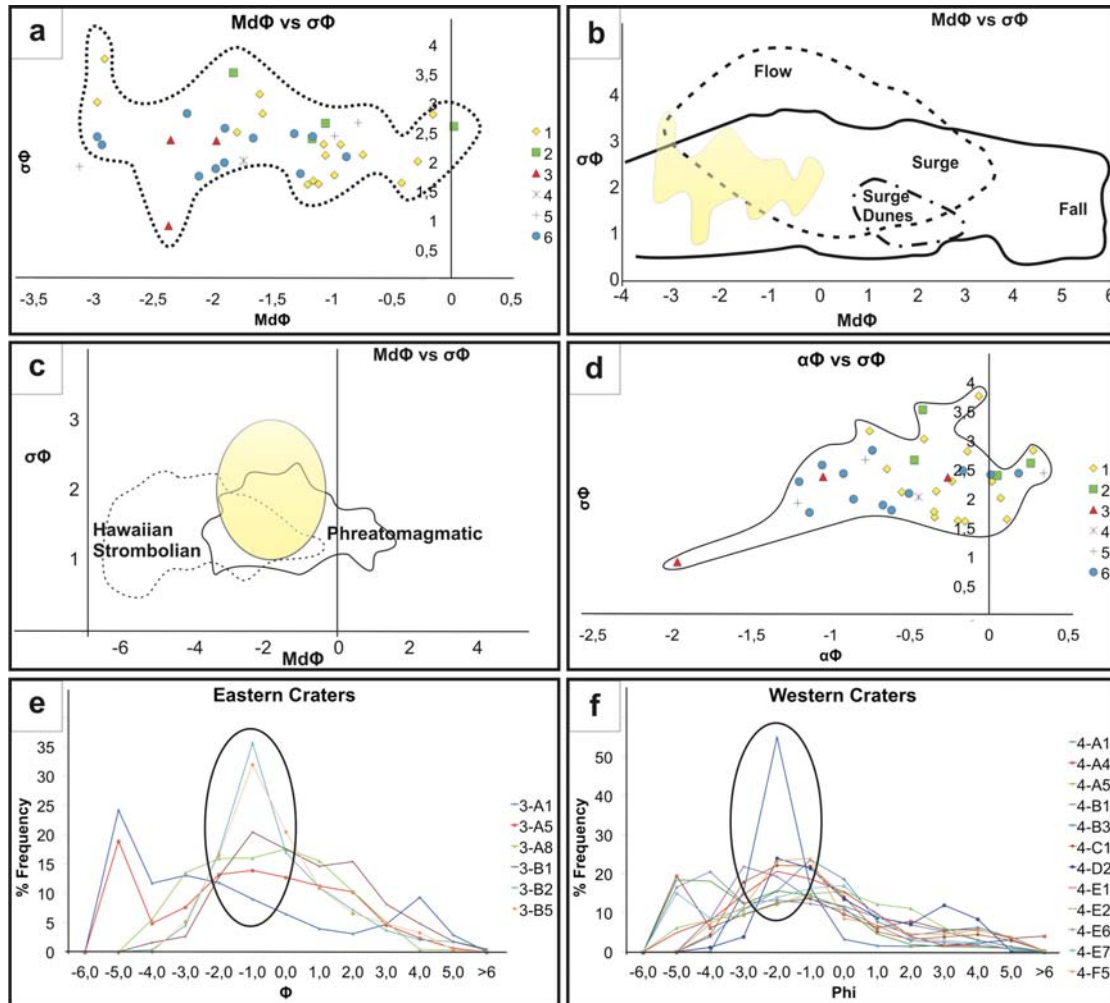


Fig. 6. Plot of grain-size data from the fall and surge deposits. (a) Sorting ($\sigma\phi$) versus Median Diameter ($Md\phi$); (b) Sorting ($\sigma\phi$) versus Median Diameter ($Md\phi$) compared with a Walker diagram (1971); (c) Houghton *et al.* (2000) diagram; (d) Sorting ($\sigma\phi$) versus Skewness ($\alpha\phi$), granulometrical frequency distribution at (e) Eastern Craters and (f) Western Craters.

An isopleth map from close to the eruptive centres is given (Fig. 7). The size values recorded on this map represent an average of the three axes of the largest clasts from any given site. Clasts are made of juvenile fragments and accidental lithics (grey aphyric lava, yellow and greenish tuff and reddish vesicular lava). Some of the lithic

clasts related to the western craters that are shown in Figure 7d might have been affected by re-distribution by streams and mudflows resulting from the unusual seasonal melt on Deception Island during the 1970–71 summer, as described in Baker and McReath (1975).

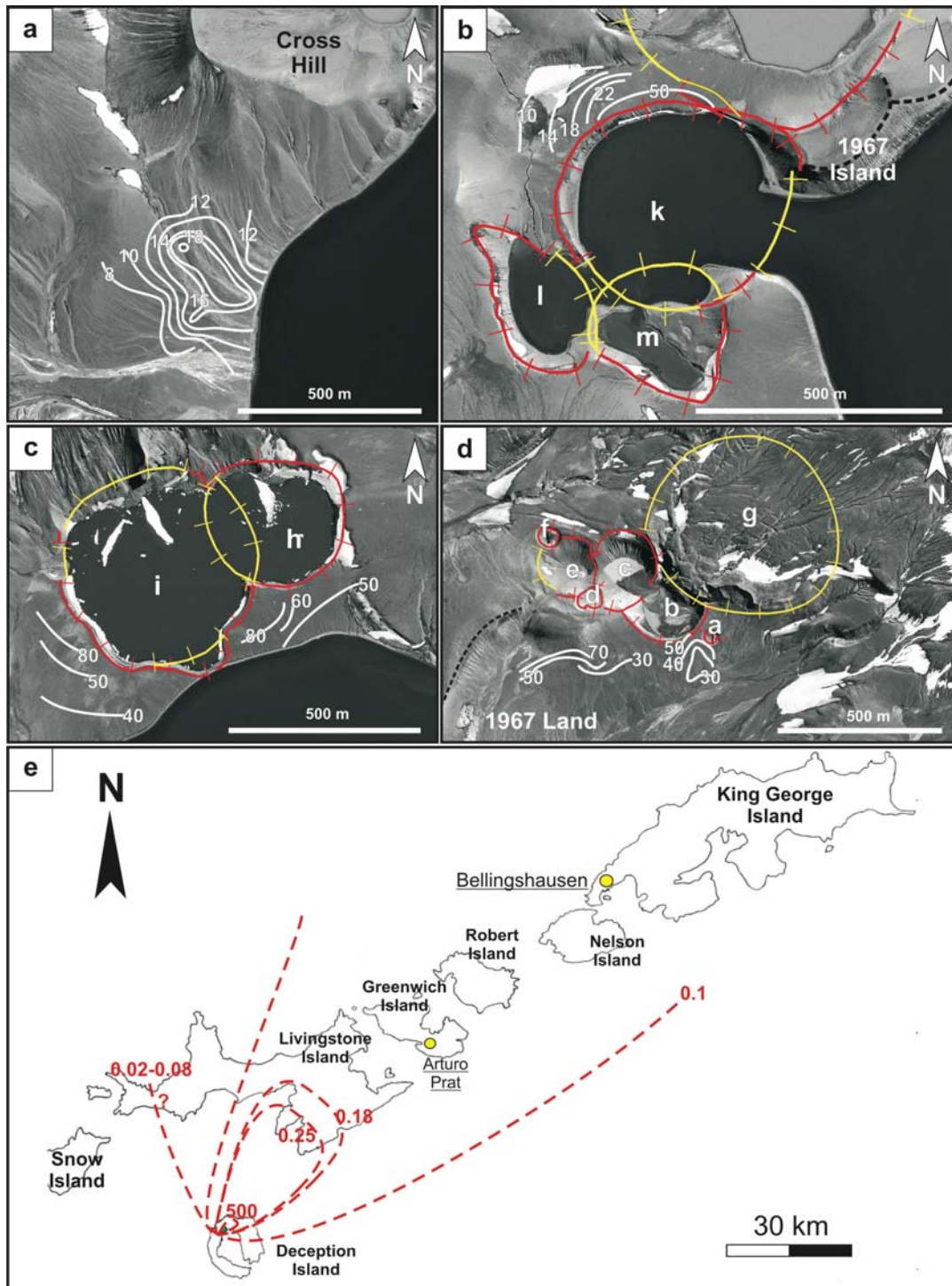


Fig. 7 Proximal isopleth map in cm (white continuous line) showing the distribution of lithics (a) south of Cross Hill; (b) Western Craters; (c) Western Craters-Lago Escondido. The red continuous line represent the crater rims and the yellow continuous lines the inferred crater rims; (d) Eastern Craters; (e) isopleth map in mm (red dashed lines) in the Shetland Archipelago.

An isolated area of relatively large bombs between Cross Hill and Wensleydale Beacon with no traces of a source crater was reported by Baker and McReath (1975). These bombs were probably discharged from another eruptive vent, as shown in Figure 7a. A preliminary isopleth map for the distal deposits (Fig. 7e) was obtained from data reported in Pallàs et al. (2001), Fretzdorff and Smellie (2002) and Geyer et al. (2006, 2008). Further data were taken from Hodgson et al. (1998), who reported an ash layer in a core from Midge Lake (Livingstone Island). Hodgson et al. (1998) suggest that this horizon might correspond to any of the documented eruptions on Deception Island (1967, 1969 or 1970) or to the earlier eruptions that occurred in 1842 and 1912–17. However, the reported dispersal area of the 1967 and 1969 eruptions (Baker and McReath, 1975; Smellie, 2002) and the shallow position in the core of this ash layer suggest that this horizon belongs to the 1970 eruption, although the 1842 and 1912–1917 episodes, which are only mentioned briefly in Wilkes (1845), Orheim (1971c) and Roobol (1973, 1980, 1982), cannot be ruled out as possible origins.

5.5.5 Componentry analysis

The products of the 1970 eruption consist of a mixture of dense, black or vesicular scoria of basaltic andesitic composition with differing proportions of accidental lithic clasts (older lava flows and yellow and greenish tuff) (Fig. 4). Variations in the occurrence of the lithic fragments can be seen in the stratigraphic succession, as well as in the different groups of craters. As observed in Fig. 4 and supplementary materials, the lava clasts are the most abundant accessory components in the successions in both groups of craters. In the Lago Escondido edifice, the lava clasts are particularly dominant in the lower part of the succession (e.g. samples 4-A4, 4-A5, 4-B1, 4-C1, 4-E2, 4-E6; Fig. 4) and also characterise the whole succession in stratigraphic log 1 (Fig. 4). Greenish and yellow tuff clasts are typically present in smaller number and in general are found in the lower part of stratigraphic log 1 (e.g. samples 3-A1; Fig. 4) and in the upper part of the sequence from Lago Escondido (e.g. samples 4-E7, 4-F5; Fig. 4).

Generally, accidental lithic clasts increase in percentage in the size range -4ϕ to -3ϕ (Fig. 4). Small variations in the amount of juvenile components can be observed throughout the first outcrop, where samples range around 90%. The second group of craters shows a general decrease in the amount of juvenile components of up to 70–80% (Fig. 4).

5.6 Discussion

Despite the limited number of exposures that we were able to study, we managed to establish one stratigraphic log from the Eastern Craters (stratigraphic log 1; Fig. 4) and five from the Western Craters from around the same vent area (Lago Escondido Edifice) (stratigraphic logs 2-6; Fig. 4). We believe that all are representative of the general succession of deposits formed by the 1970 eruption and its dynamics.

This eruption seems to have been continuous, as suggested by the absence of discontinuities in the stratigraphic sequences, and was totally pyroclastic (magmatic and hydrovolcanic) with no lava flow. The location of the craters along one of the main structural limits of the caldera (see Martí et al., 2013) suggests that caldera faults fed the eruption. Several vents opened during the eruption and generated different types of craters and cones with contrasting eruptive styles.

The Eastern Craters near Goddard Hill contrast with the western group at Telefon Bay that consist of maar-like craters. As suggested by Sohn (1996), the morphology of edifices might be controlled by depositional processes; nevertheless, morphology will also depend on the physical properties of the surrounding bedrock, vent geometry and the water/magma ratio (Kokelaar, 1986; Sohn, 1996; Vespermann and Schmincke, 2000; White Aand Houghton, 2000). The lithological and sedimentological characteristics of the deposits forming the stratigraphic succession in the eastern cones reveal that the lowest part corresponds to deposits formed from base-surge-type explosions (e.g. Crowe and Fisher, 1973; Fisher and Waters, 1970; Druitt, 1998). The high degree of fragmentation of these deposits suggests a phreatomagmatic phase with optimal magma–water energy transfer. The locus of the explosion was probably located at the limit between the shield and the syn-caldera deposits (Fig. 8a-1) due to the presence of both types of rocks as accessory lithic clasts in these deposits (sample 3-A1; Fig. 4). This episode was followed by the deposition of poorly sorted fallout breccia deposits. The nature of the lithic clasts in these breccia deposits, which mostly correspond to shield-derived lava fragments and syn-caldera ignimbrites, suggest that at this stage the locus of the eruption was located in a part of the shield structure that was below the syn-caldera deposits (Fig. 8a2). A strong unconformity (Figs. 4 and 5a,b) marks the transition towards the upper part of the succession dominated by alternating thick, coarse, well-sorted lapilli-sized breccia layers with fine and coarse lapilli layers with planar stratification, indicating the existence of continuous

changes in the efficiency of the hydromagmatic fragmentation. The presence of a strong unconformity that also coincides with a change in the layer dip suggests a shift in the locus of the explosions and a variation in the eruptive rate (e.g. Valentine and Fisher, 2000); the lower part of the succession could belong to crater c and the upper part to crater d (Fig. 2). Water could have been drawn into the conduit due to a fractured aquifer and/or to the melting of the surrounding ice-cap as a consequence of the eruption itself.

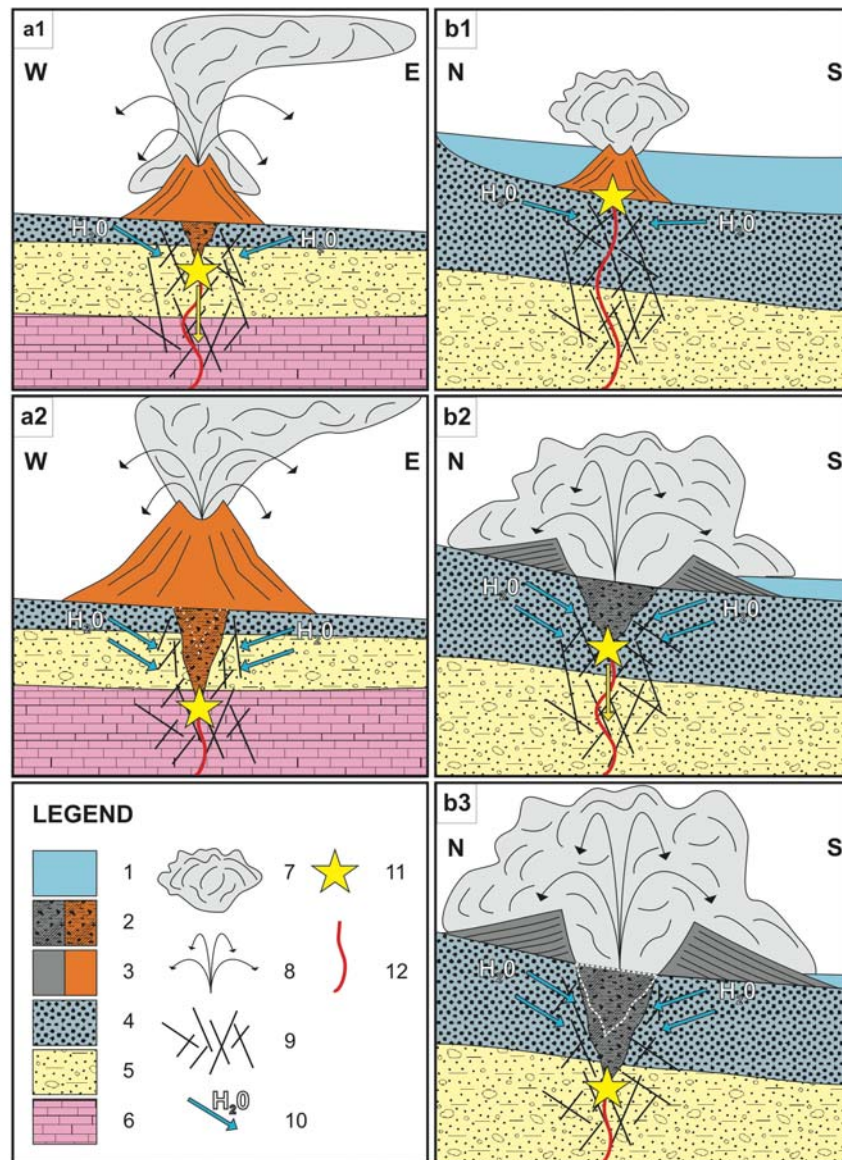


Fig. 8 Sketch not to scale of the evolution of the 1970 eruption: Eastern Craters (a1) rise of the magma and interaction with the syn-caldera deposits; (a2) decrease in the fragmentation level and interaction with a deeper part of the pre-caldera deposits; Lago Escondido (b1) interaction of the ascending magma with shallow marine water and beginning of the eruption; (b2) hydrovolcanic activity due to the interaction with water in the shallower post-caldera deposits; (b3) decrease in the fragmentation level in the conduit and interaction with the basement made of syn-caldera deposits. 1) sea, 2) breccia deposits, 3) volcanic deposits, 4) post-caldera deposits, 5) syn-caldera deposits, 6) pre-caldera deposits, 7) phreatomagmatic activity, 8) ballistic fallout, 9) fracture zone, 10) infiltration area, 11) explosion locus, 12) dyke.

Unlike the craters near Goddard Hill, the activity in the western part started with a very shallow submarine eruption (Fig. 8b1) (as deduced by the actual position of the coast line compared to the 1969 coastline; see Shultz, 1972; Baker and McReath, 1975) and then evolved into a subaerial phase (Fig. 8b2,b3), leading to the formation of a new strip of land about 1,700-m long, 400-m wide and 12 m a.s.l. The 1970 activity caused the partial destruction of the island that had formed in 1967 in Telefon Bay, which was truncated at its northeastern and southwestern ends (Baker and McReath, 1975). The stratigraphic logs (2–6; Fig. 4) studied in this sector were all located around the same vent area (Lago Escondido) whose morphology indicates the presence of two partially coalesced craters. The succession of deposits observed in all of these craters is very similar and is mainly characterised by breccia deposits with almost no evidence of depositional structures. Stratigraphic logs 2 and 4 (Fig. 4) reveal the presence at the base of the breccia deposits of a lithic-poor episode (Sample 4-A1; Fig. 4), which might correspond to the first submarine and less explosive phase of the eruption (Fig. 8b1). Stratigraphic log 6 (Fig. 4) has a uniform succession of breccia deposits and subordinate fine lapilli deposits emplaced by pyroclastic surges, above all in the upper part of the sequence (Fig. 4). The lithic content suggests an initial interaction with shallower lava flows, probably emplaced from the post-caldera phase (e.g. samples A4, 4-A5, 4-B1, 4-C1, 4-E2, 4-E6; Fig. 4) (Fig. 8b2), with a change in the upper part of the sequence characterised by an increase in the number of yellow tuff lithic clasts (e.g. samples 4-E7, 4-F5; Fig. 4) in both craters. A progressive lowering of the position of the fragmentation level in the eruption conduit during the course of the eruption might have led the magma to interact with a deeper part of the basement made of syn-caldera yellow tuff (Fig. 8b3).

On the basis of the available field data, a preliminary quantitative evaluation of the eruptive parameters can be attempted. Thickness and maximum lithic clast size measurements enable us to obtain the isopach and isopleth maps for the 1970 eruption. The minimum associated volume of the eruption was calculated using the isopach map defined by Baker and McReath (1975) and Smellie (2002). Volume calculations were carried out using the method proposed by Pyle (1989) that considers elliptical isopachs and an exponential decay.

Violent mafic eruptions described in the literature produce volumes of 0.001 to $>1 \text{ km}^3$ DRE and dispersal areas covering 10 to $>500 \text{ km}^2$ (see Wong and Larsen, 2010). The 1970 eruption is characterised by an estimated total bulk volume of less than

0.1 km³ and a dispersal area of about 4x10³ km² (Fig. 2), calculated using the isopachs extrapolated from the data collected at the Arturo Pratt and Bellingshausen stations and data from sea-cores in the Central Bransfield Basin reported by Fretzdorff and Smellie (2002). These authors found a correspondence for an ash layer with volcanic ash dating from the 1970 eruption. Deposits from the 1970 eruptions have also been reported in ice-cores from Livingston Island (Pallàs et al., 2001; Geyer et al., 2006, 2008).

Following the methods proposed by Carey and Sparks (1986) and in comparison with the 1967 eruption, we can infer a column height of about 10 km. Wind velocities for August 1970 were calculated using data from the Bellingshausen stations on King George Island (http://www.antarctica.ac.uk/met/READER/upper_air/uawind.html) with approximate values of 28–38 m/s at heights of 5,500 and 9,100 m, which confirms that the deposits were strongly affected by wind during deposition.

The wide dispersion of deposits could also be explained by the height of the tropopause above Antarctica, which is unusually low and in the range 8–10 km (Weyant, 1966); additionally, the stratosphere here is much less stratified than in the tropics or at mid-latitudes. This would allow for the rapid and widespread distribution of tephra in the area (Kyle et al., 1981) and even permit small eruptions to inject material into the stratosphere. This could also explain the generally coarse grain size character of proximal deposits, which are probably fines depleted as shown in Figs. 4 and 6e,f.

The 1970 eruption was undoubtedly one of the most violent in the past century on Deception Island and falls in the category of violent Strombolian (Wong and Larsen, 2010) and corresponds to a VEI 3 of Newhall and Self (1982).

This eruption occurred in shallow seawater and at onshore ice-free locations, in the same general area as the 1967 eruption but with more widely distributed vents. The 1967 episode was very similar in nature and size to the 1970 eruption and generated submarine and land vents. Three overlapping pyroclastic cones (Fig. 3) with water-filled craters were created in the northwestern corner of Telefon Bay, while a further centre was located 2 km east of the new island on the shore of Port Foster between Telefon Bay and Pendulum Cove (Fig. 3). The eruption has been reported in detail by Roobol et al. (1975), who described a column height of about 2.5 km at the beginning of the eruption, rising to 6 km and then reaching a maximum height of about 10 km. The wind speed was less than 10 m/s (Valenzuela et. al., 1968). As reported in Roobol et al. (1975), a thin covering of ash was noted on Livingstone Island and probably on

Greenwich Island as well. An ash-coated iceberg was reported close to Elephant Island, which is about 200 km to the northeast of Deception Island.

On Deception Island, eruptions of high explosivity due to magma/water interaction are common and are characterised by shallow submarine vents or are located on waterlogged shorelines or beneath the ice caps. The 1967 and 1970 eruptions demonstrate that similar explosive events are controlled differentially by the physical nature of the vent and the way in which the magma interacts with the surrounding environment, leading to several closely spaced episodes with different characteristics and associated hazards. Although there were 42 men in the British and Chilean stations and more in the Argentinian station during the 1967 eruption, no lives were lost (Roobol, 1982), even though some of the installations were destroyed. Despite the lack of witnesses to the 1970 eruption (Baker and McReath, 1975), its characteristics, deduced from the study of its deposits, suggest a similar or even larger event than that of 1967, but with similar associated hazards.

The Bay of Port Foster has traditionally been used as a natural harbour by sailors and, in particular, by whalers who installed the factory in Whaler's Bay that was destroyed during the 1969 eruption (Smellie, 2002). Scientific bases were built by Argentina, UK and Chile around Port Foster, the latter two being destroyed by the 1967 and 1969 eruptions (Roobol, 1982). Currently, a Spanish and an Argentinian base (Fig. 1) operate during the Antarctic summer seasons. The island has also become an important tourist attraction and was visited by almost 50,000 people in 2004–2010, with annual peaks of 10,000 visitors (IAATO, *International Association of Antarctica Tour Operators*). Thus, the volcanic risk is increasing given the high probability of an eruption in the near future. The characteristics of the 1970 and 1967 eruptions suggest that a future eruption could have a considerable impact on the people and installations on Deception Island, particularly if it occurs during the austral summer. Therefore, a detailed reconstruction of past eruptions, as we have attempted in the present study, are a necessary first step in a hazard assessment aimed at reducing the volcanic risk on Deception Island.

5.7 Conclusion

The study of the stratigraphy, lithology and sedimentological features of the eruption of 1970 on Deception Island enables us to reconstruct its eruptive dynamics and main physical parameters. The eruption occurred close to the area of 1967 vents, in

shallow seawater and at onshore ice-free locations, and led to the formation of two groups of craters – one with cone-shaped and the other with maar-like craters – that reveal the differing nature of these two eruptions. The 1970 eruption alternated magmatic and hydrovolcanic episodes that deposited fallout, ballistic blocks and bombs and pyroclastic surges. A total bulk volume of less than 0.1 km³ has been estimated for this eruption, and its tephra deposits dispersed northeastwards as far as King George Island, >150 km away. This explosive episode is classified as violent Strombolian and VEI 3, and produced a plume up to 10 km above sea level in height. The 1970 eruption was similar to the 1967 episode and confirms how this type of post-caldera volcanism on Deception Island is controlled by the location of the vents and magma interaction with the surrounding environment. This could give rise to closely spaced eruptions or even several episodes during the same eruptive event, with different characteristics and associated hazards. A similar eruption occurring in the future on Deception Island might represent a serious hazard to the increasing number of people that visit during certain periods of the year and to the scientific installations that operate there.

Acknowledgments

This research was supported by the MICINN grant CTM2011-13578-E. AG is grateful for her Juan de la Cierva Grant (JCI-2010-06092). We would like to thank all the military staff from the Spanish Antarctic Base Gabriel de Castilla for their constant help and for the logistic support, without which this research would not have been possible. The English text was corrected by Michael Lockwood.

References

- Ashcroft, W., 1972. Crustal structure of the South Shetland Islands and Bransfield Strait, 1st edn. British Antarctic Survey, London: 43 p., 41 fold. leaf p.
- Baker, P., McReath, I., Harvey, M., Roobol, M. and Davies, T., 1975. The geology of the South Shetland Islands: volcanic evolution of Deception Island. British Antarctic Survey Scientific Reports, 78: 81 pp.
- Baker, P.E. and McReath, I., 1971. Geological investigations on Deception Island. Antarctic Journal of the United States, 6: 85-86.

- Baker, P.E. and McReath, I., 1975. The 1970 eruption. in: Baker P, McReath I, Harvey M, Roobol M, Davies T (1975) The geology of the South Shetland Islands: volcanic evolution of Deception Island, British Antarctic Survey Scientific Reports (78): 52-61.
- Barclay, A.H., Wilcock, W.S.D. and Ibáñez, J.M., 2009. Bathymetric constraints on the tectonic and volcanic evolution of Deception Island Volcano, South Shetland Islands. *Antarctic Science*, 21(02): 153-167.
- Carey, S. and Sparks, R.S.J., 1986. Quantitative models of the fallout and dispersal of tephra from volcanic eruption columns. *Bulletin of Volcanology*, 48(2-3): 109-125.
- Crowe, B.M. and Fisher, R.V., 1973. Sedimentary Structures in Base-Surge Deposits with Special Reference to Cross-Bedding, Ubehebe Craters, Death Valley, California. *Geological Society of America Bulletin*, 84(2): 663-682.
- Dalziel, I.W.D., 1984. Tectonic evolution of a forearc terrane, southern Scotia Ridge, Antarctica. *Geological Society of America Special Papers*, 200: 1-32.
- Druitt, T.H., 1998. Pyroclastic density currents. In: Gilbert, J.S., Sparks, R.S.J. (Eds.), *The Physics of Explosive Volcanic Eruptions*. Geological Society, Spec. Publ. , 145: 145-182.
- Fisher, R. and Waters, A., 1970. Base surge bed forms in maar volcanoes. *American Journal of Science*, 268 (2): 157-180.
- Fretzdorff, S. and Smellie, J.L., 2002. Electron microprobe characterization of ash layers in sediments from the central Bransfield basin (Antarctic Peninsula): evidence for at least two volcanic sources. *Antarctic Science*, 14(04): 412-421.
- Geyer, A., Casas, J.M., Pallàs, R. and Gimeno, D., 2008. Chemical and physical characterization of tephra layers from Livingston Island (Antarctica): ice drill data. *Geotemas*, VII Congreso Geológico de España, vol 10: pp. 216.
- Geyer, A., Casas, J.M., Pallàs, R., Gimeno, D. and Calvet, J., 2006. Chemical and physical characterization of tephra layers from Livingston Island (Antarctica): ice drill data and methodological considerations. VII Simposio español de estudios polares Granada, University of Granada

- González-Ferrán, O., Munizafa, F. and Moreno, H., 1971. Síntesis de la evolución volcánica de Isla Decepción y la erupción de 1970. Instituto Antártico Chileno, Serie Científicas, 2: 1-14.
- Gràcia, E., Canals, M., Lí Farràn, M., José Prieto, M., Sorribas, J. and Team, G., 1996. Morphostructure and evolution of the central and Eastern Bransfield Basins (NW Antarctic Peninsula). *Marine Geophysical Researches*, 18(2-4): 429-448.
- Grad, M., Guterch, A. and Sroda, P., 1992. Upper crustal structure of Deception Island area, Bransfield Strait, West Antarctica. *Antarctic Science*, 4(04): 469-476.
- Hodgson, A.D., Dyson, C.L., Jones, V.J. and Smellie, J.L., 1998. Tephra analysis of sediments from Midge Lake (South Shetland Islands) and Sombre Lake (South Orkney Islands), Antarctica. *Antarctic Science*, 10(1): 13-20.
- Houghton, B.F., Wilson, C.J.N. and Pyle, D.L., 2000. Pyroclastic fall deposits. In: Sigurdsson, H., Houghton, B.F., McNutt, S.R., Rymer, H., Stix, J. (Eds.), *Encyclopedia of Volcanoes*. Academic Press: 555-570.
- Ibáñez, J.M., Almendros, J., Carmona, E., Martí, amp, x, nez-Arévalo, C. and Abril, M., 2003. The recent seismo-volcanic activity at Deception Island volcano. *Deep Sea Research Part II: Topical Studies in Oceanography*, 50(10–11): 1611-1629.
- Jeffers, J. and Anderson, J., 1990. Sequence stratigraphy of the Bransfield Basin, Antarctica: implications for tectonic history and hydrocarbon potential In: St. John B (ed) *Antarctica as an exploration frontier: hydrocarbon potential, geology and hazards*. *Am Ass Petrol Geol Stud Geol* 31:13–29.
- Kokelaar, P., 1986. Magma-water interactions in subaqueous and emergent basaltic volcanism. *Bulletin of Volcanology*, 48: 275-289.
- Kyle, P.R., Jezek, P.A., Mosley-Thompson, E. and Thompson, L.G., 1981. Tephra layers in the Byrd Station ice core and the Dome C ice core, Antarctica and their climatic importance. *Journal of Volcanology and Geothermal Research*, 11(1): 29-39.
- Martí, J., Geyer, A. and Aguirre-Díaz, G., 2013. Origin and evolution of the Deception Island caldera (South Shetland Islands, Antarctica). *Bulletin of Volcanology*, 75(6): 1-18.

- Newhall, C.G. and Self, S., 1982. The volcanic explosivity index (VEI) an estimate of explosive magnitude for historical volcanism. *Journal of Geophysical Research: Oceans*, 87(C2): 1231-1238.
- Orheim, O., 1971c. Volcanic activity on Deception Island, South Shetland Islands. in: ADIE, R. J., ed. *Antarctic geology and geophysics*. Oslo, Universitetsforlaget: 117-120.
- Pallàs, R., Smellie, J.L., Casas, J.M. and Calvet, J., 2001. Using tephrochronology to date temperate ice: correlation between ice tephra on Livingston Island and eruptive units on Deception Island volcano (South Shetland Islands, Antarctica). *The Holocene*, 11(2): 149-160.
- Pyle, D., 1989. The thickness, volume and grainsize of tephra fall deposits. *Bulletin of Volcanology*, 51(1): 1-15.
- Roobol, M.J., 1973. Historic volcanic activity at Deception Island. *British Antarctic Survey Bulletin*, 32: 23-30.
- Roobol, M.J., 1980. A model for the eruptive mechanism of Deception Island from 1820 to 1970. *British Antarctic Survey Bulletin*, 49: 137-156.
- Roobol, M.J., 1982. The volcanic hazard at Deception Island, South Shetland Islands. *British Antarctic Survey Bulletin*, 51: 237-245.
- Roobol, M.J., Davies, T.G. and Baker, P.E., 1975. The 1967 eruption. In: Baker P, McReath I, Harvey M, Roobol M, Davies T (1975) *The geology of the South Shetland Islands: volcanic evolution of Deception Island*: pp. 16-37.
- Sheridan, M.F. and Wohletz, K.H., 1983. Hydrovolcanism: Basic considerations and review. *Journal of Volcanology and Geothermal Research*, 17(1-4): 1-29.
- Shultz, C.H., 1972. Eruption at Deception Island, Antarctica, August 1970. *Geological Society of America Bulletin*, 83(9): 2837-2842.
- Smellie, J., Thomson, J. and Thomson, M., 2002. *Geology and geomorphology of Deception Island*. British Antarctic Survey, Cambridge: 77p. + 73 folded maps.
- Smellie, J.L., 1988 Recent observations on the volcanic history of Deception Island, South Shetland Islands. *British Antarctic Survey Bulletin* 81(83–85).

Smellie, J.L., 2001. Lithostratigraphy and volcanic evolution of Deception Island, South Shetland Islands. *Antarctic Science*, 13(02): 188-209.

Smellie, J.L., 2002. The 1969 subglacial eruption on Deception Island (Antarctica): events and processes during an eruption beneath a thin glacier and implications for volcanic hazards. in: Smellie, J.L. and Chapman, M.G., eds. *Volcano-ice interaction on Earth and Mars*. Geological Society, London, Special Publication, 202: 59- 79.

Sohn, Y.K., 1996. Hydrovolcanic processes forming basaltic tuff rings and cones on Jeju Island, Korea. *Geological Society of America Bulletin*, 108: 1199-1211.

Valencio, D.A., Mendía, J. and Vilas, J.F., 1979. Palaeomagnetism and KAr age of Mesozoic and Cenozoic igneous rocks from Antarctica. *Earth and Planetary Science Letters*, 45(1): 61-68.

Valentine, G.A. and Fisher, R.V., 2000. Pyroclastic surges and blasts. In: Sigurdsson, H., Houghton, B.F., McNutt, S.R., Rymer, H., Stix, J. (Eds.), *Encyclopedia of Volcanoes*. Academic Press: 571–580.

Valenzuela, E., Chavez, L. and Munizaga, F., 1968. Informe preliminar sobre la erupcion de Isla Decepcion ocurrida en diciembre de 1967. *Boletín Instituto Antártico Chileno*, 3: 5-16.

Vespermann, D. and Schmincke, H.U., 2000. Scoria cones and tuff rings. In: H. Sigurdsson, B.F. Houghton, S.R. McNutt, H. Rymer and J. Stix (Editors), *Encyclopedia of Volcanoes*. Academic Press, San Diego: 683-694.

Vuan, A., Robertson Maurice, S.D., Wiens, D.A. and Panza, G.F., 2005. Crustal and upper mantle S-wave velocity structure beneath the Bransfield Strait (West Antarctica) from regional surface wave tomography. *Tectonophysics*, 397(3–4): 241-259.

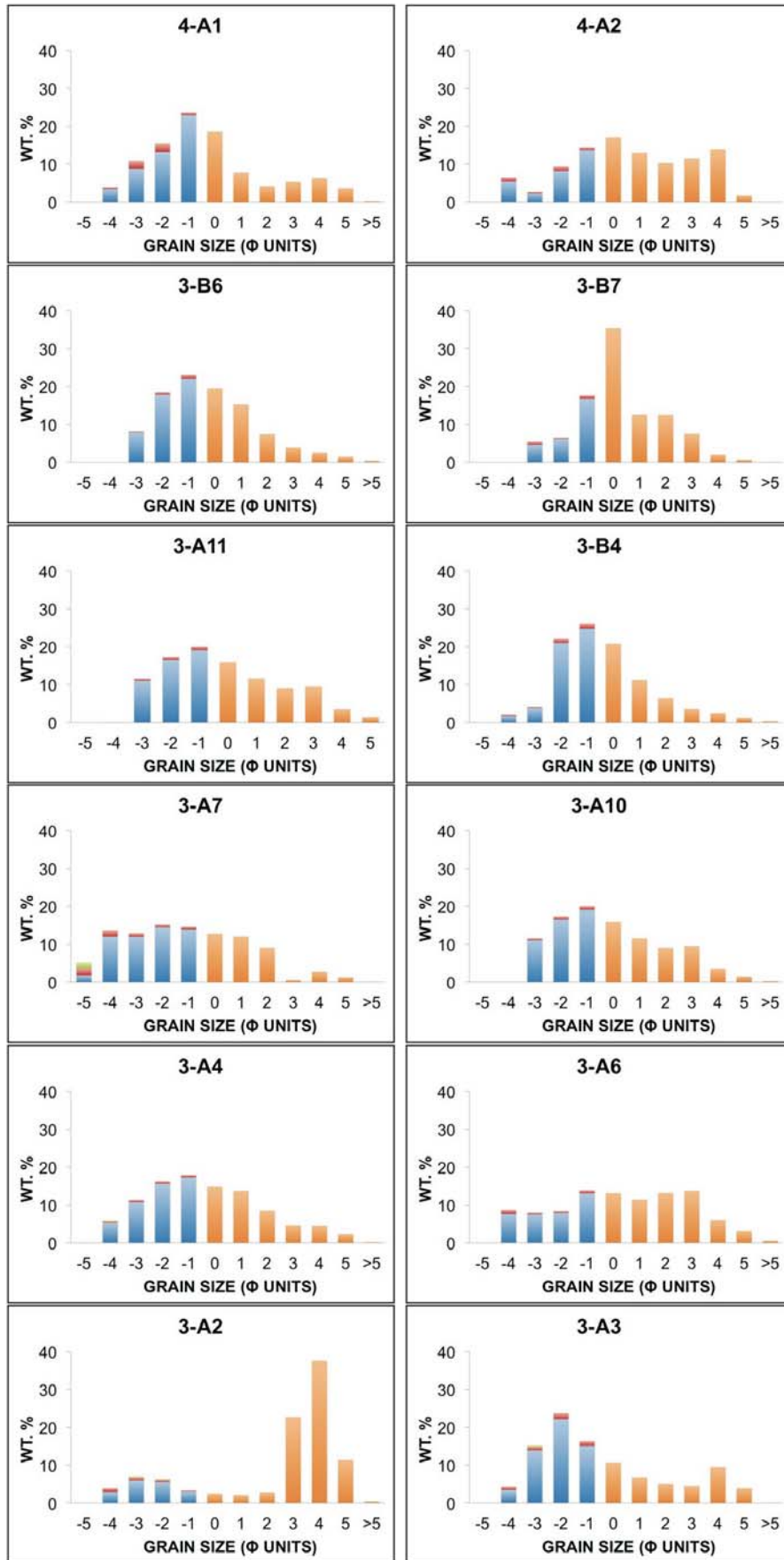
Walker, G.P.L., 1971. Grain size characteristics of pyroclastic deposits. *Journal of Geology*, 79(6): 696-714.

Weyant, W.S., 1966. The Antarctic atmosphere: climatology of the troposphere and lower stratosphere. *American Geographical Society Antarctic Map Folio Series Folio 4*.

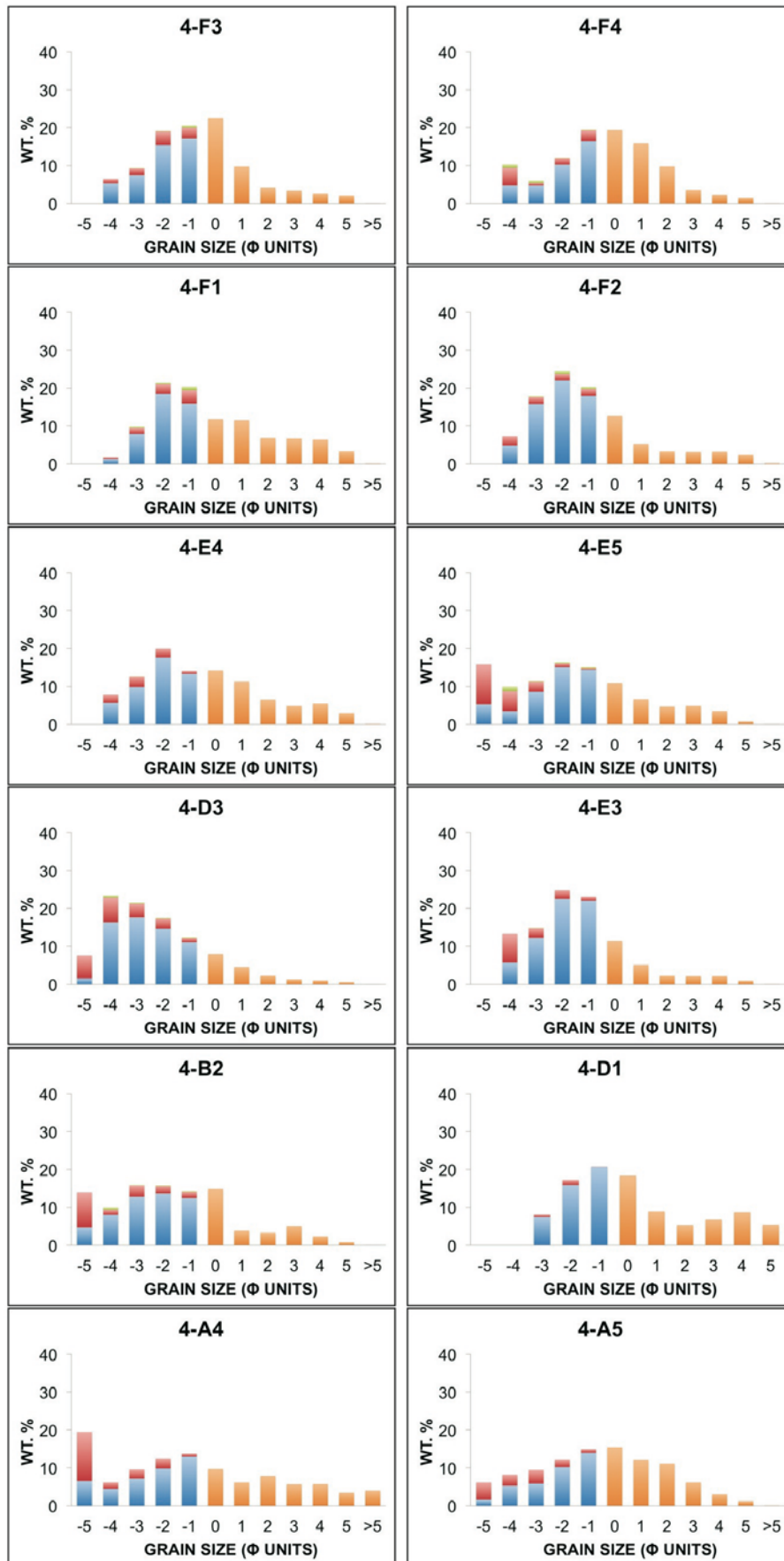
White, J.D.L. and Houghton, B., 2000. Surtseyan and related phreatomagmatic eruptions. In: Sigurdsson, H., Houghton, B.F., McNutt, S.R., Rymer H., Stix J. (Editors), Encyclopedia of Volcanoes. Academic Press, San Diego: 495-511.

Wilkes, C., 1845. Narrative of the United States Exploring Expedition, during the years 1838, 1839, 1840, 1841, 1842. I-V, Atlas(Philadelphia, Lea & Blanchard).

Wong, L. and Larsen, J., 2010. The Middle Scoria sequence: A Holocene violent strombolian, subplinian and phreatomagmatic eruption of Okmok volcano, Alaska. Bulletin of Volcanology, 72(1): 17-31.



Supp. Material. Granulometric and componentry histograms.



Supp. Material. (continued)

6. SUMMARY OF RESULTS AND DISCUSSION

The thesis consists of four research papers, which are actually published, in press or submitted in international journals, showing the evolution of the research and the main results obtained so far. The order of the papers follows the idea of showing different aspects of hydromagmatism in monogenetic volcanic fields developed in continental and ocean island environments, as well as the use of different methodologies to study such complex eruptive behaviour.

These monogenetic landforms and their successions of deposits have been analyzed and discussed, looking for the potential causes of such a wide diversity of eruptive sequences. First I have studied the Crosa de Sant Dalmai volcano, one of the most representative monogenetic centres of the Catalan Volcanic Zone, a roughly circular asymmetrical maar-diatreme, located a few km from the city of Girona. The edifice belongs to the Garrotxa Volcanic Field (GVF), which includes the youngest volcanoes in the CVZ (0.6–0.01 Ma) The edifice is an example of monogenetic volcano constructed on a mixed basement made of hard Paleozoic granites and schists rocks and soft Plio-Quaternary deposits. This type of activity occurred on a mixed environment has been poorly studied so far, highlighting the importance of understanding the eruptive dynamic of complex edifices like this. The well-preserved morphology of the edifice made it suitable for geological surveys. As reported in Pedrazzi et al. (2014), pyroclastic deposits are constituted by an alternating pyroclastic fall and subordinate surges of magmatic and phreatomagmatic origin. Four units were recognized characterized by a variable proportion of lithic and juvenile fragments. A first phreatomagmatic phase (Unit I), was followed by fallout deposition from Hawaiian-style fire fountains (Unit II), indicating that, at this stage, the water supply was not sufficient to sustain the phreatomagmatic interaction with the ascending magma. A second phreatomagmatic episode (III) passed to a final pure magmatic stage (IV) subsequently covered by lacustrine deposits. The model of the eruption was proposed taking into account a 3D geological reconstruction of the internal structure of the uppermost part of La Crosa de Sant Dalmai maar-diatreme system (Bolós et al. 2012). These informations allowed reconstructing the volcanic activity and how the magma/water interaction occurred during the eruption and the influence of the substrate. This is possibly explained by the interaction of the erupting magma with different aquifer levels located at different depths and with different hydrogeological properties, which correspond to the shallower

Plio-Quaternary deposits of La Selva Basin (clay, silt and gravel) and Paleozoic altered rocks and the deeper Paleozoic basement (granite and schists). This eruption emphasizes the role that the geological characteristics of the substrate plays in determining the eruptive style and associated hazards in this type of volcanism.

A fundamental task of this work was to study hydrovolcanic eruptions related to volcanic fields in different geological settings. Further studies were, then, carried out at the Canary Islands. A detailed sedimentological analysis was carried out at Lanzarote Island describing in detail the structure and association of facies at El Golfo tuff cone. The descriptions of the deposits as well as the detailed stratigraphic sections are reported in Pedrazzi et al. (2013). El Golfo is a tuff cone constructed close to the shoreline, in shallower marine conditions, mainly by deposition from pyroclastic surges and emplacement of minor ballistic blocks and bombs. Eight facies were recognized based on (a) sedimentary discontinuities, (b) variations in grain size and percentage of volcanic bombs and (c) variations in primary bedforms. Five facies associations can be correlated to the different stages in the eruption based on the physical appearance of the deposits that make up the succession and the differences in the inferred fragmentation, transportation and deposition mechanisms. A continuous change in the transport/depositional system was interpreted as a modification in the energy transfer efficiency from magma to water and, consequently, in the eruption explosivity and in the degree of fragmentation. A general increase in the explosive energy can be seen as one moves upwards in the pyroclastic succession, indicating possibly that there was a trend towards an optimum magma/water ratio in the second half of the eruption, which would have led to an increase in the energy-exchange efficiency and, consequently, in the magma fragmentation. Thus, El Golfo is a good example of a tuff cone where a single eruption may produce a complex sequence of eruption styles and depositional processes. Furthermore, it was observed how at a Lanzarote Island, a fissure-dominated system, characterized mainly by scoria and/or lava spatter cones, can have very different styles of eruption at the extremities of the fissure as in the case of el Golfo tuff cone, produced by the interaction of rising magma with shallow sea water. In similar geological setting, this type of volcanism might have serious repercussion in terms of potential hazard differently from small lava spatter eruptions, which are easier to manage.

A further investigation was carried out at El Hierro, the southernmost of the Canary Islands, describing in detail a pumice deposit (Malpaso Member) of

hydromagmatic origin and of felsic composition. The stratigraphic, lithological, sedimentological and petrographic characteristics are reported in Pedrazzi et al. (submitted). This deposit corresponds to the products of a single eruptive event with several pulses, giving rise to the formation of turbulent PDC as the dynamics of the eruption was controlled by magma/water interaction. The products of the eruption correspond to a single eruptive event and cover an area of about 13 km² and four units were recognized marking different phases of the eruption, with differences in fragmentation, transportation and deposition mechanisms. In general all the deposits are characterised by very fine grain size reflecting the great efficiency of the magma-water interaction. Stratigraphic data indicate that the Malpaso Member should belong to the final episodes in the construction of the composite El Golfo volcano and this implies that this eruption, the landslide of El Golfo and the eruption (and construction) of the following Tanganasoga Complex occurred sequentially in a relatively short period of time. Furthermore, it is also possible that the eruption of the Malpaso Member was the impulse behind the landslide of El Golfo and that the construction of Tanganasoga corresponds to a volumetrically significant post-collapse eruptive episode that was triggered by the decompression of the deep magmatic system caused by the massive removal of part of El Golfo. Therefore, a new felsic eruption was recognized apart from the ones of Gran Canaria and Tenerife Islands. This study, thus, represents a step forward in the hazard assessment on the island of El Hierro because a similar composition was found in the recent erupted products of the 2011–2012 eruption, highlighting the possibility that magmas from El Hierro could have the potential for producing a large volume of eruptable felsic magma, making necessary to take into account possible scenarios including felsic explosive eruptions.

The last part of the work focused on the most recent eruptive episode at Deception Island: the eruption of 1970, which led to the formation of several craters close to the beach shore at the northern sector of the island. These edifices are the result of hydrovolcanic monogenetic activity and resemble some of the ones observed at the CVZ, although they were formed in different geodynamic and geological settings. The stratigraphic sequence and the general characteristics of the eruption are described in Pedrazzi et al. (submitted). Two groups of craters were originated during the eruption, showing a different nature of the hydrovolcanic activity: maar-like and cone-shaped craters. The former were characterized by a first submarine eruption, later switching to a subaerial phase due to the interaction with the post-caldera deposits and the syn-caldera

basement. The latter were, probably, emplaced as consequence of the interaction with the syn-caldera deposits and as the eruption progressed, with the pre-caldera basement. The 1970 episode was the most violent recent volcanic activity on Deception Island being classified as violent strombolian eruption, with an estimated erupted total volume of less than 0.1 km^3 , a dispersal area of about $4 \cdot 10^3 \text{ km}^2$ and a plume of less than 10 km leading to a volcanic explosivity index (VEI) of 3. The 1970 eruption was compared with the one of 1967 showing similar characteristics, thus suggesting how at Deception Island this type of volcanism depends on the magma interaction with the surrounding environment and physical nature of the vent that might lead to several closely spaced eruptions with different dynamic. This study represents a step forward in the evaluation of volcanic hazard at Deception Island because a similar eruption occurring in the future might represent a serious threat to the increasing number of visitors it receives during certain periods of the year and to the scientific installation that are operating there.

In summary, the results obtained in this thesis prove the importance of conducting a multidisciplinary approach to understand the evolution of monogenetic centres characterized by a complex eruptive behaviour. Monogenetic volcanic fields are present in almost every tectonic setting and this type of work represents a fundamental task in order to understand the evolution and related hazards of this type of volcanism. The eruptive history of each individual monogenetic volcano within a volcanic field is usually short although the total duration of volcanism in a single volcanic field might last for a much longer span of time. The complex eruptive dynamics of monogenetic volcanic centres and the transport and emplacement mechanisms of their products are controlled by a combination of deep and shallow processes and physical environments (i.e. internal and external parameters).

Some of the examples of monogenetic eruptions shown throughout this research suggest the importance of shallow-level conditions in the formation of specific volcano types. A multidisciplinary approach as the one proposed in the present work (e.g., La Crosa de Sant Dalmai Volcano) would, then, allow to better understanding the behavior of these volcanoes in order to try to reconstruct the evolution of a certain volcanic field and to evaluate the possible volcanic hazard because similar eruptions represent a serious threat, which is often underestimated.

7. CONCLUSIONS

The present work focused on the relation between monogenetic volcanic landforms and the external variables that influenced the dynamic of the corresponding eruptions through a multidisciplinary perspective and in various settings (i.e. ocean islands and continental) under which monogenetic volcanism has developed. The results obtained show the importance of understanding the behavior of monogenetic volcanoes to reconstruct the evolution of volcanic fields. Having a good knowledge of the past behaviour of monogenetic edifices is a fundamental task in order to understand the possible future hazards associated with this type of volcanism. The results obtained in this study show the significant role that the substrate on which these volcanoes form has on their eruption dynamics. Differences in the structural, stratigraphic or hydrogeological characteristics of the volcanoes substrate may have a much stronger influence on the eruptive behaviour of these volcanoes than the magma properties themselves. That is why future research works should include a better characterization of the subsurface of the monogenetic volcanic fields and of the lithological and sedimentological and their volcanoes in terms of time and space distribution of volcanic events, in order to make them comparable in other parts of the world. Therefore, physical parameters (i.e. internal and external) controlling monogenetic volcanism are key points and need a more systematic study in each case to understand the role of shallow-level conditions in the formation of specific volcano types in such complex volcanic fields and to determine the potential hazards they may represent in the future

References

- Auer, A., Martin, U. and Németh, K., 2007. The Fekete-hegy (Balaton Highland Hungary) “soft-substrate” and “hard-substrate” maar volcanoes in an aligned volcanic complex – Implications for vent geometry, subsurface stratigraphy and the palaeoenvironmental setting. *Journal of Volcanology and Geothermal Research*, 159(1–3): 225-245.
- Baker, E., Massoth, G., de Ronde, C., Lupton, J. and McInnes, B., 2002. Observations and sampling of an ongoing subsurface eruption of Kavachi volcano, Solomon Islands. *Geology*, 30(11): 975-978.
- Barde-Cabusson, S., Bolós, X., Pedrazzi, D., Lovera, R., Serra, G., Martí, J. and Casas, A., 2013. Electrical resistivity tomography revealing the internal structure of monogenetic volcanoes. *Geophysical Research Letters*, 40(11): 2544-2549.
- Belousov, A. and Belousova, M., 2001. Eruptive process, effects and deposits of the 1996 and the ancient basaltic phreatomagmatic eruptions in Karymskoye lake, Kamchatka. Russia. *Spec. Publs int. Ass. Sediment.*, 30: 35-60.
- Bolós, X., Barde-Cabusson, S., Pedrazzi, D., Martí, J., Casas, A., Himi, M. and Lovera, R., 2012. Investigation of the inner structure of La Crosa de Sant Dalmai maar (Catalan Volcanic Zone, Spain). *Journal of Volcanology and Geothermal Research*, 247–248(0): 37-48.
- Brand, B.D. and White, C.M., 2007. Origin and stratigraphy of phreatomagmatic deposits at the Pleistocene Sinker Butte Volcano, Western Snake River Plain, Idaho. *Journal of Volcanology and Geothermal Research*, 160(3–4): 319-339.
- Branney, M.J. and Kokelaar, P., 2002. Pyroclastic density currents and the sedimentation of ignimbrites. *Geological Society of London Memoirs*, 150 pp.
- Büttner, R., Dellino, P., La Volpe, L., Lorenz, V. and Zimanowski, B., 2002. Thermohydraulic explosions in phreatomagmatic eruptions as evidenced by the comparison between pyroclasts and products from Molten Fuel Coolant Interaction experiments. *Journal of Geophysical Research: Solid Earth*, 107(B11): 2277.

- Büttner, R., Dellino, P. and Zimanowski, B., 1999. Identifying modes of magma/water interaction from the surface features of ash particles. *Nature* 401: 688-690.
- Carrasco-Núñez, G., Ort, M.H. and Romero, C., 2007. Evolution and hydrological conditions of a maar volcano (Atexcac crater, Eastern Mexico). *Journal of Volcanology and Geothermal Research*, 159(1–3): 179-197.
- Cassidy, J. and Locke, C.A., 2004. Temporally linked volcanic centres in the Auckland Volcanic Field. *New Zealand Journal of Geology and Geophysics*, 47(2): 287-290.
- Chough, S.K. and Sohn, Y.K., 1990. Depositional mechanics and sequences of base surges, Songaksan tuff ring, Cheju Island, Korea. *Sedimentology* 37(6): 1115–1135.
- Cole, P., Guest, J., Duncan, A. and Pacheco, J., 2001. Capelinhos 1957–1958, Faial, Azores: deposits formed by an emergent surtseyan eruption. *Bulletin of Volcanology*, 63(2): 204-220.
- Cole, P.D., 1991. Migration direction of sand-wave structures in pyroclastic-surge deposits; implications for depositional processes. *Geology* 19(11): 1108-1111.
- Condit, C.D. and Connor, C.B., 1996. Recurrence rates of volcanism in basaltic volcanic fields: An example from the Springerville volcanic field, Arizona. *Geological Society of America Bulletin*, 108(10): 1225-1241.
- Connor, C.B., 1987. Structure of the Michoacán-Guanajuato volcanic field, Mexico. *Journal of Volcanology and Geothermal Research*, 33(1–3): 191-200.
- Connor, C.B., 1990. Cinder cone clustering in the TransMexican Volcanic Belt: Implications for structural and petrologic models. *Journal of Geophysical Research: Solid Earth*, 95(B12): 19395-19405.
- Connor, C.B., Condit, C.D., Crumpler, L.S. and Aubele, J.C., 1992. Evidence of regional structural controls on vent distribution: Springerville Volcanic Field, Arizona. *Journal of Geophysical Research: Solid Earth*, 97(B9): 12349-12359.
- Connor, C.B. and Conway, F.M., 2000. Basaltic volcanic fields. In: Sigurdsson, H., Houghton, B.F., McNutt, S.R., Rymer H., Stix J. (Editors), *Encyclopedia of Volcanoes*. Academic Press, San Diego: p. 331–343.

Connor, C.B., Stamatakos, J.A., Ferrill, D.A., Hill, B.E., Ofoegbu, G.I., Conway, F.M., Sagar, B. and Trapp, J., 2000. Geologic factors controlling patterns of small-volume basaltic volcanism: Application to a volcanic hazards assessment at Yucca Mountain, Nevada. *Journal of Geophysical Research: Solid Earth*, 105(B1): 417-432.

Conway, F.M., Connor, C.B., Hill, B.E., Condit, C.D., Mullaney, K. and Hall, C.M., 1998. Recurrence rates of basaltic volcanism in SP cluster, San Francisco volcanic field, Arizona. *Geology*, 26(7): 655-658.

Dellino, P., Isaia, R., La Volpe, L. and Orsi, G., 2004a. Interaction between particles transported by fallout and surge in the deposits of the Agnano-Monte Spina eruption (Campi Flegrei, Southern Italy). *Journal of Volcanology and Geothermal Research*, 133(1-4): 193-210.

Dellino, P., Isaia, R. and Veneruso, M., 2004b. Turbulent boundary layer shear flows as an approximation of base surges at Campi Flegrei (Southern Italy). *Journal of Volcanology and Geothermal Research*, 133(1-4): 211-228.

Dellino, P., Isaia, R., Volpe, L. and Orsi, G., 2001. Statistical analysis of textural data from complex pyroclastic sequences: implications for fragmentation processes of the Agnano-Monte Spina Tephra (4.1 ka), Phlegraean Fields, southern Italy. *Bulletin of Volcanology*, 63(7): 443-461.

Dellino, P. and Liotino, G., 2002. The fractal and multifractal dimension of volcanic ash particles contour: a test study on the utility and volcanological relevance. *Journal of Volcanology and Geothermal Research*, 113(1-2): 1-18.

Druitt, T.H., 1998. Pyroclastic density currents. In: Gilbert, J.S., Sparks, R.S.J. (Eds.), *The Physics of Explosive Volcanic Eruptions*. Geological Society, Spec. Publ. , 145: 145-182.

Giaccio, B., Sposato, A., Gaeta, M., Marra, F., Palladino, D.M., Taddeucci, J., Barbieri, M., Messina, P. and Rolfo, M.F., 2007. Mid-distal occurrences of the Albano Maar pyroclastic deposits and their relevance for reassessing the eruptive scenarios of the most recent activity at the Colli Albani Volcanic District, Central Italy. *Quaternary International*, 171-172(0): 160-178.

Gudmundsson, M.T., Thordarson, T., Höskuldsson, Á., Larsen, G., Björnsson, H., Prata, F.J., Oddsson, B., Magnússon, E., Högnadóttir, T., Petersen, G.N., Hayward, C.L., Stevenson, J.A. and Jónsdóttir, I., 2012. Ash generation and distribution from the April-May 2010 eruption of Eyjafjallajökull, Iceland. *Sci. Rep.*, 2.

Heiken, G. and Wohletz, K., 1985. *Volcanic ash*. University of California Press, Berkeley. 246 pp.

Houghton, B.F. and Hackett, W.R., 1984. Strombolian and phreatomagmatic deposits of Ohakune craters, Ruapehu, New Zealand: A complex interaction between external water and rising basaltic magma. *Journal of Volcanology and Geothermal Research*, 21(3-4): 207-231.

Houghton, B.F., Wilson, C.J.N. and Smith, I.E.M., 1999. Shallow-seated controls on styles of explosive basaltic volcanism: a case study from New Zealand. *Journal of Volcanology and Geothermal Research*, 91(1): 97-120.

Jude-Eton, T.C., Thordarson, T., Gudmundsson, M.T. and Oddsson, B., 2012. Dynamics, stratigraphy and proximal dispersal of supraglacial tephra during the ice-confined 2004 eruption at Grímsvötn Volcano, Iceland. *Bulletin of Volcanology*, 74(5): 1057-1082.

Kienle, J., Kyle, P.R., Self, S., Motyka, R.J. and Lorenz, V., 1980. Ukinrek Maars, Alaska, I. April 1977 eruption sequence, petrology and tectonic setting. *Journal of Volcanology and Geothermal Research*, 7(1-2): 11-37.

Kokelaar, P., 1986. Magma-water interactions in subaqueous and emergent basaltic volcanism. *Bulletin of Volcanology*, 48: 275-289.

Larsen, G., 2010. 3 Katla: Tephrochronology and Eruption History. In: J.K. Anders Schomacker and H.K. Kurt (Editors), *Developments in Quaternary Sciences*. Elsevier, pp. 23-49.

Larsen, G., Guðmundsson, M.T. and Sigmarsson, O., 2009 Katla. In: Sólnes, J. et al. (Eds), *Náttúruvá á Íslandi-Tekist á við náttúruöflin í 1100 ár*. Eldgosavá. Viðlagatrygging Íslands, Reykjavík.

Machado, F., Parsons, W.H., Richards, A.F. and Mulford, J.W., 1962. Capelinhos Eruption of Fayal Volcano, Azores, 1957-1958. *J. Geophys. Res.*, 67(9): 3519-3529.

Moore, J.G., Nakamura, K. and Alcaraz, A., 1966. The 1965 Eruption of Taal Volcano. *Science*, 151(3713): 955-960.

Morimoto, R., 1960. Submarine eruption of the Myôjin reef. *Bulletin of Volcanology*, 23(1): 151-160.

Németh, K., Martin, U. and Harangi, S., 2001. Miocene phreatomagmatic volcanism at Tihany (Pannonian Basin, Hungary). *Journal of Volcanology and Geothermal Research*, 111(1–4): 111-135.

Parfitt, E.A., 2004. A discussion of the mechanisms of explosive basaltic eruptions. *Journal of Volcanology and Geothermal Research*, 134(1–2): 77-107.

Pedrazzi, D., Martí, J. and Geyer, A., 2013. Stratigraphy, sedimentology and eruptive mechanisms in the tuff cone of El Golfo (Lanzarote, Canary Islands). *Bulletin of Volcanology*, 75(7): 1-17.

Pedrazzi, D., Bolós, X. and Martí, J., 2014. Phreatomagmatic volcanism in complex hydrogeological environments: La Crosa de Sant Dalmai maar (Catalan Volcanic Zone, NE Spain). *Geosphere*.

Pedrazzi, D., Becerril, L., Martí, J., Meletlidis, S. and Galindo, I., Submitted. Explosive felsic volcanism on El Hierro (Canary Islands). *Bulletin of Volcanology*.

Pedrazzi, D., Aguirre-Diaz, G., Bartolini, S., Martí, J. and Geyer, A., Submitted. The 1970 eruption on Deception Island (Antarctica): eruptive dynamics and implication for volcanic hazard. *Journal of the geological society*.

Ross, P.-S., Delpit, S., Haller, M.J., Németh, K. and Corbella, H., 2011. Influence of the substrate on maar–diatreme volcanoes — An example of a mixed setting from the Pali Aike volcanic field, Argentina. *Journal of Volcanology and Geothermal Research*, 201(1–4): 253-271.

Rout, D.J., Cassidy, J., Locke, C.A. and Smith, I.E.M., 1993. Geophysical evidence for temporal and structural relationships within the monogenetic basalt volcanoes of the

Auckland volcanic field, northern New Zealand. *Journal of Volcanology and Geothermal Research*, 57(1–2): 71-83.

Schulz, R., Buness, H., Gabriel, G., Pucher, R., Rolf, C., Wiederhold, H. and Wonik, T., 2005. Detailed investigation of preserved maar structures by combined geophysical surveys. *Bulletin of Volcanology*, 68(2): 95-106.

Self, S., Kienle, J. and Huot, J.-P., 1980. Ukinrek Maars, Alaska, II. Deposits and formation of the 1977 craters. *Journal of Volcanology and Geothermal Research*, 7(1–2): 39-65.

Sheridan, M.F. and Wohletz, K.H., 1981. Hydrovolcanic explosions: the systematics of water-pyroclast equilibration. *Science*, 212: 1387-1389.

Sheridan, M.F. and Wohletz, K.H., 1983. Hydrovolcanism: Basic considerations and review. *Journal of Volcanology and Geothermal Research*, 17(1-4): 1-29.

Sohn, Y.K., 1996. Hydrovolcanic processes forming basaltic tuff rings and cones on Jeju Island, Korea. *Geological Society of America Bulletin*, 108: 1199-1211.

Sohn, Y.K. and Chough, S.K., 1989. Depositional processes of the Suwolbong tuff ring, Cheju Island (Korea). *Sedimentology*, 36(5): 837-855.

Sohn, Y.K. and Chough, S.K., 1992. The Ilchulbong tuff cone, Cheju Island, South Korea: depositional processes and evolution of an emergent, Surtseyan-type tuff cone. *Sedimentology* 39: 523-544.

Solgevik, H., Mattsson, H.B. and Hermelin, O., 2007. Growth of an emergent tuff cone: Fragmentation and depositional processes recorded in the Capelas tuff cone, São Miguel, Azores. *Journal of Volcanology and Geothermal Research*, 159(1): 246-266.

Sottili, G., Taddeucci, J., Palladino, D.M., Gaeta, M., Scarlato, P. and Ventura, G., 2009. Sub-surface dynamics and eruptive styles of maars in the Colli Albani Volcanic District, Central Italy. *Journal of Volcanology and Geothermal Research*, 180(2–4): 189-202.

Thorarinsson, S., 1965. The Surtsey Eruption: course of events and development of the new island. *Surtsey Research Progress Report*, 1: 51-55.

Valentine, G.A. and Gregg, T.K.P., 2008. Continental basaltic volcanoes — Processes and problems. *Journal of Volcanology and Geothermal Research*, 177(4): 857-873.

Valentine, G.A., Perry, F.V., Krier, D., Keating, G.N., Kelley, R.E. and Cogbill, A.H., 2006. Small-volume basaltic volcanoes: Eruptive products and processes, and posteruptive geomorphic evolution in Crater Flat (Pleistocene), southern Nevada. *Geological Society of America Bulletin*, 118(11-12): 1313-1330.

Valenzuela, E., Chavez, L. and Munizaga, F., 1968. Informe preliminar sobre la erupcion de Isla Decepcion ocurrida en diciembre de 1967. *Boletín Instituto Antártico Chileno*, 3: 5-16.

Vespermann, D. and Schmincke, H.U., 2000. Scoria cones and tuff rings. In: H. Sigurdsson, B.F. Houghton, S.R. McNutt, H. Rymer and J. Stix (Editors), *Encyclopedia of Volcanoes*. Academic Press, San Diego: 683-694.

Walker, G.P.L., 1993. Basaltic-volcano systems. in: Prichard, H.M., Alabaster, T., Harris, N.B.W., and Nearly, C.R., eds., *Magmatic Processes and Plate Tectonics*, Geological Society [London] Special Publication 76 [A volume in commemoration of the work of Ian Gass]: p. 3–38.

Walker, G.P.L., 2000. Basaltic volcanoes and volcanic systems. in: Sigurdsson, H., Houghton, B.F., McNutt, S.R., Rymer H., Stix J. (Editors), *Encyclopedia of Volcanoes*. Academic Press, San Diego: p. 283-290.

White, J.D.L., 1996. Impure coolants and interaction dynamics of phreatomagmatic eruptions. *Journal of Volcanology and Geothermal Research*, 74(3–4): 155-170.

White, J.D.L. and Houghton, B., 2000. Surtseyan and related phreatomagmatic eruptions. In: Sigurdsson, H., Houghton, B.F., McNutt, S.R., Rymer H., Stix J. (Editors), *Encyclopedia of Volcanoes*. Academic Press, San Diego: 495-511.

White, J.D.L. and Ross, P.S., 2011. Maar-diatreme volcanoes: A review. *Journal of Volcanology and Geothermal Research*, 201(1–4): 1-29.

Wohletz, K., 1986. Explosive magma-water interactions: Thermodynamics, explosion mechanisms, and field studies. *Bulletin of Volcanology*, 48(5): 245-264.

Wohletz, K. and Heiken, G., 1992. *Volcanology and geothermal energy*. University of California Press, Berkeley, California: 432.

Wohletz, K.H. and Sheridan, M.F., 1983. Hydrovolcanic explosions; II, Evolution of basaltic tuff rings and tuff cones. *American Journal of Science*, 283(5): 385-413.

Wong, L. and Larsen, J., 2010. The Middle Scoria sequence: A Holocene violent strombolian, subplinian and phreatomagmatic eruption of Okmok volcano, Alaska. *Bulletin of Volcanology*, 72(1): 17-31.

Zanon, V., Pacheco, J. and Pimentel, A., 2009. Growth and evolution of an emergent tuff cone: Considerations from structural geology, geomorphology and facies analysis of São Roque volcano, São Miguel (Azores). *Journal of Volcanology and Geothermal Research*, 180(2-4): 277-291.

Zimanowski, B., Lorenz, V. and Frohlich, G., 1986. Experiments on phreatomagmatic explosions with silicate and carbonatitic melts. *Journal of Volcanology and Geothermal Research*, 30(1): 149-153.

APPENDIX 1 CONTRIBUTION TO THE PAPERS

Inform from the director of the thesis on the impact factor or the categorization of magazine publications to be found in the doctoral thesis and the report of the thesis director explaining the participation in the paper of the coauthors.



JOAN MARTÍ I MOLIST, Professor d'Investigació del CSIC adscrit a l'Institut de Ciències de la Terra "Jaume Almera" de Barcelona i Director de la Tesi Doctoral realitzada per Dario Pedrazzi titulada "HYDROMAGMATIC MONOGENETIC VOLCANISM IN CONTINENTAL AND OCEANIC ISLAND ENVIRONMENTS"

CERTIFICA:

1) que, d'acord amb la normativa vigent de la Universitat de Barcelona referent a la presentació de Teses Doctorals, aquest Tesi Doctoral es presenta com a compendi de les següents publicacions científiques de les que s'indica el seu factor d'impacte a l'any de la publicació:

Pedrazzi D, Xavier B, Martí J (2014, in press) Phreatomagmatic volcanism in complex hydrogeological environments: La Crosa de Sant Dalmai maar (Catalan Volcanic Zone, NE Spain) (Geosphere). Factor d'impacte: 2,023

Pedrazzi D, Martí J, Geyer A (2013) Stratigraphy, sedimentology and eruptive mechanisms in the tuff cone of El Golfo (Lanzarote, Canary Islands). Bulletin of Volcanology 75(7):1-17. Factor d'impacte: 2,205

Pedrazzi D, Becerill L, Martí J, Meletlidis S, Galindo I, (submitted) Explosive felsic volcanism on El Hierro (Canary Islands) (Bulletin of Volcanology). Factor d'impacte: 2,205

Pedrazzi D, Aguirre Díaz G, Bartolini S, Geyer A, Martí J (submitted) The 1970 eruption on Deception Island (Antarctica): eruptive dynamics and implication for volcanic hazard (Journal of the Geological Society). Factor d'impacte: 3,196

2) que tots els treballs han estat realitzats en col·laboració amb altres investigadors, havent estat el doctorant la persona encarregada de realitzar la major part del treball, la seva planificació, redacció i revisió, en totes les publicacions, i que el paper dels altres firmants ha estat l'assessorament científic, aportació de dades complementaries i/o participació en els treballs de camp.

I perquè així consti i a tots el efectes oportuns signo el present certificat en Barcelona a setze de dos mil catorze.

APPENDIX 2

PHREATOMAGMATIC VOLCANISM IN COMPLEX HYDROGEOLOGICAL ENVIRONMENTS: LA CROSA DE SANT DALMAI MAAR (CATALAN VOLCANIC ZONE, NE SPAIN)

Phreatomagmatic volcanism in complex hydrogeological environments: La Crosa de Sant Dalmai maar (Catalan volcanic zone, NE Spain)

Dario Pedrazzi*, Xavier Bolós, and Joan Martí

Institute of Earth Sciences Jaume Almera, ICTJA-CSIC, Group of Volcanology.SIMGEO (UB-CSIC) Lluís Sole i Sabaris s/n, 08028 Barcelona, Spain

ABSTRACT

The volcano of La Crosa de Sant Dalmai is a roughly circular asymmetrical maar that forms part of the Catalan volcanic zone (Girona Province, NE Spain). The edifice is an example of a maar-diatreme volcano constructed on a mixed basement of hard Paleozoic granites and schists and soft Pliocene and Quaternary deposits. The heterogeneities and differences in these rocks' hydraulic properties and fracturing patterns influenced the way in which the magma-water interaction took place during the eruption and, consequently, the style of the eruption and the resulting deposits. The eruption of La Crosa de Sant Dalmai consisted of four consecutive eruptive phases characterized by alternating phreatomagmatic and magmatic fragmentation. The eruptive sequence and the variety of deposits—mainly fallout with subordinate surges—generated by this single eruption are a stark contrast to the compositional monotony of the magma, which thus highlights the role played by the geological and hydrological characteristics of the substrate in determining the eruptive style and associated hazards in this type of volcanism.

INTRODUCTION

Maar-diatreme volcanoes are typical products of phreatomagmatism (e.g., Fisher and Waters, 1970; Lorenz, 1973, 1974, 1986; Fisher and Schmincke, 1984). They represent one of the most interesting examples of the explosive excavation of geological substrate because the lithic components in the maar deposits are an excellent source of information that reveals much about the substrate and the depth of the explosions. These monogenetic volcanoes are created by comparatively low-volume and low-intensity

eruptions, but this form of volcanism represents a localized, unpredictable volcanic hazard.

These volcanic explosions are caused by the interaction of magma with phreatic water, and their exact nature depends on the substrate and the proportions and extent to which magma and water interact (Wohletz and Sheridan, 1983; Houghton and Hackett, 1984; Kokelaar, 1986; White and Houghton, 2000; Mastin et al., 2004). The type of substrate controls the characteristics of the aquifer(s) in which the external water is stored (fracture-controlled vs. porous aquifers) and has an important influence on the eruption dynamics and the characteristics of the resulting pyroclastic deposits. The substrate also affects the resulting overall shape of the volcano—for example, the diatreme and the posteruptive lacustrine architecture of the maar crater (Lorenz, 2003)—and gives rise to a wide range of maar types and maar processes (e.g., Tihany maar volcanic complex in Hungary [Németh et al., 2001]; Balaton Highland, Hungary [Auer et al., 2007]; Campo de Calatrava, Spain [Martín-Serrano et al., 2009]; Atexcac crater, eastern Mexico [Carrasco-Núñez et al., 2007]; Pali Aike volcanic field, Argentina [Ross et al., 2011]).

Maars commonly display evidence of complex eruptive dynamics and different phases during individual eruptive events that can include phreatic, phreatomagmatic, and magmatic episodes (e.g., Houghton et al., 1996; White and Houghton, 2000; Carrasco-Núñez et al., 2007; Németh et al., 2001).

The Catalan volcanic zone (Martí et al., 1992), one of the Quaternary volcanic regions related to the European rift system, exhibits a wide range of phreatomagmatic episodes that depend on the stratigraphic, structural, and hydrogeological characteristics of the subsoil below each volcano (Martí et al., 2011). Of these hydrovolcanic edifices, La Crosa de Sant Dalmai offers the most characteristic example of a maar structure in this volcanic field (Martí et al., 1986; Martí and Mallarach, 1987) and

reveals how much the resulting volcanic edifice depends on the substrate (Bolós et al., 2012). La Crosa de Sant Dalmai represents, in fact, an example of an edifice emplaced in a mixed substrate. These types of edifices are so far less well documented (e.g., White, 1991; Sohn, 1996; Sohn and Park, 2005; Ross et al., 2011) compared to examples of maars emplaced in hard substrates (e.g., Lorenz, 1987; Lorenz and Zimanowski, 2008).

In order to determine how the magma-water interaction occurred during the eruption of La Crosa de Sant Dalmai and how it was influenced by the stratigraphic, lithological, and hydrological characteristics of the substrate, we performed a detailed lithological and sedimentological analysis of the stratigraphic succession of this volcano and interpreted it in terms of its eruption dynamics. In this paper, we describe the main characteristics of the deposits in La Crosa de Sant Dalmai and discuss the influence of the substrate on its eruption behavior. The results obtained here help to explain changes in the explosive behavior of a maar volcano emplaced in a mixed substrate with complex hydrogeological behavior and can be extrapolated to other phreatomagmatic volcanoes of similar characteristics.

GEOLOGICAL SETTING

The Catalan volcanic zone is situated in the NE Iberian Peninsula and is one of the Quaternary alkaline volcanic provinces that belong to the European Cenozoic rift system. The Catalan volcanic zone is mainly represented by alkali basalts and basanites and includes several distinct volcanic fields ranging in age from older than 12 Ma to early Holocene (Fig. 1; Martí et al., 1992). The volcanic activity in the Catalan volcanic zone is characterized by small scoria cones that were produced during short-lived monogenetic eruptions associated with widely dispersed fractures of short lateral extent.

*E-mail: dpedrazzi@ictja.csic.es.

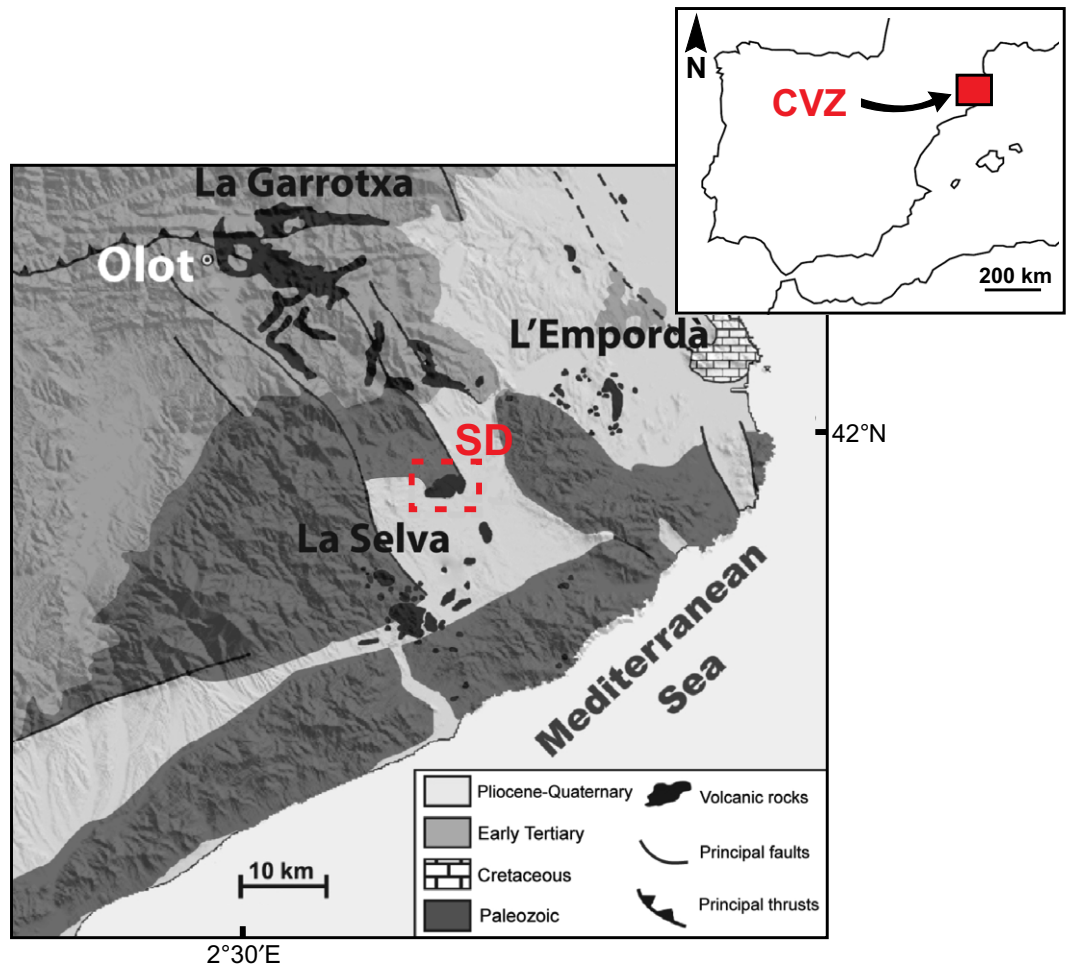


Figure 1. Simplified geological map of the Catalan volcanic zone (CVZ) and its three sub-zones, La Selva (7.9–1.7 Ma), L'Empordà (12–8 Ma), and La Garrotxa (0.5–0.01 Ma) (modified from Guérin et al., 1986; Martí et al., 1992). Dashed red square and SD indicate La Crosa de Sant Dalmai location.

The total volume of extruded magma in each eruption was small (0.01–0.2 km³ dense rock equivalent [DRE]), suggesting that the amount of magma available to feed each eruption was also very limited. Strombolian and phreatomagmatic episodes alternated in most of these eruptions and gave rise to complex stratigraphic sequences displaying a wide range of pyroclastic deposits (Martí et al., 2011).

With a diameter of 1200 m, the maar of La Crosa de Sant Dalmai is the largest edifice in the Catalan volcanic zone. It belongs to the Garrotxa volcanic field (0.6–0.01 Ma), which includes the youngest volcanoes in the Catalan volcanic zone (Fig. 1). This volcano is located at the northern border of La Selva graben, a Neogene tectonic depression bounded by ENE-WSW- and NW-SE-oriented normal fault systems that affect the Paleozoic basement, and it is infilled with Pliocene and Quaternary sediments (Fig. 1).

La Crosa de Sant Dalmai is an example of a maar-diatreme volcano consisting of a circular tephra ring, 30 m and 50 m high on its eastern and western sides, respectively. Volcanic deposits cover an area of 7 km², extending up to 4 km

eastward but only a few hundred meters westward (Fig. 2). Geophysical studies (Bolós et al., 2012) have found that La Crosa de Sant Dalmai developed on a NW-SE-oriented fault through which deep magmas were transported to the surface. This maar volcano is mostly composed of phreatomagmatic deposits with subordinate Strombolian phases. La Crosa de Sant Dalmai eruption ended with the formation of a scoria cone in the northern part of the main maar crater (Fig. 2). This small edifice emitted a basaltic lava flow that flowed southward and filled much of the maar crater (Bolós et al., 2012). Currently, postvolcanic lacustrine sediments cover this lava flow. The age of this volcano is not well constrained, but stratigraphic relations and existing U-Th and C¹⁴ ages of the lava flow and post-eruptive sediments suggest that it dates from the end of the Quaternary age.

METHODS

An important part of the research was carried out in the field in an area of ~10 km² surrounding the edifice of La Crosa de Sant Dalmai using

as a reference the geological map produced by Bolós et al. (2012). In total, six stratigraphic sections were carefully studied. The stratigraphic criteria used to distinguish the different units forming the succession of volcanic deposits included color, nature and relative content of the components, and variations in grain size, texture, and sedimentary structures. Estimates of grain size were conducted partially in the field using a comparative grain size chart and then completed in the laboratory.

Grain-size analyses consisting of dry-sieving techniques and componentry analysis were performed by weighing/counting 47 representative samples of the identified units. Large boulders were not considered for sieving but were measured and considered as part of the stratigraphic column for comparison with other layers. Samples were sieved with a set of sieves with a mesh size ranging from -6φ to +4φ units (64 to 1/16 mm). Grain-size data were used to define the median diameter (*Md*φ) and sorting (*σ*φ) (Inman, 1952) to help discriminate between deposits emplaced by fall and flow mechanisms. Clast compositions were characterized immedi-

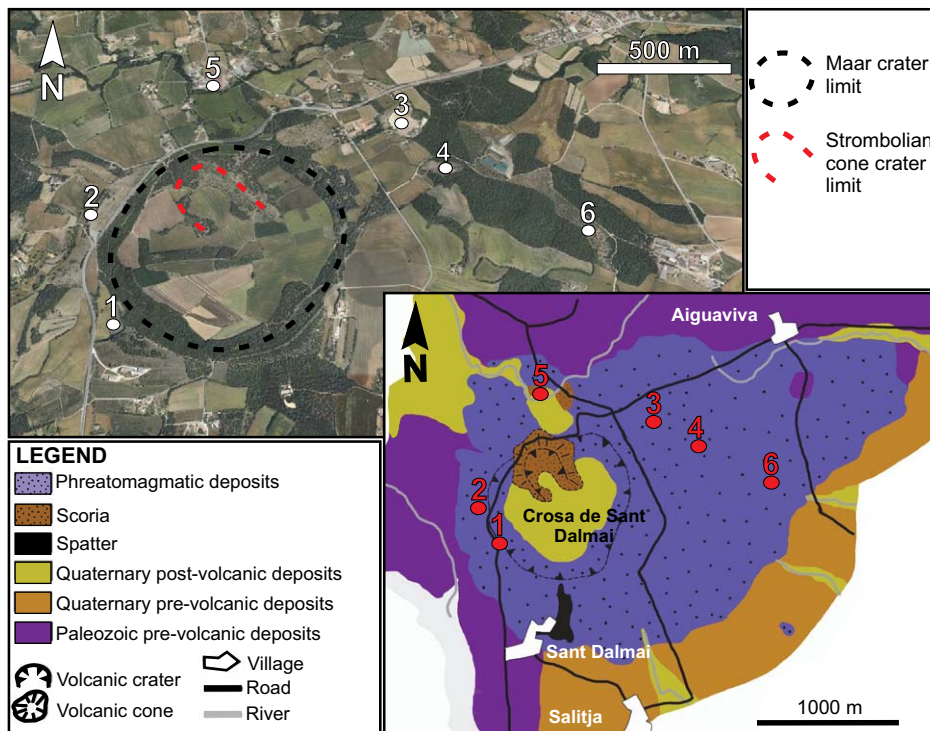


Figure 2. Google Earth image and geological map of the volcano of La Crosa de Sant Dalmai (modified from Martí et al., 2011) showing the main crater and the inner scoria cone, as well as the extent of the phreatomagmatic deposits and the pre- and postvolcanic deposits. The studied outcrops are also shown (numbers).

ately in the field by hand-sample observation and then confirmed in the laboratory using a binocular microscope and petrographic analysis. Component analysis was carried out on the -4ϕ , -3ϕ , -2ϕ fractions of the deposits. Clasts were separated into juvenile and accidental lithics classes belonging to the Paleozoic basement and La Selva infill succession. The main difference lies in the roundness and alteration of the clasts; nevertheless, this difference was not sufficient to discriminate between clasts in fractions smaller than -2ϕ . Maximum juvenile (scoria and cauliflower bombs) and lithic clast sizes were determined by measuring and averaging the long axes of 5–10 of the largest clasts in each bedset.

In order to establish a qualitative idea of the different degrees of vesiculation of the juvenile clasts, comparative petrographic and image analyses were carried out using a binocular microscope and ImageJ software (www.ImageJ.com).

Samples obtained from the lava flow and organic matter from a drill core made on the northeastern side of the maar crater (Bolós et al., 2012) were used for dating. A prevolcanic organic sediment sample was sent for dating to the Beta Analytics Laboratory (UK). The analy-

sis was performed through accelerator mass spectrometry (AMS) (radiocarbon.com/accelerator-mass-spectrometry.htm). The chemical procedure and mass spectrometry for lava samples are described in Sigmarsson et al. (1998).

CHARACTERISTICS OF THE PYROCLASTIC SUCCESSION

In order to reconstruct the complete succession of deposits, we carried out a detailed characterization of six stratigraphic sections in which six different facies were identified (Fig. 3). The lateral correlation of individual beds was possible using stratigraphic markers (Fig. 3); the maximum thickness of the observed succession was ~ 20 m (column 1, Fig. 3).

Facies Analysis

Facies SDA: Large Lithic Ballistic Deposits

This facies (Fig. 4A) has a maximum thickness of 200 cm (Fig. 3). It is clast supported and well sorted (e.g., samples SD1–1E, SD1–19E, SD2–1, SD3–2D; Fig. 5), with block- and lapilli-sized angular prevolcanic accidental lithic clasts (up to 70%; Fig. 3), as well as poorly vesiculated scoria fragments (Fig. 6A) and a scarce

interstitial matrix of juvenile coarse lapilli-sized to coarse ash-sized clasts and the same prevolcanic accidental lithic clasts. The largest lithic clasts—up to 70–80 cm in diameter (Fig. 5)—are horizontally aligned and mainly correspond to granites and schists; they are subangular in shape, and some have partly or totally oxidized surfaces. Subordinate bombs of the same size are also present.

Facies SDB: Clast-Supported Deposits

The deposits of this facies (Fig. 4B) have a maximum thickness of ~ 300 cm (Fig. 3). They are clast supported and medium to well sorted (e.g., samples SD1–3CG, SD1–20, SD2–1B, SD2–5AB, SD2–7A, SD3–4G; Fig. 5), and they have coarse lapilli-sized fragments of poorly vesiculated scoriae (Fig. 6A) and granite and schist lithic clasts, with an interstitial matrix of lapilli and coarse ash fragments of the same composition. The largest clasts have a maximum size of 50 cm (Fig. 5). Facies SDB looks very similar to facies SDA (Fig. 4B), but it is characterized by a different percentage of non-volcanic lithic clasts (up to 50%) compared to facies SDA (up to 70%; Fig. 3), and by poor stratification.

Facies SDC: Scoriaceous Clast-Supported Deposits

This facies (Fig. 4C) has a maximum thickness of 70 cm (Fig. 3). Its deposits are clast supported and moderately to well sorted (e.g., samples SD1–5AS, SD2–15BI; Fig. 5) and have vesiculated scoria (up to 70%; Fig. 3) the size of coarse lapilli (Fig. 6C), as well as granite and schist lithic clasts with a maximum size of 40 cm (Fig. 5) and an interstitial matrix mainly consisting of juvenile fine lapilli and coarse ash fragments. Impact structures are generally absent. These deposits are characterized by normal and reverse grading.

Facies SDD: Scoriaceous Deposits

This facies (Fig. 4D) occurs in the middle of the sequence, where it reaches a maximum thickness of 250 cm (Fig. 3) and also corresponds to the last episode of the eruption, which led to the formation of a Strombolian cone (Fig. 2). No deposits directly connected to the scoria cone located inside the crater were present in the studied sections. The facies mantles the topography and consists of black-and-red, well-vesiculated bombs and lapilli scoriae (Fig. 6D) covered by a subordinate fine lapilli and coarse ash matrix. These deposits are generally well sorted (e.g., samples SD1–18E, SD3–2AI; Fig. 5). A few accidental lithic (granites and schists) clasts with a maximum size of 10–15 cm are found at certain levels (Figs. 4D and 5).

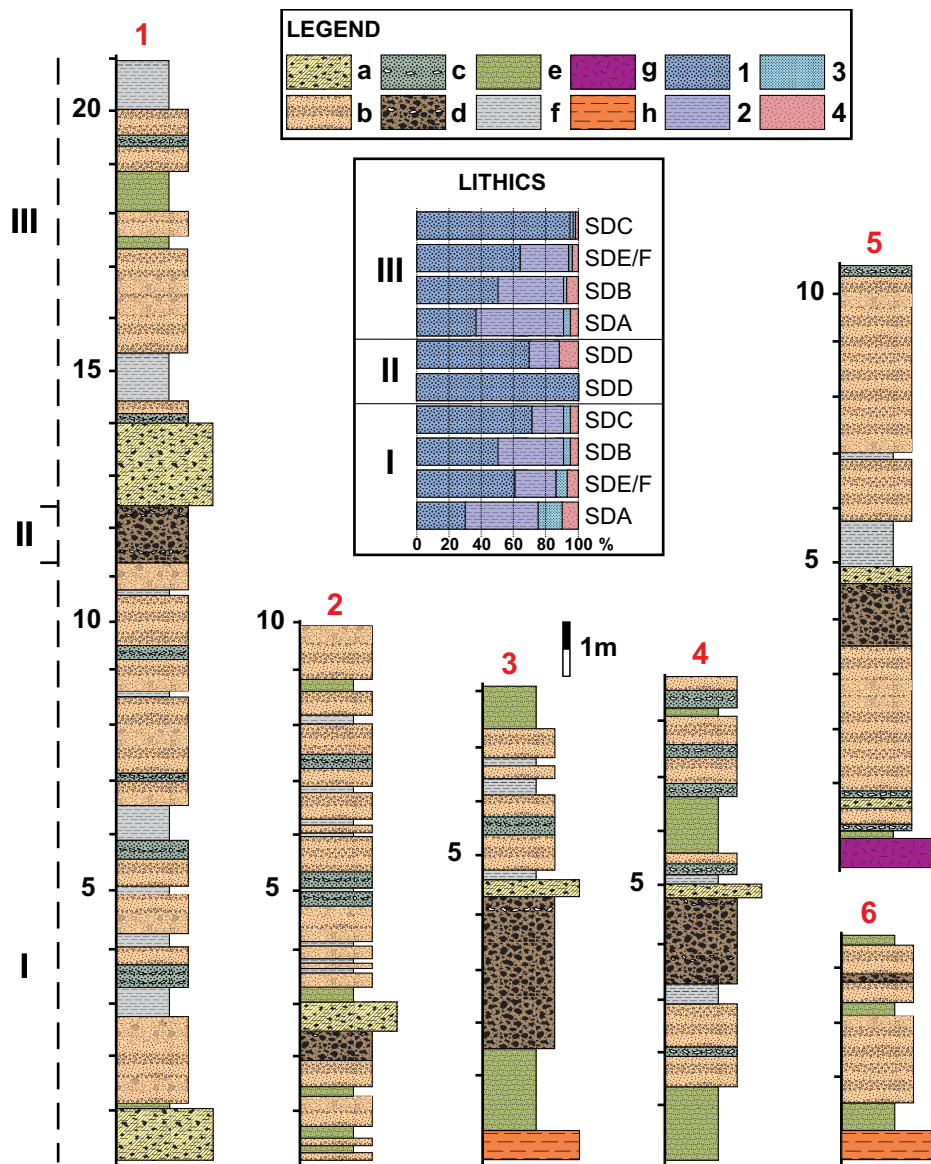


Figure 3. Composite stratigraphic column of the deposits at La Crosa de Sant Dalmai showing the main facies: (a) facies SDA—large lithic ballistic deposits; (b) facies SDB—clast-supported deposits; (c) facies SDC—scoriaceous clast-supported deposits; (d) facies SDD—scoriaceous deposits; (e) facies SDE—thinly bedded deposits; (f) facies SDF—diffusely stratified deposits; (g) Paleozoic basement; (h) Pliocene–Quaternary basement. Lithics contents in the various units are reported as well: (1) juvenile clasts; (2) Paleozoic lithic clasts; (3) Pliocene–Quaternary lithic clasts; (4) altered lithic clasts. Four lithofacies associations and four units are identified based on the depositional processes and resulting deposits. Unit IV corresponds to the product of the inner scoria cone shown in Figure 2.

Facies SDE: Thinly Bedded Deposits

This facies (Fig. 4E) consists of thinly bedded, poorly vesiculated scoria of fine lapilli size (Fig. 6E) with subangular accidental lithic clasts (up to 30%–40%; Fig. 3) having a maximum size of few centimeters. This deposit occurs overall at the bottom and top of the stratigraphic sequence with a maximum thickness of 50–70 cm (Fig. 3). The deposits are poorly sorted (e.g., samples

SD1–2, SD3–1B; Fig. 5). The bed surfaces have planar and low-angle cross-stratified laminations and basal erosional contact (Fig. 4E).

Facies SDF: Diffusely Stratified Deposits

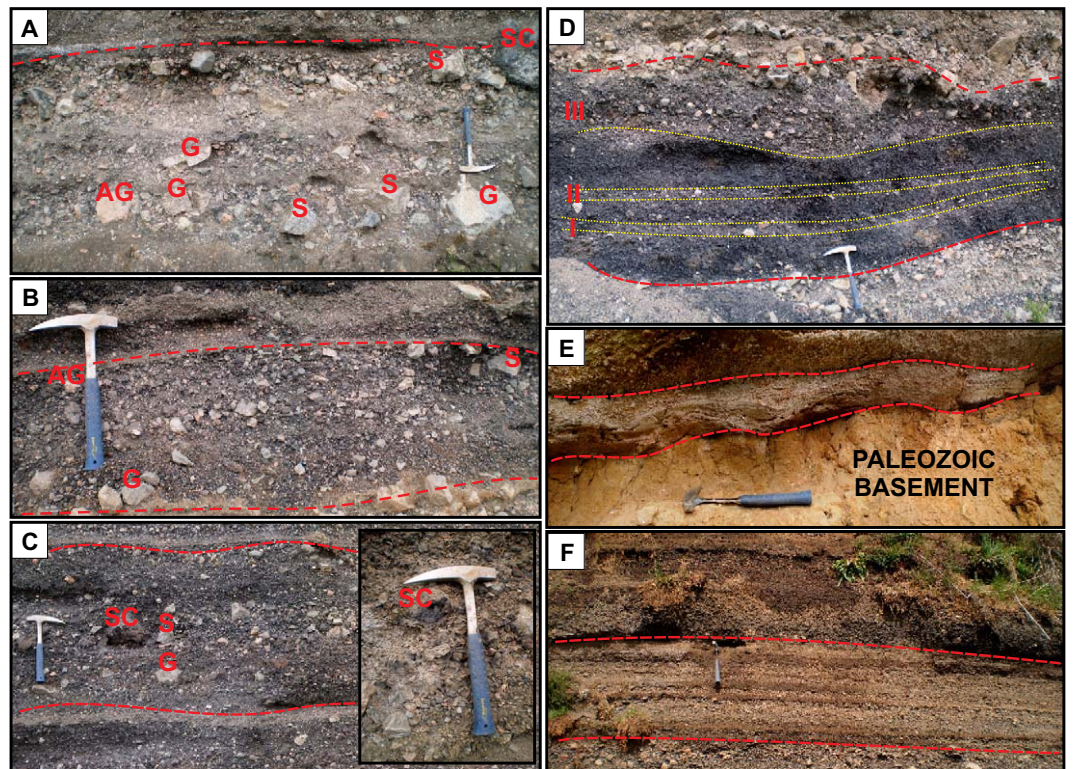
This facies (Fig. 4F) has a maximum thickness of 50 cm (Fig. 3) and consists of poorly sorted deposits (e.g., samples SD1–14, SD2–10; Fig. 5) with coarse, poorly vesiculated scoria lapilli

(Fig. 6F) and accidental lithics (up to 30%–40%; Fig. 3) with a maximum size of 10 cm. The bed surfaces have diffuse stratification.

Stratigraphic Units and Facies Associations

Four stratigraphic units (Figs. 2, 3, and 7) can be described from the study of the facies associations, each of which represents a successive stage in the construction of the volcano (Fig. 3). Unit I is represented by the lithofacies association I (facies SDA–SDB–SDC–SDE–SDF). Its thickness varies from 11 m in the western section (column 1, Fig. 3) to only 3 m in the east (column 6, Fig. 3). It is dominated by clast-supported deposits with relatively minor intercalated layers of lapilli-size material. The base of this unit is only visible in a few outcrops (columns 3, 5, and 6, Fig. 3), and it has thick layers of lithic-rich, fine lapilli (facies SDE) that correspond to the beginning of the eruption. On the eastern side, this initial deposit is overlain, in almost all the outcrops, by a series of thick deposits of coarse angular to subangular, lapilli-sized clasts (facies SDB) alternating with thin layers, just a few centimeters thick, of lapilli-sized clasts (facies SDE and SDF). The following clast-supported, well-sorted deposit (facies SDA), with decimetric angular prevolcanic accidental lithic clasts, is a good stratigraphic marker found throughout almost all of these outcrops (Fig. 3). A monotonous sequence characterized by facies SDB, facies SDC, facies SDE, and facies SDF completes unit I. In the eastern section (columns 3 and 6, Fig. 3; Fig. 7), the sequence is more uniform and is characterized mainly by thin, bedded deposits of fine and coarse lapilli-sized clasts (facies SDE). Unit II (lithofacies association II, facies SDD) is represented by deposits that are almost 3 m thick in section 3 (Fig. 3) but that overall decrease to 1 m (column 1, Fig. 3) or less (column 2, Fig. 3). The unit is made up of highly vesiculated bombs and scoria lapilli with a certain percentage (up to 30%; Fig. 5) of accidental lithic clasts in certain levels. Unit III is somewhat similar to unit I, and it is composed of the lithofacies association III (facies SDA–SDB–SDC–SDE–SDF). All the stratigraphic logs (Figs. 3 and 7) have a similar pattern. Their thickness varies from 8 m to less than 1 m (Fig. 3). This unit begins with a breccia (facies SDA) that has the same grain size as unit I and large blocks of accidental lithic clasts up to 70 cm (Fig. 5). The following deposits are dominated by thick, coarse layers of lapilli-sized breccia with accidental lithics up to 30 cm and non-vesiculated (juvenile) scoria (facies SDB), and occasional deposits with more vesiculated juvenile scoriae (facies SDC), intercalated with a

Figure 4. Field photographs of the characteristic facies of the maar of La Crosa de Sant Dalmai: (A) Facies SDA: block- and lapilli-sized angular prevolcanic accidental lithic clasts (AG, G, and S) and poorly vesiculated scoriae (SC); (B) facies SDB: clast-supported, medium to well sorted, with coarse lapilli consisting of poorly vesiculated lithics (AG, G, and S); facies SDB resembles facies SDA closely but has a different percentage of lithics (up to 50%); (C) facies SDC: clast-supported deposits with coarse lapilli consisting of vesiculated scoriae (SC) and subordinate lithics (G and S) in a mainly juvenile matrix with fine lapilli and coarse ash; (D) facies SDD: angular- to fluidally shaped, black-and-red, well-vesiculated bombs and lapilli scoriae, where I and II represent lithic-rich levels (delimited by yellow dotted lines), and III represents the lithic-rich transitional upper part toward the following breccia deposit; (E) facies SDE: thinly bedded, poorly vesiculated fine scoria lapilli with subangular accidental lithics, where the bed surfaces show planar and low-angle cross-stratified laminations and basal erosional contact; and (F) facies SDF: poorly sorted deposits with coarse, poorly vesiculated scoria lapilli and accidental lithics, where the bed surfaces show a diffuse stratification. AG—altered granite, G—granite, S—schists, SC—scoriae. Dashed red lines represent the facies limits.



small proportion of thin fine lapilli layers with planar stratification (facies SDE). Unit IV corresponds to a small scoria cone with an associated lava flow formed inside the maar (lithofacies association IV-SDD).

No evidence of stratigraphic discontinuities was observed in the sequence, and in some cases, slightly diffused contacts were observed among the different facies (Fig. 4). Mantle-derived nodules in the juvenile fragments are present in all of the units.

GRAIN SIZE, MODAL VARIATIONS, AND LITHIC DISTRIBUTION

Grain Size and Modal Variations

Vertical variations in the grain-size distribution and modal variations were analyzed by selecting representative samples from both the coarse- and fine-grained layers (Fig. 5). The maximum clast size is related to the energy conditions and efficiency of magma fragmentation, vent excavation, ejection, and emplacement. In the lowermost unit (unit I), fine layers dominate in the first part, with a general increase in grain

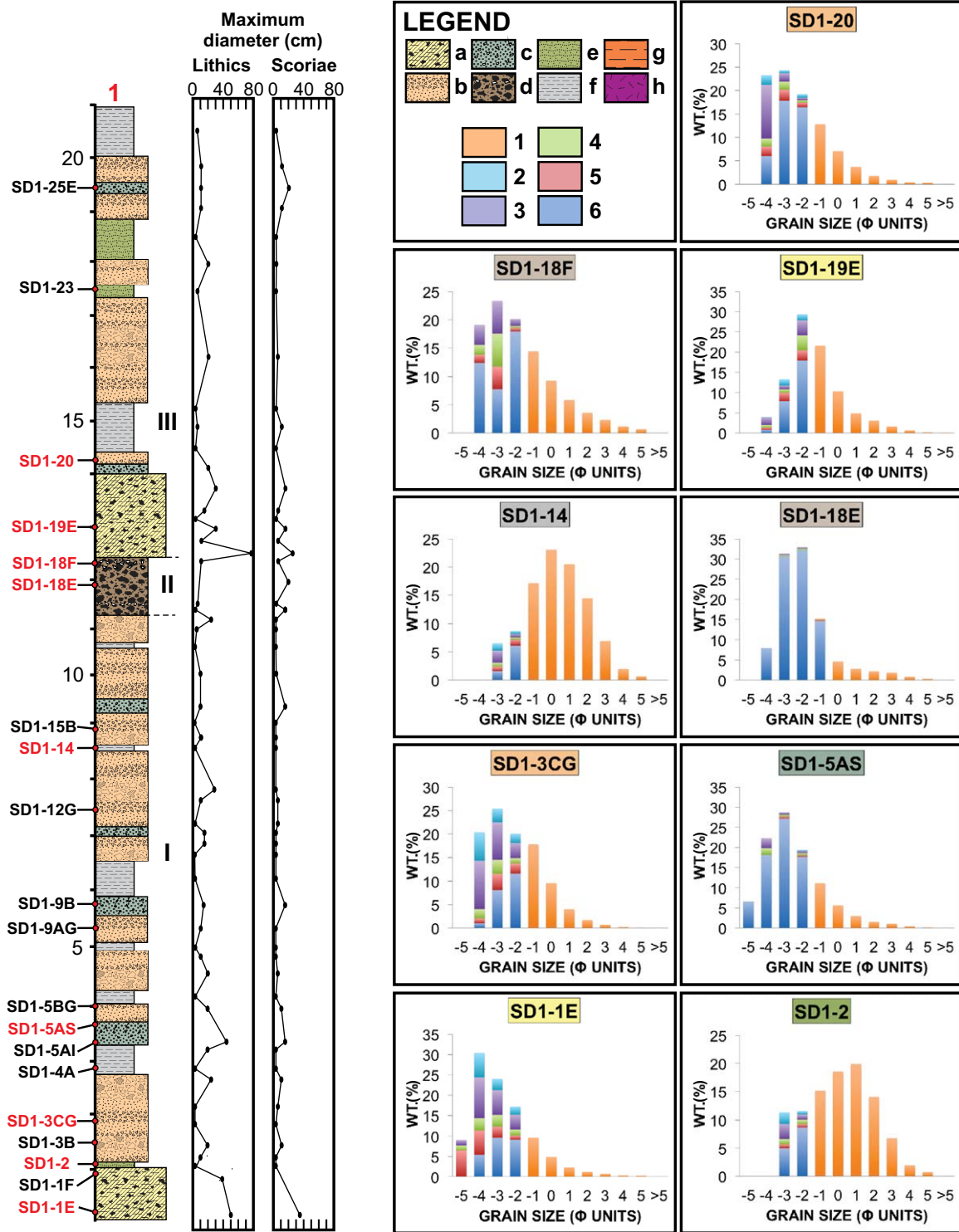
size up to the first lithic-rich breccia. A general trend of alternating, well-sorted coarse lithic-rich lapilli deposits and poorly sorted fine lapilli deposits characterizes the first unit. As shown in Figure 5, the largest blocks measure up to 50–70 cm. Unit II includes coarse juvenile fragment-rich layers. Unit III is similar to unit I and is dominated by coarse deposits, particularly in the lower half of the unit, and a grain size that gradually decreases toward its upper part. Both units show the same characteristics and can be distinguished by being above or below unit II, which is an important stratigraphic marker of the eruption. Although the distribution of large blocks is variable, units I and III clearly include the largest proportion of blocks of the whole sequence.

Based on the grain-size data, Inman parameters (Inman, 1952) of median diameter ($Md\phi$) and sorting ($\sigma\phi$) were obtained and plotted on frequency histograms (Fig. 8) in order to help discriminate between fall and surge deposits. Sorting ($\sigma\phi$) values for La Crosa de Sant Dalmai samples range between 1ϕ and 2.25ϕ , while the median diameter $Md\phi$ values generally range between -4.3ϕ and -0.2ϕ (Fig. 8).

Componentry Analysis

La Crosa de Sant Dalmai deposits consist of a mixture of juvenile scoria and accidental lithic clasts in differing proportions (Figs. 3 and 5 and the Supplemental Figure¹). Juvenile fragments are fresh, black, dense or vesicular scoria with a basaltic composition. The lithic fragments found in the different beds throughout the succession include granite and schist from the Paleozoic basement, as well as the same type of fragments—but with a different grade of roundness—from the Pliocene–Quaternary sediments that fill La Selva depression. These latter fragments were formed by the erosion and reworking of the Paleozoic basement. Although the juvenile material is present at all stratigraphic levels, its distribution is variable (Figs. 3 and 5).

¹Supplemental Figure. Lithics content of additional samples from the composite stratigraphic columns shown in Figure 5. If you are viewing the PDF of this paper or reading it offline, please visit <http://dx.doi.org/10.1130/GES00959.S1> or the full-text article on www.gsapubs.org to view the Supplemental Figure.



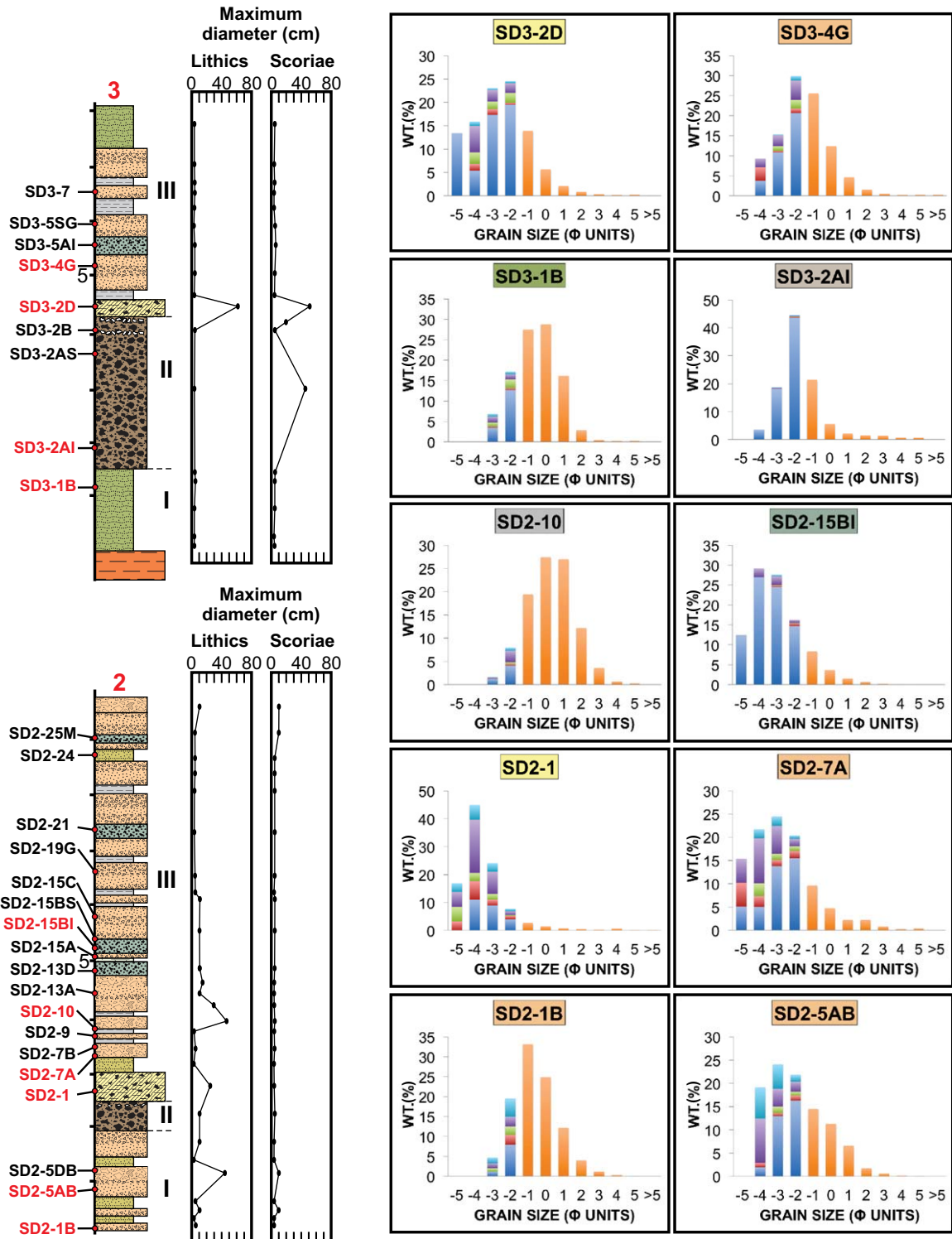


Figure 5 (continued).

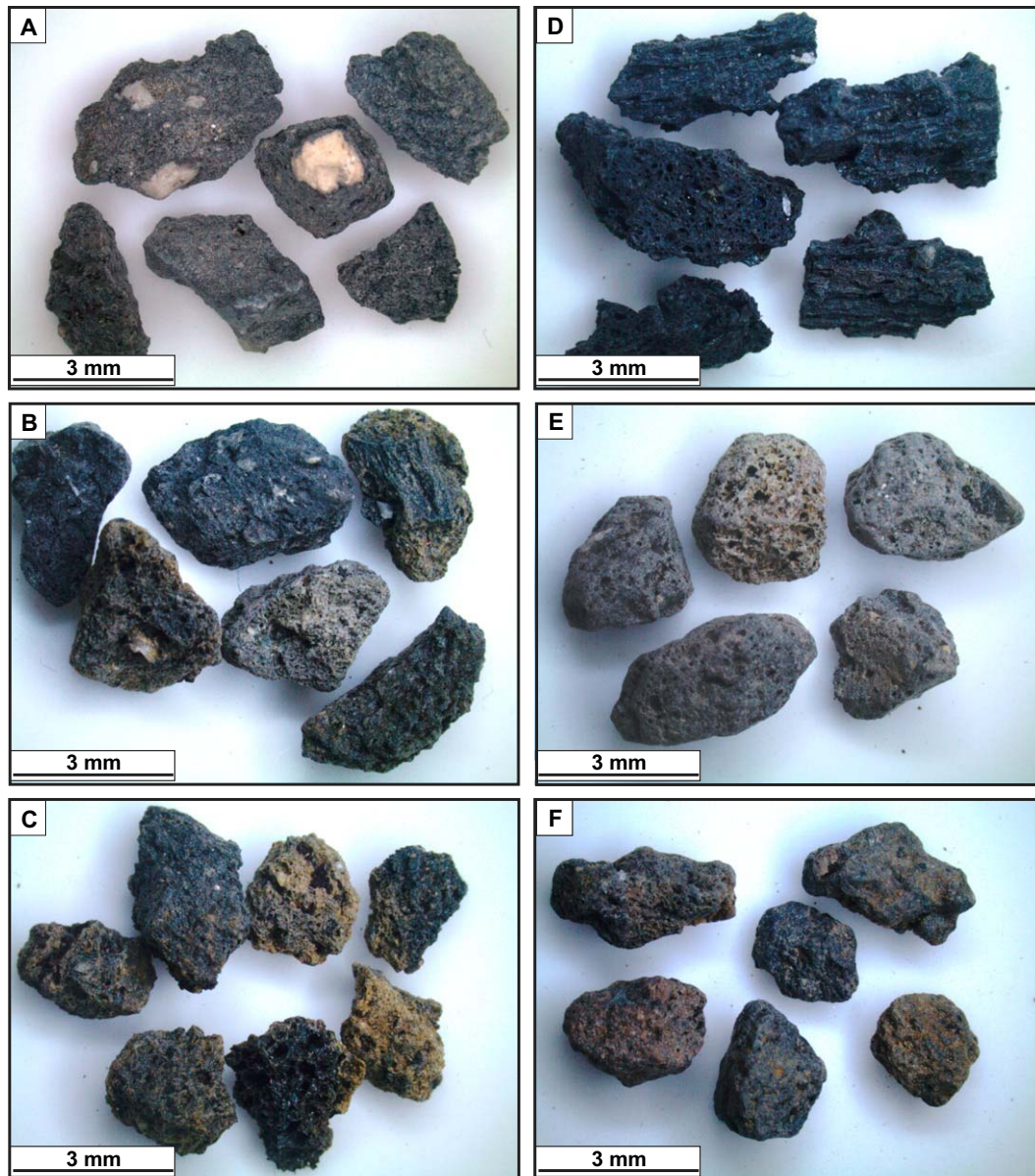


Figure 6. Photographs comparing the juvenile fragments of different lithofacies: (A) facies SDA; (B) facies SDB; (C) facies SDC; (D) facies SDD; (E) facies SDE; and (F) facies SDF. Most of the samples are made of poorly vesiculated scoriae except that in D, which represents a pure Strombolian deposit (facies SDD).

Small systematic variations in the occurrence of the lithic fragments can be seen in the stratigraphic succession. The lower part of unit I is characterized by a breccia deposit (e.g., sample SD1-1E; Fig. 5) with angular lithic fragments, mainly granites and schists (up to 40%), and Pliocene-Quaternary fragments (around 15%) with subordinate altered clasts (~10%). The whole of unit I is dominated by alternating coarse-grained deposits (e.g., samples SD1-3CG, SD2-1B, SD2-5AB; Fig. 5) that contain ~45%–50% juvenile lithic clast fragments (10% of Pliocene-Quaternary fragments, less than 5%

of altered clasts, and around 40% of fragments from the Paleozoic basement), as well as fine lapilli deposits (e.g., samples SD1-2, SD1-14, SD3-1B; Fig. 5) with lithic fragment contents of around 30%–40%. Only a few levels (e.g., sample SD1-5AS; Fig. 5) of unit I are dominated by juvenile material with lithic fragments reaching 20%–30% in abundance (with less than 5% of Pliocene-Quaternary lithic clasts). The highest proportion of juvenile clasts is found in unit II, where the accidental lithic fragments from the Paleozoic basement represent less than 1% (e.g., samples SD1-18E, SD3-2AI;

Fig. 5). However, some levels in unit II show a notable increase in granite and schist fragments (up to 30%) and a very high content of altered clasts and metamorphic fragments with almost no Pliocene-Quaternary content (e.g., samples SD1-18F; Fig. 5). In unit III, the same trends as in unit I are present. The sequence starts with a lithic-rich breccia with a lithic content of 50%–60% (mainly from the Paleozoic basement; e.g., samples SD1-19E, SD2-1, SD3-2D; Fig. 5) and continues with the same alternating succession as in unit I, with a variable amount of lithic clasts (20%–40%), which mainly originate from

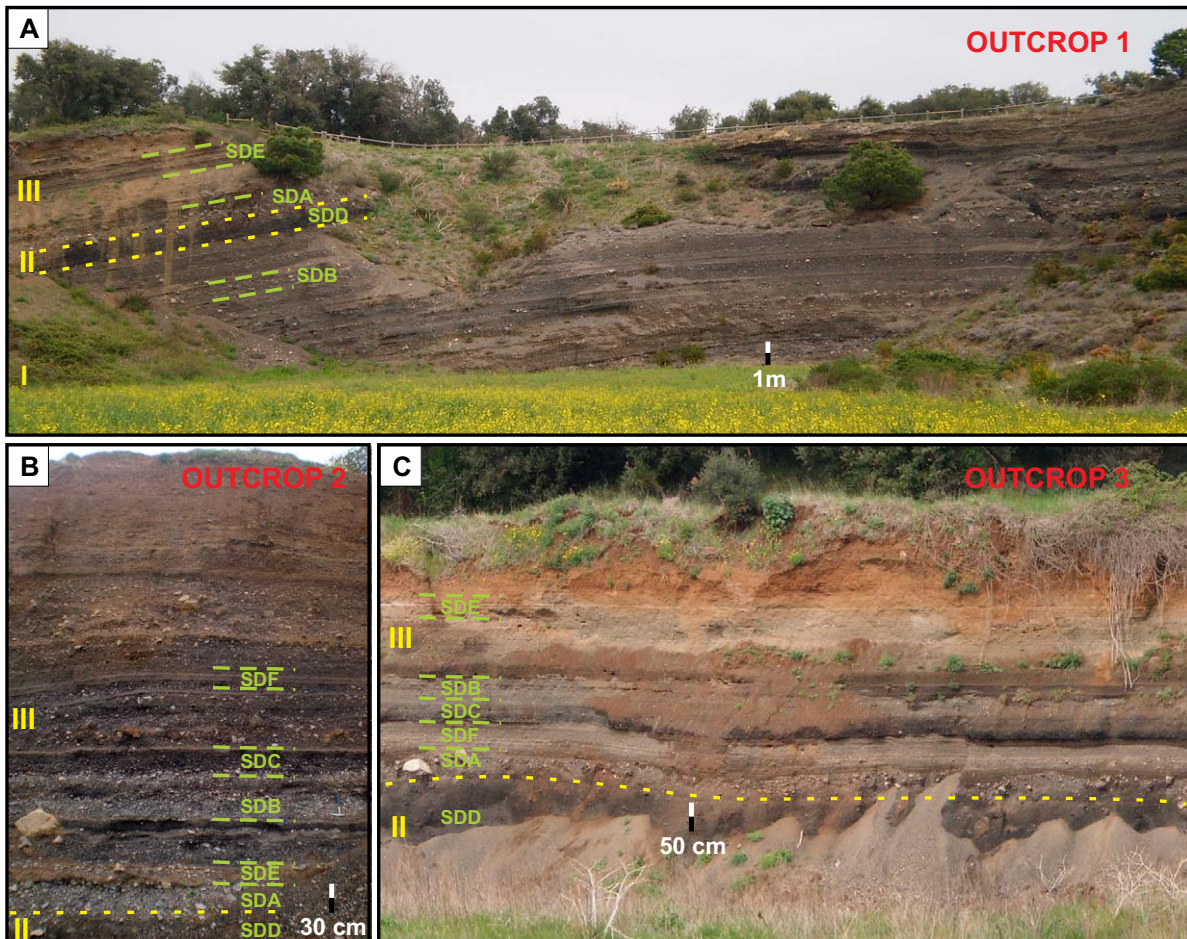
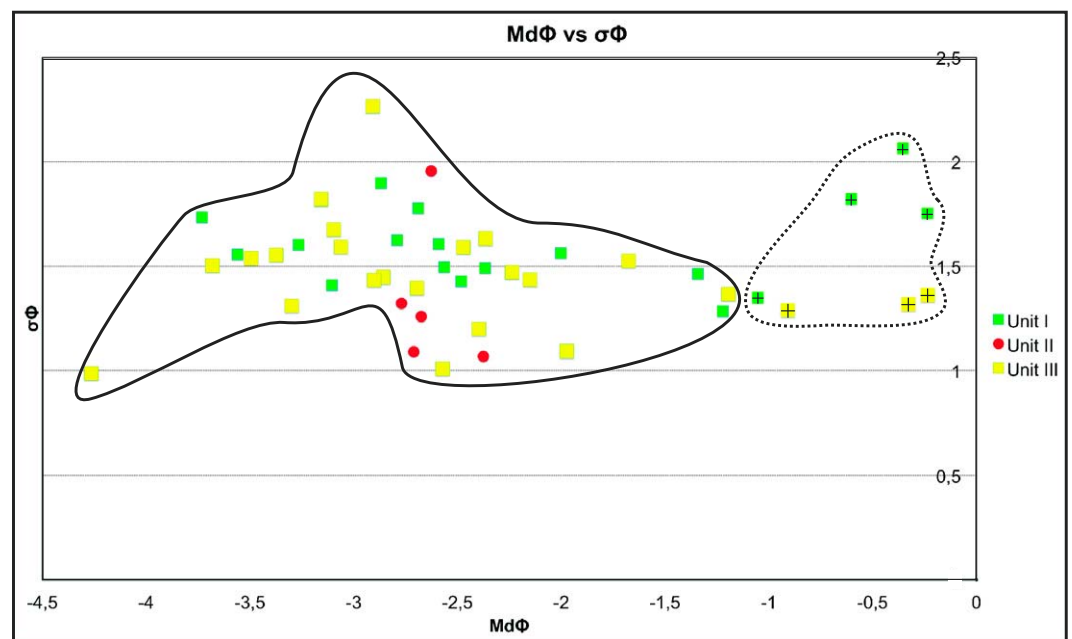


Figure 7. The three main outcrops (1, 2, and 3) showing the main characteristics of the La Crosa de Sant Dalmai sequence. I, II, and III refer to the different units of the eruption, and the green letters represent the facies as shown in Figure 4.

Figure 8. Sorting ($\sigma\phi$) versus median diameter ($Md\phi$) plot of grain-size data from the fall and surge deposits. Dotted line defines samples from surge deposits, while continuous line shows samples from fall-out deposits.



the Paleozoic basement (e.g., samples SD1–20, SD2–7A, SD3–4G; Fig. 5) and with lesser amounts of Pliocene–Quaternary lithics (~5%). Unit IV is represented by a scoria cone (Fig. 2) largely made up of juvenile scoria fragments.

LITHOLOGICAL AND HYDROGEOLOGICAL CHARACTERISTICS OF THE PREVOLCANIC SUBSTRATE

The maar of La Crosa de Sant Dalmai is located on the northern border of La Selva Basin on the fault contact between the Paleozoic basement and the Pliocene–Quaternary sediments that fill the depression (Bolós et al., 2012). La Selva Basin covers an area of 565 km² and is located in NE Catalonia (Fig. 9). It has a graben structure (Pous et al., 1990) and is bounded on four sides by mountain ranges with greater relief, including the Guilleries range to the west, the Transversal range to the north, the massif of Gavarres to the east, and the Selva Marítima mountains to the south. This basin was created during the Neogene extensional period following the Alpine orogeny. Two main watersheds in the area correspond to the basins of the Santa Coloma and Onyar Rivers (Fig. 9). The Santa Coloma River Basin extends along the whole southwestern side of La Selva Basin and part of its headwaters are in the Montseny–Guilleries Mountains (Fig. 9). The Onyar River basin, on the other hand, occupies the northeastern side of the basin (Fig. 9) and has its headwaters in the Gavarres and Selva Marítima ranges. As proposed by Menció (2005) and Folch et al. (2011), three main hydrogeological units are present in La Selva Basin (Figs. 9 and 10): (1) alluvial materials, surface Neogene sedimentary layers, and highly porous and permeable weathered igneous rocks; (2) layers of arkosic sands, gravels, and conglomerates with a low clay content and Neogene sediment alternating with layers of low-permeability clays and silt, which compose the main infilling in this basin (where the transmissivity and permeability of the Neogene sediments are both very low; except for the conglomerate-rich levels); and (3) crystalline materials (Paleozoic igneous and metamorphic rocks), which generally have low permeabilities but also have a set of structural heterogeneities (fractures, schistosity, presence of dikes and alteration) that act as zones of preferential flow.

As proposed by Menció et al. (2010) (Fig. 9), based on hydrochemical and isotopic data, the general model for underground flow requires a local flow system generated by the subsurface topography of the basin that is related to the main alluvial aquifers and more superficial Neogene layers. Furthermore, a regional flow

system runs across La Selva Basin, and its recharge zone is located in the adjacent massifs (the Guilleries and Transversal ranges and, to a lesser extent, in the Gavarres and Selva Marítima ranges). Piezometric data proposed by Folch et al. (2011) indicate the presence in the La Selva area of unconfined aquifers less than 30 m deep and confined or semiconfined aquifers over 30 m deep. Furthermore, based on hydrochemical and isotopic data, the same authors proposed a lateral hydraulic connection between the range-front areas and the basin aquifers, which would indicate an effective recharge through fault zones and fracture networks within the basement. Similar behavior is also suggested to occur at the contact between the sedimentary infill of the basin and the basement, with the magnitude of the recharge depending on distinct geological features such as the hydraulic conductivity of the lowest Neogene sediments, the thickness of the weathered granite on top of the basement, and the fracture network. At the same time, hydraulic head data indicate a vertical connection between sedimentary aquifer levels at various depths, which allows distinct vertical connections between the Neogene sedimentary aquifer layers (Folch et al., 2011). Additionally, hydraulic head records indicate that the regional hydraulic head decline due to water withdrawal is recovered annually despite the rainfall regime. This behavior is attributable to the effective recharge from the aforementioned regional flow system (Menció, 2005).

In general, the distribution of the water table is consistent with the topography of the area. The western, eastern, and southeastern areas of La Selva Basin are characterized by a steep gradient (coinciding with the mountainous areas of Guillerias, Gavarres, and Selva Marítima), while in the central part of the basin, the distance between the isopiezes (equipotential curves representing the phreatic surfaces of the aquifer) grows, and the gradient decreases (Menció, 2005).

DISCUSSION

The eruption of La Crosa de Sant Dalmai included episodes that were clearly dominated by a magma–water interaction and magma–poor phases as shown by field evidence (Fig. 4), the abundance of lithics fragments (Figs. 3 and 5 and the Supplemental Figure [see footnote 1]), and the general low vesicularity of the juvenile fragments (Fig. 6). The lithological and depositional characteristics (Fig. 4) as well as the granulometrical analysis (Fig. 8) of the resulting deposits reveal that most were formed by fall-out mechanisms of ballistic blocks and bombs

impact sags, and subordinate pyroclastic surges. The characteristics of the lithofacies and lithofacies associations, as well as the results of the componentry analysis, provide the necessary clues for understanding the evolution of the eruption and the construction of the volcanic edifice.

The sequence starts with lithic-rich fine lapilli layers (facies SDE) deposited by pyroclastic surges, as suggested by the presence of cross laminations (Fig. 4E). This first episode corresponds to an initial phreatomagmatic phase during which the efficiency in the energy transfer from the magma to the phreatic water was optimal, as indicated by the characteristic high degree of fragmentation in the resulting deposit. At this stratigraphic level, it is very likely that the locus of the explosions was located between the weathered surface of the granite basement and the Quaternary deposits (stage I, Fig. 10), as shown by the relative abundance of Quaternary fragments compared to the rest of the sequence (Fig. 5). The characteristics of these initial deposits and their radial distribution reflect the presence of a base-surge–type explosion (Crowe and Fisher, 1973; Fisher and Waters, 1970; Druitt, 1998), as has occurred at the beginning of other phreatomagmatic eruptions (e.g., Atexcac crater [eastern Mexico], Carrasco-Núñez et al., 2007; Tihany [Hungary], Németh et al., 2001). The first episode was followed by the deposition of mainly lithic-rich fallout lapilli-sized clast layers (e.g., samples SD2–1B, SD2–5AB; Fig. 5). As proposed by Carrasco-Núñez et al. (2007), the deposition of these layers could have been associated with the formation of an ephemeral eruptive column. This vent-opening episode was immediately followed by the formation of a thick breccia deposit (facies SDA), with abundant angular lithic clasts of block and lapilli size, derived from the mixed (Paleozoic and Pliocene–Quaternary) substrate rocks, and poorly vesiculated scoria fragments (Fig. 6A). This breccia corresponds to the main vent-enlargement phase caused by a major influx of phreatic water into the eruption conduit. The largest clasts, mainly granites and schists, are horizontally aligned and did not generate impact structures. Martí et al. (1986) suggested that this breccia originated from a very shallow explosion that generated ballistic trajectories with an important lateral component. Following this major explosive phase, a thick sequence formed the rest of unit I, dominated by poorly stratified, clast-supported deposits (facies SDB; Fig. 6B) alternating occasionally with deposits of more vesiculated scoriae (facies SDC; Fig. 6C) and diffusely stratified deposits of lapilli-sized clasts (facies SDF; Fig. 6F) and subordinate thinly bedded deposits (facies SDE; Fig. 6E).

La Crosa de Sant Dalmai maar

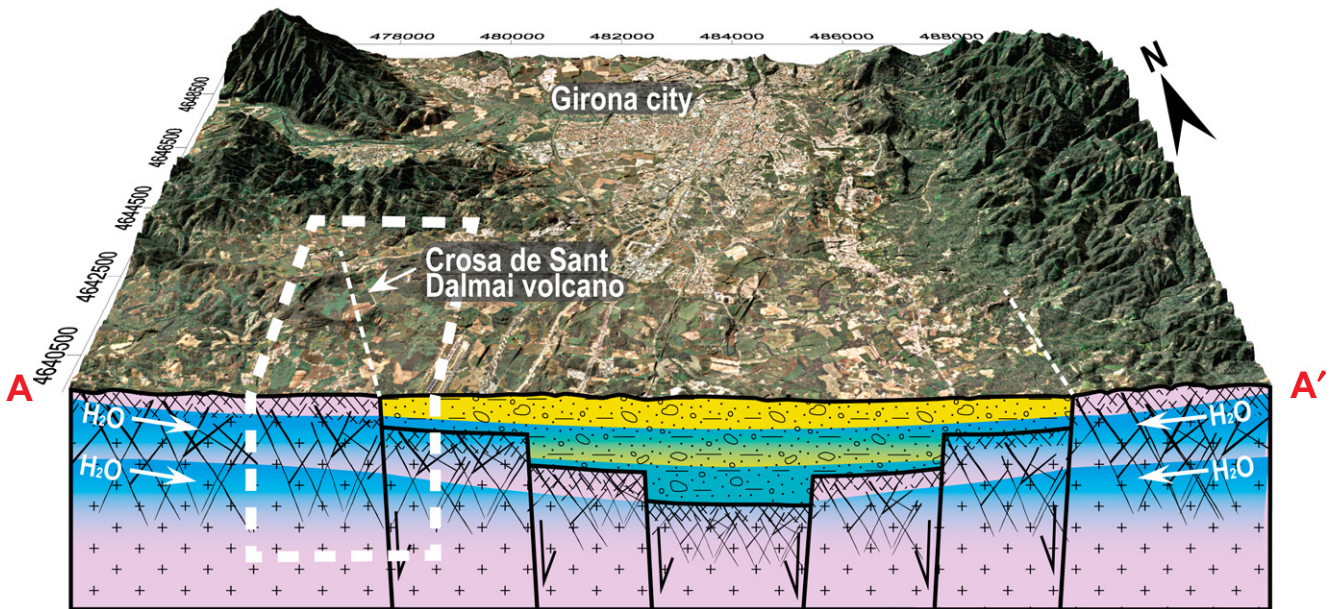
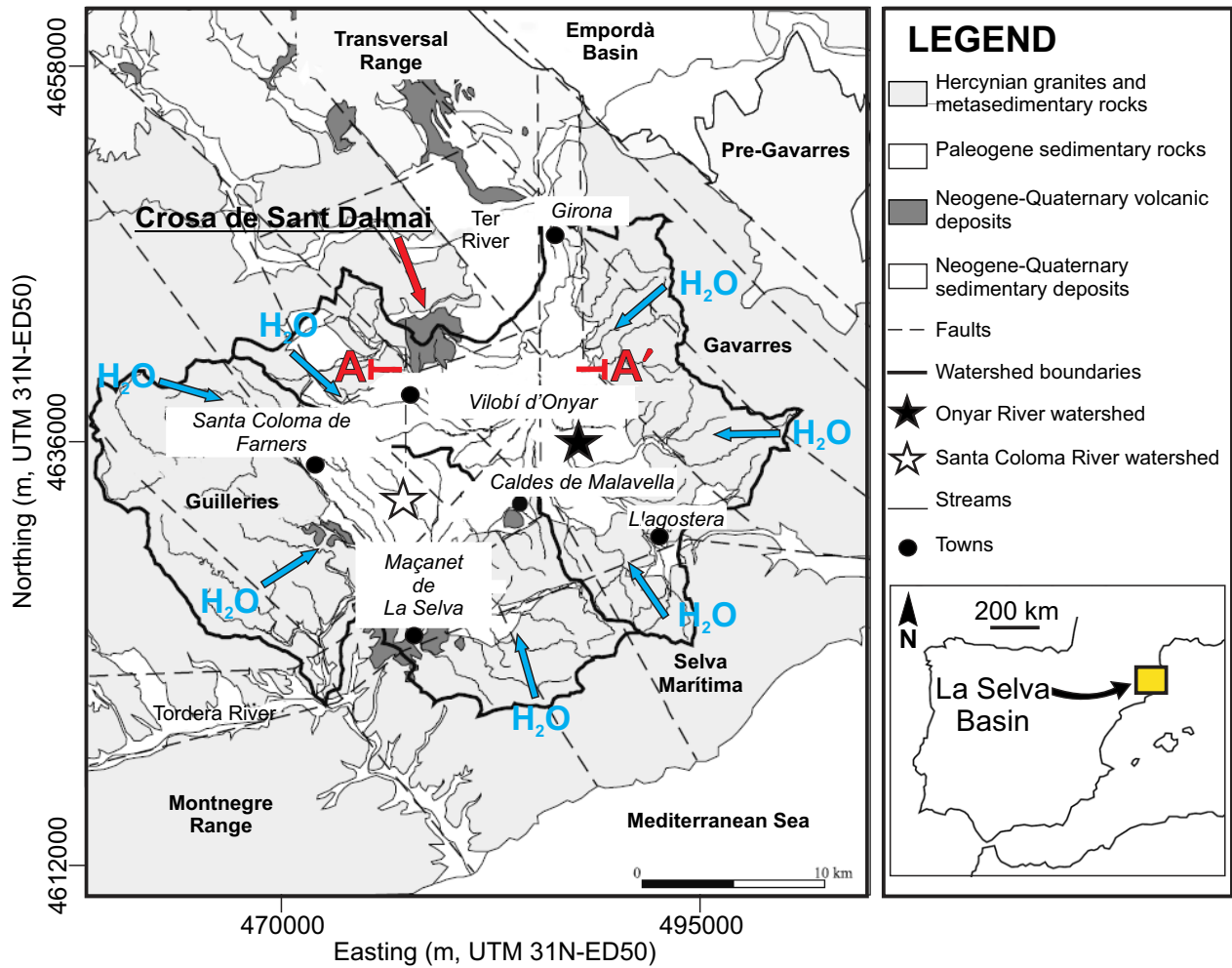


Figure 9. Geographical and geological setting of La Selva Basin, with the watershed boundaries with the two main subbasins (Onyar and Santa Coloma Rivers) marked. Arrows indicate the recharging area of the basin (modified after Folch et al., 2011). The A-A' profile consists of a block diagram showing the general hydrogeological characteristics of the substrate below La Crosa de Sant Dalmai and La Selva depression and the infilling of the tectonic graben of La Selva Basin and the crystalline materials (igneous and metamorphic rocks). The orthophoto was provided by ICC ((UTM 31N-ED50 Institut Cartogràfic de Catalunya, 2013, www.icc.cat).

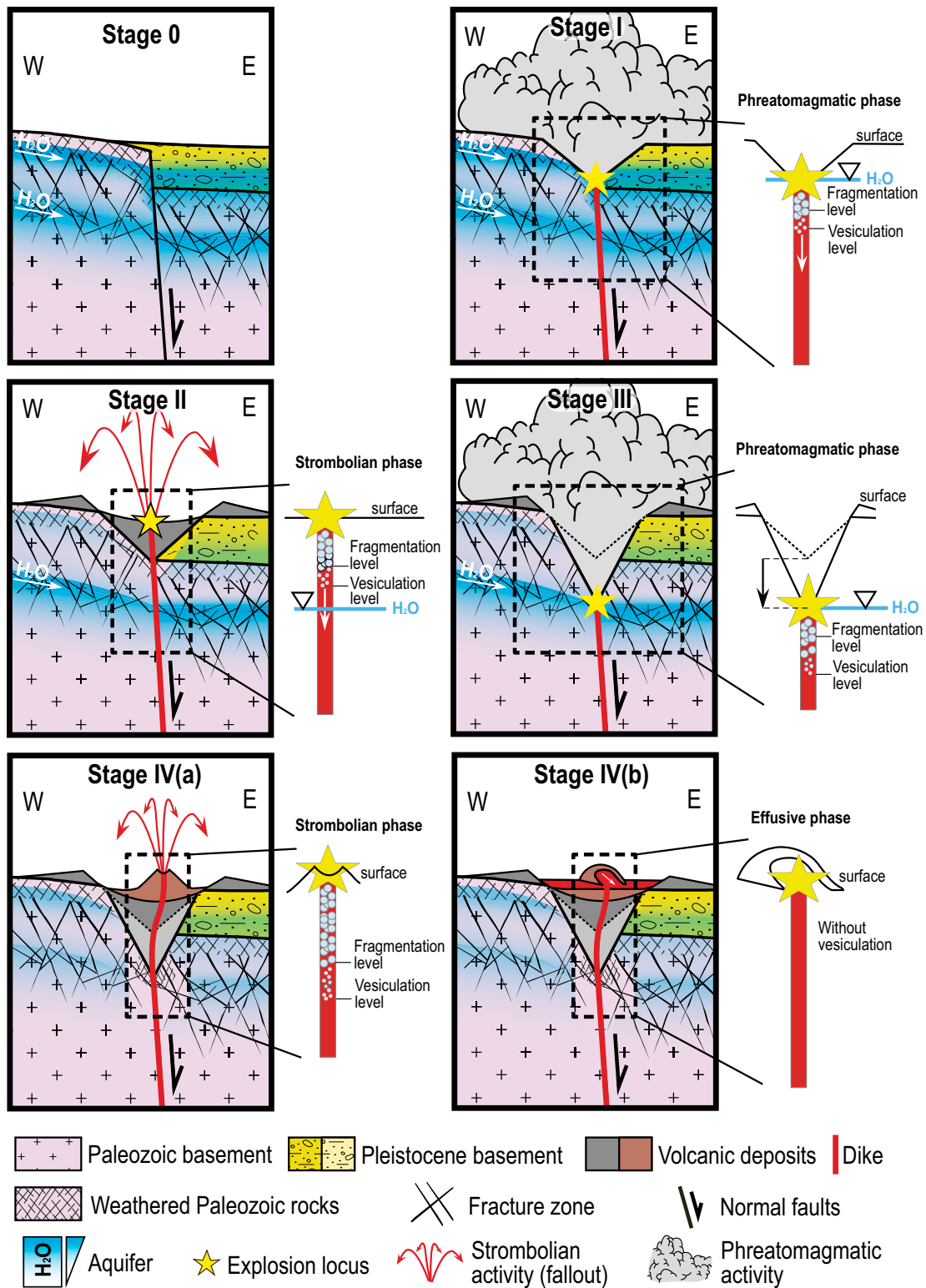


Figure 10. Four stages of the evolution of La Crosa de Sant Dalmai edifice: Stage 0—formation of La Selva Basin with the associated aquifers; stage I—interaction of the ascending magma with the shallower Quaternary and Paleozoic altered granite aquifers; stage II—first magmatic phase, probably due to a general decreasing of the water content in the shallower aquifer; stage III—decrease in the fragmentation level in the conduit and a new phreatomagmatic episode in a deeper aquifer; stage IVa—pure Strombolian phase, with the rise and eruption of the magma and no interaction with the probably almost exhausted aquifer; stage IVb—emplacement of a lava flow inside the maar crater.

We suggest that the whole of unit I derived from explosions occurring in the weathered granitic basement, which would have contained abundant water (stage I, Fig. 10). This idea is supported by the large proportion of basement-derived granite and schist clasts in the beds that form this part of the succession (Fig. 5). Presumably, the rising magma would have occupied existing fractures in the granite and schist that would have probably filled with water. The lack of interaction with the first aquifer could be related to a high and rapid input of magma, as suggested by the presence of large mantle-derived nodules in the deposits, which would not have allowed the required energy transfer efficiency to permit magma-water interaction.

Facies SDA, SDB, and SDC suggest fallout and ballistic emplacement (Fig. 8; see Németh et al., 2001). In particular, facies SDC includes some horizons of juvenile scoria lapilli with few prevolcanic lithic fragments (Fig. 5), probably indicating episodes involving less water recharge from the aquifer. Generally, these latter explosions did not have the same energy transfer efficiency during the magma-water interaction as during the first explosion, as shown by the abundance of breccia deposits. The stratified beds (facies SDE and SDF) could be interpreted as deposits originating from a high-concentration suspension with little tractional transport (e.g., Chough and Sohn, 1990).

These deposits, different than facies SDA–SDD, suggest other transport and depositional mechanisms, probably related to changes in the eruption dynamics caused by changes in the efficiency of the hydromagmatic fragmentation. The efficiency of hydromagmatic fragmentation and the corresponding eruption dynamics depend on the pressure differences between magma and water, the water-magma contact mode, and magma temperature and viscosity (Wohletz and Sheridan, 1983), as well as on the exact nature of the coolant (White, 1996). This implies that the eruption responsible for the construction of La Crosa de Sant Dalmai maar was continuous but included several pulses in which different types of deposits were formed.

Unit II reflects an important change in the eruption dynamics (stage II, Fig. 10). It is made up of well-vesiculated (Fig. 6D) scoria bombs and lapilli (facies SDD) with a few (less than 1%; Fig. 5) accidental lithic clasts in some levels. This facies is the result of fallout deposition from Hawaiian-style fire fountains. The fact that this scoria deposit appears in stratigraphic continuity (as suggested by the absence of erosional surfaces) with phreatomagmatic unit I and immediately precedes a new phreatomagmatic episode (Figs. 4D and 7) indicates that, at this stage, the water supply from the aquifer located

between the altered granites and the Quaternary sediments (stage II, Fig. 10) was not sufficient to sustain the phreatomagmatic interaction with the ascending magma.

Due to the effect of hydromagmatic eruptions, a large amount of water is vaporized, causing a large and almost instantaneous withdrawal of groundwater from the aquifer. A lowering of the water table can be expected if hydromagmatic activity lasts over a period of several days (Lorenz, 1986). As suggested by Németh et al. (2001), in a porous media aquifer, with lateral heterogeneities, water might not flow fast enough to the vent area to maintain the phreatomagmatic character of the eruption, despite the abundance of groundwater in the rest of the aquifer. Thus, the conditions for a purely magmatic eruption might be reached, and Strombolian explosions may occur.

Unit III (stage III, Fig. 10) started with a new breccia episode (facies SDA) characterized by abundant large heterolithologic blocks (up to almost 1 m in diameter) originating from the Paleozoic basement, and poorly vesiculated juvenile scoria (Fig. 6) resulted from the intermittent fallout deposition (facies SDB and SBC) and the subordinate pyroclastic surges (facies SDE and SDF). The lithic fragment contents, which mostly correspond to Paleozoic basement clasts with lesser amounts of Pliocene–Quaternary clasts (Fig. 5), indicate that the locus of the explosions migrated downward.

A possible water transmissivity is thought to occur at the contact between the sedimentary infill of the basin and the basement, although it would depend on hydraulic conductivity of the lowest Neogene sediments, the thickness of the weathered granite on the top of the basement, and the fracture networks. As the eruption progressed, the fracture-controlled aquifer could have been disrupted by the initial shock wave, causing an increase of secondary permeability and further excavation of the maar crater. This might have led to a decrease of the lithostatic pressure and a progressive lowering of the position of the fragmentation level in the eruption conduit during the course of the eruption (see Papale et al., 1998; Macedonio et al., 2005). This would have permitted a new phreatomagmatic episode when the magma interacted with a deeper aquifer located in the fractured Paleozoic basement, as indicated by the nature of the lithic fragments included in unit III.

A second line of evidence of the existence of a deeper aquifer was provided by Menció (2005) and Folch et al. (2011) with field data, where multilayer aquifers were recognized in the La Selva area. Furthermore, investigations carried out by Folch and Mas-Pla (2008) highlighted the relevance of fault geometry upon the flow

system and the connection between the upper basin-fill formations and the Paleozoic basement. Moreover, the same authors explained how some deep wells located close to La Crosa de Sant Dalmai area showed a confined type of behavior according to structural characteristics, fault geometry, and scaling. This might suggest a similar behavior for La Crosa de Sant Dalmai, enhancing the hypothesis of multilayer aquifers acting at different depth.

The eruption ended with a Strombolian episode (unit IV) (stage IV, Fig. 10) focused in the interior of the maar crater, which gave rise to the formation of a small scoria cone (stage IVa, Fig. 10) and the emission of a lava flow (stage IVb, Fig. 10) that was subsequently covered by lacustrine deposits. The transition from wet to dry conditions might suggest a significant decrease in the volumetric water content in the deeper levels of the aquifer as well as a changing water supply that thus ensured that the eruption would continue in a pure Strombolian phase. As suggested by Németh et al. (2001), a fracture-controlled aquifer might have a very strong seasonality, with an increasing or decreasing groundwater supply. Another hypothesis could suggest a magma conduit able to seal itself off from the surrounding aquifer, leading to a final purely magmatic phase.

The eruption sequence deduced for La Crosa de Sant Dalmai follows the generalized model proposed by Lorenz (1986). The proportion of lithic and juvenile fragments in the phreatomagmatic deposits and the presence of pure Strombolian phases in the middle and at the end of the eruption suggest that water supply was not constant. Even assuming that magma supply was not continuous, the changes observed in the eruption sequence and the resulting deposits are better explained by changes in the water supply. This variation in the amount of water interacting with the erupting magma could be due either to the intermittent recharge of the aquifer during the eruption or to the magma interacting with a heterogeneous aquifer (in which the levels had different hydraulic characteristics) at different depths in the conduit. The first case would account for a relatively long eruption in which seasonal recharges of the aquifer could have induced this type of pulsating behavior. However, the eruption of La Crosa de Sant Dalmai seems to have occurred in a continuous fashion and over a short period of time, as is suggested by the absence of discontinuities in the stratigraphic sequence (Figs. 3 and 4). The intermittent magma-water interaction would thus seem to result from the interaction of the erupting magma with different aquifer levels located at different depths and with different hydrogeological properties, an explanation that matches

the hydrogeological characteristics of the study area. Alluvial and weathering materials with high permeabilities composing the main infilling deposits of La Selva Basin would have allowed the first phreatomagmatic phase, while the crystalline materials characterized by structural heterogeneities, enhanced by the presence of a fault system connected to La Selva Basin, would explain the second phreatomagmatic phase. Similar to La Crosa de Sant Dalmai, the same types of stratigraphic successions can be observed in other edifices of the Catalan volcanic zone. Martí et al. (2011) explained the differences in the eruptive behavior of the Catalan volcanic zone as related to the occasional interaction of the ascending magma with groundwater rather than to changes in magma composition rheology or magma supply.

The succession of deposits that form La Crosa de Santa Dalmai has uniform stratigraphy all around the vent, albeit with smaller, thicker units and steeper angles in the west, and thinner units, gentler angles, and a broader distribution in the east, thereby suggesting a radial but asymmetrical distribution of the deposits (Fig. 2). This highlights the importance of differences in rock strength in mixed substrates, as already emphasized by Smith and Lorenz (1989), Sohn and Park (2005), and Auer et al. (2007) in other maar examples, which, in the case of La Crosa de Sant Dalmai (Bolós et al., 2012), made it easier for the phreatomagmatic explosions to excavate the eastern side where the soft Pliocene–Quaternary sediments were found. This is also suggested by the strong eastward horizontal component in the fallout deposits, which were probably influenced by this type of rheological contrast with the host rocks

CONCLUSION

La Crosa de Sant Dalmai maar formed on the northern border of the Neogene La Selva Basin on a NW–SE–oriented normal fault that was probably used by deep magma to reach the surface. This maar volcano is an example of the way in which a tephra ring develops in a mixed setting characterized by a hard (Paleozoic granites and schists) and soft (Quaternary filling) basement with heterogeneities and differences in the hydrogeological structure of the area, and aquifer levels with different hydraulic properties and fracturing patterns. These differences clearly influenced the way in which the magma–water interaction occurred throughout the eruption and, consequently, the style of the eruption and the resulting deposits. The eruption at La Crosa de Sant Dalmai included four eruptive phases with alternating phreatomagmatic and magmatic fragmentation. As occurs in many

other volcanoes in the same monogenetic field, the eruptive sequence and resulting deposits that formed La Crosa de Sant Dalmai contrast with the compositional monotony of the magma, thereby emphasizing the role played by the geological characteristics of the substrate in determining the eruptive style and associated hazards in this type of volcanism.

ACKNOWLEDGMENTS

This study was partially funded by the grant CROSAND and the European Commission (FT7 Theme: ENV.2011.1.3.3-1; grant 282759: “VUELCO”). We would like to thank Lluís Motjé (Consortium of La Crosa de Sant Dalmai: management of field geology in La Crosa volcanic area) for his logistical support during the field work. We are also grateful to Llorenç Planagumà and Leandro d’Elia for their help with the field work and Guillem Serra for his contribution to the discussion of this paper. We are also grateful to Editor Tim Wawrzyniec, Associate Editor Dave Hirsch, and Pete Stelling and an anonymous reviewer for their constructive reviews of this manuscript. English text was corrected by Michael Lockwood.

REFERENCES CITED

- Auer, A., Martin, U., and Németh, K., 2007, The Feketehegy (Balaton Highland, Hungary) “soft-substrate” and “hard-substrate” maar volcanoes in an aligned volcanic complex—Implications for vent geometry, subsurface stratigraphy and the palaeoenvironmental setting: *Journal of Volcanology and Geothermal Research*, v. 159, no. 1–3, p. 225–245, doi:10.1016/j.jvolgeores.2006.06.008.
- Bolós, X., Barde-Cabusson, S., Pedrazzi, D., Martí, J., Casas, A., Himi, M., and Lovera, R., 2012, Investigation of the inner structure of La Crosa de Sant Dalmai maar (Catalan volcanic zone, Spain): *Journal of Volcanology and Geothermal Research*, v. 247–248, p. 37–48, doi:10.1016/j.jvolgeores.2012.08.003.
- Carrasco-Núñez, G., Ort, M.H., and Romero, C., 2007, Evolution and hydrological conditions of a maar volcano (Atexcac crater, eastern Mexico): *Journal of Volcanology and Geothermal Research*, v. 159, no. 1–3, p. 179–197, doi:10.1016/j.jvolgeores.2006.07.001.
- Chough, S.K., and Sohn, Y.K., 1990, Depositional mechanics and sequences of base surges, Songaksan tuff ring, Cheju Island, Korea: *Sedimentology*, v. 37, no. 6, p. 1115–1135, doi:10.1111/j.1365-3091.1990.tb01849.x.
- Crowe, B.M., and Fisher, R.V., 1973, Sedimentary structures in base-surge deposits with special reference to cross-bedding, Ubehebe Craters, Death Valley, California: *Geological Society of America Bulletin*, v. 84, no. 2, p. 663–682, doi:10.1130/0016-7606(1973)84<663:SSIBDW>2.0.CO;2.
- Druitt, T.H., 1998, Pyroclastic density currents, in Gilbert, J.S., and Sparks, R.S.J., eds., *The Physics of Explosive Volcanic Eruptions*: Geological Society of London Special Publication 145, p. 145–182.
- Fisher, R.V., and Schmincke, H.U., 1984, *Pyroclastic Rocks*: Berlin, Springer-Verlag, 474 p.
- Fisher, R.V., and Waters, A., 1970, Base surge bed forms in maar volcanoes: *American Journal of Science*, v. 268, no. 2, p. 157–180, doi:10.2475/ajs.268.2.157.
- Folch, A., and Mas-Pla, J., 2008, Hydrogeological interactions between fault zones and alluvial aquifers in regional flow systems: *Hydrological Processes*, v. 22, no. 17, p. 3476–3487, doi:10.1002/hyp.6956.
- Folch, A., Menció, A., Puig, R., Soler, A., and Mas-Pla, J., 2011, Groundwater development effects on different scale hydrogeological systems using head, hydrochemical and isotopic data and implications for water resources management: The Selva basin (NE Spain): *Journal of Hydrology (Amsterdam)*, v. 403, no. 1–2, p. 83–102, doi:10.1016/j.jhydrol.2011.03.041.
- Guérin, G., Benhamou, G., and Mallarach, J.M., 1986, Un exemple de fusión parcial en medi continental: El vulcanisme quaternari de Catalunya: *Vitruva*, v. 1, p. 20–26.
- Houghton, B.F., and Hackett, W.R., 1984, Strombolian and phreatomagmatic deposits of Ohakune craters, Ruapehu, New Zealand: A complex interaction between external water and rising basaltic magma: *Journal of Volcanology and Geothermal Research*, v. 21, no. 3–4, p. 207–231, doi:10.1016/0377-0273(84)90023-4.
- Houghton, B.F., Wilson, C.J.N., Rosenberg, M.D., Smith, I.E.M., and Parker, R.J., 1996, Mixed deposits of complex magmatic and phreatomagmatic volcanism: An example from Crater Hill, Auckland, New Zealand: *Bulletin of Volcanology*, v. 58, no. 1, p. 59–66, doi:10.1007/s004450050126.
- Inman, D., 1952, Measures for describing the size distribution of sediments: *Journal of Sedimentary Petrology*, v. 22, p. 125–145.
- Kokelaar, P., 1986, Magma–water interactions in subaqueous and emergent basaltic volcanism: *Bulletin of Volcanology*, v. 48, p. 275–289, doi:10.1007/BF01081756.
- Lorenz, V., 1973, On the formation of maars: *Bulletin Volcanologique*, v. 37, no. 2, p. 183–204, doi:10.1007/BF02597130.
- Lorenz, V., 1974, Studies of the Surtsey tephra deposits: *Surtsey Research Progress Report*, v. 7, p. 72–79.
- Lorenz, V., 1986, On the growth of maars and diatremes and its relevance to the formation of tuff rings: *Bulletin of Volcanology*, v. 48, no. 5, p. 265–274, doi:10.1007/BF01081755.
- Lorenz, V., 1987, Phreatomagmatism and its relevance: *Chemical Geology*, v. 62, no. 1–2, p. 149–156, doi:10.1016/0009-2541(87)90066-0.
- Lorenz, V., 2003, Maar-diatreme volcanoes, their formation, and their setting in hard-rock or soft-rock environments: *Geolines (Prague)*, v. 15, p. 72–83.
- Lorenz, V., and Zimanowski, B., 2008, Volcanology of the West Eifel Maars and Its Relevance to the Understanding of Kimberlite Pipes Field Trip for the 9th IKC Held in Frankfurt Am Main, Germany, University of Würzburg, Physical Volcanological Laboratory, 84 p.
- Macedonio, G., Neri, A., Martí, J., and Folch, A., 2005, Temporal evolution of flow conditions in sustained magmatic explosive eruptions: *Journal of Volcanology and Geothermal Research*, v. 143, no. 1–3, p. 153–172, doi:10.1016/j.jvolgeores.2004.09.015.
- Martí, J., and Mallarach, J.M., 1987, Erupciones hidromagmáticas en el vulcanismo cuaternario de Olot: *Estudios Geológicos*, v. 43, p. 31–40.
- Martí, J., Ortiz, R., Claudin, F., and Mallarach, J.M., 1986, Mecanismos eruptivos del volcán de la Closa de Sant Dalmai (Prov. Gerona): *Anales de Física*, v. 82, special series B, p. 143–153.
- Martí, J., Mitjavila, J., Roca, E., and Aparicio, A., 1992, Cenozoic magmatism of the Valencia trough (western Mediterranean): Relationship between structural evolution and volcanism: *Tectonophysics*, v. 203, p. 145–165, doi:10.1016/0040-1951(92)90221-Q.
- Martí, J., Planagumà, L., Geyer, A., Canal, E., and Pedrazzi, D., 2011, Complex interaction between Strombolian and phreatomagmatic eruptions in the Quaternary monogenetic volcanism of the Catalan volcanic zone (NE of Spain): *Journal of Volcanology and Geothermal Research*, v. 201, no. 1–4, p. 178–193, doi:10.1016/j.jvolgeores.2010.12.009.
- Martín-Serrano, A., Vegas, J., García-Cortés, A., Galán, L., Gallardo-Millán, J.L., Martín-Alfageme, S., Rubio, F.M., Ibarra, P.I., Granda, A., Pérez-González, A., and García-Lobón, J.L., 2009, Morphotectonic setting of maar lakes in the Campo de Calatrava volcanic field (central Spain, SW Europe): *Sedimentary Geology*, v. 222, no. 1–2, p. 52–63, doi:10.1016/j.sedgeo.2009.07.005.
- Mastin, L.G., Christiansen, R.L., Thorner, C., Lowenstern, J., and Beeson, M., 2004, What makes hydromagmatic eruptions violent? Some insights from the Keanakākoʻi Ash, Kīlauea Volcano, Hawaii: *Journal of Volcanology and Geothermal Research*, v. 137, no. 1–3, p. 15–31, doi:10.1016/j.jvolgeores.2004.05.015.
- Menció, A., 2005, Anàlisi Multidisciplinària de l’Estat de l’Aigua a la Depressió de la Selva [Ph.D. thesis]: Barcelona, Spain, Universitat Autònoma de Barcelona, 265 p.

La Crosa de Sant Dalmai maar

- Menció, A., Folch, A., and Mas-Pla, J., 2010, Analyzing hydrological sustainability through water balance: *Environmental Management*, v. 45, no. 5, p. 1175–1190, doi:10.1007/s00267-010-9461-y.
- Németh, K., Martin, U., and Harangi, S., 2001, Miocene phreatomagmatic volcanism at Tihany (Pannonian Basin, Hungary): *Journal of Volcanology and Geothermal Research*, v. 111, no. 1–4, p. 111–135, doi:10.1016/S0377-0273(01)00223-2.
- Papale, P., Neri, A., and Macedonio, G., 1998, The role of magma composition and water content in explosive eruptions: 1. Conduit ascent dynamics: *Journal of Volcanology and Geothermal Research*, v. 87, no. 1–4, p. 75–93, doi:10.1016/S0377-0273(98)00101-2.
- Pous i Fàbregas, J., Solé Sugrañes, L., and Badiella, P., 1990, Estudio geoelectrico de la depresión de la Selva (Girona): *Acta Geologica Hispanica*, v. 25, no. 4, p. 261–269.
- Ross, P.-S., Delpit, S., Haller, M.J., Németh, K., and Corbella, H., 2011, Influence of the substrate on maar–diatreme volcanoes—An example of a mixed setting from the Pali Aike volcanic field, Argentina: *Journal of Volcanology and Geothermal Research*, v. 201, no. 1–4, p. 253–271, doi:10.1016/j.jvolgeores.2010.07.018.
- Sigmarrsson, O., Carn, S., and Carracedo, J.C., 1998, Systematics of U-series nuclides in primitive lavas from the 1730–36 eruption on Lanzarote, Canary Islands, and implications for the role of garnet pyroxenites during oceanic basalt formations: *Earth and Planetary Science Letters*, v. 162, no. 1–4, p. 137–151, doi:10.1016/S0012-821X(98)00162-9.
- Smith, C.B., and Lorenz, V., 1989, Volcanology of the Ellendale lamproite pipes, Western Australia, in Ross, J., ed., *Kimberlites and Related Rocks: Geological Society of Australia Special Publication 14*, p. 505–519.
- Sohn, Y.K., 1996, Hydrovolcanic processes forming basaltic tuff rings and cones on Jeju Island, Korea: *Geological Society of America Bulletin*, v. 108, p. 1199–1211, doi:10.1130/0016-7606(1996)108<1199:HPFBTR>2.3.CO;2.
- Sohn, Y.K., and Park, K.H., 2005, Composite tuff ring/cone complexes in Jeju Island, Korea: Possible consequences of substrate collapse and vent migration: *Journal of Volcanology and Geothermal Research*, v. 141, no. 1–2, p. 157–175, doi:10.1016/j.jvolgeores.2004.10.003.
- White, J.D.L., 1991, Maar-diatreme phreatomagmatism at Hopi Buttes, Navajo Nation (Arizona), USA: *Bulletin of Volcanology*, v. 53, no. 4, p. 239–258, doi:10.1007/BF00414522.
- White, J.D.L., 1996, Impure coolants and interaction dynamics of phreatomagmatic eruptions: *Journal of Volcanology and Geothermal Research*, v. 74, no. 3–4, p. 155–170, doi:10.1016/S0377-0273(96)00061-3.
- White, J.D.L., and Houghton, B., 2000, Surtseyan and related phreatomagmatic eruptions, in Sigurdsson, H., Houghton, B.F., McNutt, S.R., Rymer, H., and Stix, J., eds., *Encyclopedia of Volcanoes: San Diego, Academic Press*, p. 495–511.
- Wohletz, K.H., and Sheridan, M.F., 1983, Hydrovolcanic explosions: II. Evolution of basaltic tuff rings and tuff cones: *American Journal of Science*, v. 283, no. 5, p. 385–413, doi:10.2475/ajs.283.5.385.

APPENDIX 3

STRATIGRAPHY, SEDIMENTOLOGY AND ERUPTIVE MECHANISMS IN THE TUFF CONE OF EL GOLFO (LANZAROTE, CANARY ISLANDS)

Stratigraphy, sedimentology and eruptive mechanisms in the tuff cone of El Golfo (Lanzarote, Canary Islands)

Dario Pedrazzi · Joan Martí · Adelina Geyer

Received: 4 September 2012 / Accepted: 10 June 2013
© Springer-Verlag Berlin Heidelberg 2013

Abstract The tuff cone of El Golfo on the western coast of Lanzarote (Canary Islands) is a typical hydrovolcanic edifice. Along with other edifices of the same age, it was constructed along a fracture oriented NEE–SWW that coincides with the main structural trend of recent volcanism in this part of the island. We conducted a detailed stratigraphic study of the succession of deposits present in this tuff cone and here interpret them in light of the depositional processes and eruptive dynamics that we were able to infer. The eruptive sequence is represented by a succession of pyroclastic deposits, most of which were emplaced by flow, plus a number of air-fall deposits and ballistic blocks and bombs. We distinguished five different eruptive/depositional stages on the basis of differences in inferred current flow regimes and fragmentation efficiencies represented by the resulting deposits; the different stages may be related to variations in the explosive energy. Eight lithofacies were identified based on sedimentary discontinuities, grain size, components, variations in primary laminations and bedforms. The volcanic edifice was constructed very rapidly around the vent, and this is inferred to have controlled the amount of water that was able to enter the eruption conduit. The sedimentological characteristics of the deposits and the nature and distribution of palagonitic alteration suggest that most of the pyroclastic succession in El Golfo was deposited in a subaerial environment. This type of hydrovolcanic explosive activity is common in the coastal zones of Lanzarote and the other Canary Islands and is one of the main potential hazards that could threaten the human population of this archipelago. Detailed studies of these hydrovolcanic eruptions such as the one we

present here can help volcanologists understand the hazards that this type of eruption can generate and provide essential information for undertaking risk assessment in similar volcanic environments.

Keywords El Golfo · Lanzarote · Canary Islands · Tuff cone · Hydrovolcanism · Facies analysis

Introduction

Hydrovolcanism is a volcanic phenomenon in which magma or magmatic heat interacts with an external source of water (Macdonald 1972; Sheridan and Wohletz 1981). Typically, it takes place in deep or shallow submarine, littoral, lacustrine, phreatic or subglacial environments. Common volcanic landforms produced by hydrovolcanic eruptions include tuff cones, tuff rings and maar-diatreme volcanoes. Varieties of landforms are attributable to differences in eruption intensities, in styles of explosions and in depositional processes (Sheridan and Wohletz 1983). These differences are determined by variables such as the exact nature of the magma and water involved, the proportions and properties of the interacting fluids, the lithology and mechanical properties of the rocks of the conduit wall, and vent geometry (Kokelaar 1986; Sohn and Chough 1989; Sohn 1996; White 1996; White and Houghton 2000; White and Ross 2011). Also of importance is the geometry of the water-to-magma interface. Due in some cases to their short duration and often remote location, these hydrovolcanic eruptions have only ever been observed or documented on a few occasions in places such as Myojin, Japan (Morimoto 1960), Surtsey, Iceland (Thorarinsson 1965), Taal, Philippines (Moore et al. 1966), Capelinhos, Faial Island, Azores (Machado et al. 1962; Cole et al. 2001), Ukinrek, Alaska (Kienle et al. 1980; Self et al. 1980), Karymskoye Lake, Kamchatka (Belousov and Belousova 2001), Kavachi, Solomon Islands (Baker et al.

Editorial responsibility: T. Thordarson

D. Pedrazzi (✉) · J. Martí · A. Geyer
Group of Volcanology, SIMGEO (UB-CSIC) Institute of Earth
Sciences Jaume Almera, c/Lluís Sole Sabaris s/n,
08028 Barcelona, Spain
e-mail: dpedrazzi@ictja.csic.es

Published online: 03 July 2013

2002), Katla eruptions (Larsen et al. 2009; Larsen 2010), Grimsvotn, Iceland (Jude-Eton et al. 2012; IMO/IES websites, Iceland) and Eyjafjallajökull, Iceland (Gudmundsson et al. 2012).

Hydrovolcanic eruptions are common in coastal environments where erupting magma is prone to interact with seawater in either subaquatic or subaerial settings depending on the location of the eruption conduit and vent (Sheridan and Wohletz 1983). Water may gain access to magma either in the subsurface as groundwater or at the surface, and water entry is controlled largely by the exact nature of the rocks enveloping the vent site and eruption-related. Near-shore and shallow subaqueous activity may generate high-intensity explosions characterised by ballistic blocks, ash fall and pyroclastic density currents that can represent a hazard for nearby population centres. This is a threat above all on volcanic islands where basaltic magmas, which can erupt relatively passively under magmatic conditions, may become highly explosive when interacting with seawater in coastal environments (Moore et al. 1966; Waters and Fisher 1971; Sumner 1998; Cole et al. 2001; Baker et al. 2002; Sohn et al. 2003; Cronin et al. 2006; Clark et al. 2009; Németh and Cronin 2009, 2011).

Although examples of basaltic hydrovolcanic eruptions can be found on all the Canary Islands in the form of maars and tuff cones and rings, very few have ever been studied in detail. Published studies include those of include Montaña Amarilla, Montaña Escachada and Caldera del Rei on Tenerife (De La Nuez et al. 1993), Bandama on Gran Canaria (Araña et al. 1988), La Palma's 1949 eruption (White and Schmincke 1999) and Montaña Los Erales on Tenerife (Clark et al. 2009). Canarian hydrovolcanic events include both inland phreatomagmatic eruptions generated by erupting magmas interacting with groundwater and surtseyan eruptions caused by the interaction of magma with water in coastal or shallow offshore settings.

In the present paper, we study the tuff cone of El Golfo, located on the west coast of Lanzarote and a very typical of Canarian hydrovolcanic coastal edifice (Fig. 1). Our main objective was to describe in detail the structure and association of the facies in an archetypal tuff cone and use this information to infer changes in eruption style and depositional processes applicable to tuff cones worldwide. In the case of El Golfo, eruption of the basaltic magma was modified by interaction with seawater, and the eruptive sequence is characterised by a simple pyroclastic succession. In order to identify and characterise the different eruptive phases and pulses that constructed El Golfo, we here (1) describe the stratigraphy of the succession of deposits, (2) analyse their lithological and sedimentological characteristics, and (3) interpret these deposits in terms of the depositional regime and the efficiency of the magma fragmentation, which in turn are used to infer changes in the eruption dynamics and the degree of the magma-to-water interaction (Wohletz and

Sheridan 1983). Finally, we discuss the implications for human settlements on Lanzarote of the hazards that are inherent in this type of eruption.

Geological setting and general description of the tuff cone of El Golfo

The Canary Islands are a group of seven large islands and several islets that form a 450-km-long archipelago located 100 km off the northwest coast of Africa (Fig. 1). They were constructed by volcanic and tectonic activities that started at around 60 Ma ago and continue to the present day (Robertson and Stillman 1979; Le Bas et al. 1986; Marinoni and Pasquarè 1994; Marinoni and Gudmundsson 2000).

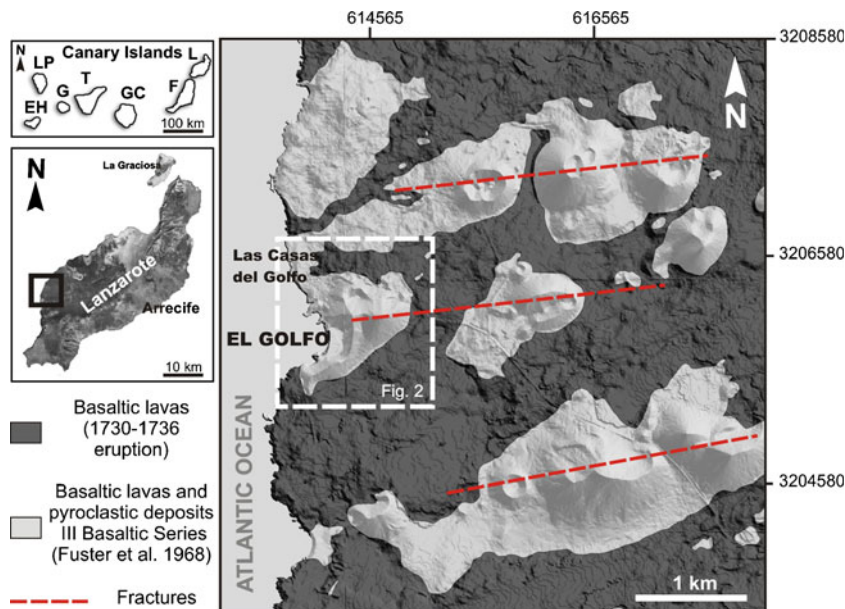
Lanzarote is the north easternmost of the Canary Islands (Fig. 1). It represents the emergent part of the East Canary Ridge, a NNE–SSW linear volcanic structure located on typical oceanic crust that is at least 11 km thick (Banda et al. 1981). The shallow basement of the island is probably about 4–5 km thick (Banda et al. 1981) and is composed of sedimentary (quartzite and shales), plutonic (basic and ultrabasic) and subvolcanic rocks (basaltic and trachytic dikes). The erupted magma contains an abundance of quartzite and sandstone xenoliths (Araña and Carracedo 1978). Although the island's lavas are almost all basaltic, there are small outcrops of massive trachytes in the oldest parts of the island (NW and SE).

The volcanic stratigraphy of Lanzarote was first classified by Fuster et al. (1968) as having four eruptive series: (I) a tableland with basalts dated at 6–12 Ma (Miocene–Pliocene); (II–III) Quaternary volcanism dated at 1 Ma and separated from stage I by an erosional unconformity; and (IV) recent volcanism including the 1730–1736 eruption, the largest eruption in modern times on the Canary Islands.

Marinoni and Pasquarè (1994) divided the geological evolution of the emergent part of Lanzarote into two principal construction stages named the 'Pre-erosional or Shield stage' and the 'Post-erosional or Differentiated stage'. The main volcanostratigraphic units of the former stage are exposed locally on the west coast of the island and correspond to scoriaceous lavas of basaltic composition and subordinate trachytic intrusions, scoria and tuff cones, as well as lavas of basaltic composition. The post-erosional Quaternary stage is characterised mainly by aligned scoria cones and associated lava flows.

The volcanic edifice of El Golfo, located on the western coast of Lanzarote (Fig. 1), reaches 60 m a.s.l. and has a basal diameter of approximately 1 km, which gives it an aspect ratio of about 0.05. The volcanic edifice has been partially destroyed by marine erosion, and only its eastern part remains intact. The age of this volcano is not well known, but it is assumed to be a product of recent volcanism on the island (since 2 Ma) (Abdel-Monem et al. 1972).

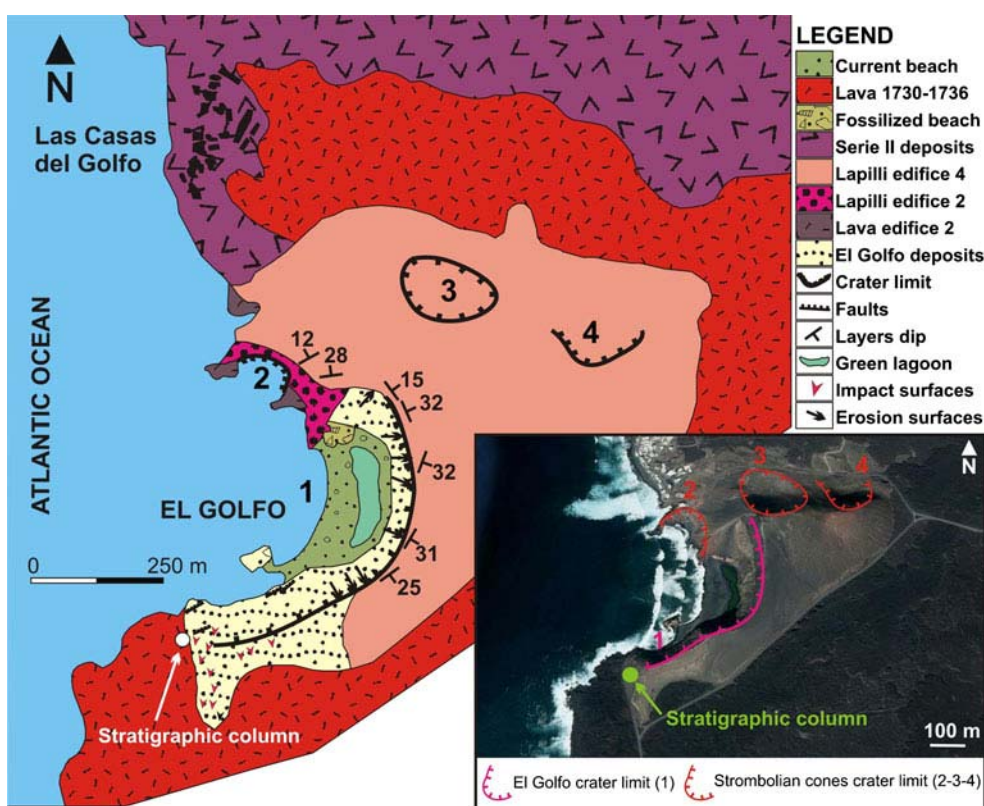
Fig. 1 Location and simplified geological map of the study area: *EH* El Hierro, *F* Fuerteventura, *G* Gomera, *GC* Gran Canaria, *L* Lanzarote, *LP* La Palma, *T* Tenerife



A simplified geological map of El Golfo is given in Fig. 2. Its deposits are covered by the lavas that were generated by the 1730–1736 event. El Golfo, together with other edifices of the same age, forms a linear vent system running NEE–SWW that coincides with the main orientation of recent volcanism in this part of the island (Marinoni and Pasquare 1994), whose products, today eroded by wave action, partially cover the area of El Golfo.

The tuff cone consists entirely of a succession of pyroclastic deposits with different lithological and sedimentological characteristics. The composition of its juvenile fragments is homogeneous which are of poorly evolved intraplate alkali basalt that does not vary through the whole eruptive sequence (Martí and Colombo 1990). The pyroclasts are rich in olivine and pyroxene phenocrysts, which are enclosed within the glassy groundmasses of the pyroclasts. A number of lapilli

Fig. 2 Geological map of the tuff cone of El Golfo (modified from Martí and Colombo 1990) from a Google Earth image of the volcanic edifice showing the main crater (1), the three subsequent craters (2–3–4) located to the north of the volcanic edifice, and the location of the studied stratigraphic sequence



are highly vesicular (>70 % vesicles) and have a very low density (<1 g/cm³); nevertheless, their mineralogical and chemical compositions do not differ from those of the other, denser, juvenile pyroclasts. Dunite and gabbro xenoliths ranging in size from 5–30 cm are common (Fig. 3). An irregularly distributed palagonitic alteration of the juvenile vitric fragments, which were devitrified and transformed into smectites, zeolites (mainly phillipsite) and Fe oxides, is another distinctive feature of the deposits on El Golfo (Martí and Colombo 1990) (Fig. 4).

Methods

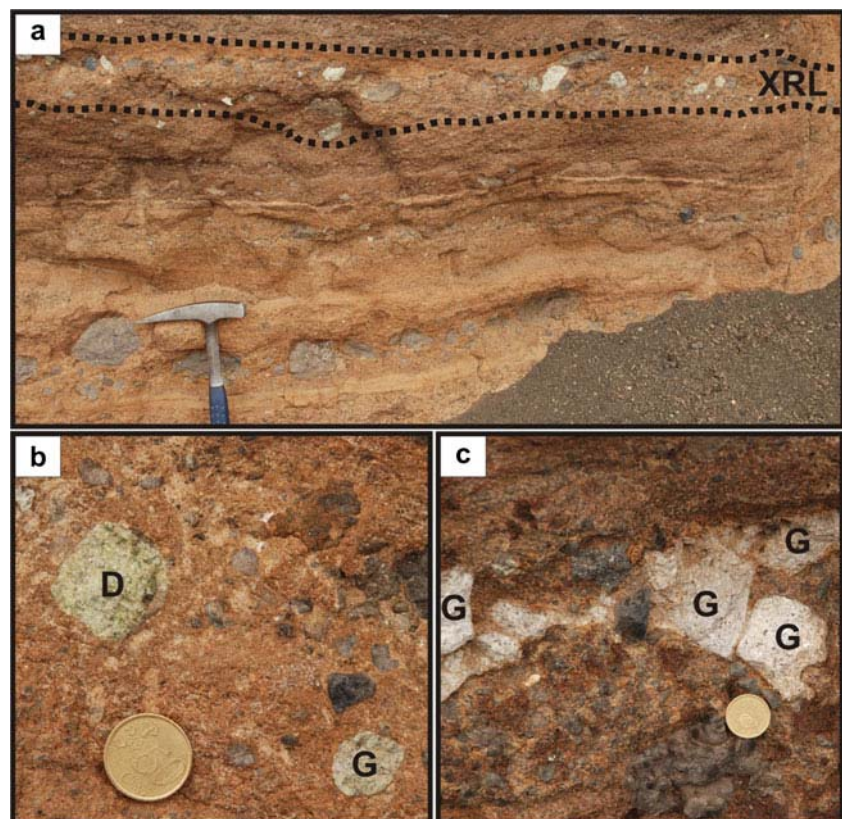
The research we present here is above all the result of new fieldwork. An investigation was carried out in order to establish the relationships between the different volcanic edifices present in an area 2 km² around El Golfo. Relative ages were determined on the basis of stratigraphic correlations. Detailed field measurements of the succession were then conducted on the main outcrop located in the southern part of the edifice (Fig. 2). Unfortunately, access to the other parts of the cone for close observation is impossible. Our studies included bed-by-bed thickness measurements of the deposits and facies analysis. Deposits were divided into lithofacies (Table 1) based on different criteria (see below) and following the facies model and nomenclature proposed by Chough

and Sohn (1990) and Solgevik et al. (2007). Due to the post-depositional palagonitisation that affects an important part of the sequence, it was not possible to obtain samples for mechanical sieving in the laboratory. Therefore, grain size determinations for the >64 mm fraction were performed partially in the field using grain size comparators. The grain size of clasts smaller than 64 mm was determined from thin sections using image analysis techniques (e.g., ImageJ software). The grain size classification is modified after Chough and Sohn (1990) due to field conditions and comprises ash <2 mm, fine lapilli = 2–8 mm; medium lapilli = 8–32 mm and coarse lapilli = 32–64 mm. Bed thickness is based on Ingram (1954): lamina (<1 cm); very thin bed (1–3 cm), thin bed (3–10 cm), medium bed (10–30 cm), thick bed (30–100 cm) or very thick bed (>100 cm). Scanning electron microscopy data for juvenile particles were taken from Martí and Colombo (1990).

Facies description

The tuff cone of El Golfo stands at sea level and has a well-exposed 45-m-thick stratigraphic section that exhibits differences in the size and shape of the clasts, in the levels of alteration and in the depositional features. We grouped the cone's deposits into eight facies and facies associations based on the following criteria: (1) sedimentary discontinuities such as erosion surfaces, (2) variations in grain size and percentage

Fig. 3 Field photographs of: **a** detail of the deposits in which the levels with gabbro and dunite xenoliths are visible (XRL); **b** detail of dunite (D) and gabbro (G) xenoliths; **c** detail of gabbro (G) xenoliths



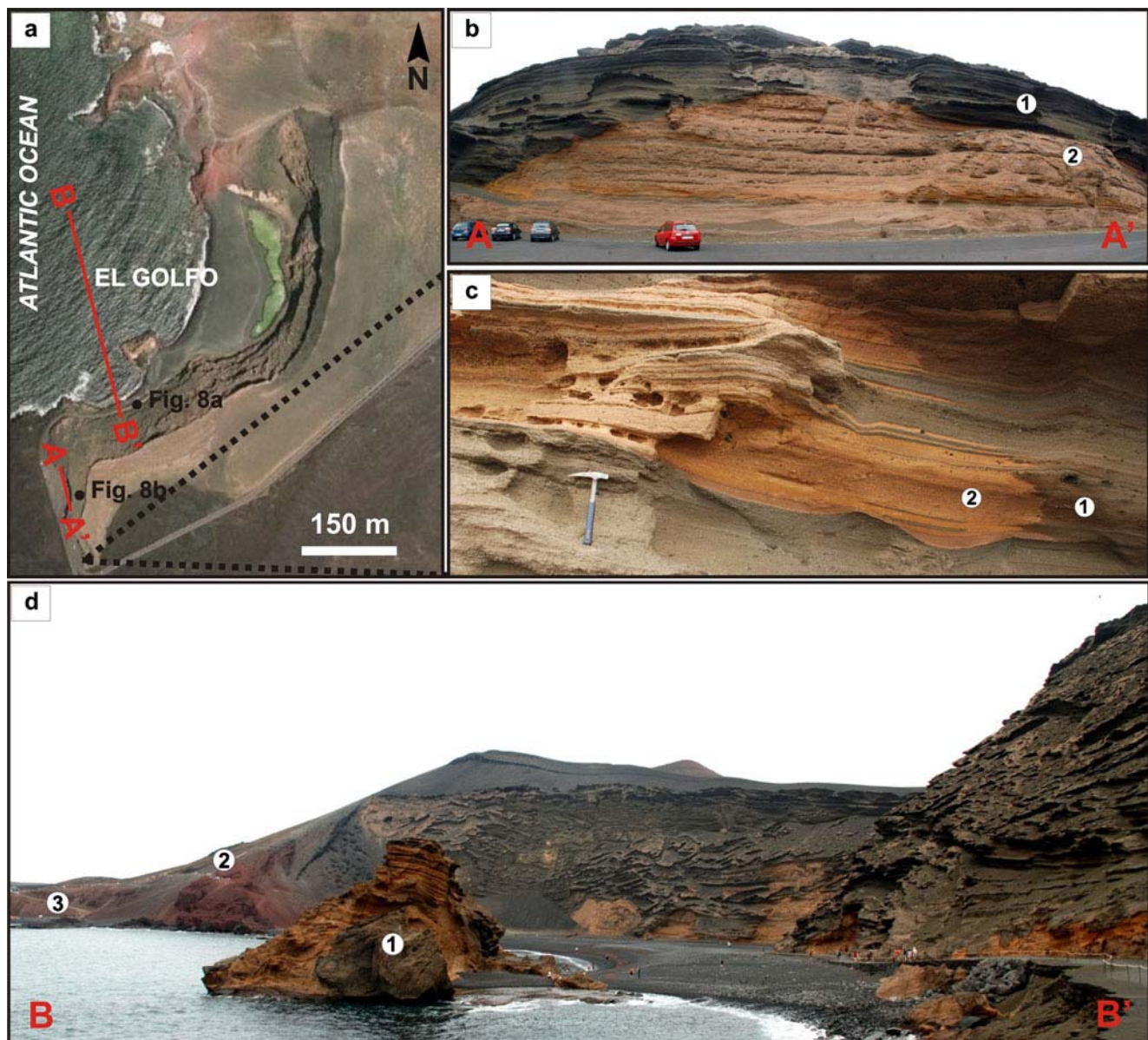


Fig. 4 **a** Google Earth image of the volcanic edifice of El Golfo; **b** field photographs of a NNW–SSE cross-section of the deposit sequence at El Golfo (*A–A'*); **c** detail of the deposits, where both the non-altered deposits (*1*) and the palagonitised deposits (*2*) are visible. Note the irregularity of the limit between the altered and non-altered zones that

is independent of the current topographical surface; **d** field photograph of El Golfo showing (*1*) the fallen block of the tuff cone in the present-day beach and (*2* and *3*) the Strombolian deposits (posterior to the emplacement of the tuff cone) located to the northeast (*B–B'*)

of volcanic bombs and (*3*) variations in primary bedforms. Erosion surfaces constitute the main discontinuity between deposits but only affect specific levels, the rest of the stratigraphic column being depositionally continuous (Fig. 5).

Channel fill facies (*A*)

This facies consists predominantly of thin structureless beds of juvenile and lithic clasts (Fig. 6a). Juvenile ash and medium lapilli fragments are rounded, dense and non-vesicular. Juvenile vesicular ballistic fragments (up to 3 cm) occur on

specific levels. Angular lithic fragments of lavas and xenoliths (up to 3 cm) can be found alongside accretionary lapilli of 1 cm. The average size of matrix grains is about 2 mm. The coarsest lithic fragments tend to be concentrated in the lowest part of the deposits. This facies is present mainly as fillings of depressions and occurs as lenses (maximum depth of 0.5 m and width of 0.4 m) (Fig. 7a–c) or in V- or U-shaped channels (depth of 1.5 m with a maximum width of 2 m) (Fig. 7d). The bedding planes are marked by sharp variation in grain size. Individual beds are generally ungraded and have irregular and erosive boundaries.

Table 1 Lithofacies and lithofacies association

Units	Lithofacies associations	Lithofacies	Interpretation
I	G1	B E	High rate of direct suspension sedimentation that alternate with tractional deposition (depending on the deposition rate)
II	G2	D E	Upper flow-regime bedforms
III	G3	A C E	A Erosive initial phase with a following depositional stage C–E Deposition of turbulent pyroclastic surges fluctuating in velocity and particle concentration with episodes of high shear stress
IV	G4	A D G H	A Eroding current with erosive surfaces with larger size than G3 D–G–H Multiple pyroclastic surges with “wet” hydromagmatic explosion
V	G5	D E F G H	Continuous changing conditions of the surge with possible moderate amount of liquid water

Letters indicate the different lithofacies: *A* channel-fill facies, *B* massive crudely stratified facies, *C* diffusely stratified facies, *D* stratified facies, *E* undulate ash-bed facies, *F* dune facies, *G* antidune facies and *H* accretionary lapilli facies

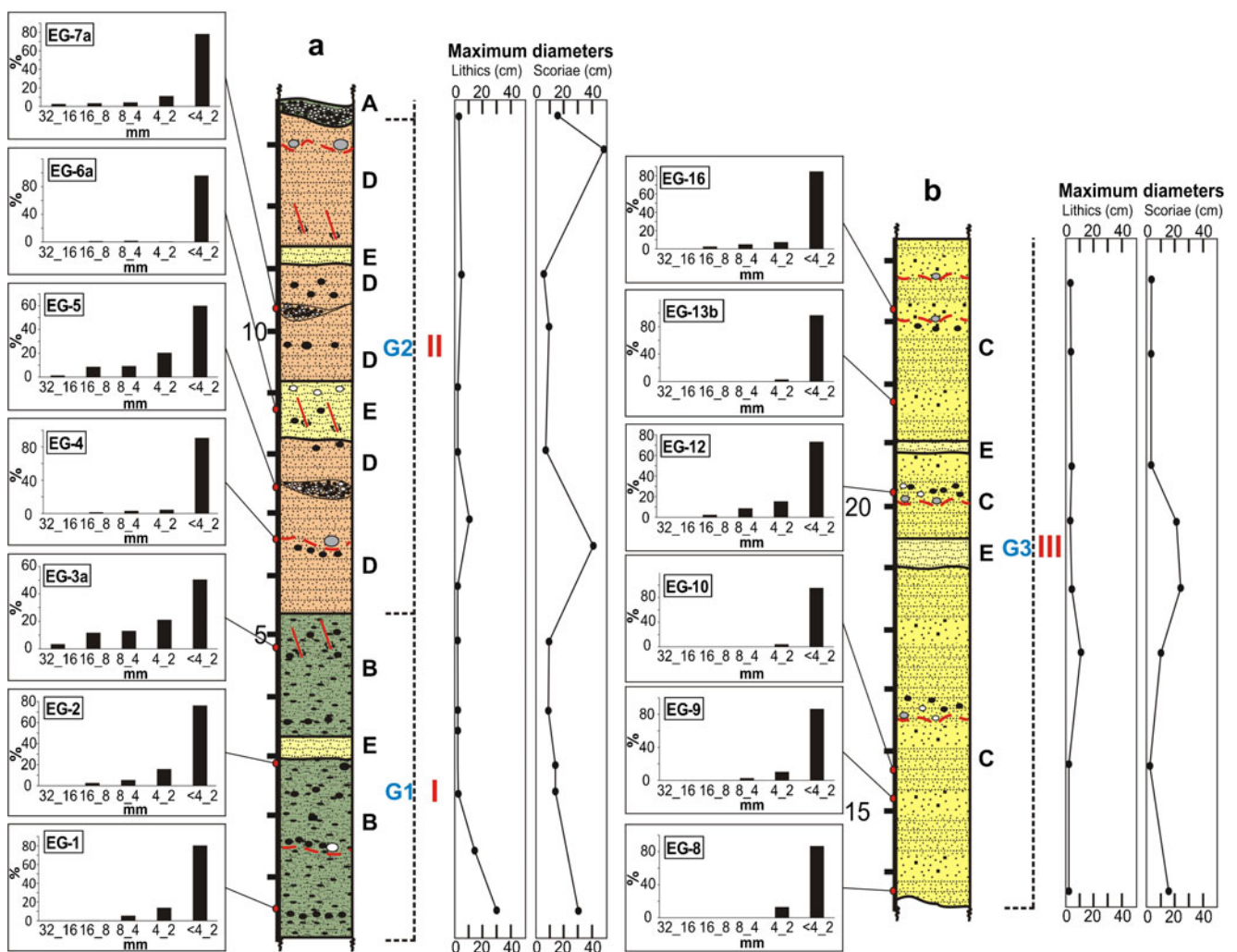


Fig. 5 Composite stratigraphic column of the deposits at El Golfo showing the main facies: **a** channel fill facies, **b** crudely stratified facies, **c** diffusely stratified facies, **d** planar stratified facies, **e** undulate ash-bed facies, **f** dune facies, **g** antidune facies and **h** accretionary lapilli facies.

Five stages (I–V) are identified based on the depositional processes and resulting deposits. Vertical variations in grain size and the maximum diameter of lithics and scoriae clasts are also indicated

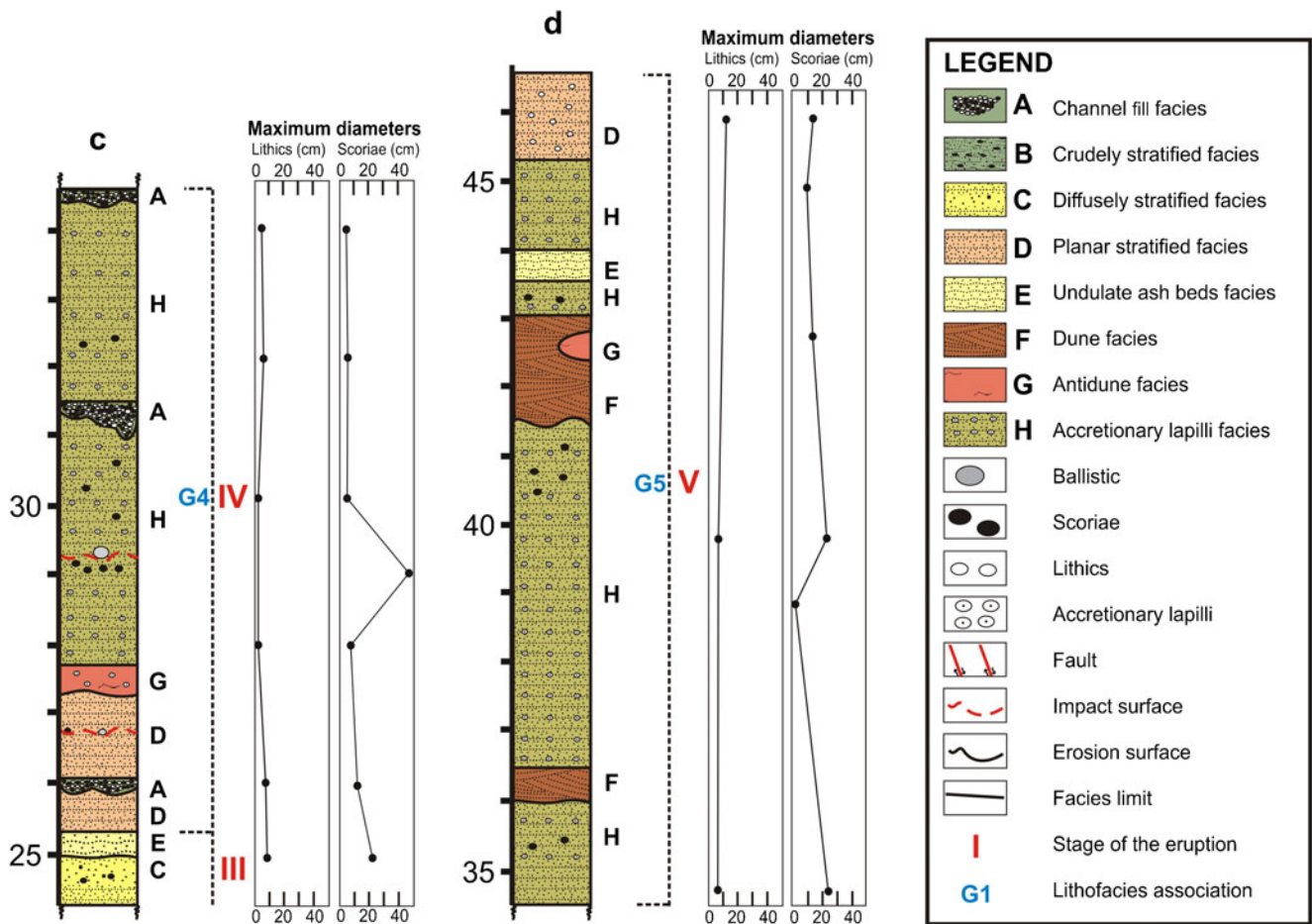


Fig. 5 (continued)

Crudely stratified facies (B)

This facies has a maximum thickness of 3 m (Fig. 5) with crude thin to medium beds (Fig. 6b). It consists of clast-supported layers, with subrounded, poorly vesicular juvenile coarse-to-medium lapilli with ballistic ejecta (up to 30 cm) in a matrix of fine lapilli and coarse ash (EG1; EG2; EG3A: Fig. 5). The fragment population in this facies is dominantly juvenile. However, many of the ballistic blocks are accidental basaltic fragments. The crude layering in this facies is defined by the presence of thick-bedded packets containing several indistinct and discontinuous boundaries with about 10–30 cm vertical spacing. Overall, the sequences are laterally continuous with single beds pinching and swelling laterally, and grading that varies vertically from normal to reverse.

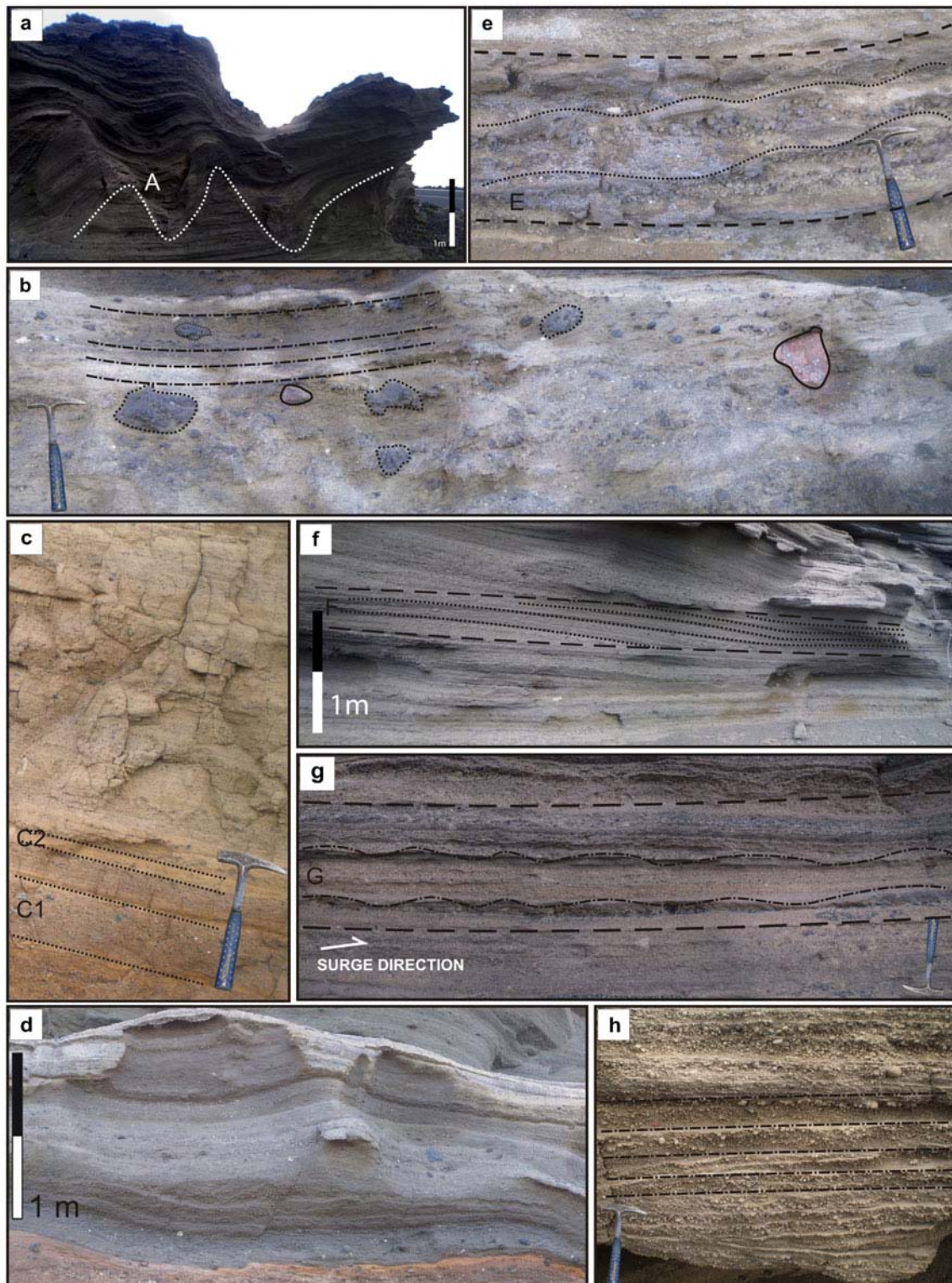
Diffusely stratified facies (C)

This facies has a maximum thickness of 5 m (range, 1–5 m) (Fig. 5) and consists of alternating ash and lapilli beds (Fig. 6c). The juvenile fine lapilli are rounded and non-vesicular. The matrix is palagonitised basaltic ash with crystal fragments of olivine and clinopyroxene. In a few levels

(often in the middle of the deposits), there is a significant increase in the number of bombs and blocks (plutonic xenoliths). Bombs can be up to 35 cm in size, while blocks are no larger than 20 cm. This facies is characterised by a visually obvious separation between layers. It consists of laterally continuous beds where, on the one hand, poorly sorted fine, lapilli-rich massive layers with a coarse ash matrix (EG9; EG13B; EG16: Fig. 5) and thicknesses ranging from a few centimetres to several decimetres thick alternate with, on the other hand, a coarse ash matrix and well-sorted ash-rich layers (EG8; EG10: Fig. 5) with thin laminations.

Planar stratified facies (D)

This facies is represented by a set of up to 2-m-thick homogeneous planar (Fig. 5) and laterally continuous multiple layers moderately sorted with bedding planes plus internal planar laminations (Fig. 6d). Juvenile fine lapilli are commonly subangular and non-vesicular. The coarse fraction (up to 10 cm) consists of lava fragments and poorly vesicular juvenile ballistic scoria bombs, with somewhat fewer xenolith fragments (max 3–5 cm). The matrix is made up of palagonitised basaltic ash with crystal fragments of olivine



and clinopyroxene. Planar lamination is locally visible in the less palagonitised layers; otherwise, the matrix appears generally to be massive due to textural modification by alteration. Typically, the contact below each bed is well-defined and non-erosive. Ballistic fragments up to 50 cm can be

found. Individual beds are thin (1–5 cm) and vary from fine lapilli-rich beds to ash and exhibit good sorting with both normal and reverse grading. Some levels are characterised by poorly sorted deposits (EG5; EG7a; Fig. 5) with coarse and medium lapilli in a matrix of fine lapilli and coarse ash that

Fig. 6 Field photographs of the characteristic facies at the tuff cone of El Golfo: **a** channel-fill facies made of heterogeneous bedded ash and lapilli. Individual beds are generally ungraded with irregular and erosive boundaries. The *dashed white line* indicates the erosion surface; **b** massive crudely stratified facies including a thin- to medium-bedded, massive-to crudely stratified unit (*dotted-dashed line*). It is also possible to distinguish the ballistic clasts corresponding to accidental basaltic fragments (*continuous line*) and bombs (*dotted line*); **c** diffusely stratified facies with continuous beds (C1) of poorly sorted lapilli-rich layers alternating with (C2) lapilli-poor layers with a yellow ash matrix; **d** planar stratified facies composed of planar and laterally continuous beds with internal stratification. This facies can be distinguished from the diffusely stratified facies because this has continuous lateral planar bedding with constant moderately sorted layers 2–3 cm and better sorting in each bed; **e** undulate ash-bed facies consisting of laterally continuous, well-sorted ash and lapilli beds with pinch-and-swell structures and undulate laminations (*dotted line*); **f** dune facies with crests up to 40 cm and sets with foresets dipping downstream migrating downstream (*dotted line*); **g** antidune facies with crest (*dotted-dash line*) up to 40 cm height with a wavelength of 15 cm; **h** accretionary lapilli facies commonly containing cores of coarse ash and fine lapilli. Individual plane-beds (*dotted-dash line*) alternate from fine lapilli-rich to ash-rich layers

fill in the small depressions. Despite resembling a diffusely stratified facies, this planar stratified facies is distinguished by the presence of continuous lateral planar bedding with constant moderately sorted layers of 2–3 cm and better sorting of each bed.

Undulate ash bed facies (E)

This facies, with a maximum detected thickness of just a few decimetres (Fig. 5), is represented by laterally continuous, well-sorted ash beds alternating with fine lapilli beds (EG6a: Fig. 5), which have undulate laminations and pinch-and-swell structures (Fig. 6e). Crests can be up to 5 cm in height and wavelengths vary from 5 to 10 cm. Some beds display brittle rupture due to the impact of ballistic ejecta.

Dune facies (F)

This facies is only present in the upper part of the succession at El Golfo. It has a maximum thickness of 1.5 m (Fig. 5) and forms large dunes (Fig. 6f). These can be up to 40 cm in height, and their wavelengths vary from 1.5 to 2 m. Individual thin beds are generally moderately sorted, structureless or reversely graded. The coarse fraction consists of juvenile medium lapilli, accretionary lapilli up to 1 cm and accidental lithic fragments (up to 4 cm) that are basaltic in nature with a matrix of coarse ash. The laminae are defined by a clast-supported fabric from which all fine material has disappeared. In front of these structures, the foresets (maximum length 50 cm) are well-preserved and exhibit clear sigmoidal geometry. Both the top and bottom set laminations are still observable, the latter asymptotic to the basal bedding plane (Fig. 6f). These dunes are similar to the ones described as Type A by Cole (1991).

Antidune facies (G)

This facies, with a maximum thickness of a few decimetres (Fig. 5), consists of small bedforms with stoss sides preserved (Fig. 6g). These deposits are generally moderately sorted with individual beds alternating between juvenile fine lapilli-rich and ash-rich and loose accretionary lapilli with a maximum size of 1 cm. Crests are up to 15 cm in height with a wavelength of 40 cm (Fig. 5).

Accretionary lapilli facies (H)

This facies is only found in the upper part of the sequence, where it has a maximum thickness of 5 m (Fig. 5) and represents a level of mainly accretionary lapilli (Fig. 6h). Although present in small amounts in other facies, the accretionary lapilli are mostly concentrated in this level. They commonly contain cores of juvenile coarse ash and fine lapilli with coarser clasts up to about 3 cm in size and are defined as rim type (Schumacher and Schmincke 1991, 1995). Deposits are usually moderately sorted, showing planar and laterally continuous beds with internal lamination. Individual plane beds are 5 cm thick and alternate between fine lapilli-rich and ash-rich layers.

Facies associations

We distinguished five lithofacies associations between the base and the top of the succession at El Golfo (Fig. 5, Table 1). As we explain below (see “Discussion”), these facies associations can be correlated to the different stages in the eruption that constructed the volcanic edifice on the basis of, on the one hand, the physical appearance of the deposits that make up the succession and, on the other, the differences in the inferred fragmentation, transportation and deposition mechanisms.

The first lithofacies association (G1) (stage I; Fig. 5) is represented by deposits exposed at sea level, mainly correspond to crudely stratified facies alternating with a small proportion of undulate ash-bed facies. Both of these facies are clearly characterised by juvenile clasts with accidental basaltic ballistic fragments, as well as notable differences in the distribution of the grain size of the deposits (Fig. 5). This lithofacies association represents the lowest part of the volcanic sequence at El Golfo (Fig. 5). The second lithofacies association (G2) (stage II; Fig. 5) exhibits a gradual transition from the previous stage and has planar stratified facies with minor undulate ash-bed facies. These deposits are finer-grained, planar and laterally continuous with episodes with undulate beds. Both facies are characterised by impact lithics of basalt. The following lithofacies association (G3) (stage III; Fig. 5) is characterised by an abrupt change, and deposits

are present mainly as fillings of depressions and as lenses (channel-fill facies). As the construction of the edifice progressed, deposits became progressively more poorly sorted: Massive lapilli-rich facies alternate with deposits characterised by well-sorted lapilli-poor, thinly bedded, internally stratified (diffuse stratified deposits) and, to a lesser extent, undulate facies. Accidental fragments (basaltic and xenoliths) characterise specific levels of the lithofacies (Fig. 5). This lithofacies association corresponds to the mid-part of the volcanic sequence. The next facies association (G4) (stage IV; Fig. 5) is characterised by a transitional change to planar stratified facies, accretionary lapilli and antidune facies, all followed by abundant lenses and V- and U-shaped channels associated with larger-sized channel-fill facies than those in G3. The final stage (G5) (stage V; Fig. 5) produced dunes and antidunes and accretionary lapilli, along with undulate and planar stratified facies. This lithofacies association is the uppermost in the depositional sequence and reveals an important change in the bedforms: Dunes and antidunes predominate, with a decrease in the average grain size of the matrix from fine lapilli/coarse ash to coarse-fine ash.

Discussion

Facies interpretation

Based on the stratigraphic and geological features discussed in this study, the volcano of El Golfo is revealed as a tuff cone constructed close to the shoreline mainly by deposition from pyroclastic surges and emplacement of minor ballistic blocks and bombs. The interpretation of the lithofacies and the lithofacies associations identified in this study provides the necessary clues for understanding the eruption, transport and depositional mechanisms involved in the construction of the volcanic edifice of El Golfo. A channel-fill facies (A) consists of beds confined to channels formed by an eroding current with an erosive initial phase followed by a depositional stage. Massive muddy ash and lapilli lenses (Fig. 6a) can be interpreted as volcanoclastic water-logged gravity currents (Cas and Wright 1987) based on the observed clearly defined boundaries and massive fine ash appearance. These geometries are in fact replaced in the lower part of the facies by massive deposits (Fig. 7a). In some cases, it is possible to infer that a two-stage process filled these channels (Fig. 7b–c): first of all, erosion by a passing current generated the V-shaped geometries that were subsequently coated by a thin veneer of fine ash deposited presumably by an ash-rich current through the channels (Fisher 1977; Verwoerd and Chevallier 1987); secondly, the channels were completely filled in by the materials transported the later pyroclastic surges. In other cases such as the U- and V-

shaped rills (Fig. 7d), the erosive surfaces are larger and were probably formed by surface runoff from flows after the deposition of the pyroclastic material. Erosional features in surge deposits are well documented (e.g. Moore 1967; Fisher 1977; Kieffer and Sturtevant 1986). As proposed in Wohletz (1998), the two-phase flow behaviour of a surge is influenced by topographic variability and implies particle deposition in cases of subsonic surges or erosion in supersonic surges.

As suggested by Valentine (1987), for any given stratified flow encountering an obstacle, there will be a level (streamline) above which all fluid has sufficient energy to surpass the obstacle and below which all fluid either is stopped (blocked) or simply moves around the obstacle with no upward motion. This critical level is referred to as the 'dividing streamline'. An increasing Rouse number, that is, the ratio of particle settling velocity to the scale of turbulence (Middleton and Southard 1978), due possibly to the confinement of the surge, causes lower parts to become dense enough to assume the characteristics of a pyroclastic flow. This leads to the deposition of the characteristic facies observed at El Golfo, where the deposits tend to have a massive fine ash appearance, and the coarsest lithics tend to be found in the lowest part of the deposits.

As suggested by Solgevik et al. (2007) for the Capelas tuff cone (Sao Miguel Island, Azores), crudely stratified facies (B) (Fig. 6b) might be the result of a rapid emplacement from a high concentration boundary layer with weak tractional transport. Alternatively (in the case of more pronounced tractional transport), this facies might be interpreted as deposits from a traction carpet in a highly concentrated boundary layer. The presence of blocks and bombs is indicative of ballistically emplaced ejecta.

The diffusely stratified facies (C) is characterised by a visible difference in grain size and sorting between the lapilli and ash-rich layers (Fig. 6c) and could be interpreted as the result of either an unsteady pyroclastic surge or multiple, closely spaced events (Dellino et al. 2004a). Poorly sorted, lapilli-rich, massive layers with crude associated stratification might be the result of rapid deposition from suspension with little traction, whereas well-sorted lapilli-poor layers with thin internal laminations could be indicative of a relatively slow deposition rate resulting in grain segregation (Arnott and Hand 1989).

In the planar stratified facies (D), it is difficult to discriminate the depositional mechanisms due to a lack of outcrops. Planar lamination, sometimes visible in the less palagonitised layers (Fig. 6d), could suggest that the facies was the product of a pyroclastic surge in which a single couplet consisting of fine lapilli and ash-grade beds was formed by a single surge (Sohn and Chough 1989; Dellino et al. 2004a, b).

The undulate ash beds (E) can be interpreted as pyroclastic surge deposits primarily on the basis of the low-angle cross

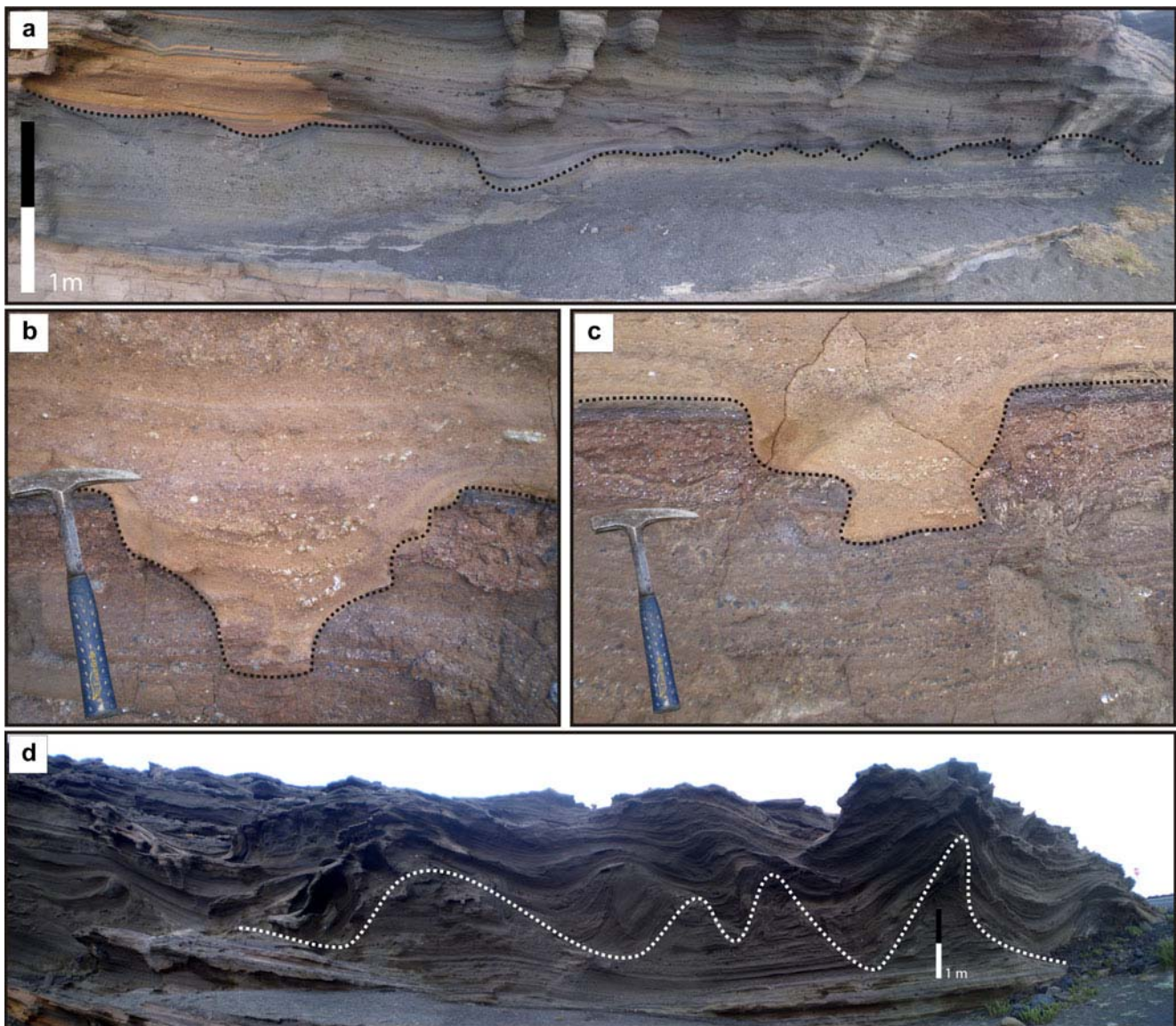


Fig. 7 Field details of channel-fill facies: **a** V-shaped geometry (*dotted line*) and crudely stratified replenishment of the erosion cavities excavated in plane beds by pyroclastic surge deposits; **b c** channels filled in two stages: First, the flow generated the V-shaped geometries (*dotted line*) that were subsequently coated by the massive dense flows that circulated

through the channels. Finally, the materials transported by the latter pyroclastic surges replenished the cavities; **d** U- and V-shaped rill geometries (*white dotted line*). The erosive surfaces have larger geometries and are thought to have been formed by surface runoff from flows after the deposition of the pyroclastic material

lamination. The existence of these structures (Fig. 6e) may be the result of variations in the flow regime (Valentine and Fisher 2000) and in particle concentration (Sohn and Chough 1989; Sohn 1996). Given the relationship between flow regimes and resulting bedforms (Cas and Wright 1987), low-angle undulate ash-beds with weak stratification could be interpreted as the result of a low-flow regime, thereby indicating a decreasing velocity of the flow or lower to transitional regime produced by a relatively low concentration pyroclastic surge.

Aside from undulate ash-beds, the dune facies (F) (Fig. 6f) are classified as lower-flow-regime bedforms (Cas and Wright 1987). Fisher and Schmincke (1984) argued that sand-wave migration direction is controlled by velocity and flow regime,

and a similar situation was proposed by Druitt (1992) for the May, 1980, Mount St. Helens blast deposits: regressive sand waves (antidunes) formed where the blast was accelerating and progressive sand waves (dunes) where it was decelerating.

The antidune facies (G) (Fig. 6g) occurs where there is supercritical flow (Cas and Wright 1987). The presence of accretionary lapilli might indicate that the corresponding pyroclastic surges were wet (i.e. they consisted of three-phase flows with gas, particles and liquid water), as suggested by Lorenz (1974a, 1974b), Walker (1984) and Sohn and Chough (1992).

Accretionary lapilli facies (H) (Fig. 6h) commonly form in steam-rich hydrovolcanic eruption columns (Self and Sparks 1978) or in convecting pyroclastic surge clouds when solid

particles pick up sticky wet ash (Waite and Dzurisin 1981). During the lateral spreading of surges, particles form core agglomerate due to accidental collisions and when the binding forces of liquid bridges from condensed moisture exceed the grain-dispersive forces (Schumacher and Schmincke 1995).

The depositional characteristics of the pyroclastic surge deposits at El Golfo and the absence of secondary reworking by sea waves suggest that the emplacement of the deposits and the construction of the cone occurred in a subaerial environment. In addition, the irregular distribution of palagonitic alteration indicate that, given the depositional characteristics of the deposits, the palagonitisation was produced in a subaerial environment, as suggested by Martí and Colombo (1990).

Most of the pyroclastic deposits in the edifice consist of a fine-grained matrix embedding coarse scoria, lithic fragments and volcanic bombs and blocks (emplaced ballistically) (Figs. 6 and 8), which suggests that the transportation process of this pyroclastic material was not able to develop any proper grain-sorting process. The lack of clear fallout deposits is a remarkable feature of the succession at El Golfo. This, together with lithological and depositional features such as ripples, dunes, antidunes and tabular forms, as well as the circular distribution of deposits, indicates that most pyroclastic deposits formed from turbulent, highly dilute pyroclastic surges (see Druitt 1998; Freundt and Bursik 1998; Huppert 1998; Branney and Kokelaar 2002) expanding radially from the eruptive vent. In fact, variations in vertical facies are usually

related to variable rates of energy release occurring during an ongoing eruption (Sohn and Chough 1989). The apparent lack of fallout deposits may be interpreted either as a direct consequence of the eruption dynamics (i.e. absence of fallout mechanisms in proximal areas) or of their erosion and assimilation by the pyroclastic surges.

Eruptive dynamics

Along with accretionary lapilli and accidental lithics, particles with morphology and textures related to hydromagmatic fragmentation (block-like shapes, low vesicularity, presence of adhered dust, tephra size and superficial chemical alteration) (Martí and Colombo 1990) dominate the deposits found in the tuff cone of El Golfo. The dynamics of hydrovolcanism are controlled by the complex thermodynamics of magma–water interaction, which determines the nature of explosive activity, and are characterised by variable energy outputs and different degrees of magmatic or hydromagmatic fragmentation (Wohletz and Sheridan 1983; Houghton and Hackett 1984; Kokelaar 1986; White and Houghton 2000; Mastin et al. 2004). Depending on the extent of the magma–water interaction and the modes of transport and deposition, hydrovolcanic deposits show remarkable variability in between-layer and within-layer. The efficiency of hydromagmatic fragmentation and the corresponding eruption dynamics are controlled by magma viscosity, temperature, the pressure differences between magma

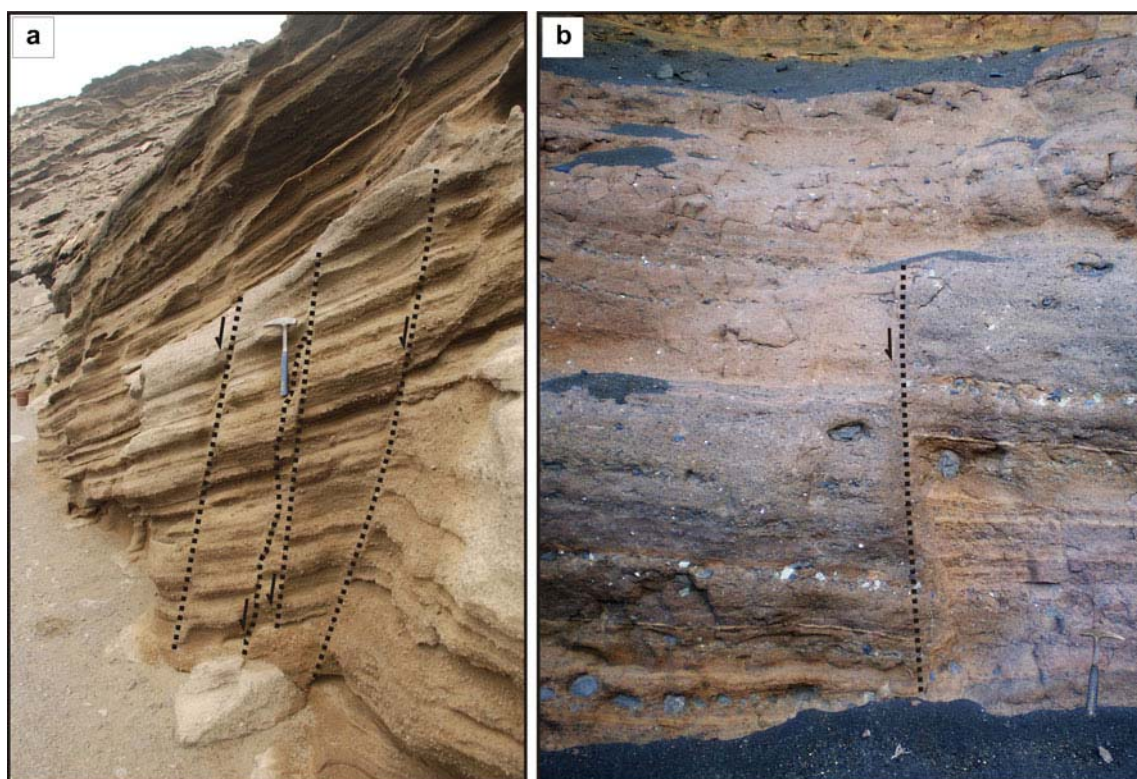


Fig. 8 Field photographs showing examples of subvertical settlement faults existing around the edifice

and water, and the water/magma contact mode (supply rate of magma and the external water; Wohletz and Sheridan 1983), as well as by the exact nature of the coolant (White 1996).

The lithological and stratigraphic variations shown by the deposits at El Golfo (Fig. 5) suggest that the different transport and depositional mechanisms that characterize them were a product of changes in the eruption dynamics caused by changes in the efficiency of the hydromagmatic fragmentation. This implies that the eruption responsible for the construction of this tuff cone was continuous but had several pulses in which different types of deposits were formed. According to the resulting facies associations described above and their interpretation in light of the mechanisms of fragmentation, transportation and deposition, we are able to distinguish five stages or pulses in the eruption of this volcano (Table 1).

The first stage (I) is represented by the lithofacies association G1 (Fig. 5, Table 1), which consists of deposits characterised by the effects of the high rate of direct suspension sedimentation that alternate with tractional deposition (depending on the deposition rate). The general aspect of this lithofacies, characterised by poor sorting with coarse-grained tephra (coarse lapilli) alternating with beds of coarse ash, along with large clasts and blocks up to 30 cm in diameter, reflects in general high-energy transport with changes in the rate of deposition. The trajectories of the ballistic impacts indicate north-to-south transportation. The large amount of accidental basaltic lithic clasts can be interpreted as a vent-opening episode that occurred during the initial stages of the subsurface hydrovolcanic explosions.

The second stage (II) corresponds predominantly to the emplacement of multiple pyroclastic surges with subordinate undulate ash-beds (lithofacies association G2) (Fig. 5, Table 1). The resulting deposits show characteristic planar bedding, which may be considered as an upper flow-regime bedform. Higher fragmentation efficiency is suggested by the abundance of ash matrix in these deposits. This suggests an increase in the energy of the explosions, probably associated with greater efficiency in the energy transfer during the hydromagmatic process. Similar deposits can be observed at Surtsey, Capelinhos and Capelas (Waters and Fisher 1971; Kokelaar 1983, 1986; Solgevik et al. 2007). The presence of a number of ballistic blocks up to 50 cm in diameter (Fig. 5) suggest episodes of higher explosive energy.

The third stage (III) of the eruption is reflected in the succession of deposits in the lithofacies association G3 (Fig. 5, Tab. 1), which represents a further change in the transportation and depositional conditions. This stage consists of beds confined to channels formed by an eroding current with an initial erosive phase followed by a depositional stage. The rest of the unit is interpreted as resulting from the deposition of turbulent pyroclastic surges with fluctuating velocity and particle concentration, as well as

episodes of high shear stress leading to the formation of undulate deposits. These deposits are similar to the ones described in Solgevik et al. (2007) and Cole et al. (2001). These features—by comparison with those of the previous stage—indicate that this stage was characterised by higher-energy transport related to episodes of higher explosive energy, which also generated bomb- and block-rich (up to 35 cm in diameter) horizons.

Stage four (IV) can be correlated with wet explosions (lithofacies association G4) (Fig. 5, Tab. 1) in which a remobilisation of material occurred due to an excess of water (e.g. Sohn and Chough 1992). Individual explosions could also have produced water-charged tephra jets that landed on the flanks of the growing cone and acted as a source of ready-to-move free water. The U-shaped channels might also be the result of topographic variability with particle deposition or erosion. The presence of antidunes, planar stratified and accretionary lapilli suggest a complex emplacement of pyroclastic density currents with continuous changes in transportation and depositional conditions. The presence in smaller proportions of bedforms with ripple-type geometries and slopes in the opposite direction to the propagation direction of the main pyroclastic surges (i.e. antidunes) suggests an important increase in the energy of the flow (Fisher and Schmincke 1984), whilst the dunes represent lower-flow-regime bedforms.

Stage five (V) corresponds to the lithofacies association G5 (Fig. 5, Tab. 1) and is characterised by deposits containing large dunes, accretionary lapilli, antidunes, and undulate and planar stratified facies. The duration of the pyroclastic surges that caused their deposition was probably very short, and there is no evidence that during flow emplacement the materials of the bedform were eroded and adapted to the new flow conditions. The lack of fine material, probably elutriated during the transport process, in the cross-bedded levels, indicates that the flows generating these dunes were gas-supported. However, the presence of a facies with accretionary lapilli in the deposits of this last stage suggests that occasionally there was a moderate amount of liquid water (or moisture) in the surges and/or eruption clouds from which they formed (e.g. Fisher and Schmincke 1984; Heiken and Wohletz 1985). As a surge moves laterally away from the vent, it loses heat, solids and momentum, resulting in a decreasing wavelength and amplitude of the cross-stratified surge deposits as the distance from the vent increases (e.g. Waters and Fisher 1971; Wohletz and Sheridan 1979; Sohn and Chough 1989). The loss of heat results in the condensation of steam, which explains the increase in wet features. The amount of water might thus be related to the dynamics of the flow rather than the changing eruption conditions. This hypothesis was first proposed by Wohletz and Sheridan (1983).

In summary, the diversity of emplacement mechanisms inferred and grain size distributions observed in the stratigraphic sequence indicates that the eruptive and emplacement

mechanisms were not constant during the eruptive episode that generated the tuff cone of El Golfo. A general increase in the explosive energy can be seen as one moves upwards in the pyroclastic succession, indicating possibly that there was a trend towards an optimum magma/water ratio in the second half of the eruption, which would have led to an increase in the energy-exchange efficiency and, consequently, in the magma fragmentation. This is illustrated by the progressive increase in the degree of fragmentation (i.e. decrease in grain size) and in the energy of the resulting pyroclastic surges, which was probably related to a progressive reduction in the amount of sea water entering the vent as the volcanic edifice was being built. However, there is no evidence of any Strombolian phase during the eruption, which would seem to imply that to the west the tuff cone remained open to the sea during the whole eruption sequence, even at its end when the eastern side of the edifice had reached around 60 m a.s.l. This might probably be due to the continuous partial collapse of part of the edifice. The absence of any significant volume of lithic clasts derived from the substrate (e.g. fragments of older lavas or fossil beaches) suggests that the eruption did not excavate deeply into the substrate, and so we can assume that the magma–water interaction occurred mostly at a very shallow depth or even at sea level and can discard the idea that water could have been drawn into the conduit from a subsurface aquifer.

Post-depositional processes

The irregular geometry of the different alteration zones suggests that some primary causes for the palagonitisation should have existed. This process may be almost contemporaneous to tuff deposition (e.g. Capelas, Capelinhos and Sao Roque tuff cones in Azores, Solgevik et al. 2007, Cole et al. 2001, Zanon et al. 2009; Sinker Butte Volcano in USA, Brand and White 2007). The fact that the materials that are in contact with the highest topographic surface are the least altered indicates that, during the late depositional stages, the pyroclastic materials retained a small amount of steam shortly after being deposited. By contrast, the materials located in the lower half of the sequence are more altered, which implies that at the moment of deposition they retained a greater proportion of water as steam. In these lower sections, the steam remained trapped for longer, which may be related to the fact that the accumulation of materials occurred very rapidly and thus prevented the steam from escaping. Thus, once covered by the successive pyroclastic surges, the deposits would have acted as an aquatard that could explain the different degree of alteration between the upper and lower parts of the sequence at El Golfo, despite the lack of any clear (eruptive) separation.

The presence of interstitial water in the lower part of the sequence of deposits is also shown by the existence of tephra-slips that affected the whole wall and which are associated

with circular compaction faults (Fig. 8). The palagonitisation induced high secondary resistance in the tuff, resulting in a stress response that changed from pseudo-plastic to pseudo-brittle in behaviour. As a consequence, the response to this oriented stress was the formation of fractures and an immediate failure. During these slides, the entire block behaved as a single rigid unit (but sufficiently plastic). It is important to note that the downdropped section in front of El Golfo (Fig. 4d) exhibits the same type of alteration as the rest of the edifice but with the addition of a chaotic structure due to the slumping process. This suggests that the main landslide occurred once the palagonitization processes had already started. However, as has been demonstrated in the case of the Surtsey eruption (Kokelaar 1983; Moore 1985), it is possible that slumps occurred during the construction of the volcanic edifice and that the material displaced towards the vent was re-ejected during subsequent explosions.

Hazard implications

El Golfo is a good example of a tuff cone demonstrating how a single eruption may produce a complex sequence of eruption styles and depositional processes. Nonetheless, an examination of this volcano sheds light on a number of important implications for hazard assessment when considered within the framework of the fissural volcanism present in the Canary Islands. After the construction and partial erosion of its edifice, another eruptive episode took place in the northern section of El Golfo (Fig. 2). Three craters were formed, and lavas and Strombolian pyroclasts were emitted (Fig. 4d). Despite not occurring during the same eruptive episode, the formation of these new edifices can be linked to the same NEE–SWW fracture system that originated the tuff cone at El Golfo. We can see here how a fissure-dominated system in which scoria and/or lava spatter cones form long chains exhibits very different styles of eruptions at the extremities of the fissure. Subaerial conditions changing to shallow submarine conditions allowed for the development of a hydrovolcanic landform in the area. Sea-level changes during the long time in which the overall fissure system was active (as shown by the presence of fossil beaches) may have led to the construction of a complex set of volcano types in this lowland area with contrasting eruption styles and, consequently, a variety of associated hazards. While a small lava spatter eruption may be manageable, a full tuff cone or maar eruption would cause havoc on a local scale and would have very different repercussions in terms of its potential hazards. Furthermore, the pyroclastic deposits at El Golfo are very rich in xenoliths, and the existence of these plutonic enclaves in the basalts of Lanzarote would seem to suggest that on occasions a rapid ascent of magma to the surface occurs. On Lanzarote and the other Canary Islands, this type of long-lived fissure-dominated volcanism incorporating contrasting

eruption styles is not uncommon and should be studied in more detail as a means of conducting appropriate hazard assessment for this area.

Conclusions

The tuff cone at El Golfo is an example of a coastal volcanic edifice caused by simple hydrovolcanic activity without any evidence of Strombolian phases. Interaction of water with magma, mostly at sea level, dominated the whole eruptive process. The lithological and stratigraphic features present in the deposits at El Golfo suggest that most were formed by deposition from turbulent pyroclastic surges. These characteristics, together with the type and distribution of the palagonitic alteration that affects part of the materials and the absence of hyaloclastites, suggest that they were emplaced in a subaerial environment. The growth of the tuff cone can be divided roughly into five stages on the basis of the resulting deposits and different corresponding eruption mechanisms inferred. A continuous change in the transport/depositional system is revealed, with a possible progressive increase in the energy-transfer efficiency from magma to water and, consequently, in the eruption explosivity and in the degree of fragmentation. This volcano forms part of a long-lived fissural system that reaches down to the coastal plains, along which several monogenetic cones showing a large diversity of eruptive styles have formed. It reminds us that eruption dynamics and associated hazards may differ considerably within the same volcanic system if external variables (e.g. the availability of water) change.

Acknowledgements This research was partially funded by CTM2009-05919-E/ANT. The authors are grateful to the Cabildo of Lanzarote and the National Park of Timanfaya for giving permission to undertake this research, and to Orlando Hernandez (Casa de Los Volcanes-Cabildo de Lanzarote) for his assistance with the logistics. We are also grateful to the Editor James White, the Associated Editor Thorvaldur Thordarson and the reviewers Danilo Palladino, Karoly Németh and Christopher Hamilton for their constructive reviews of this manuscript.

References

- Abdel-Monem A, Watkins ND, Gast PW (1972) Potassium-argon ages, volcanic stratigraphy, and geomagnetic polarity history of the Canary Islands; Tenerife, La Palma and Hierro. *Am J Sci* 272(9):805–825
- Araña V, Carracedo J (1978) Cañarian volcanoes: Gran Canaria. Editorial Rueda, Madrid:1–175
- Araña V, Hansen A, Martí J (1988) La caldera y el Pico de Vandama (Gran Canaria). *Boletín Geológico y Minero T XCIX-I*:47–58
- Amott RWC, Hand BM (1989) Bedforms, primary structures and grain fabric in the presence of suspended sediment rain. *J Sediment Petrol* 59:1062–1069
- Baker E, Massoth G, de Ronde C, Lupton J, McInnes B (2002) Observations and sampling of an ongoing subsurface eruption of Kavachi volcano, Solomon Islands. *Geology* 30(11):975–978
- Banda E, Dan̄obeitia JJ, Surin̄ach E, Ansoorge J (1981) Features of crustal structure under the Canary Islands. *Earth Planet Sci Lett* 55(1):11–24
- Belousov A, Belousova M (2001) Eruptive process, effects and deposits of the 1996 and the ancient basaltic phreatomagmatic eruptions in Karymskoye lake Kamchatka, Russia. *Spec Publ int Assoc Sediment* 30:35–60
- Brand BD, White CM (2007) Origin and stratigraphy of phreatomagmatic deposits at the Pleistocene Sinker Butte Volcano, Western Snake River Plain, Idaho. *J Volcanol Geotherm Res* 160(3–4):319–339
- Branney MJ, Kokelaar P (2002) Pyroclastic density currents and the sedimentation of ignimbrites. *Geological Society of London Memoirs*, p 150
- Cas RAF, Wright JV (1987) Volcanic successions, modern and ancient. A geological approach to processes products and successions. Chapman and Hall, London, 528 pp
- Chough SK, Sohn YK (1990) Depositional mechanics and sequences of base surges, Songaksan tuff ring, Cheju Island, Korea. *Sedimentology* 37(6):1115–1135
- Clarke H, Troll VR, Carracedo JC (2009) Phreatomagmatic to Strombolian eruptive activity of basaltic cinder cones: Montaña Los Erales, Tenerife, Canary Islands. *J Volcanol Geotherm Res* 180(2–4):225–245
- Cole PD (1991) Migration direction of sand-wave structures in pyroclastic-surge deposits; implications for depositional processes. *Geology* 19(11):1108–1111
- Cole PD, Guest J, Duncan A, Pacheco J (2001) Capelinhos 1957–1958, Faial, Azores: deposits formed by an emergent surtseyan eruption. *Bull Volcanol* 63(2):204–220
- Cronin SJ, Bonte-Grapentin M, Nemeth K (2006) Samoa technical report—review of volcanic hazard maps for Savai'i and Upolu. EU-SOPAC, MUIR, Massey, New Zealand
- De La Nuez J, Alonso J, Quesada M, Macu M (1993) Edificios hidromagmáticos costeros de Tenerife (Islas Canarias). *Rev Soc Geol España* 6(1–2):47–59
- Dellino P, Isaia R, La Volpe L, Orsi G (2004a) Interaction between particles transported by fallout and surge in the deposits of the Agnano-Monte Spina eruption (Campi Flegrei, Southern Italy). *J Volcanol Geotherm Res* 133(1–4):193–210
- Dellino P, Isaia R, Veneruso M (2004b) Turbulent boundary layer shear flows as an approximation of base surges at Campi Flegrei (Southern Italy). *J Volcanol Geotherm Res* 133(1–4):211–228
- Druitt TH (1992) Emplacement of the 18 May 1980 lateral blast deposit ENE of Mount St. Helens, Washington. *Bull Volcanol* 54(7):554–572
- Druitt TH (1998) Pyroclastic density currents. In: Gilbert, J.S., Sparks, R.S.J. (eds.), *The physics of explosive volcanic eruptions*. *Geol Soc Spec Publ* 145:145–182
- Fisher RV (1977) Erosion by volcanic base-surge density currents: U-shaped channels. *Geol Soc Am Bull* 88(9):1287–1297
- Fisher RV, Schmincke HU (1984) *Pyroclastic rocks*. Springer-Verlag Inc, Berlin, p 474
- Freundt A, Bursik M (1998) Pyroclastic flow transport mechanisms. In: Freundt A, Rosi M (eds) *From magma to tephra, modeling physical processes of explosive volcanic eruptions*, vol 4. Elsevier Science, Amsterdam, pp 173–231
- Fuster JM, Cendrbro A, Gastesi P, Ibarróla E, Ruiz JL (1968) *Geología y volcanología de las islas Canarias: Tenerife*. Instituto 'Lucas Mallada', CSIC, Madrid:218 pp
- Gudmundsson MT, Thordarson T, Höskuldsson Á, Larsen G, Björnsson H, Prata FJ, Oddsson B, Magnússon E, Högnadóttir T, Petersen GN, Hayward CL, Stevenson JA, Jónsdóttir I (2012) Ash generation and distribution from the April-May 2010 eruption of Eyjafjallajökull, Iceland. *Sci. Rep.* 2
- Heiken G, Wohletz K (1985) *Volcanic ash*. University of California Press, Berkeley, p 246

- Houghton BF, Hackett WR (1984) Strombolian and phreatomagmatic deposits of Ohakune craters, Ruapehu, New Zealand: a complex interaction between external water and rising basaltic magma. *J Volcanol Geotherm Res* 21(3–4):207–231
- Huppert HE (1998) Quantitative modelling of granular suspension flows. *Phil Trans R Soc Lond* 356:2471–2496
- (IMO) (Icelandic Meteorological Office) <http://en.vedur.is/earthquakes-and-volcanism/articles/nr/1884>
- Ingram RL (1954) Terminology for the thickness of stratification and parting units in sedimentary rocks. *Geol Soc Am Bull* 65(9):937–938
- Jude-Eton TC, Thordarson T, Gudmundsson MT, Oddsson B (2012) Dynamics, stratigraphy and proximal dispersal of supraglacial tephra during the ice-confined 2004 eruption at Grímsvötn Volcano, Iceland. *Bull Volcanol* 74(5):1057–1082
- Kieffer S, Sturtevant B (1986) Erosional furrows formed during the lateral blast at Mount St. Helens, May 18, 1980: indicators of longitudinal vortices in the boundary layer. *Abstr. Intl. Volcanol. Cong. New Zealand* 53
- Kienle J, Kyle PR, Self S, Motyka RJ, Lorenz V (1980) Ukinrek Maars, Alaska, I. April 1977 eruption sequence, petrology and tectonic setting. *J Volcanol Geotherm Res* 7(1–2):11–37
- Kokelaar BP (1983) The mechanism of surtseyan volcanism. *J Geol Soc* 140(6):939–944
- Kokelaar BP (1986) Magma–water interactions in subaqueous and emergent basaltic volcanism. *Bull Volcanol* 48:275–289
- Larsen G (2010) 3 Katla: Tephrochronology and eruption history. In: Anders Schomacker JK, Kurt HK (eds) *Developments in Quaternary sciences*. Elsevier, pp 23–49
- Larsen G, Guðmundsson M, Sigmarsson O (2009) Katla. In: Sólnes J et al (eds) *Náttúruvá á Íslandi-Tekist á við náttúruöflin í 1100 ár. Eldgosavá. Viðlagatrygging Íslands, Reykjavík*
- Le Bas MJ, Rex DC, Stillman CJ (1986) The early magmatic chronology of Fuerteventura, Canary Islands. *Geol Mag* 123:287–298
- Lorenz V (1974a) Studies of the Surtsey tephra deposits. *Surtsey Res Prog Rep* 7:72–79
- Lorenz V (1974b) Vesiculated tuffs and associated features. *Sedimentology* 21:273–291
- Macdonald GA (1972) *Volcanoes*. Prentice-Hall, Inc, N.J, p 510
- Machado F, Parsons WH, Richards AF, Mulford JW (1962) Capelinhos eruption of Fayal Volcano, Azores, 1957–1958. *J Geophys Res* 67(9):3519–3529
- Marinoni LB, Gudmundsson A (2000) Dykes, faults and palaeostresses in the Teno and Anaga massifs of Tenerife (Canary Islands). *J Volcanol Geotherm Res* 103(1–4):83–103
- Marinoni LB, Pasquarè G (1994) Tectonic evolution of the emergent part of a volcanic ocean island: Lanzarote, Canary Islands. *Tectonophysics* 239(1–4):111–137
- Martí J, Colombo F (1990) Estratigrafía, sedimentología y mecanismos eruptivos del edificio hidromagmático de El Golfo (Lanzarote). *Bol Geol Min* 101(4):560–579
- Mastin LG, Christiansen RL, Thorber C, Lowenstern J, Beeson M (2004) What makes hydromagmatic eruptions violent? Some insights from the Keanakākoʻi Ash, Kīlauea Volcano, Hawaiʻi. *J Volcanol Geotherm Res* 137(1–3):15–31
- Middleton G, Southard J (1978) *Mechanics of sediment movement*. Soc Econ Paleontol Mineral Short Course 3, Eastern Section: pp 6.37–36.41
- Moore J (1967) Base surge in recent volcanic eruptions. *Bull Volcanol* 30(1):337–363
- Moore JG (1985) Structures and eruptive mechanisms at Surtsey Volcano, Iceland. *Geol mag* 122(6):649–661
- Moore JG, Nakamura K, Alcaraz A (1966) The 1965 eruption of Taal Volcano. *Science* 151(3713):955–960
- Morimoto R (1960) Submarine eruption of the Myōjin reef. *Bull Volcanol* 23(1):151–160
- Németh K, Cronin SJ (2009) Volcanic structures and oral traditions of volcanism of Western Samoa (SW Pacific) and their implications for hazard education. *J Volcanol Geotherm Res* 186(3–4):223–237
- Németh K, Cronin SJ (2011) Drivers of explosivity and elevated hazard in basaltic fissure eruptions: the 1913 eruption of Ambrym Volcano, Vanuatu (SW-Pacific). *J Volcanol Geotherm Res* 201(1–4):194–209
- Robertson AHE, Stillman CJ (1979) Late Mesozoic sedimentary rocks of Fuerteventura, Canary Islands: implications for West African continental margin evolution. *J Geol Soc* 136(1):47–60
- Schumacher R, Schmincke HU (1991) Internal structure and occurrence of accretionary lapilli—a case study at Laacher See Volcano. *Bull Volcanol* 53(8):612–634
- Schumacher R, Schmincke HU (1995) Models for the origin of accretionary lapilli. *Bull Volcanol* 56(8):626–639
- Self S, Sparks R (1978) Characteristics of widespread pyroclastic deposits formed by the interaction of silicic magma and water. *Bull Volcanol* 41(3):196–212
- Self S, Kienle J, Huot J-P (1980) Ukinrek Maars, Alaska, II. Deposits and formation of the 1977 craters. *J Volcanol Geotherm Res* 7(1–2):39–65
- Sheridan MF, Wohletz KH (1981) Hydrovolcanic explosions: the systematics of water-pyroclast equilibration. *Science* 212:1387–1389
- Sheridan MF, Wohletz KH (1983) Hydrovolcanism: basic considerations and review. *J Volcanol Geotherm Res* 17(1–4):1–29
- Sohn YK (1996) Hydrovolcanic processes forming basaltic tuff rings and cones on Jeju Island, Korea. *Geol Soc Am Bull* 108:1199–1211
- Sohn YK, Chough SK (1989) Depositional processes of the Suwolbong tuff ring, Cheju Island (Korea). *Sedimentology* 36(5):837–855
- Sohn YK, Chough SK (1992) The Ilchulbong tuff cone, Cheju Island, South Korea: depositional processes and evolution of an emergent, surtseyan-type tuff cone. *Sedimentology* 39:523–544
- Sohn YK, Park JB, Khim BK, Park KH, Koh GW (2003) Stratigraphy, petrochemistry and Quaternary depositional record of the Songaksan tuff ring, Jeju Island, Korea. *J Volcanol Geotherm Res* 119(1–4):1–20
- Solgevik H, Mattsson HB, Hermelin O (2007) Growth of an emergent tuff cone: fragmentation and depositional processes recorded in the Capelas tuff cone, São Miguel, Azores. *J Volcanol Geotherm Res* 159(1):246–266
- Sumner JM (1998) Formation of clastogenic lava flows during fissure eruption and scoria cone collapse: the 1986 eruption of Izu-Oshima Volcano, eastern Japan. *Bull Volcanol* 60(3):195–212
- Thorarinsson S (1965) The Surtsey eruption: course of events and development of the new island. *Surtsey Res Prog Rep* 1:51–55
- Valentine GA (1987) Stratified flow in pyroclastic surges. *Bull Volcanol* 49(4):616–630
- Valentine GA, Fisher RV (2000) Pyroclastic surges and blasts. In: Sigurdsson, H., Houghton, B.F., McNutt, S.R., Rymer, H., Stix, J. (Eds.), *Encyclopedia of volcanoes*. New York, Academic Press: 571–580
- Verwoerd WJ, Chevallier L (1987) Contrasting types of surtseyan tuff cones on Marion and Prince Edward islands, southwest Indian Ocean. *Bull Volcanol* 49(1):399–413
- Waitt RB, Dzurisin D (1981) Devastating pyroclastic density flow and attendant air fall of May 18—Stratigraphy and sedimentology deposits. In: *The 1980 eruptions of Mount St. Helens, Washington* (ed. by P.W. Lipman & D.R. Mullineaux), Pap. US Geol. Surv. 1250 439–458
- Walker GPL (1984) Characteristics of dune-bedded pyroclastic surge bedsets. *J Volcanol Geotherm Res* 20(3–4):281–296
- Waters AC, Fisher RV (1971) Base surges and their deposits: Capelinhos and Taal volcanoes. *J Geophys Res* 76(23):5596–5614
- White JDL (1996) Impure coolants and interaction dynamics of phreatomagmatic eruptions. *J Volcanol Geotherm Res* 74(3–4):155–170
- White JDL, Houghton B (2000) Surtseyan and related phreatomagmatic eruptions. In: Sigurdsson H, Houghton BF, McNutt SR, Rymer H,

- Stix J (eds) Encyclopedia of volcanoes. Academic Press, 511, p 495
- White JDL, Ross PS (2011) Maar-diatreme volcanoes: a review. *J Volcanol Geotherm Res* 201(1–4):1–29
- White JDL, Schmincke H-U (1999) Phreatomagmatic eruptive and depositional processes during the 1949 eruption on La Palma (Canary Islands). *J Volcanol Geotherm Res* 94(1–4):283–304
- Wohletz KH, Sheridan MF (1979) A model of pyroclastic surge. In: Chapin, C.E., Elston, W.E. (eds.). *Geol Soc Am Spec Pap* 180:177–194
- Wohletz KH, Sheridan MF (1983) Hydrovolcanic explosions; II, Evolution of basaltic tuff rings and tuff cones. *Am J Sci* 283(5):385–413
- Wohletz KH (1998) Pyroclastic surges and compressible two-phase flow. In: Freundt A, Rosi M (eds) *From magma to tephra: modelling physical processes of explosive volcanic eruptions*. Elsevier, Amsterdam
- Zanon V, Pacheco J, Pimentel A (2009) Growth and evolution of an emergent tuff cone: considerations from structural geology, geomorphology and facies analysis of São Roque volcano, São Miguel (Azores). *J Volcanol Geotherm Res* 180(2–4):277–291

APPENDIX 4

EXPLOSIVE FELSIC VOLCANISM ON EL HIERRO (CANARY ISLANDS)

Bulletin of Volcanology

Explosive felsic volcanism on El Hierro (Canary Islands)

--Manuscript Draft--

Manuscript Number:	BUVO-D-13-00096R1
Full Title:	Explosive felsic volcanism on El Hierro (Canary Islands)
Article Type:	Research Article
Corresponding Author:	Dario Pedrazzi Institute of Earth Sciences Jaume Almera, Group of Volcanology of Barcelona (GVB-CSIC). SIMGEO (UB-CSIC) Barcelona, Barcelona SPAIN
Corresponding Author Secondary Information:	
Order of Authors:	Dario Pedrazzi Laura Becerril Carretero, Geologist, Ph.D. student Joan Martí Molist, Geologist; Researcher Stavros Meletlidis, Geologist. Ph.D. student Inés Galindo, Ph.D.
Abstract:	The Canary Islands consist of a number of complex basaltic shield edifices whose submerged portion is much more voluminous than the emerged islands. Like so many other oceanic volcanic islands, the presence of explosive felsic volcanism is not a common feature in this archipelago and has only been reported from the central islands of Gran Canaria and Tenerife, where it has been responsible for the formation of large central volcanic complexes. On the other Canary Islands, the presence of felsic rocks is mostly restricted to subvolcanic intrusions and a few lava flows, generally associated with the oldest parts of the islands. In this paper we present a detailed stratigraphic, lithological, and sedimentological study of a significant trachytic pumice deposit on the island of El Hierro, referred here as the Malpaso Member, which represents the only explosive episode of felsic composition found on the Canary Islands (apart from those on Gran Canaria and Tenerife). Four different subunits were identified on the basis of their lithological and granulometrical characteristics. The products of the eruption correspond to a single eruptive event and cover an area of about 13 km ² . This work provides a detailed stratigraphic and chronological framework for El Hierro Island and demonstrates the importance of an explosive eruption within an environment in which effusive basaltic activity predominates. Bearing in mind the style and the spatial extent of the Malpaso eruption, a future event with similar characteristics would have a serious impact on the population, infrastructures, and economy of the island of El Hierro.
Response to Reviewers:	Response to reviewers and editor comment was included in a a separate file.



MINISTERIO
DE ECONOMÍA
Y COMPETITIVIDAD



CSIC  **ICTJA**

INSTITUTO DE CIENCIAS DE LA TIERRA JAUME ALMERA (ICTJA)

Barcelona, January 31th, 2014

Dear Editor and Associate Editor of Bulletin of Volcanology,

Enclosed you will find the revised version of the on the manuscript entitled: "Felsic explosive volcanism at El Hierro (Canary Islands)" by Dario Pedrazzi, Laura Becerril, Joan Martí, Stavros Meletlidis and Inés Galindo, and we hope you will find it acceptable for publication as a Research Article in Bulletin of Volcanology.

To prepare the revision we have taken into account all the reviewers and associated editor's comments, which we have much appreciated as they have allowed us to improve the original manuscript. All the changes made on the original manuscript have been indicated with different colours depending on the referee in an annotated copy also included in this submission. The specific referees' comments and our responses to them are detailed below

Yours Sincerely,

Dario Pedrazzi



Associate Editor:

I have now received three reviews for your manuscript (see attached), of which two are favourable and make useful suggestion for improvement. The third is somewhat more critical but at the same time constructive. After reading carefully through your manuscript, I agree with the assessment and concern raised by Reviewer 3 in that the manuscript needs significant improvements and modifications in terms of presentation and organization before it can be considered and accepted for publication. This applies, in particular, to the presentation and analyses of chemical and mineralogical data, which should be presented in a more comprehensive manner and in context with the petrology/geochemistry of El Hierro in general. By the same token, the stratigraphic data (especially the graphical part) could be presented in a more logical manner (for example, present sections in logical order). Hence, based upon the reviewers' comments and my own reading, I am advising that you make moderate revisions to your paper.

The manuscript has been revised following the proposed suggestions. We include the following changes:

- a) Petrology and geochemistry analysis are not included in the revised version of the paper because are they are not relevant for the purpose of the paper and created some confusion. We only present mineralogical data in a different section, highlighting the general petrographic characteristics of the Malpaso Member, which so far represent a unique case in the geological context of El Hierro Island. The mineralogical composition is sufficient to identify the trachyphonolitic nature of the deposit-
- b) Stratigraphy section has been simplified and shortened and the stratigraphic data are now presented in a more logical manner. Figures 2 and 3 were merged and the number of general stratigraphic sections has been reduced.
- c) Sedimentological description (see: lines 200 to 254) and discussion (see: lines 363 to 409) has been improved taking into account some recent and classical sedimentological papers on PDCs. Furthermore discussion on hydrovolcanism has been enhanced (see: lines 414 to 443) to better support the hypothesis of magma/water interaction as the main fragmentation mechanism of the eruption.
- d) The volcanic hazard section has been changed and improved, suggesting how this type of eruption is of great importance in the evaluation of hazards on El Hierro Island (see: lines 508 to 537).
- e) Additional comments proposed by Reviewers 1, 2 and 3 have also been considered and the corresponding changes realized throughout the text.

Reviewer #1

This is a very well written and well illustrated manuscript. The fieldwork has been very detailed and meticulous and the laboratory work to document the textural and componentry characteristics has been very detailed. However, there was one small matter of ash particle characteristics being presented in the discussion section, without having been described in the description section, unless I missed it. This is an important part of the basis for the phreatomagmatic interpretation and needs to be described in a sub-section of the description section of the paper.



This part has been changed making a separate paragraph in the description section (see: lines 306 to 320) and data are analyzed in the discussion section (see: lines 403 to 409) as an important basis to support magma/water interaction.

The discussion section is excellent, coming to very sound conclusions based on deposit characteristics. Very importantly, the authors have argued convincingly that the apparently small volume explosive trachytic eruption could have had a major consequence in terms of a major sector collapse. This is extremely important in terms of future hazard and risk assessment.

I have suggested some minor expression corrections. I enjoyed reading this very well documented and written paper, and congratulate the authors, especially the graduate students, on an excellent piece of research.

Expressions and commentaries have been revised and corrected.

Reviewer #2

I edited the manuscript (attached) in which you can find revision notes and minor text modifications of your manuscript. Figures are of good quality. The authors need to change paleosoil by paleosol in many figures.

Text modifications as well as some changes in figures have been made accordingly.

Reviewer #3

I revised the manuscript BUVO-D-13-00096.

The manuscript describe an explosive felsic eruption of Holocene time occurred at El Hierro, Canary Islands. The eruption is an exception in common eruptive style and magma composition of El Hierro Island. The Authors studied the eruption deposits through field and laboratory data, and extracted some considerations about future volcanic hazard for the island of El Hierro. The argument is certainly of interest for the readers of BV, and the English text is, for the most part, clearly written. However, the manuscript, at present, has some major flaws that need to be addressed by Authors before consideration for publication.

I listed several major points in the following, while other minor points are in the edited pdf I attached to this report.

Main points

- Chemical data is not correctly presented. Table 1a contains only one analysis, which is a non-sense. It is unclear if it is a mean of several analyses or the Authors performed just one XRF analysis. In both cases it has not scientific significance. All the data need to be presented in the paper. Indeed, the geochemical data need also to be presented using Harker diagrams, at least for illustrating their place within the El Hierro magmatic series. The same still holds for chemical analyses of mineral phases.

see main change a) above and lines 321 to 329

Table 1a and 1b need to be presented separately.



Table 1a and 1b were removed (see: first point).

Figure 2 and 3 should be merged.

Figure 2 and 3 were merged

Chemical and mineralogical data need to be illustrated in a different section than the stratigraphic one.

Mineralogical data are now shown in a different section (see: point a).

Ages. Please, specify what kind of data you are reporting. If they are from radiocarbon dating you need to show error and calibration.

We are reporting radiometric ages. Error is shown in the text as well (e.g. line 118).

Isopach and isopleth data are not stratigraphy. You need to present them separately from stratigraphy.

You have to choose the best method to express the erupted volume.

Isopach and isopleth data are now reported in a different section (see: lines 225 to 263). The method to express the erupted volume is Kriging interpolation technic as explained in line 144.

Stratigraphy paragraph needs to be simplified and shortened. Also the stratigraphic sections shown in Figure 2 need to be reduced.

Stratigraphy section has been simplified and shortened and the stratigraphic data are now presented in a more logical manner (see: lines 174 to 186). The number of general stratigraphic sections has been reduced and is now reported in the new Figure 2 (Figure 2 and 3 were merged)

What is modal distribution?

We meant the distribution of the different size classes from a single sample. To clarify this, the section is now called “Componentry characteristics and grain size distribution” (see: lines 264 to 305).

What means fresh hydromagmatic?

This sentence was removed.

When presenting grain size histograms you have to use the same scale of x and y axes for all diagrams.

Grain size histograms (new Fig. 6) are now presented with the same scale for X and Y.

Sedimentological discussion needs substantial improvement. At present it is too vague and highly speculative. There are a huge mess of sedimentological papers on PDCs in recent and less recent literature to take as an example for improving sedimentological description and interpretation.

Sedimentological description (see: lines 200 to 254) and discussion (see: lines 363 to 409) has been improved taking into account some specific bibliography on PDCs. In the subsection “Eruption and emplacement of the Malpaso Member” (lines 331 to 443) a better interpretation is now given characterizing each unit of the Malpaso Member (lines 366 to 397) in terms of transport and emplacement mechanisms.

Avoid repeating description of different Units in the discussion section. You already did it in the stratigraphic paragraph.

These repetitions have been removed only mentioning, when necessary, some peculiar characteristics of the deposits.

The discussion on hydrovolcanism is too vague and not convincing, and it lacks in citation of more recent literature on this topic (e.g. Buttner et al., 1999; 2002). Also the use of particles <1 mm for image analyses



MINISTERIO
DE ECONOMÍA
Y COMPETITIVIDAD



INSTITUTO DE CIENCIAS DE LA TIERRA JAUME ALMERA (ICTJA)

is questionable, since it is recommended to use particles in the size range between 90 and 125 μm for performing morphoscopic analysis (Dellino and La Volpe, 1995).

Discussion on hydrovolcanism has been improved (see: [lines 414 to 443](#)) considering the more recent literature on this topic, highlighting the major role played by magma/water interaction in the dynamics of the eruption. Furthermore we considered for morphoscopic analysis particles around 125 μm (eg [line 150](#)) as shown in the new Figure 8.

At present, the volcanic hazard section is highly speculative and not conclusive.

The volcanic hazard section has been improved, suggesting how this type of eruption is of great importance in the evaluation of hazards on El Hierro Island (see: [lines 508 to 537](#)), and that both long- and short-term hazard assessment on the island should take into account possible scenarios related to the eruption of felsic magmas

1

2

3

4

Explosive felsic volcanism on El Hierro (Canary Islands)

5

6

Dario Pedrazzi¹, Laura Becerril^{1,2}, Joan Martí¹, Stavros Meletlidis³, Inés Galindo²

7

8

¹ Group of Volcanology, Institute of Earth Sciences Jaume Almera (GVB-CSIC). SIMGEO

9

(UB-CSIC) c/Lluis Sole Sabaris s/n, 08028 Barcelona, Spain.

10

² Instituto Geológico y Minero de España (IGME) c/ Alonso Alvarado, 43-2⁰A 35003-Las

11

Palmas de Gran Canaria, Spain.

12

³ Centro Geofísico de Canarias, IGN, Santa Cruz de Tenerife, Spain.

13

14

Corresponding author: dpedrazzi@ictja.csic.es

15

16

Submitted to:

17

18

Bulletin of Volcanology

19

20

21 Abstract

22 The Canary Islands consist of a number of complex basaltic shield edifices whose
23 submerged portion is much more voluminous than the emerged islands. Like so many other
24 oceanic volcanic islands, the presence of explosive felsic volcanism is not a common feature
25 in this archipelago and has only been reported from the central islands of Gran Canaria and
26 Tenerife, where it has been responsible for the formation of large central volcanic complexes.
27 On the other Canary Islands, the presence of felsic rocks is mostly restricted to subvolcanic
28 intrusions and a few lava flows, generally associated with the oldest parts of the islands. In
29 this paper we present a detailed stratigraphic, lithological, and sedimentological study of a
30 significant trachytic pumice deposit on the island of El Hierro, referred here as the Malpaso
31 Member, which represents the only explosive episode of felsic composition found on the
32 Canary Islands (apart from those on Gran Canaria and Tenerife). Four different subunits were
33 identified on the basis of their lithological and granulometrical characteristics. The products
34 of the eruption correspond to a single eruptive event and cover an area of about 13 km². This
35 work provides a detailed stratigraphic and chronological framework for El Hierro Island and
36 demonstrates the importance of an explosive eruption within an environment in which
37 effusive basaltic activity predominates. Bearing in mind the style and the spatial extent of the
38 Malpaso eruption, a future event with similar characteristics would have a serious impact on
39 the population, infrastructures, and economy of the island of El Hierro.

40 **Keywords:** El Hierro, Canary Islands, phreatomagmatism, explosive volcanism, volcanic
41 hazard

42 Introduction

43 The island of El Hierro (Canary Archipelago) is a typically complex basaltic shield
44 volcano characterised by mainly effusive volcanism that exhibits both Strombolian and

45 Hawaiian activity. Most of the rocks that form the subaerial succession on El Hierro are of
46 basic composition and include, above all, basanites, basalts, and trachybasalts (Pellicer 1975;
47 Ballcels and Gómez 1997; Carracedo et al. 2001). Although the presence of subordinate
48 trachytic compositions on El Hierro has been reported by previous studies (Pellicer 1975;
49 Pellicer 1977; Fuster et al. 1993; Ballcels and Gómez 1997; Carracedo et al. 2001), its
50 relevance in the volcanological evolution of this island has never been discussed in detail,
51 probably because these rocks are volumetrically subordinate to the island's mafic rocks.
52 Felsic rocks appear as dikes and lava flows associated with the older parts of the island, where
53 minor pumice deposits interbedded with basanitic lavas occur, above all in the upper part of
54 the stratigraphic sequence that forms the shield edifice of El Golfo. These felsic deposits have
55 been interpreted as normal products of the basaltic differentiation that occurs in this type of
56 volcanic system (Carracedo et al. 2001). Radiometric ages ranging from 8.13 ± 0.06 to
57 3.95 ± 0.07 ka have been determined for these pumice deposits (Pellicer 1977; Pérez Torrado et
58 al. 2011).

59 The submarine eruption that lasted from early October 2011 to the end of February
60 2012 about 2 km off the southern coast of El Hierro increased awareness of the possibility
61 that felsic (i.e. more explosive) eruptions could occur on an island that is mostly characterised
62 by mafic (i.e. less explosive) volcanism. Although this eruption mostly extruded basanitic
63 magmas in the form of lava flows and pyroclastic fragments (Martí et al. 2013 a, b), the first
64 observed products corresponded to lava balloons of highly vesiculated, low density aphyric
65 white core, surrounded by a thin, highly vesiculated basanitic carapace. The white component
66 was identified as being the result of the remobilization of a small volume of stagnant rhyolitic
67 melt formed as the result of the incorporation of approximately 10 % quartz-rich sediment
68 into a late differentiate magma of trachytic composition by a gas-rich basanitic melt
69 (Meletlidis et al. 2012; Sigmarsson et al. 2013).

70 The fact that felsic episodes have occurred in Holocene times is significant for hazard
71 assessment given that this island has just entered into a period of renewed activity; likewise,
72 these episodes are particularly relevant since an explosive episode could represent a major
73 threat to the island. In the recent geological record of El Hierro only one explosive felsic
74 episode of trachytic composition – which would have produced pumice-rich deposits and
75 whose characteristics are unknown – has ever been reported by previous studies (Pellicer
76 1977; Balcells and Gómez 1997; Carracedo et al. 2001; Pérez-Torrado et al. 2011).

77 In this study we describe a detailed stratigraphic, lithological, and sedimentological
78 study of these pumice deposits, which we name here as the Malpaso Member. We present the
79 field descriptions and the petrographic and granulometric data of these felsic deposits and
80 discuss their relative age, transport/depositional mechanisms, the corresponding eruption
81 dynamics, and implications for hazard assessment on the island of El Hierro.

82 Geological setting

83 Located 100 km off the east coast of Africa, the Canary Archipelago is composed of
84 seven major volcanic islands and a number of smaller islets and has a total surface area of
85 almost 500 km² (Fig. 1). The islands are Neogene in age (Schmincke 1982; Araña and Ortiz
86 1991) and their subaerial activity began around 24 Ma (Robertson and Stillman 1979; Le Bas
87 et al. 1986; Marinoni and Pasquare` 1994; Marinoni and Gudmundsson 2000). El Hierro is the
88 southwesternmost and smallest island in the archipelago, with an area of 269 km². It has an
89 estimated total edifice volume (subaerial and submarine) of 5,500 km³ and rises about 5,500
90 m from its submarine base at a depth of 4,000 m (Schmincke 1990). The highest point on the
91 island is Malpaso (1,501 m a.s.l.).

92 With its oldest subaerial deposits dated at 1.12 Ma, this island is considered to be the
93 youngest in the Canary Archipelago (Guillou et al. 1996; Fuster et al. (1993); Carracedo
94 (1996) and Carracedo et al. (1998) have cited El Hierro as a classic case of a triple-armed rift

95 system (Fig. 1) inasmuch as it is the result of three main volcanic cycles corresponding to the
96 construction and partial destruction of successive volcanic edifices (Guillou et al. 1996;
97 Balcells and Gómez 1997). The first edifice corresponds to the Tiñor volcano (1.12–0.88 Ma),
98 the second to El Golfo-Las Playas edifice (545–176 ka) and the third to the island's rift or
99 dorsal volcanism (158 ka–Present time) (Fig. 1). During the island's growth at least five
100 debris avalanches occurred (Masson 1996; Urgeles et al. 1996, 1997; Carracedo et al. 1999,
101 2001; Masson et al. 2002; Longpré et al. 2011) that notably changed its morphology. The ages
102 of these debris avalanches range from <880 ka and 545–176 ka for the first at Tiñor and Las
103 Playas I, and was followed by landslides at Las Playas II (176–145 ka) and El Julan (>158
104 ka), located at SE and at SW of the island respectively (Fig. 1). The most recent landslide
105 corresponds to El Golfo, whose age has been recently proposed more precisely as between
106 87–39 ka (Longpré et al. 2011) (Fig. 1). The latest eruption took place on the submarine south
107 rift in the sea off Las Calmas (Fig. 1) and lasted from 10 October 2011 to the end of February
108 2012 (Martí et al. 2013).

109 The geology of the island is characterised by effusive magmatic eruptions of basic
110 composition, mainly Hawaiian-Strombolian in nature, fed by subvertical dykes (Becerril et al.
111 2013), combined with a number of hydromagmatic episodes (Becerril 2009). In general the
112 island's eruptions have been monotonous in composition and mainly basanitic in nature
113 (Pellicer 1977; Carracedo et al. 2001). An example of one of the few types of felsic deposits
114 that have been described from the island are the trachytic lava flows near Las Puntas dated by
115 Guillou et al. (1996) at an age of 176 ka. Other trachytic lava flows are present in the east of
116 the island, above all close to Playa del Pozo and on the uppermost part of the cliff of Las
117 Playas (Ballcels and Gómez 1997). Pellicer (1977) remarked on the presence of trachytic
118 pyroclastic deposits around Malpaso (Fig. 1), which were dated by ¹⁴C at an age of 6.74±0.15
119 ka and attributed to an explosive eruption subsequent to the construction of the Tanganasoga

120 edifice (Fig. 1). Balcells and Gómez (1997) described these deposits as laminated “surge-
121 type” trachytic materials originating during a previous eruption of Tanganasoga. Carracedo et
122 al. (2001) interpreted these deposits as volcanic differentiates from the terminal stages of
123 activity of the volcano of El Golfo (176 ka) prior to the establishment of the Rift volcanism.
124 More recently, Pérez Torrado et al. (2011) obtained ^{14}C ages ranging from 8.13 ± 0.06 to
125 3.95 ± 0.07 ka for charcoal located in a paleosol under these deposits and suggested that their
126 emplacement was coeval to the construction of Tanganasoga inside the landslide depression
127 of El Golfo.

128 Methods

129 A preliminary study and interpretation of 1:5,000-scale orthophotos was carried out to
130 obtain a complete overview of the area, to identify possible outcrops of interest, and to
131 discriminate the different morphologies occurring in the field. In order to understand the
132 general geological framework of the area and to define the characteristics and extent of the
133 deposits, we undertook extensive field mapping at 1:5,000 scale in an area covering about 13
134 km^2 . The stratigraphic criteria used to distinguish different units included primarily
135 sedimentary structures and the apparent component content (juvenile and lithic fragments), as
136 well as characteristics such as grading, colour, and sorting. Nomenclature used in the text for
137 bed thickness, grain size, and sorting of the pyroclastic deposits follows the one proposed by
138 Sohn and Chough (1989).

139 In all, 152 stratigraphic sections were measured and used to document the geometry of
140 the deposits and their component proportions (Online Resource 1). Maximum clast sizes and
141 thickness of the units were measured to create isopleth and isopach maps; sections with
142 eroded tops were not considered for calculations. All data were managed and processed using
143 the software ARCGIS 10.0 by ESRI and Surfer 7. To obtain volumetric data from the maps
144 we used Kriging interpolation technic by Surfer 7.

145 The geographical coordinates of relevant locations, as well as the stratigraphic sections
146 and sampling points, were recorded using a portable GPS to a precision of about 3 m
147 (additional data are given in Online Resource 1). The reference zone used was the UTM
148 projection Datum: D_WGS_1984, zone 27–28N.

149 Binocular and electron microscopes were used to determine the main petrographic and
150 textural characteristics of the juvenile components. As well, pumice particles $\sim 125\mu\text{m}$
151 diameter from each unit were analysed with the scanning electron microscope (SEM,
152 QUANTA 200-FEI) at the University of Barcelona (UB) to discriminate the magmatic-
153 phreatomagmatic mechanism of the eruption. In addition petrographic analyses were carried
154 out in order to to identify the mineralogy and general composition of the studied deposits.

155 The most representative levels of each stratigraphic unit were sampled and analysed
156 (11 samples in total) for grain-size distribution and componentry. Grain-size analysis was
157 performed by dry sieving at 1Φ (ϕ) with sieves with aperture sizes ranging from 32 to $1/32$
158 mm (-5Φ to 5Φ). The weight percentages of the sieved fractions were calculated and then
159 plotted as cumulative curves to give grain-size distribution and the Inman parameters (median
160 grain size, $Md\Phi$ and sorting coefficient, $\sigma\Phi$). The proportion of juveniles from -5Φ to 0Φ was
161 defined by hand picking and from 0Φ to 5Φ using a binocular microscope and image analysis
162 techniques (e.g. ImageJ software).

163 Stratigraphy

164 The studied deposits (Malpaso Member) form a succession of pyroclastic units of
165 variable thickness ranging from 3 to 81 cm and are exposed around the area of Malpaso
166 (1,500 m a.s.l.) (Figs. 2–3), the highest point on the island of El Hierro. These deposits overlie
167 unconformably previous massive-to-stratified Strombolian scoria fall deposits and lava flows
168 originated from the uppermost part of the edifice of El Golfo (Carracedo et al. 2001). They
169 are discontinuously covered by younger lava flows and by later deposits from the volcano

170 Tanganasoga and other nearby vents, all of which are constructed inside the embayment of El
171 Golfo (Fig. 2). Well-developed paleosols have formed at the base and top of the studied
172 sequence, indicating that a significant period of time elapsed between its deposition and
173 previous and posterior eruptive events.

174 Figure 2 shows the stratigraphic correlation among 8 synthetic stratigraphic columns
175 constructed around the whole area. In the central sector of the study area, close to Malpaso
176 (Column 1 and 2; Fig. 2), the Malpaso Member lies above a paleosol developed on older
177 mafic Strombolian deposits, and consists of a lithic-rich pumice deposit directly overlain by
178 the Tanganasoga deposits (Column 8; Fig. 2). Beyond the headwall of the landslide at El
179 Golfo, on the northern flank of El Hierro, the Malpaso Member could not be identified. In the
180 eastern area (Column 3,4,5, Fig. 2) a series of Strombolian deposits – including material from
181 Montaña Cueva del Guanche, probably corresponding to the vents located inside the
182 embayment of El Golfo (e.g. Hoya del Pino and Montaña Colorada) (Fig. 2) – and a lava flow
183 originating from El Tomillar, overlie the Malpaso Member. The southern sector is mainly
184 covered by lava flows and subordinate Strombolian deposits (Column 6 and 7, Fig. 2). The
185 western side of the area shows a similar sequence with Strombolian deposits of magmatic and
186 hydromagmatic origin covering the Malpaso Member (Column 8, Fig. 2).

187 The Malpaso Member consists of different units (Fig. 3) with no field evidence of any
188 temporal hiatus. These units cover the whole of the terrain in the Malpaso area (Fig. 2) and
189 tend to thicken in depressions and valleys. Investigated in 152 outcrops (Fig. 2), these
190 deposits extend mostly in a southeastern direction, reaching a maximum distance of >2.5 km
191 from the peak of Malpaso (Fig. 2). Simplified stratigraphic sections from 11 key localities are
192 shown in Fig. 3. The area was divided into proximal (0-1 km), medial (1-2.5 km) and distal
193 zones (≥ 2.5 km) based on thickness and grain size characteristics of the deposit (Fig. 2). The
194 maximum observed thickness of the entire succession lie in the range 40–81 cm at Malpaso

195 and 3–5 cm in the most distal outcrops (≥ 2.5 km). Some apparently anomalously thick values
196 occur inside some channels and depressions. We divided the Malpaso Member into four units
197 (from base to top: N1, N2, N3, N4) in terms of their lithological and sedimentological
198 characteristics (Fig. 3 and 4) that can be recognised throughout almost all of the area covered
199 by these deposits.

200 Unit N1

201 This unit is up to 21-cm thick (Figs. 3 and 4) and is composed mainly of well-sorted,
202 clast-supported, pumice thin lapilli beds alternating with matrix-supported, poorly stratified
203 thin beds of fine lapilli/ash with well-defined boundaries (Fig. 4). The pumice is light grey in
204 colour and has small vesicles (millimetric to submillimetric in size) and lithic clasts consisting
205 mainly of lava fragments. The base of Unit N1 is erosive as observed by the interaction with
206 the underlying topography (Fig. 4a,b). Unit N1 rests directly on a paleosol that, according to
207 radiocarbon ages given by Pellicer (1977) and Pérez Torrado et al. (2011), was dated as
208 6.74 ± 0.15 ka BC or 8.1 ± 0.06 ka BP, respectively. To the north, south, and east N1 thins out
209 rapidly to just a few centimetres.

210 Two subunits are distinguishable: N1a and N1b (Fig. 3). N1a at Malpaso reaches a
211 maximum thickness of 8–10 cm and has alternated centimetric clasts supported pumice lapilli
212 (< 1 cm) very thin beds and ash-rich 1–2-cm beds. Lava lithic fragments reach up to 2 cm in
213 size. N1b is similar but shows a remarkable increase in the size of pumices, which reach up to
214 10 cm in diameter. N1 is similar in the proximal zone (0-1 km) than in the medial zone (1-2.5
215 km) (Figs. 2, 3 and 4b) and the distinction between the two subunits is unclear; at greater
216 distances (≥ 2.5 km; Fig. 2) the subunits are thinner and finer-grained making almost
217 impossible to separate them (Fig. 4c).

218 Unit N2

219 This unit has a maximum thickness of about 20 cm (Fig. 3). It consists of poorly
220 stratified, dark-brown, matrix-supported thin ash beds with some interbedded very thin beds
221 that are up to 5-mm thick of lapilli-rich poorly vesiculated pumices (Fig. 4a), which contain
222 lava lithic clasts of the same size. At proximal exposures (0-1 km; Fig. 3) it is possible to
223 differentiate four sub-levels (N2a, N2b, N2c, and N2d). N2a is made up of 1–2-mm thick ash-
224 rich laminae that progressively increase in grain size and merge into the up-to-5-mm thick
225 lapilli-rich beds that form N2b. The same pattern is repeated for sub-levels N2c and N2d.
226 Lithic fragments reach a maximum size of 5 mm in the lapilli-rich layers. At more distal
227 exposures (Figs. 2 and 4b), it becomes harder to distinguish the different sub-levels, which
228 progressively fade away (Fig. 4c) until they disappear completely.

229 Unit N3

230 Within the area around Malpaso (Fig. 2), Unit N3 shows an apparent massive aspect
231 but it is predominantly composed of stratified thin ash beds with a maximum total thickness
232 of 25 cm (Figs. 3 and 4). Minor fine-grained lapilli beds up to 5-cm thick are interbedded with
233 individual very thin ash beds in its lower part. Loose lava lithic clasts are also recognisable.
234 N3 is lighter in colour than N2 and there is a clear contrast at the contact zone (Fig. 4a). Four
235 sub-levels, N3a, N3b, N3c, and N3d, are identifiable in the proximal outcrops (0-1 km; Fig. 2)
236 although in the outermost distal zone (≥ 2.5 km; Fig. 2) the various sub-levels disappear and
237 become a single fine-grained very thin (2–3 cm) massive bed (Fig. 4c). N3a consists of lithic-
238 poor finely stratified ash-rich beds with subordinate cross-bedded undulate millimetric very
239 thin lapilli-rich beds with loose millimetric lava lithic clasts; N3b is more massive, lithic-poor,
240 homogeneous, and ash-rich, although with a few coarse-grained interbedded horizons; N3c
241 and N3d follow the same pattern with a general decrease in grain size from lapilli to ash-rich
242 beds. In intermediate zones (1-2.5 km; Fig. 2) N3 is perfectly visible with the same

243 characteristics (Fig. 4b) as in the proximal outcrops although tends to be massive (Fig. 4c)
244 with poor evidence of cross-bedded structures in the most distal outcrops (≥ 2.5 km.; Fig. 2).

245 Unit N4

246 This unit is up to 20-cm thick (Fig. 3) in the proximal outcrops (0-1 km; Fig. 2) and is
247 composed of ash and lithic-rich lapilli thin beds. Abundant lithic clasts from older lava flows,
248 millimetric to centimetric in size, are found throughout the entire unit and give it a
249 characteristic gray-black colour (Fig. 4a). Some loose, white-coloured beds (like unit N3 in
250 appearance) are also present. N4 is either normally or reversely graded with coarse- and fine-
251 grained stratifications. At intermediate distances (1-2.5 km; Fig. 2) N4 is still perfectly
252 recognisable because it has the same characteristics as in the proximal outcrops (Fig. 4b);
253 nevertheless, in most distal exposures (≥ 2.5 km; Fig. 3) it is 1–2-cm thick before it becomes a
254 massive layer (Fig. 4c).

255 Isopach and Isopleth maps

256 Isopach and isopleth maps of the Malpaso Member (Fig. 5) were obtained from the
257 field data. The isopach map was computed using 134 sections that illustrate that the thickness
258 of the deposit changes sharply over short distances. This map enabled us to calculate the area
259 of the deposit at 13 km^2 with a volume of about $1.81 \cdot 10^6 \text{ m}^3$ using kriging with Surfer 7. The
260 isopleth map was based on 30 measurements of the five largest pumice clasts in level N1 in
261 the study area. The largest pumice clast, 10 cm in diameter, was found in the Malpaso area.
262 The pumice diameter represented on the isopleth map ranges from <1 cm to the maximum
263 diameter measured.

264 Componentry characteristics and grain size distribution

265 The vertical variations in grain size distribution and componentry of individual beds
266 are described in Figure 6 and Figure 7. They show median grain size ($Md\Phi$) and sorting ($\sigma\Phi$)

267 parameters, as well as a comparison between F1 (wt% <1 mm diameter) and F2 (wt% <1/16
268 mm diameter). Juvenile pumice fragments, free crystals, and accidental lithic fragments
269 (mostly derived from older lava flows) can be distinguished in each class size. Modal
270 components are unevenly distributed among the various grain-size fractions and the different
271 subunits. Although all the samples belonging to N1 have the same component distribution
272 with crystals and lithic fragments increasing in percentage in the $1\Phi - 5\Phi$ size range, the
273 pumice component typically has a wider range of sizes (Fig. 6). The total amount of juvenile
274 fragments (pumices and free crystals) ranges from 60% (N1BF) to a maximum of 75%
275 (N1BG). N2 samples are not significantly different and the percentage of juvenile fragments
276 is around 70%. As in the N1 subunits, this same trend is noticeable in N2 and crystals and
277 lithic fragments increase in proportion in the greatest Φ size range. Compared to the previous
278 units, Unit N3 is significantly different. Sample N3A taken from the lowest part of the unit
279 exhibits the same trend as in previous units, with a c. 65% content of juvenile fragments.
280 However, this content increases in the upper part of the unit as the obvious change in colour
281 from dark-gray to light-gray occurs; on the other hand, samples N3C and N3D have juvenile
282 fragment content of around 90% and of free crystals of about 25%. The contact with the
283 following unit (N4) is marked by a clear change in colour from light grey to dark brown. This
284 variation in color may be due to an increase in lithic clasts with total values of 55–60% with a
285 constant percentage throughout almost all of the range in grain sizes.

286 In terms of grain size distribution, the two subunits (N1A and N1B) that conform the
287 basal unit (N1) of the Malpaso Member are characterised by an alternation of ash and lapilli
288 layers and a general increase in grain size in the lapilli layers towards the upper part of the
289 unit (Fig. 6). Both subunits are characterised by well-sorted unimodal (N1AG and N1BG) and
290 poorly sorted polymodal (N1AF and N1BF) samples with $\sigma\Phi$ values ranging from 1.68 to
291 2.55 (Fig. 7a). N1AG and N1BG are characterised respectively by 3% and 2% of fine ash

292 (<63 μm). N1AF and N1BF show an increase in the amount of fine ash with 16% and 11% in
293 weight, respectively (Fig. 7b). Two representative samples (N2 and N2G) from Unit N2 with
294 similar characteristics as those from Unit N1 layers were analysed: N2 is a polymodal poorly
295 sorted fine-ash-poor sample ($\sigma\Phi=2.39$), with 28% by weight of fine ash, whereas N2G is well
296 sorted, unimodal with $\sigma\Phi=1.61$ and 4.6% of fine ash. The N3 subunit is the most
297 distinguishable unit in the field due to its peculiar white/grey colour. Three representative
298 samples were considered for grain size analysis: N3A from the first subunit and N3C and
299 N3D from the second (Fig. 7). N3A and N3C are well-sorted, lapilli-ash samples with $\sigma\Phi$
300 values in the range 1.46–1.63 (Fig. 7a). N3D is a well-sorted sample mainly made up of ash
301 with $\sigma\Phi$ values reaching 1.63 (Fig. 7a). N3D is richer in fine ash (41%) than subunit N3A
302 (28%) and N3C (14%) (Fig. 7b). Unit N4 is mainly made up of ash, although some lapilli-rich
303 horizons can also be found toward its upper part. As observed in Figure 7a,b, N4F is a
304 polymodal, poorly sorted ($\sigma\Phi= 2.06$) ash-rich layer with 25% by weight of fine ash, while
305 N4G is a unimodal, well-sorted ($\sigma\Phi= 1.59$) lapilli-rich layer with 6.5% of fine ash.

306 Morphology of the juvenile material

307 The morphology of juvenile clasts $\sim 125 \mu\text{m}$ in diameter was examined with the
308 electron microscope (SEM) in order to discriminate between purely magmatic and
309 phreatomagmatic fragmentation processes during the Malpaso Member formation.

310 Texturally, individual particles in levels N2–N4 are subangular with spherical forms
311 tending to have blocky and stepped morphologies with poor or no vesicularity (Figs. 8). Fine
312 particles ($<32 \mu\text{m}$) commonly adhere to larger surface fragments as dust (Fig. 8c). Another
313 characteristic feature of these particles is the presence of quenching cracks (Fig. 8e).

314 Knowledge of certain morphological and textural features of the particles can help to
315 resolve whether the eruption mechanisms were purely magmatic or hydromagmatic due to
316 magma-water interaction. In particular, blocky shapes, low vesicularities and glass shards,

317 although not unique to, are characteristic of eruptions in which water intervenes (Wohletz
318 1983; Heiken and Wohletz 1985). Another common feature of hydrovolcanic eruptions is the
319 presence of micron-sized dust particles adhering to the fragment surfaces and aggregate
320 multicomponent particles (Wohletz 1983; Heiken and Wohletz 1985).

321 Mineralogy

322 Juvenile components have identical mineralogy that suggests a trachiphonolitic
323 composition throughout the whole Malpaso Member but there are variations in texture
324 between units. Pumice fragments are porphyritic, with 25–30% of phenocrysts in volume that
325 are surrounded by a glassy groundmass with a variable amount of vesicles of different sizes
326 (6–<0.05 mm) and forms (elongated and spherical). The mineral assemblage consists of
327 euhedral-to-subhedral plagioclase, amphiboles and, to a lesser extent, clinopyroxene (Fig. 9).
328 The same phases were also found in the groundmass, along with oxides and glass. The
329 maximum size of the phenocrysts is 2.5 mm (plagioclase) and 2 mm (amphiboles).

330 Discussion

331 *Eruption and emplacement of the Malpaso Member*

332 The Malpaso Member covers an area of approximately 13 km² (Fig. 2), almost 5% of
333 the total area of El Hierro Island. Calculations of the volume of the exposed deposit is about
334 1.81·10⁶ m³. However, its original extent and volume was significantly larger since most of
335 the original deposits have been removed by subsequent erosion, in particular during the
336 landslide at El Golfo. The stratigraphic relationships and distribution of the Malpaso Member
337 demonstrate that it was emplaced before this landslide occurred (87-39 Ka; Longpré et al.
338 2011) as it is clearly barren by this sector collapse. Consequently, the mapped distribution of
339 the Member does not represent its original extent. Despite these practical limitations,

340 variations in distribution and thickness can still be observed suggesting an emplacement
341 direction spreading radially from the vent.

342 The stratigraphic, lithological, and sedimentological characteristics of the Malpaso
343 Member suggest that it corresponds to the products of a single eruptive event with several
344 pulses of PDCs (Pyroclastic Density Currents) generation.

345 The presence of subrounded/rounded pumice clasts, as well as lateral variations in
346 thickness and sedimentary features such as undulate deposits, tendency to fill channels of the
347 pre-eruptive surface on outcrop scale, and the poor sorting and polymodality of grain size
348 curves, might be indicative of a lateral flow component of transport. The very low aspect ratio
349 and regular thickness decaying with distance are consistent with an origin from a dilute,
350 turbulent pyroclastic density current. Furthermore, thinning and fining of the deposits from
351 proximal to distal locations indicate a base surge in which concentration decreased down-
352 current (Sohn and Chough 1989; Dellino et al. 2004a,b).

353 Grain-size data [median diameter ($Md\Phi$) and sorting ($\sigma\Phi$); Fig. 7a and the F1 vs. F2
354 diagram of Walker (1983) (Fig. 7b) support the idea that the Malpaso Member was formed by
355 PDCs currents although some grain size histograms seem describing fallout deposits (N1AG,
356 N1BG, N2G, N4G; Fig. 7a). These samples refer to the thin coarse-grained layers observed
357 throughout the sequence but field evidence such as rounding of pumice, and lateral changes of
358 texture and thickness on local scale, allow the distinction from fall deposits. Furthermore, a
359 granulometrical shift toward finer values from an increasing distance from the vent is
360 observed for the same deposit, in accordance with the sequential fragmentation/transportation
361 model of grain-size distribution of Wohletz et al. (1989). This is due to a selective
362 transportation mechanism related to turbulent suspensions.

363 The four recognized units (N1, N2, N3, N4) marked different phases of the eruption
364 and can be interpreted in terms of changing of eruptive dynamics and of the transport and
365 depositional systems.

366 Unit N1 is characterized by an alternation of centimetre beds of well sorted fines-poor
367 pumice lapilli and poorly sorted ash layers. This unit is characterised by a visible difference in
368 grain size and sorting between the lapilli and ash-rich layers (Fig. 3 and 4) and could be
369 interpreted as the result of either an unsteady pyroclastic surge or multiple, closely spaced
370 events (Dellino et al. 2004a). These types of deposits resemble the type 1a deposit described
371 in Palladino and Simei (2002). Deposition from dilute, turbulent suspensions commonly
372 produces normally graded beds or ungraded beds for high depositional rates. Prolonged,
373 unsteady currents may also produce multiple graded deposits by progressive aggradation
374 (Branney and Kokelaar 1992). These deposits, thus, might be the result of sedimentation from
375 a turbulent and low concentrated unsteady current with direct suspension sedimentation. As
376 proposed by Fisher (1966), deposition occurs progressively during the passage of the current.

377 Unit N2 shows similar characteristics respect to N1, but it is made of matrix-supported
378 thin ash beds with interbedded very thin beds of fine pumice lapilli. Lapilli-poor layers with
379 thin internal laminations could be indicative of a relatively slow deposition rate resulting in
380 grain segregation, whereas lapilli-rich layers with crude associated stratification might be the
381 result of rapid deposition from suspension with little traction (Arnott and Hand 1989).

382 Unit N3 looks massive but it is characterized by stratified thin ash beds and minor
383 fine-grained lapilli beds. This unit can be interpreted as pyroclastic surge deposits based on
384 plane parallel and low-angle cross laminations. The lower part of Unit N3 is characterized by
385 minor fine-grained lapilli interbedded with individual very thin ash beds, which might reflect
386 the presence of a turbulent and unsteady current with deposition, under a tractive regime
387 passing to a slower sedimentation rate as reflected by the presence of the finer-grained beds.

388 Some ash layers have variations in lateral thickness, as well as in cross-bedding and
389 undulating structures. The existence of these structures may be the result of variations in the
390 flow regime (Valentine and Fisher 2000) and in particle concentration (Sohn and Chough
391 1989; Sohn 1996).

392 Unit N4 is composed of ash and lithic-rich lapilli thin beds where each alternation
393 between coarse and fine-grained layers could be interpreted as deposits emplaced from a
394 single surge (see Sohn and Chough 1989; Dellino et al. 2004). These alternating fine and
395 coarse grained beds might be the result of deposition under a tractive regime. As proposed by
396 Valentine (1987) a turbulent pyroclastic current tends to develop stratification by particle
397 sizes and densities to form a more concentrated dispersion towards the base.

398 Pyroclastic density currents (PDCs) might be associated with either magmatic or
399 phreatomagmatic fragmentation (e.g. Cas and Wright 1987; Carey 1991; Branney and
400 Kokelaar 2002). The lithological and stratigraphic variations shown by the Malpaso Member
401 units imply that the eruption responsible for the emplacement of these deposits was
402 continuous but had several pulses.

403 Based on field evidences (thinly laminated, fine- and coarse-grained beds) (Fig. 4),
404 grain size and componentry of deposits (fine-grained, negatively skewed grain size
405 distribution, high lithic content; see Self and Sparks 1978; Barberi et al. 1989) (Fig. 6) and
406 textural features of the juvenile fragments (shape of the fragments; presence of quenching
407 cracks and fine adhering dust on particle surfaces; see Heiken and Wohletz 1985; Buttner et
408 al. 1999; Buttner et al. 2002) (Fig. 8), it is possible to assume that magma/water interaction
409 played a major role in the dynamics of the eruption.

410 The absence, in general, of any fall deposits at the base of each unit, rules out the
411 possibility of a column collapse and supports the idea that most of the studied deposits were

412 formed directly from base surges radially expanding from the vent during vulcanian-type
413 explosions with no rise of any sustained convective column.

414 The N1 (Figs. 3 and 4) with a total amount of lithic clasts (35–40%) (Fig. 6) –
415 consisting of lava fragments – suggests that significant erosion of the conduit might have
416 occurred during the first phase of the eruption. Within the N2 unit (Figs. 3 and 4) layers are
417 more massive and fine-grained, reflecting a better efficiency in the magma-water interaction
418 with an increase in the energy of the explosions (e.g. Wohletz 1986). Magma/water
419 interaction is supported by the occurrence of accidental lithics (30%) (Fig. 6) and textural
420 surfaces of juvenile fragments (Fig. 8). The transition from N2 to N3 seems gradual, although
421 the evident change to a lighter grey colour in N3 (Fig. 4) reveals a rapid decrease in lithics of
422 around 10% (Fig. 6). The lithological features of the deposits in N3 (extremely fine grained
423 tephra) suggest efficient fragmentation of the magma although the presence of only a few
424 accidental lithics hint at the secondary role played by magma/water interaction during this
425 phase of the eruption. Furthermore, the absence of fall deposit at the base of N3 beds rules out
426 the possibility of a gravitational collapse from a sustained column. This type of deposits might
427 be associated with sharp increases in magma discharge and/or changes in upper conduit-crater
428 geometries as observed in the case of Mt. Pinatubo (Hoblitt et al. 1996), Greenish eruption of
429 Somma-Vesuvius (Cioni et al. 2003a), Montserrat (Formenti et al. 2003), or Pollena (Sulpizio
430 et al. 2005).

431 Hydromagmatic activity characterised the final phase of the eruption. A clearly
432 defined limit marks the change from N3 to N4 and a rapid change in the overall aspect of the
433 deposit (Fig. 4). The lithology (lava lithics up to 55–60%) (Fig. 6), bedding characteristics
434 (ash layers, generally with lapilli-rich horizons toward the upper part of the unit) (Fig. 4) and
435 textural characteristics (Fig. 8) of N4 reflecting the great efficiency of the magma-water
436 interaction (e.g. Wohletz 1986).

437 As proposed by Sulpizio et al. (2005), the presence of lithic-enriched layers might not
438 be indicative of magma/water interaction, but it might reflect the clearing of the conduit and
439 restoration of the pristine magma discharge conditions. In such cases, density of the erupting
440 mixture increases due to incorporation of large amounts of cold and heavy lithics. However,
441 we can exclude this possibility because the lithic-enriched layers are associated with textural,
442 stratigraphic and grain-size features suggesting that magma/water interaction exerted the main
443 control on magma fragmentation during the eruption.

444 *Age of the Malpaso Member and of the landslide at El Golfo*

445 The authors who have mentioned the presence of the trachytic pumice deposit on El
446 Hierro have offered contrasting explanations for its origin, significance, and age. Pellicer
447 (1977) attributed this deposit to an explosive eruption subsequent to the Tanganasoga eruption
448 (dated at 6.74 ± 0.15 ka), whilst Balcells and Gómez (1997) described this deposit as a
449 laminated “surge-type” deposit originating during an eruption that predates Tanganasoga.
450 Carracedo et al. (2001) assumed that this deposit represents later evolutionary stages of the El
451 Golfo volcano construction, thereby interpreting it as a pre-El Golfo sector collapse dated
452 around 176 ka. Finally, Pérez Torrado et al. (2011) dated a paleosol at the base of the pumice
453 deposit at 8.13 ± 0.06 ka attributing the overlying deposit to Tanganasoga.

454 Given the new stratigraphy described in this paper, the dates hitherto ascribed to this
455 deposit and their interpretations do not match the stratigraphic position of the Malpaso
456 Member. Bearing in mind that Tanganasoga and other vents (e.g Hoya del Pino, Montaña
457 Colorada) postdate the landslide of El Golfo, and that their deposits cover the pumice
458 products, no stratigraphic evidence exists to support the idea that the Malpaso Member was
459 associated with Tanganasoga or to any subsequent eruption. Therefore, stratigraphically
460 speaking, the Malpaso Member must belong to the final episodes in the construction of the
461 composite El Golfo volcano, as has been suggested by Carracedo et al. (2001). However,

462 between the deposition of the Malpaso Member and the deposits on Tanganasoga there is no
463 paleosol that could indicate any significant time lapse between the two events. This implies
464 that the eruption of the Malpaso Member, the landslide of El Golfo and the eruption (and
465 construction) of Tanganasoga occurred sequentially in a relatively short period of time.
466 Furthermore, it is also possible that the eruption of the Malpaso Member was the impulse
467 behind the landslide of El Golfo. The construction of Tanganasoga could correspond to a
468 volumetrically significant post-collapse eruptive episode that was triggered by the
469 decompression of the deep magmatic system caused by the massive removal of part of El
470 Golfo. This matches well with the model proposed by Manconi et al. (2009) and similar
471 successions of events that have occurred after the formation of volcanic landslides on other
472 oceanic volcanic islands (Lipman et al. 1990; Presley et al. 1997; Hildenbrand et al. 2004).

473 These stratigraphic constraints also generate an inconsistency with published data
474 regarding the date of the landslide at El Golfo. Using radio-isotopic dating this event has been
475 established as occurring between 134 ± 4 and 21 ± 3 ka (Guillou et al. 1996; Széreméta et al.
476 1999; Carracedo et al. 1999, 2001); on the other hand, marine geological studies, primarily
477 concerned with the age of turbidite deposits associated with the massive landslide avalanche,
478 give a younger age of 17–13 ka (Masson 1996; Urgelés et al. 1997; Masson et al. 2002). A
479 more recent study using new radio-isotopic data from pre- and post-landslide materials from
480 El Golfo valley dates the event at between 87 ± 8 and 39 ± 13 ka (Longpré et al. 2011).
481 However, if the emplacement of the Malpaso Member took place between 8.13 ± 0.06 and
482 3.95 ± 0.07 ka– as suggested by Pérez-Torrado et al. (2011) – and given that it clearly predates
483 the formation of the landslide on El Golfo (as demonstrated in this study), the age of this
484 destructive event must be at least the same as that of the Malpaso Member or younger. Thus,
485 either the age attributed to the landslide by the above-quoted authors is mistaken or the age of
486 the Malpaso Member (Pérez Torrado et al. 2011) is wrong. We only found charcoal samples

487 in the paleosol near Malpaso (same location of previous ^{14}C dates) and found no evidence of
488 any charcoal in the paleosol in distal parts of the deposits. This finding, coupled with the facts
489 that in proximal and intermediate areas the Malpaso member is overlain by several pyroclastic
490 deposits of local eruptions, and that these deposits are separated by well-developed paleosols
491 (e.g. Column 2 and Column 3; Figs. 2 and Fig. 10), suggesting that between these eruptions
492 occur long periods of repose that once thought between the emplacement of the Malpaso
493 Member and the present day. In addition, morphological characteristics of the paleosol, where
494 the charcoal dated by Pérez Torrado et al. (2011) was found, indicate that it is an Andosol
495 (Padrón 1993). The formation of this type of soils requires between several tens of thousands
496 to hundreds of thousands of years (~ 150 ka) in areas as Hawaii (Torn et al. 1997). If we
497 assume that El Hierro has similar climatic characteristics as Hawaii (mild temperatures,
498 although lower rainfall rates) we can think that the paleosol formation required more than few
499 thousand years. This leads us to conclude that the ages obtained by Pérez-Torrado et al.
500 (2001) are too young and that the charcoal they used may correspond to charcoal from
501 younger plant roots growing on Malpaso or to younger deposits.

502 The distribution of the pumice deposits (in particular the isopach map), variations in
503 lateral grain-size, and the isopleth map (Fig. 5a, b) suggest that the position now occupied by
504 Tangansoga is the most suitable location for the vent of the Malpaso Member. This would be
505 consistent with the distribution of all the products from El Golfo in the area and with the
506 location of Tangansoga itself, and would provide a site for the main vent of El Golfo and its
507 eruptive activity in the area.

508 *Volcanic Hazard Implications*

509 The style and magnitude of this type of eruption is clearly of great importance in
510 assessing the potential volcanic hazard on El Hierro. The presence of similar compositions in
511 the erupted products during the recent 2011–2012 eruption raises the question as to whether

512 this felsic magma represents an assimilated product from a previous eruption or whether it
513 represents a juvenile component (i.e. differentiated product) from the last eruption. Needless
514 to say, the most important question to answer is whether or not El Hierro's magmas have the
515 potential to generate a large volume of eruptable felsic magma. The sequence of unrest
516 episodes following this very recent eruption, characterized by heightened seismicity mostly
517 located at a depth of about 20–25 km and significant surface deformation that has already
518 accumulated more than 25 cm of total vertical uplift (www.ign.es), suggests that fresh magma
519 has continued to accumulate below the surface of the island.

520 These petrological issues are beyond the scope of this paper but nevertheless still
521 should be investigated in detail. From the results obtained we can see that an eruption of
522 similar characteristics to that of the Malpaso Member does not require a large amount of
523 eruptable magma and that its associated hazards are much greater than those related to the
524 mafic volcanism that has characterised most of the recent eruptions on El Hierro. The results
525 of our study show that the pumice deposits reached a radial distance of at least 3 km from the
526 hypothetical vent site (Fig. 3) and it seems likely that the pyroclastic density currents that
527 produced these deposits could have travelled much further. The degree of hazard depends on
528 the location of the vent and the topography of the surrounding area, as well as the initial
529 energy in the flow. Our data suggest that the vent area of the Malpaso Member eruption was
530 located in a similar position to that currently occupied by Tanganasoga, probably due to the
531 position of the main feeding system from the previous El Golfo volcano. However, the
532 characteristics of the 2011–2012 eruption and of the preceding episode of unrest (Martí et al.
533 2013) suggest that the position of future vents (i.e. current volcanic susceptibility; see Becerril
534 et al. 2013) is not controlled by the same stress configuration as during the construction of El
535 Golfo and Tanganasoga. This introduces additional uncertainty into the evaluation of hazards

536 on El Hierro and thus is an indication that both long- and short-term hazard assessment on the
537 island should take into account possible scenarios related to the eruption of felsic magmas.

538 Conclusion

539 In this study we conducted a detailed stratigraphic, lithological, and sedimentological
540 study of a trachytic pumice deposit, named here as the Malpaso Member. This deposit
541 originated from a base-surge-type explosive eruption with a subsequent radial emplacement of
542 dilute PDC currents from the vent that would have been located in a similar position to the
543 volcano of Tanganasoga. The low vesicularity of juvenile fragments and the morphological
544 characteristics of the fine particles, as well as the high proportion of lithic fragments and the
545 ash-rich nature of the deposit, suggest that magma/water interaction controlled the dynamics
546 of the eruption.

547 In the light of the new stratigraphy described in this paper and previously available
548 data, we thus conclude that the Malpaso Member was not associated with the eruption of
549 Tanganasoga or any subsequent eruption and instead corresponds to the final episodes in the
550 construction of the composite volcano of El Golfo.

551 The presence of similar compositions in the erupted products of the recent 2011–2012
552 eruption indicate that the magmas from El Hierro could have the potential for producing a
553 large volume of eruptable felsic magma, a finding that obliges both long- and short-term
554 hazard assessment to take into account possible scenarios that include the eruption on El
555 Hierro of felsic magmas.

556 Acknowledgments

557 This research was partially funded by the MINECO grant CGL2011-16144-E and the
558 European Commission (FT7 Theme: ENV.2011.1.3.3-1; Grant 282759: "VUELCO"). The
559 authors are grateful to the Cabildo of El Hierro for permission to undertake this research and,

560 above all, to the Consejo Insular de Aguas de El Hierro for its support and to Orlando
561 Hernandez, Xavier Bolós, Daniele Giordano, Jose Morales de Francisco, and Llorenç
562 Planagumà for their assistance in the field as well as Olaya García for some contributions to
563 the paper. We are also grateful to the Associated Editor Thorvaldur Thordarson, to the
564 reviewer Roberto Sulpizio and the two anonymous reviewers for their constructive reviews of
565 this manuscript. The English text was corrected by Michael Lockwood.

566 References

- 567 Araña V, Ortiz R (1991) The Canary Islands: Tectonics, Magmatism and Geodynamic
568 Framework. In: Kampunzu AB, Lubala RT (eds) Magmatism in Extensional Structural
569 Settings. Springer Berlin Heidelberg, pp 209-249
- 570 Arnott RWC, Hand BM (1989) Bedforms, primary structures and grain fabric in the presence
571 of suspended sediment rain. *Journal of Sedimentary Petrology* 59:1062-1069
- 572 Balcells R, Gomez JA (1997a) Memorias y mapas geológicos del Plan MAGNA a escala
573 1:25.000 de las Hojas correspondientes a la isla de El Hierro. Hoja de Frontera, Instituto
574 Geológico y Minero de España, Spain
- 575 Balcells R, Gomez JA (1997b) Memorias y mapas geológicos del Plan MAGNA a escala
576 1:25.000 de las Hojas correspondientes a la isla de El Hierro. Hoja de Sabinosa, Instituto
577 Geológico y Minero de España, Spain
- 578 Barberi F, Cioni R, Rosi M, Santacroce R, Sbrana A, Vecci R (1989) Magmatic and
579 phreatomagmatic phases in explosive eruptions of Vesuvius as deduced by grain-size and
580 component analysis of the pyroclastic deposits. *Journal of Volcanology and Geothermal
581 Research* 38(3–4):287-307

582 Becerril L (2009) Approach to volcanic hazard and its effects in coastal areas of the Canary
583 Islands. Master's thesis, Universidad de Las Palmas de Gran Canaria, Spain

584 Becerril L, Cappello A, Galindo I, Neri M, Del Negro C (2013) Spatial probability
585 distribution of future volcanic eruptions at El Hierro Island (Canary Islands, Spain). *Journal of*
586 *Volcanology and Geothermal Research* 257(0):21-30

587 Branney M, Kokelaar P (1992) A reappraisal of ignimbrite emplacement: progressive
588 aggradation and changes from particulate to non-particulate flow during emplacement of
589 high-grade ignimbrite. *Bulletin of Volcanology* 54(6):504-520

590 Branney MJ, Kokelaar P (2002) Pyroclastic density currents and the sedimentation of
591 ignimbrites. *Geological Society of London Memoirs*, p 150

592 Büttner R, Dellino P, La Volpe L, Lorenz V, Zimanowski B (2002) Thermohydraulic
593 explosions in phreatomagmatic eruptions as evidenced by the comparison between pyroclasts
594 and products from Molten Fuel Coolant Interaction experiments. *Journal of Geophysical*
595 *Research: Solid Earth* 107(B11):2277

596 Büttner R, Dellino P, Zimanowski B (1999) Identifying modes of magma/water interaction
597 from the surface features of ash particles. *Nature* 401:688-690

598 Carey SN (1991) Transport and deposition of tephra by pyroclastic flows and surges. In:
599 Fisher RV, Smith GA (eds) *Sedimentation in volcanic setting*. Society of Economic
600 Paleontologists and Mineralogists, Special publications, pp 39-57

601 Carracedo JC (1996) Morphological and structural evolution of the western Canary Islands:
602 hotspot-induced three-armed rifts or regional tectonic trends? *Journal of Volcanology and*
603 *Geothermal Research* 72(1-2):151-162

604 Carracedo JC, Day S, Guillou H, Rodríguez Badiola E, Canas JA, Pérez Torrado FJ (1998)
605 Hotspot volcanism close to a passive continental margin: the Canary Islands. Geological
606 Magazine 135(05):591-604

607 Carracedo JC, Day SJ, Guillou H, Pérez Torrado FJ (1999) Giant Quaternary landslides in the
608 evolution of La Palma and El Hierro, Canary Islands. Journal of Volcanology and Geothermal
609 Research 94(1-4):169-190

610 Carracedo JC, Rodríguez Badiola E, Guillou H, de La Nuez HJ, Pérez Torrado FJ (2001)
611 Geology and volcanology of the western Canaries: La Palma and El Hierro. Estudios
612 Geológicos 57:171-295

613 Cas RAF, Wright JV (1987) Volcanic successions, modern and ancient. A geological
614 approach to processes products and successions. 528 pp

615 Cioni R, Sulpizio R, Garruccio N (2003a) Variability of the eruption dynamics during a
616 Subplinian event: the Greenish Pumice eruption of Somma-Vesuvius (Italy). Journal of
617 Volcanology and Geothermal Research 124(1-2):89-114

618 Dellino P, Isaia R, La Volpe L, Orsi G (2004a) Interaction between particles transported by
619 fallout and surge in the deposits of the Agnano-Monte Spina eruption (Campi Flegrei,
620 Southern Italy). Journal of Volcanology and Geothermal Research 133(1-4):193-210

621 Dellino P, Isaia R, Veneruso M (2004b) Turbulent boundary layer shear flows as an
622 approximation of base surges at Campi Flegrei (Southern Italy). Journal of Volcanology and
623 Geothermal Research 133(1-4):211-228

624 Fisher RV (1966) Mechanism of deposition from pyroclastic flows. American Journal of
625 Science 264(5):350-363

626 Formenti Y, Druitt TH, Kelfoun K (2003) Characterisation of the 1997 Vulcanian explosions
627 of Soufrière Hills Volcano, Montserrat, by video analysis. *Bulletin of Volcanology* 65(8):587-
628 605

629 Fuster JM (1993) Geochronología de la Isla de El Hierro (Islas Canarias). *Bol. R. Soc. Esp.*
630 *Hist. Nat (Sec. Geol)* 88((1-4)):85-97

631 Guillou H, Carracedo JC, Torrado FP, Badiola ER (1996) K-Ar ages and magnetic
632 stratigraphy of a hotspot-induced, fast grown oceanic island: El Hierro, Canary Islands.
633 *Journal of Volcanology and Geothermal Research* 73(1–2):141-155

634 Heiken G, Wohletz K (1985) *Volcanic ash*. University of California Press, Berkeley. 246 pp

635 Hildenbrand A, Gillot P-Y, Le Roy I (2004) Volcano-tectonic and geochemical evolution of
636 an oceanic intra-plate volcano: Tahiti-Nui (French Polynesia). *Earth and Planetary Science*
637 *Letters* 217(3–4):349-365

638 Hoblitt R, Wolfe E, Scott W, Couchman M, Pallister J, Javier D (1996) The preclimatic
639 eruptions of Mount Pinatubo, June 1991. In: Newhall CG, Punongbayan RS (eds) *Fire and*
640 *mud: eruptions and lahars of mount Pinatubo, Philippines*. Philippines Institute of
641 *Volcanology and Seismology, Quezon 766 City and University of Washington Press, Seattle*
642 *and London:pp 457–511*

643 Le Bas MJ, Rex DC, Stillman CJ (1986) The early magmatic chronology of Fuerteventura,
644 Canary Islands. *Geological Magazine* 123:287-298

645 Lipman P, Rhodes JM, Dalrymple G (1990) The Ninole Basalt — Implications for the
646 structural evolution of Mauna Loa volcano, Hawaii. *Bulletin of Volcanology* 53(1):1-19

647 Longpré M-A, Chadwick JP, Wijbrans J, Iping R (2011) Age of the El Golfo debris
648 avalanche, El Hierro (Canary Islands): New constraints from laser and furnace $^{40}\text{Ar}/^{39}\text{Ar}$
649 dating. *Journal of Volcanology and Geothermal Research* 203(1–2):76-80

650 Manconi A, Longpré M-A, Walter TR, Troll VR, Hansteen TH (2009) The effects of flank
651 collapses on volcano plumbing systems. *Geology* 37(12):1099-1102

652 Marinoni LB, Gudmundsson A (2000) Dykes, faults and palaeostresses in the Teno and
653 Anaga massifs of Tenerife (Canary Islands). *Journal of Volcanology and Geothermal*
654 *Research* 103(1-4):83-103

655 Marinoni LB, Pasquarè G (1994) Tectonic evolution of the emergent part of a volcanic ocean
656 island: Lanzarote, Canary Islands. *Tectonophysics* 239(1-4):111-137

657 Martí J, Castro A, Rodríguez C, Costa F, Carrasquilla S, Pedreira R, Bolos X (2013)
658 Correlation of Magma Evolution and Geophysical Monitoring during the 2011–2012 El
659 Hierro (Canary Islands) Submarine Eruption. *Journal of Petrology* 54(7):1349-1373

660 Martí J, Pinel V, López C, Geyer A, Abella R, Tárrega M, Blanco MJ, Castro A, Rodríguez C
661 (2013) Causes and mechanisms of the 2011–2012 El Hierro (Canary Islands) submarine
662 eruption. *Journal of Geophysical Research: Solid Earth* 118(3):823-839

663 Masson DG (1996) Catastrophic collapse of the volcanic island of Hierro 15 ka ago and the
664 history of landslides in the Canary Islands. *Geology* 24:231-234

665 Masson DG, Watts AB, Gee MJR, Urgeles R, Mitchell NC, Le Bas TP, Canals M (2002)
666 Slope failures on the flanks of the western Canary Islands. *Earth-Science Reviews* 57(1–2):1-
667 35

668 Meletlidis S, Di Roberto A, Pompilio M, Bertagnini A, Iribarren I, Felpeto A, Torres PA,
669 D'Oriano C (2012) Xenopumices from the 2011–2012 submarine eruption of El Hierro
670 (Canary Islands, Spain): Constraints on the plumbing system and magma ascent. *Geophysical*
671 *Research Letters* 39(17):L17302

672 Padrón Padrón P (1993) Estudio edafoambiental de la isla de El Hierro. In: Tesis Doctoral
673 inédita. Departamento de Edafología y Geología. Universidad de La Laguna. 285 p.+ mapas

674 Palladino DM, Simei S (2002) Three types of pyroclastic currents and their deposits:
675 examples from the Vulsini Volcanoes, Italy. *Journal of Volcanology and Geothermal*
676 *Research* 116(1–2):97-118

677 Pellicer MJ (1975) Estudio vulcanológico, petrológico y geoquímico de la isla de El Hierro
678 (Archipiélago Canario). Tesis Doctoral. Facultad de Ciencias Geológicas. Universidad
679 Complutense de Madrid:179 pp

680 Pellicer MJ (1977) Estudio vulcanológico de la Isla de El Hierro, Islas Canarias. *Estudios*
681 *Geológicos* 33:181-197

682 Perez-Torrado FJ, Rodríguez-Gonzalez A, Carracedo JC, Fernández-Turiel JL, Guillou H,
683 Hansen A, Rodríguez Badiola E (2011) Edades C-14 Del Rift ONO de El Hierro (Islas
684 Canarias). In: *El Cuaternario en España y Áreas Afines, Avances en 2011* (Turu, V. &
685 Constante, A., eds.), Asociación Española para el Estudio del Cuaternario (AEQUA), Andorra
686 101-104

687 Presley TK, Sinton JM, Pringle M (1997) Postshield volcanism and catastrophic mass wasting
688 of the Waiaanae Volcano, Oahu, Hawaii. *Bulletin of Volcanology* 58(8):597-616

689 Robertson AHF, Stillman CJ (1979) Late Mesozoic sedimentary rocks of Fuerteventura,
690 Canary Islands: Implications for West African continental margin evolution. *Journal of the*
691 *Geological Society* 136(1):47-60

692 Schmincke H-U (1982) Volcanic and Chemical Evolution of the Canary Islands. In: Rad U,
693 Hinz K, Sarnthein M, Seibold E (eds) *Geology of the Northwest African Continental Margin*.
694 Springer Berlin Heidelberg, pp 273-306

695 Schmincke HU (1990) *Geology and Geological Field Guide of Gran Canaria*. Pluto Press,
696 Kiel. 212 pp

697 Self S, Sparks RSJ (1978) Characteristics of widespread pyroclastic deposits formed by the
698 interaction of silicic magma and water. *Bulletin Volcanologique* 41(3):196-212

699 Sigmarsson O, Laporte D, Carpentier M, Devouard B, Devidal J-L, Marti J (2013) Formation
700 of U-depleted rhyolite from a basanite at El Hierro, Canary Islands. *Contributions to*
701 *Mineralogy and Petrology* 165(3):601-622

702 Sohn YK (1996) Hydrovolcanic processes forming basaltic tuff rings and cones on Jeju
703 Island, Korea. *Geological Society of America Bulletin* 108:1199-1211

704 Sohn YK, Chough SK (1989) Depositional processes of the Suwolbong tuff ring, Cheju
705 Island (Korea). *Sedimentology* 36(5):837-855

706 Sulpizio R, Mele D, Dellino P, Volpe L (2005) A complex, Subplinian-type eruption from
707 low-viscosity, phonolitic to tephri-phonolitic magma: the AD 472 (Pollena) eruption of
708 Somma-Vesuvius, Italy. *Bulletin of Volcanology* 67(8):743-767

709 Széreméta N, Laj C, Guillou H, Kissel C, Mazaud A, Carracedo J-C (1999) Geomagnetic
710 paleosecular variation in the Brunhes period, from the island of El Hierro (Canary Islands).
711 Earth and Planetary Science Letters 165(3–4):241-253

712 Torn MS, Trumbore SE, Chadwick OA, Vitousek PM, Hendricks DM (1997) Mineral control
713 of soil organic carbon storage and turnover. Nature 389(6647):170-173

714 Urgeles R, Canals M, Baraza J, Alonso B (1996) The submarine “El Golfo” debris avalanche
715 and the Canary debris flow, West Hierro Island: the last major slides in the Canary
716 archipelago. Geogaceta 20:390–393

717 Urgeles R, Canals M, Baraza J, Alonso B, Masson DG (1997) The most recent megaslides on
718 the Canary Islands: the El Golfo Debris Avalanche and the Canary Debris Flow, west El
719 Hierro Island. J. Geophys. Res. 102:20305-20323

720 Valentine GA (1987) Stratified flow in pyroclastic surges. Bulletin of Volcanology 49(4):616-
721 630

722 Valentine GA, Fisher RV (2000) Pyroclastic surges and blasts. In: Sigurdsson, H., Houghton,
723 B.F., McNutt, S.R., Rymer, H., Stix, J. (Eds.), Encyclopedia of Volcanoes. Academic
724 Press:571–580

725 Walker GPL (1983) Ignimbrite types and ignimbrite problems. Journal of Volcanology and
726 Geothermal Research 17(1–4):65-88

727 Wohletz K (1986) Explosive magma-water interactions: Thermodynamics, explosion
728 mechanisms, and field studies. Bulletin of Volcanology 48(5):245-264

729 Wohletz KH, Sheridan MF (1983) Hydrovolcanic explosions; II, Evolution of basaltic tuff
730 rings and tuff cones. American Journal of Science 283(5):385-413

731 Wohletz KH, Sheridan MF, Brown WK (1989) Particle size distributions and the sequential
732 fragmentation/transport theory applied to volcanic ash. *Journal of Geophysical Research:*
733 *Solid Earth* 94(B11):15703-15721

734 Figures and table caption

735 Fig. 1 Location and simplified geological map of El Hierro.

736 Fig. 2 Aerial distribution of the Malpaso Member deposits, with all the studied outcrops
737 indicated. Selected stratigraphic columns showing the field relationships between the Malpaso
738 Member and the older and younger deposits are shown as well.

739 Fig. 3 Detailed stratigraphic sections of the Malpaso Member and its different units and
740 subunits. See text for further details.

741 Fig. 4 Field photographs of the Malpaso Member deposits at (a) proximal, (b) medial, and (c)
742 distal outcrops.

743 Fig. 5 a) Isopach map showing the variations in thickness of the Malpaso Member; b) Isopleth
744 map of the distribution of the average maximum pumice-clast diameter (cm) in level N1 in the
745 Malpaso Member

746 Fig. 6 Grain-size distribution and modal composition of representative samples from the
747 Malpaso Member. N1: pumice lapilli layers alternating with poorly stratified ash layers; N2:
748 ash layers with loose pumice-lapilli-rich layers; N3: massive poorly stratified ash beds with
749 interbedded lapilli layers; N4: ash and pumice-rich lapilli layers with abundant lava lithic
750 clasts. The different sublevels (e.g. N1a) are indicated.

751 Fig. 7 a) graphic standard deviation versus median diameter; b) F2 (wt% <1 mm diameter)
752 versus F1 (wt% <1/16 mm diameter)

753 Fig. 8 Scanning electron microscope (SEM) images of pumice from Units 2, 3 and 4. Clasts
754 show little abrasion due to transport. Several examples of the most typical morphological
755 features are shown. (a-b): poorly vesiculated particles from Unit N2 with mainly blocky
756 morphologies; (c-d): poorly vesiculated clasts from Unit N3 with tiny adhering particles and
757 elongate vesicles; (e-f): dense and poorly vesiculated grains with blocky morphology,
758 quenching crack structures and stepped textures.

759 Fig. 9 Petrographic composition of juvenile samples from the eruption: a) Amphibole, b)
760 Plagioclase, c) Pyroxene and oxide.

761 Fig. 10 Pyroclastic deposits corresponding to local Strombolian eruptions and to the studied
762 eruption close to Malpaso but separated by well-developed paleosols.

763 Online Resource 1 Geographical coordinates of relevant locations, as well as stratigraphic
764 sections and sampling points

Figure1
[Click here to download high resolution image](#)

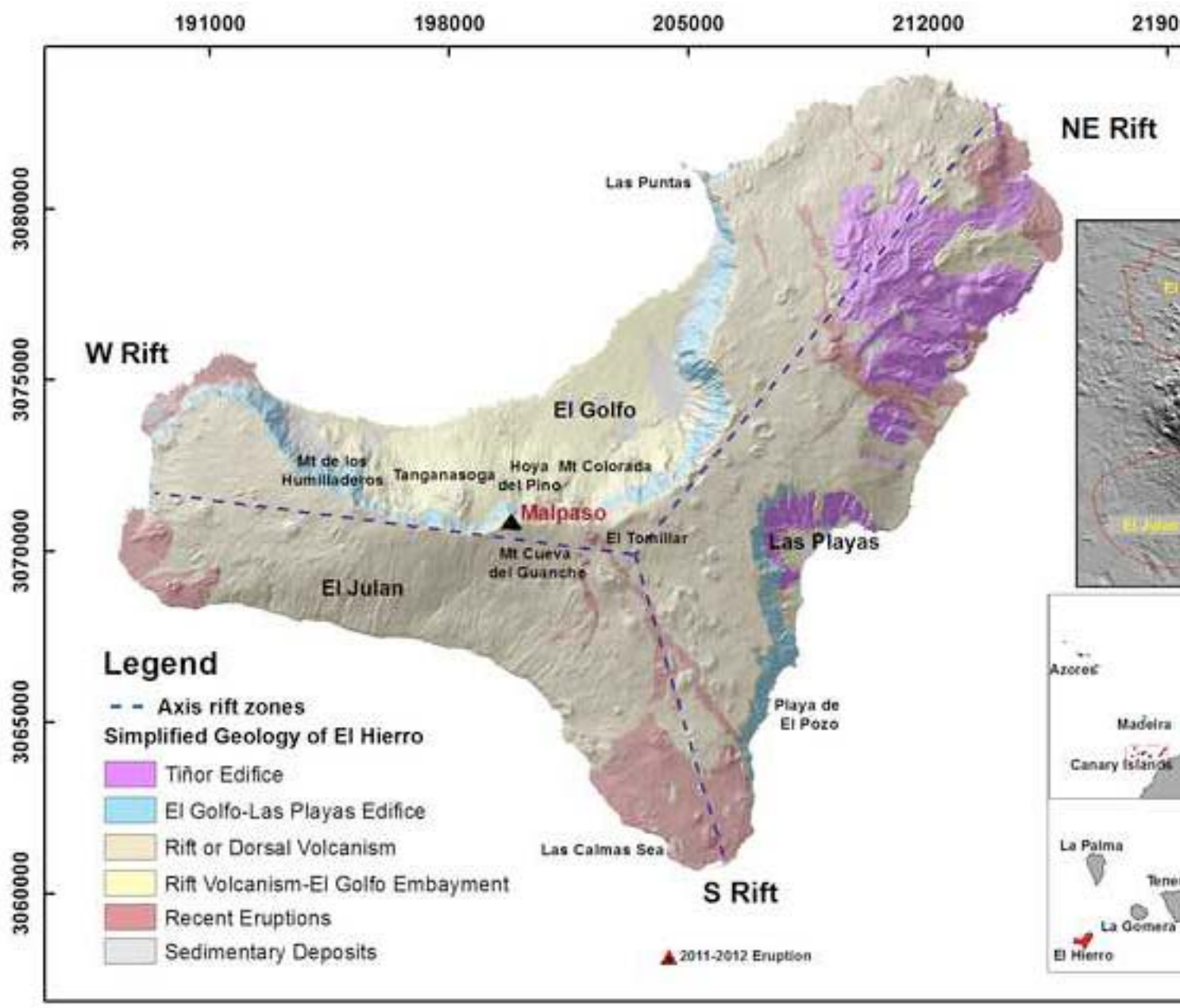


Figure2
[Click here to download high resolution image](#)

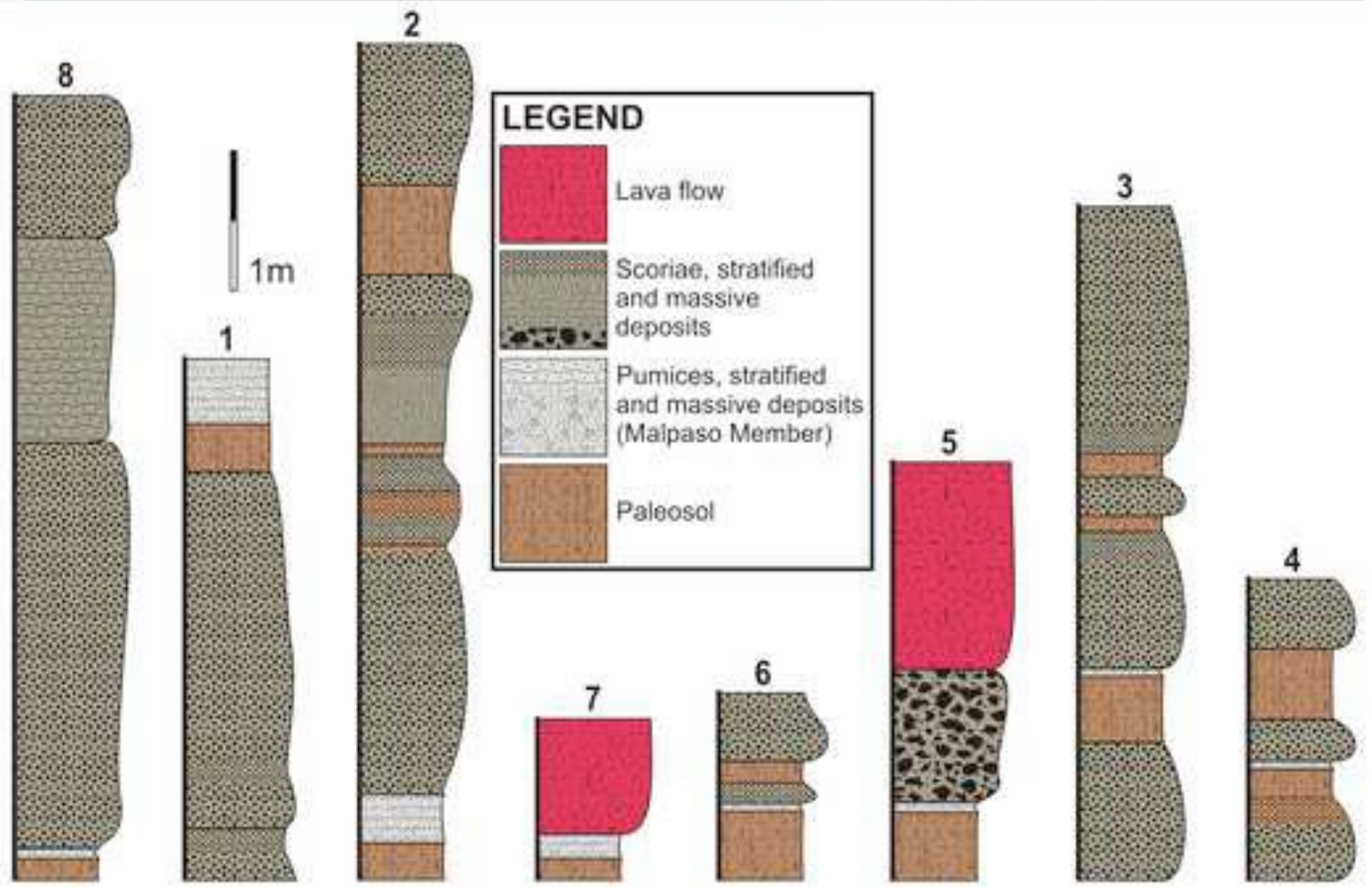
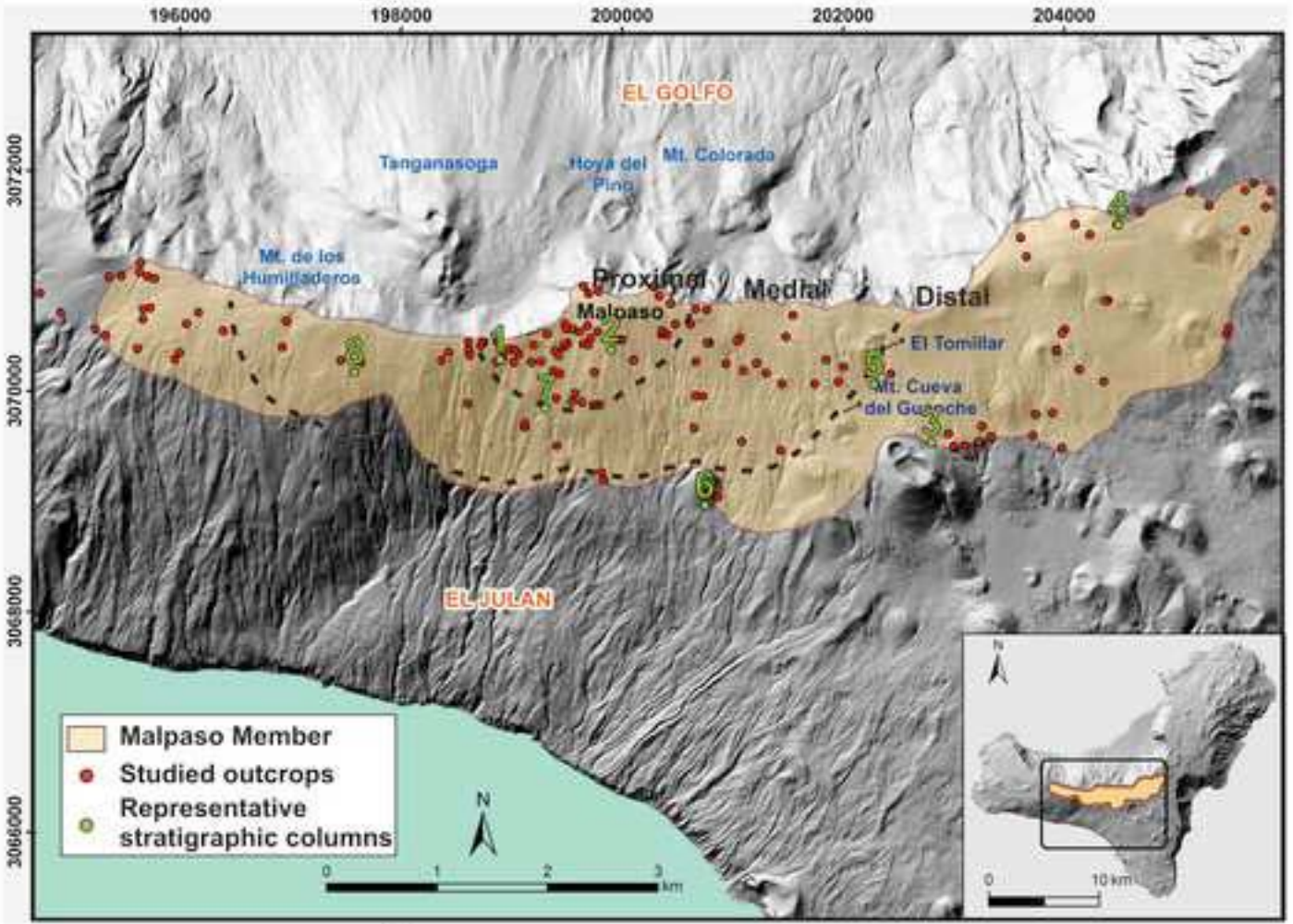


Figure3
[Click here to download high resolution image](#)

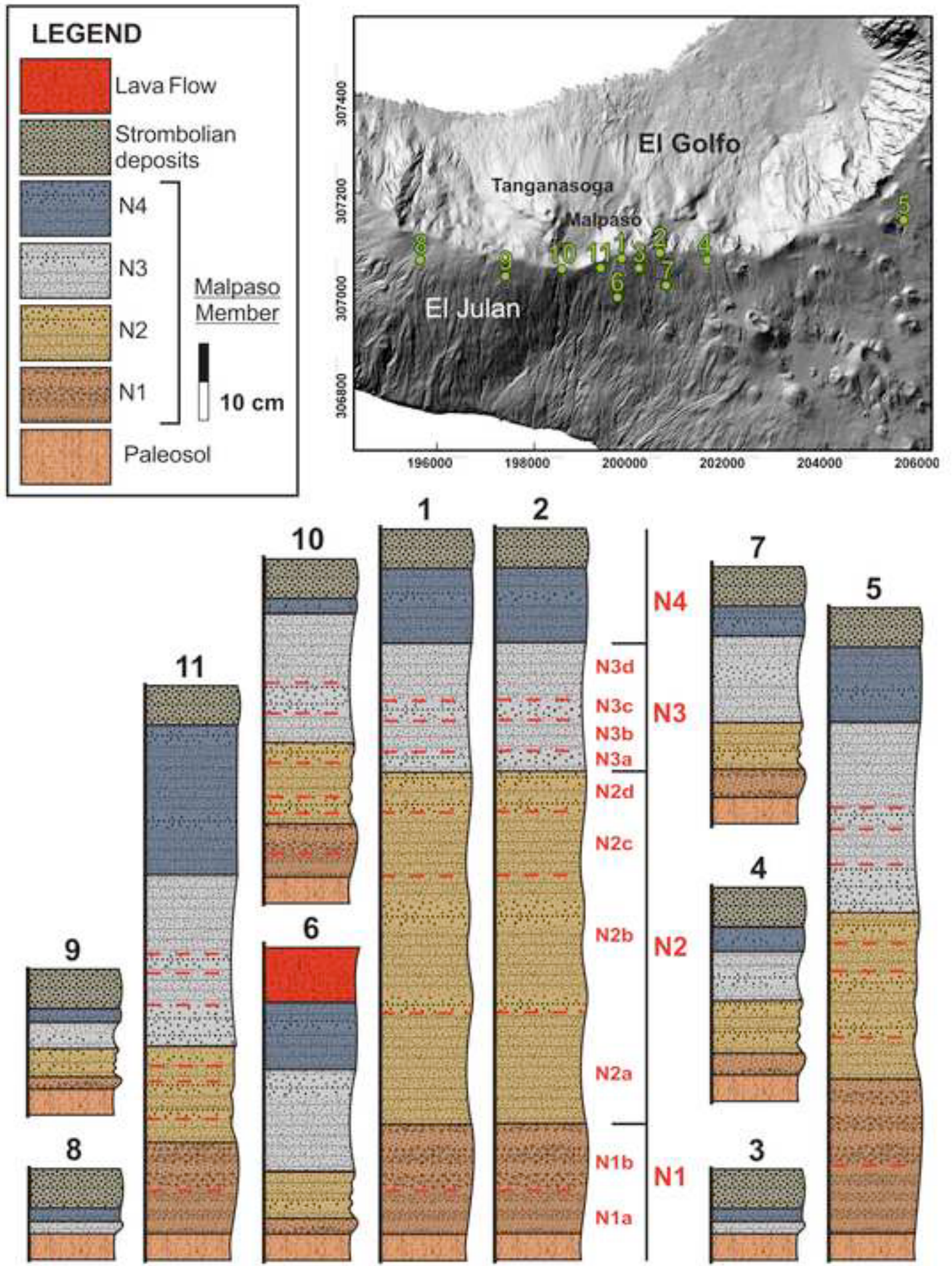


Figure4
[Click here to download high resolution image](#)

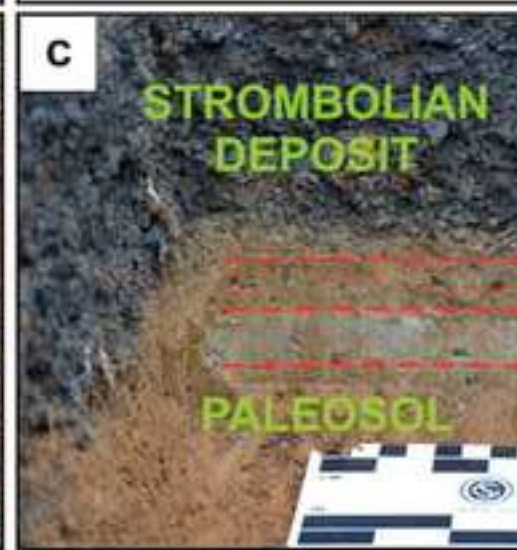
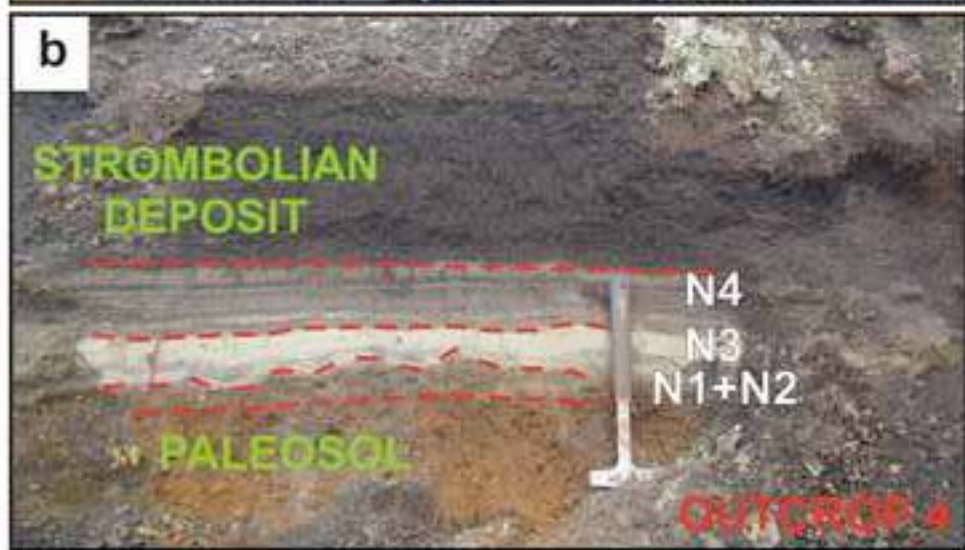
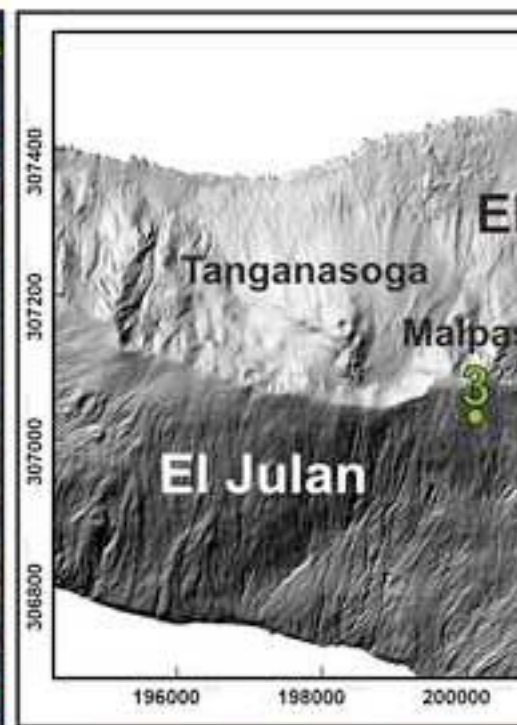
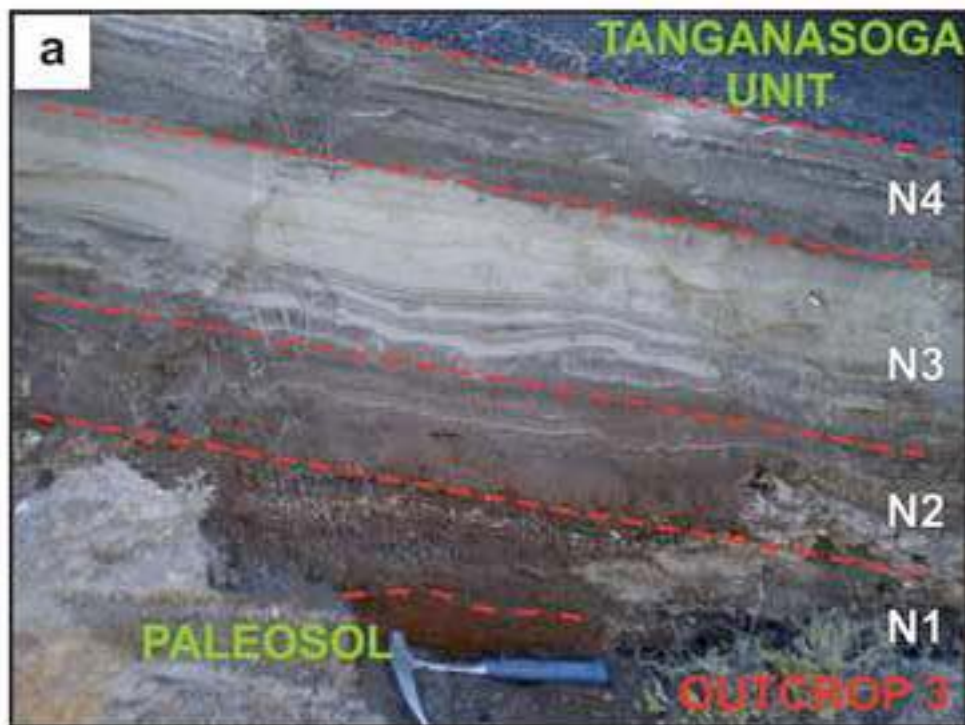


Figure5
[Click here to download high resolution image](#)

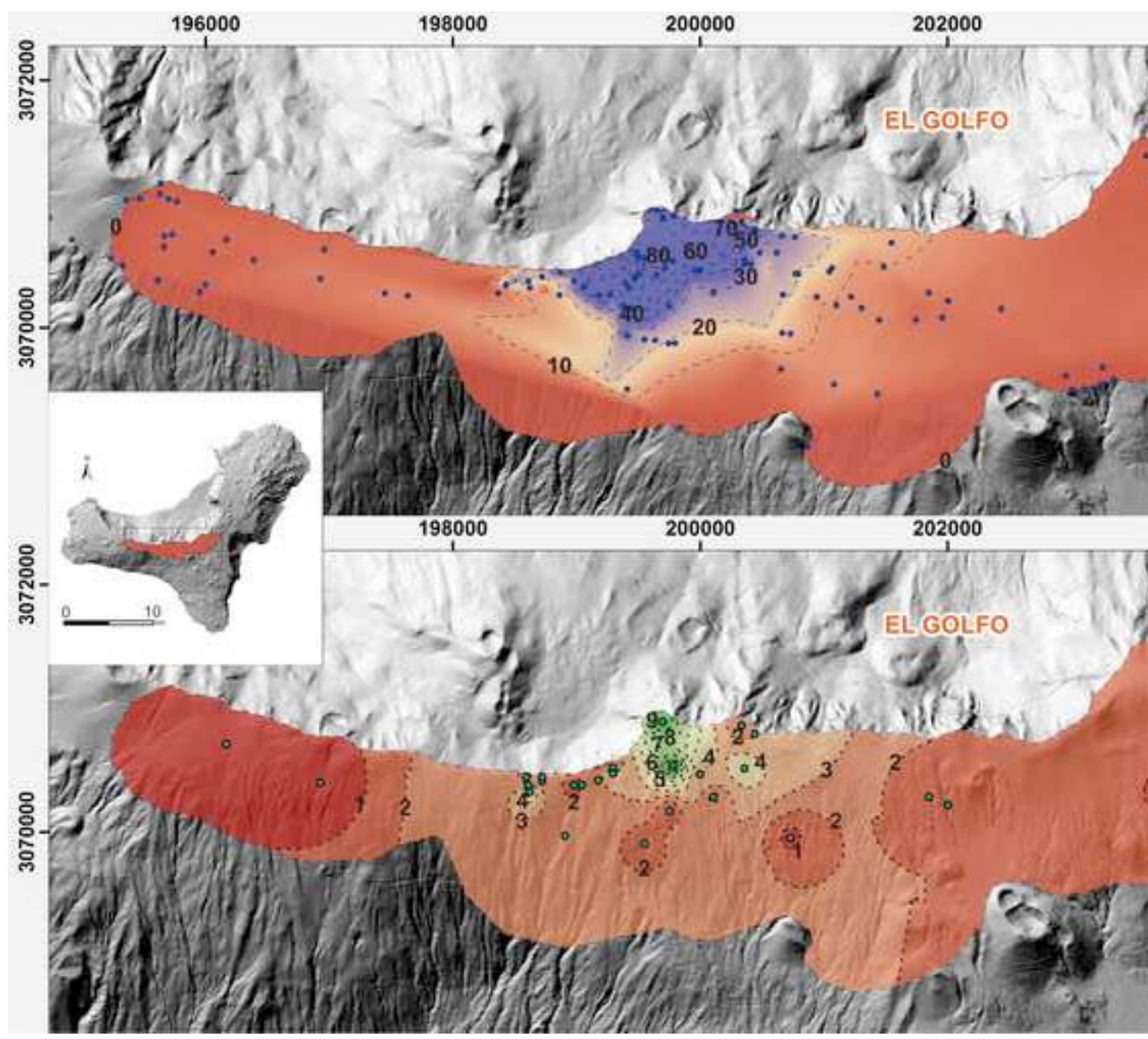


Figure6
[Click here to download high resolution image](#)

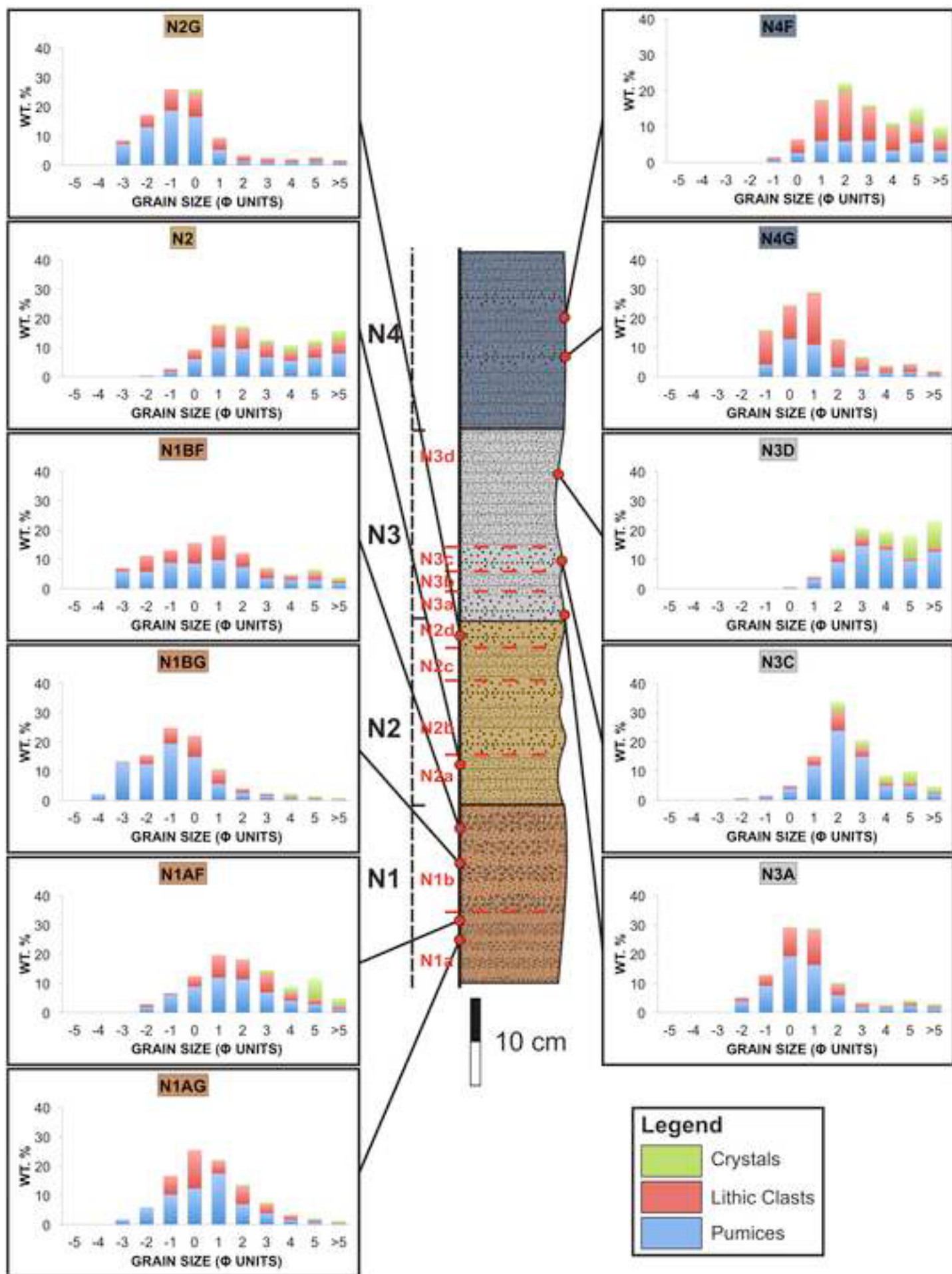


Figure 7

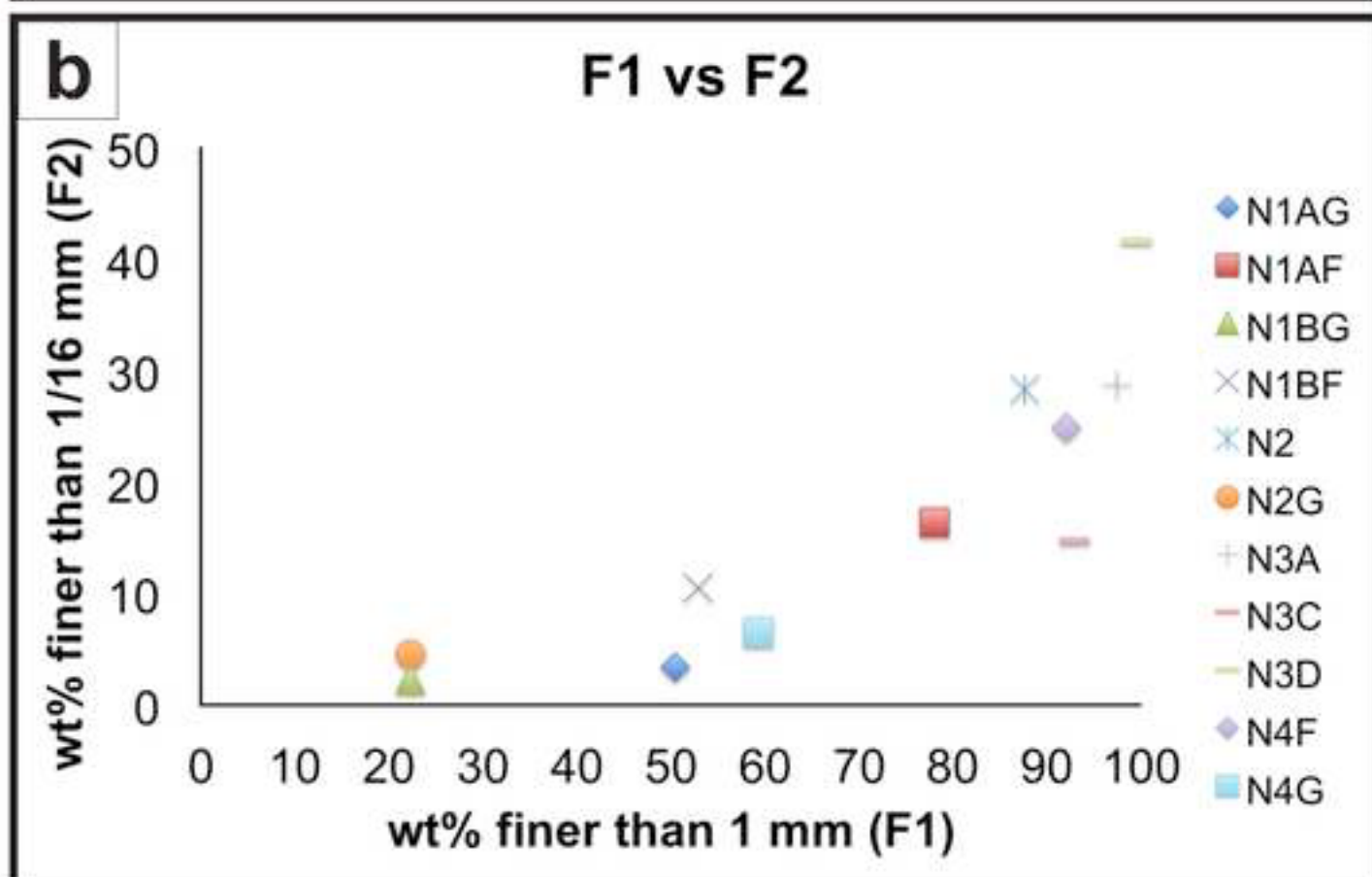
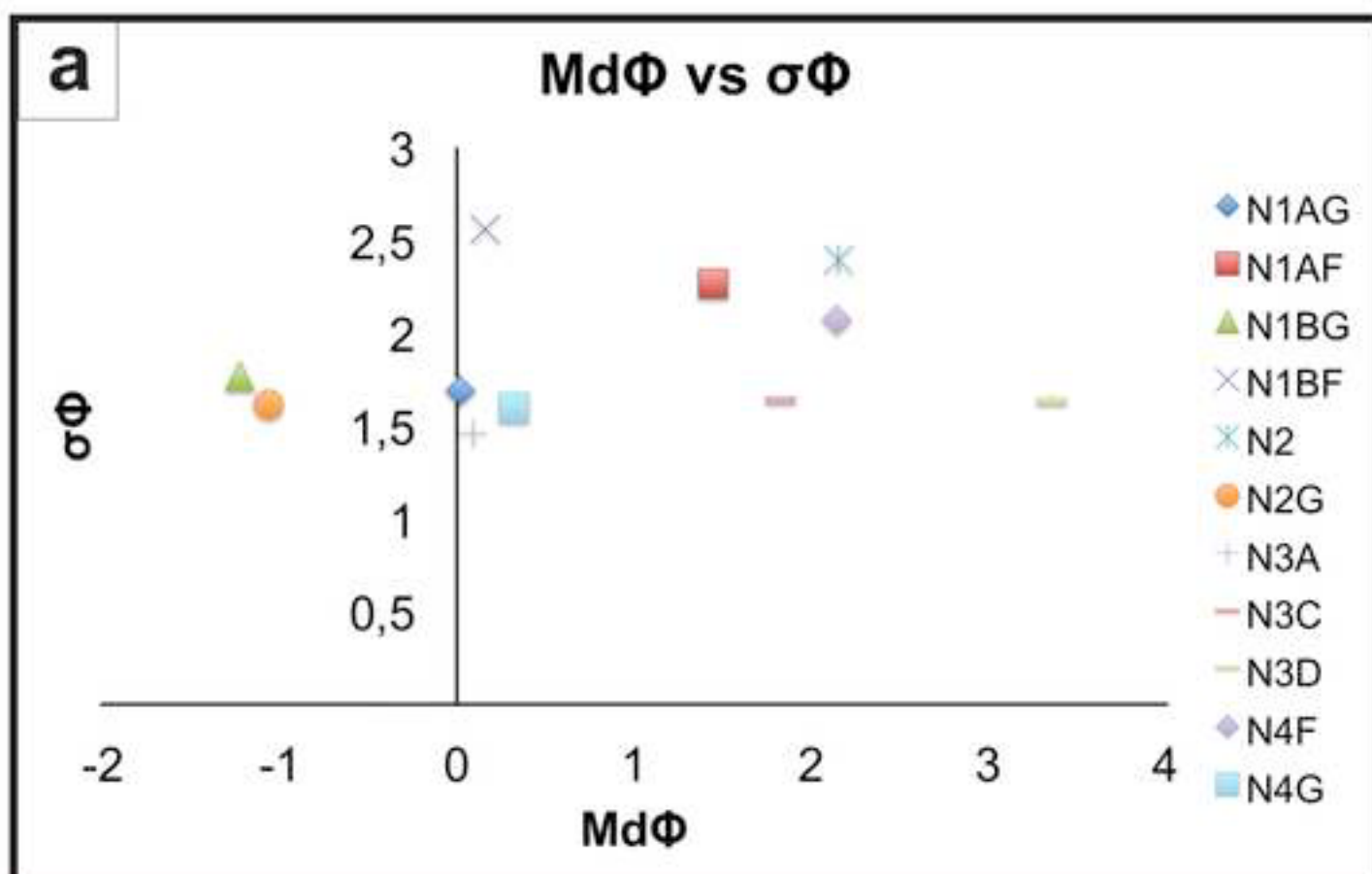
[Click here to download high resolution image](#)

Figure8
[Click here to download high resolution image](#)

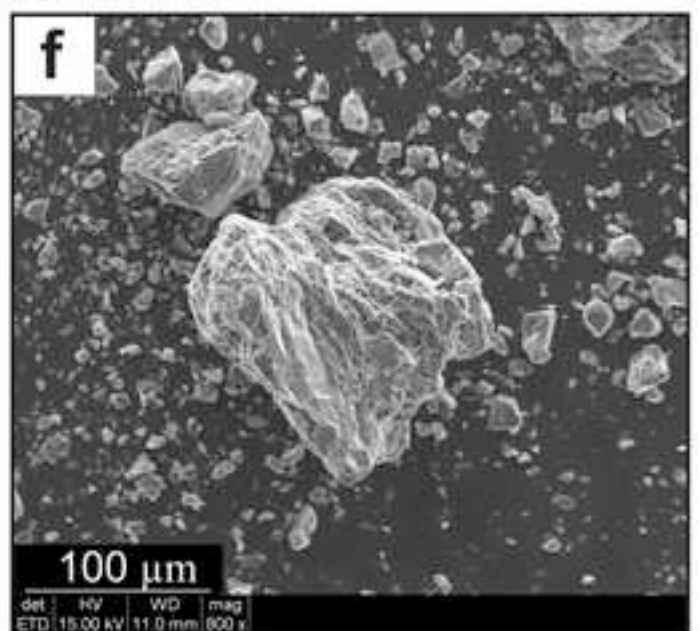
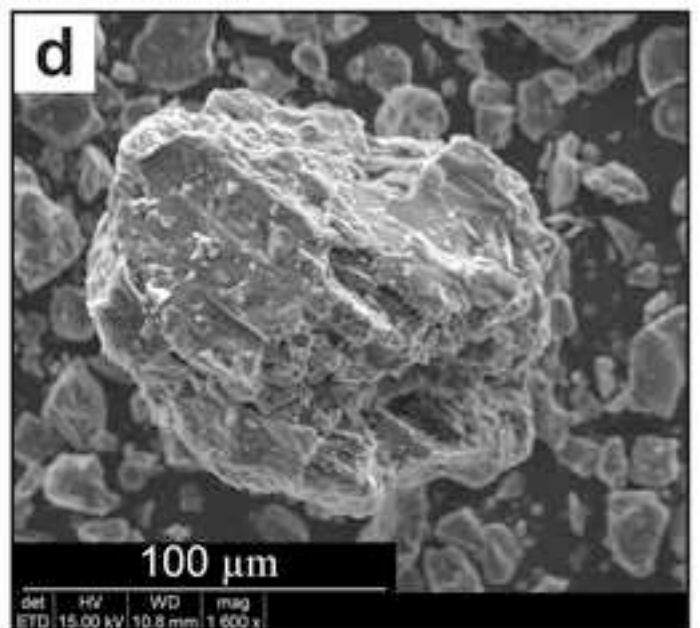
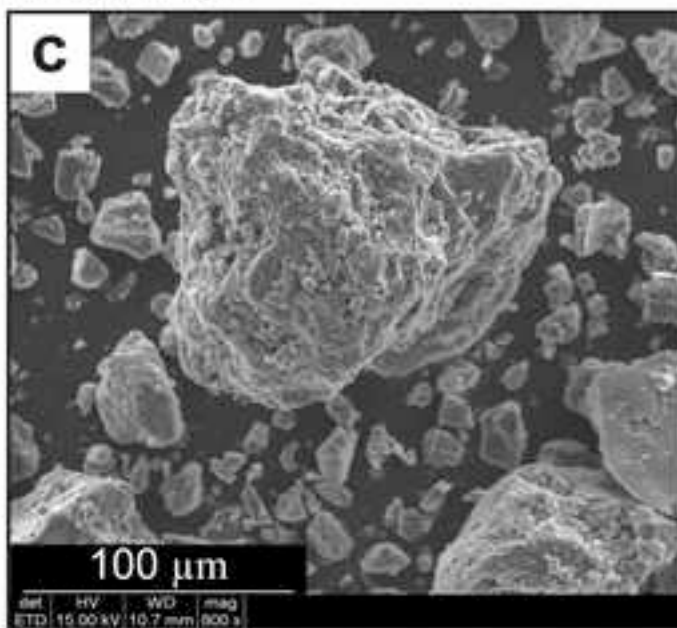
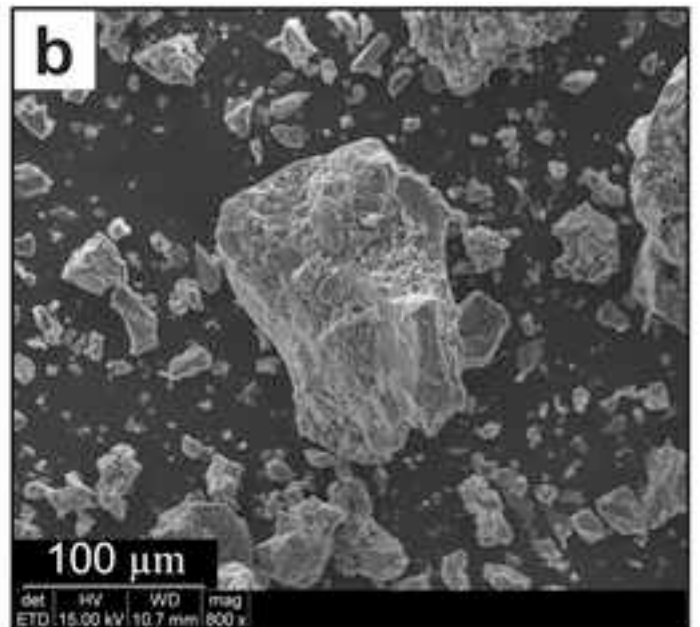
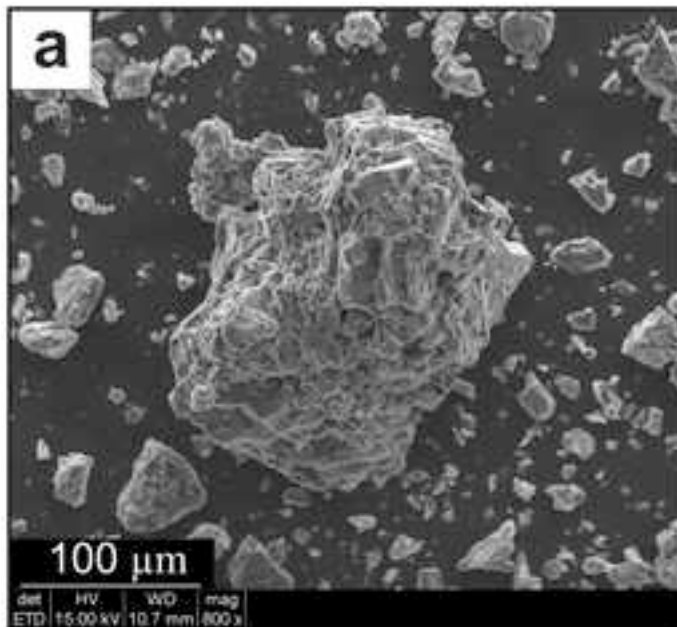


Figure9
[Click here to download high resolution image](#)

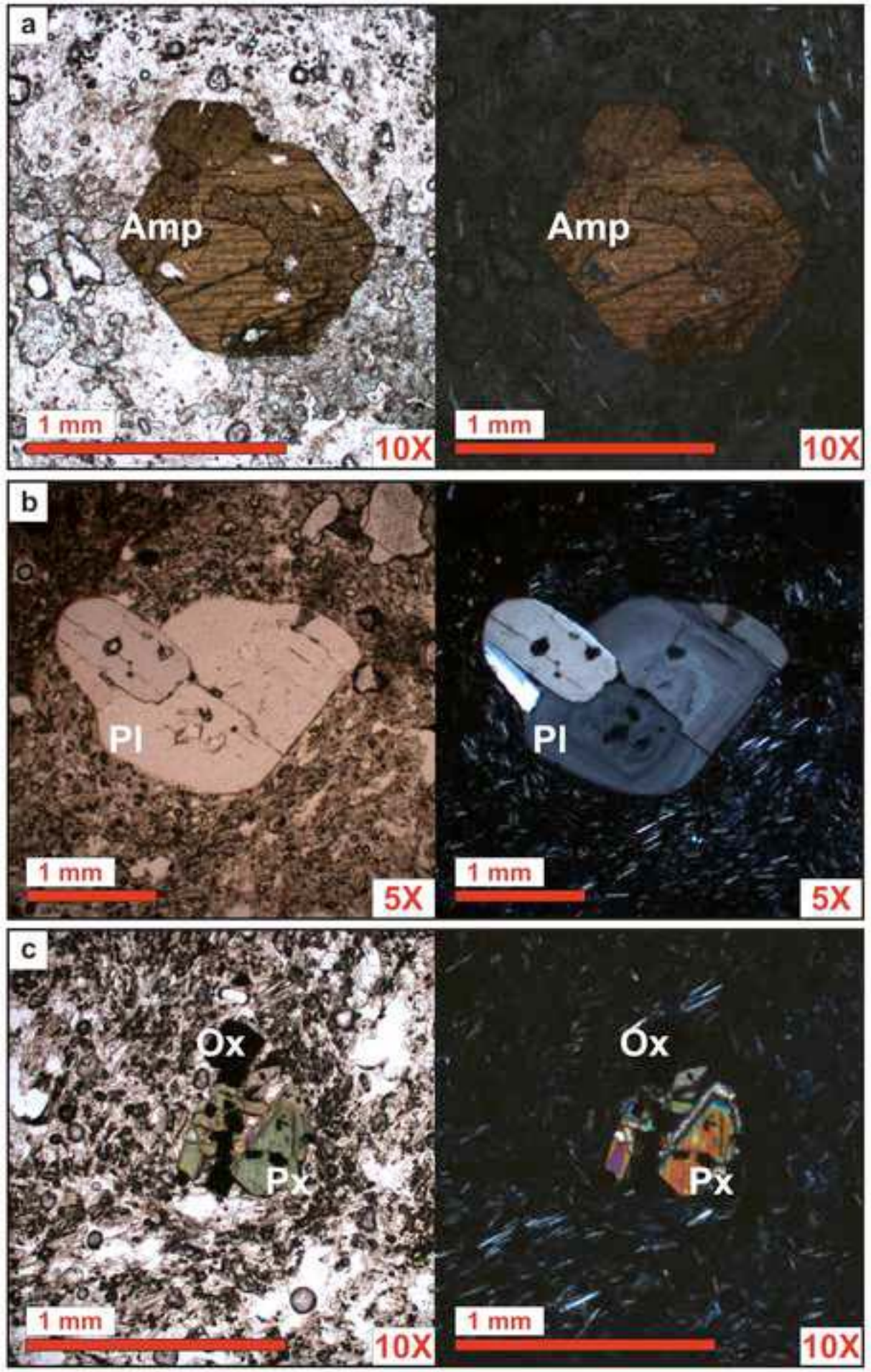
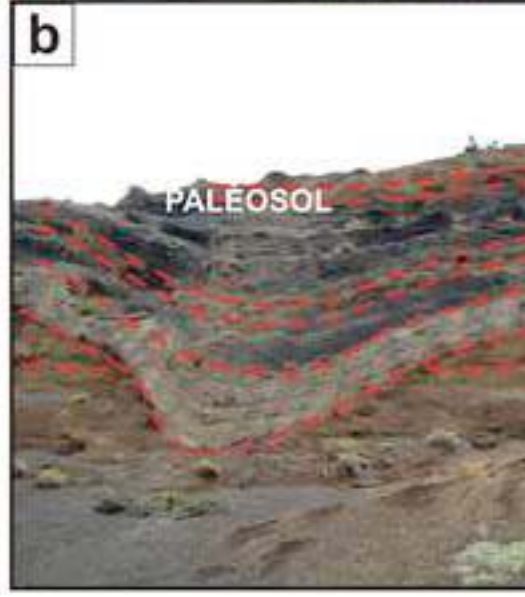
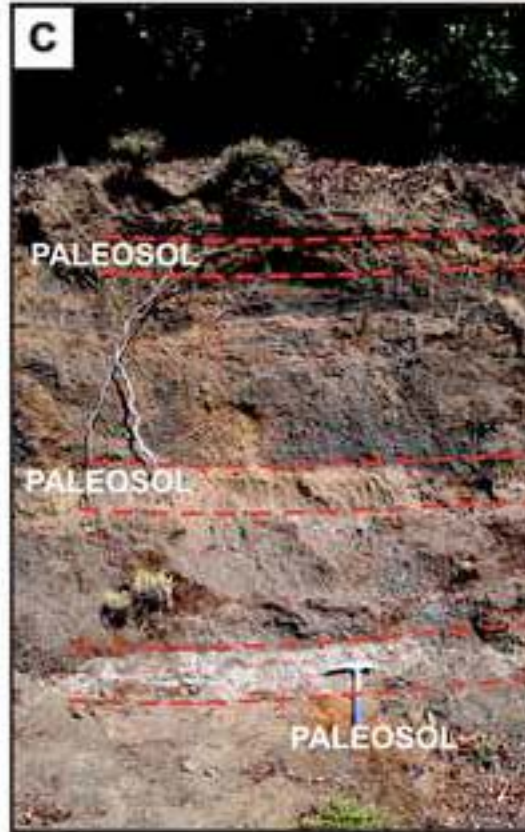
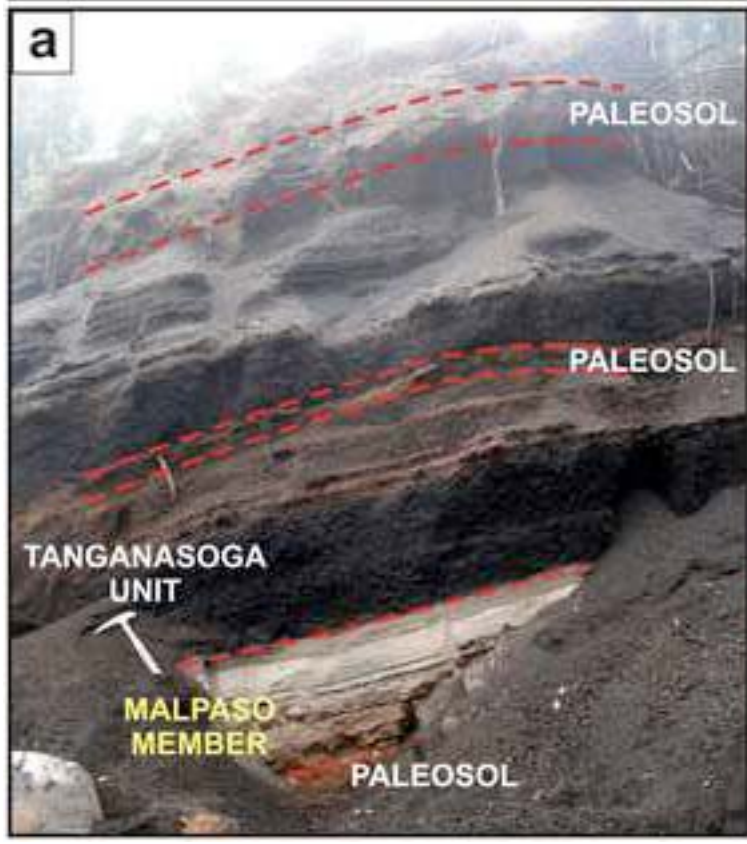
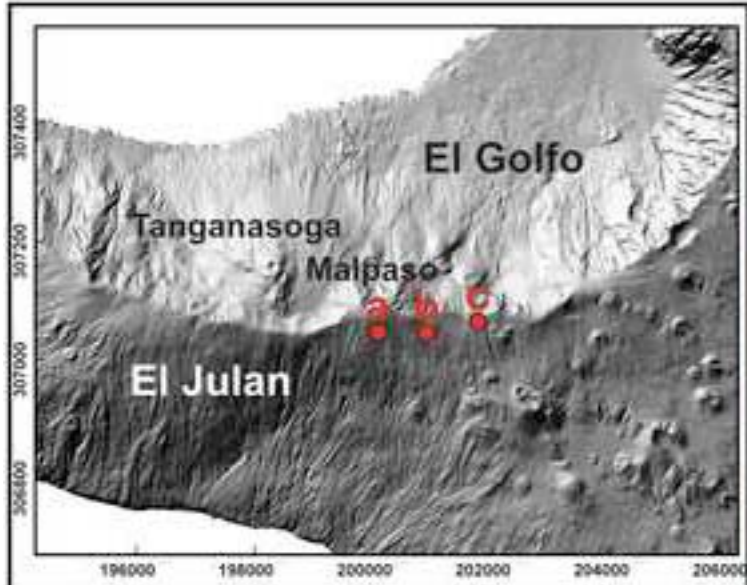


Figure10
[Click here to download high resolution image](#)



Supplementary Material

[Click here to download Supplementary Material: Online Resource 1.docx](#)

1
2
3
4
5
6
7
8
9
10
11
12
13
14
15
16
17
18
19
20

Explosive felsic volcanism on El Hierro (Canary Islands)

Comment [Dario Ped1]: reviewer1 green, reviewer 2 blue, reviewer 3 red.

Dario Pedrazzi¹, Laura Becerril^{1,2}, Joan Martí¹, Stavros Meletlidis³, Inés Galindo

¹ Group of Volcanology, Institute of Earth Sciences *Jaume Almera* (GVB-CSIC). SIMGEO (UB-CSIC) c/Lluis Sole Sabaris s/n, 08028 Barcelona, Spain.

² Instituto Geológico y Minero de España (IGME) c/ Alonso Alvarado, 43-2⁰A 35003-Las Palmas de Gran Canaria, Spain.

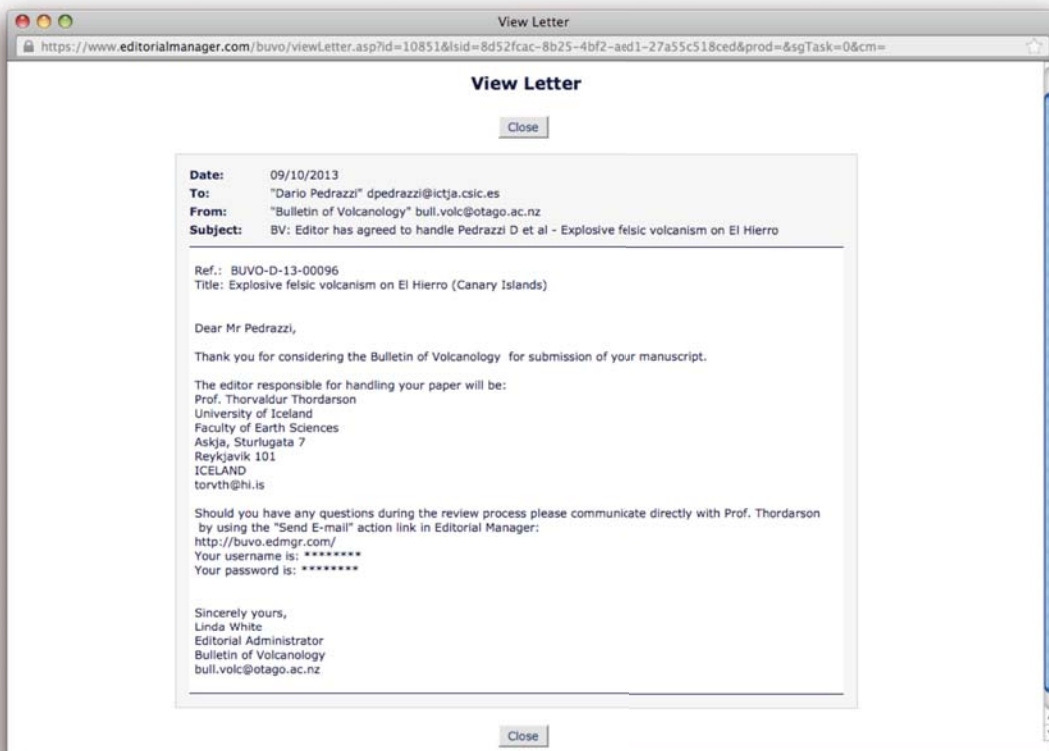
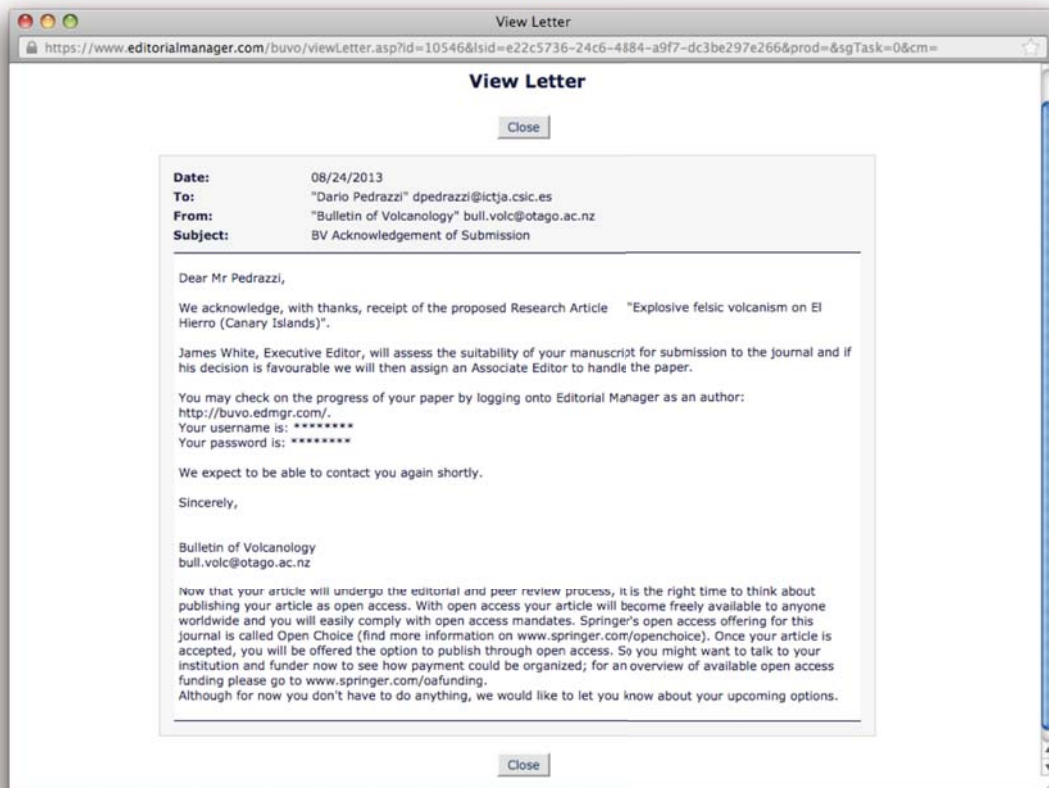
³ Centro Geofísico de Canarias, IGN, Santa Cruz de Tenerife, Spain.

Corresponding author: dpedrazzi@ictja.csic.es

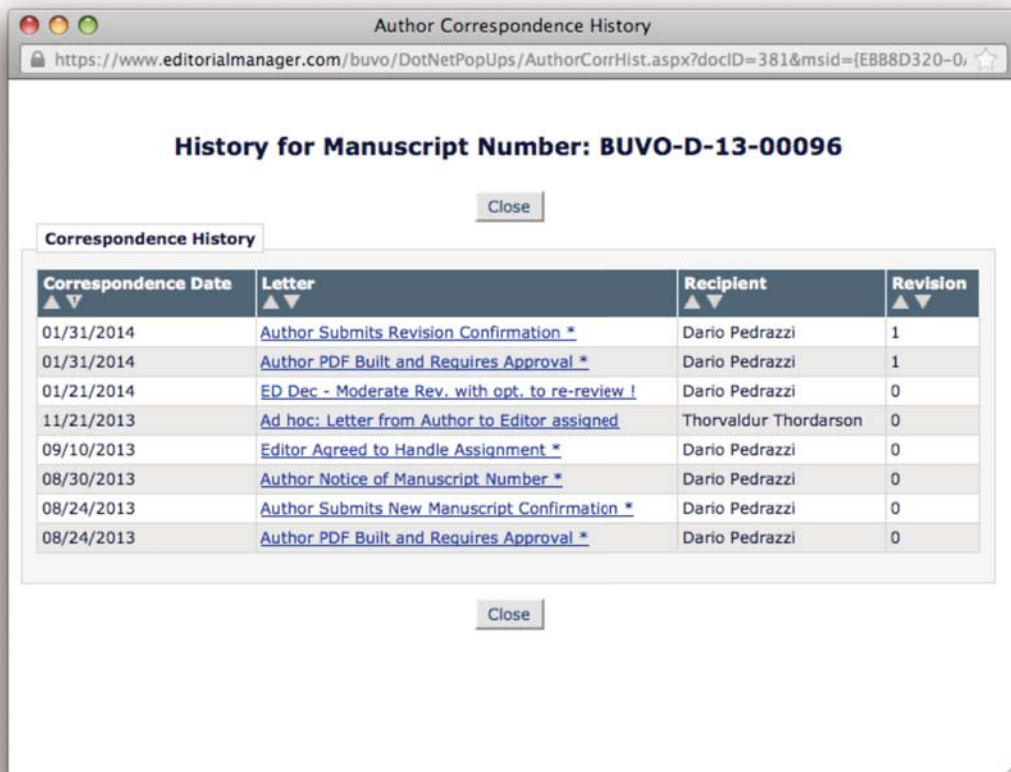
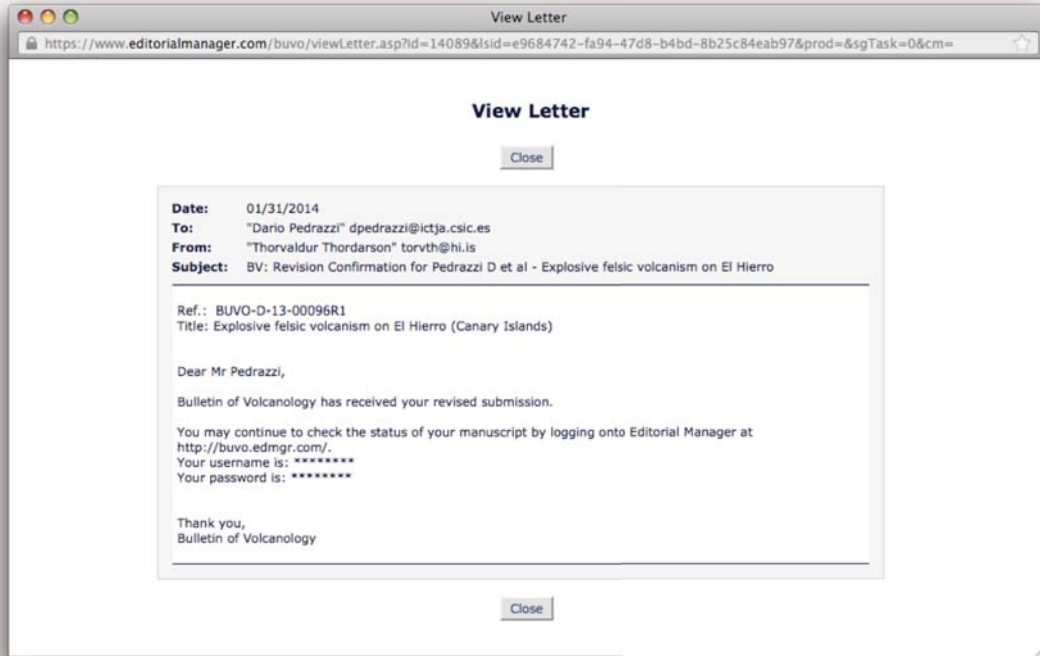
Submitted to:

Bulletin of Volcanology

Appendix 4.1 Proof of delivery of the paper: “*Explosive felsic volcanism on El Hierro (Canary Islands)*” in Bulletin of Volcanology



Appendix 4.2 Proof of delivery of the revised version of the accepted paper: “Explosive felsic volcanism on El Hierro (Canary Islands)” in Bulletin of Volcanology



APPENDIX 5

THE 1970 ERUPTION ON DECEPTION ISLAND (ANTARCTICA): ERUPTIVE DYNAMICS AND IMPLICATION FOR VOLCANIC HAZARD

1 **The 1970 eruption on Deception Island (Antarctica): eruptive dynamics and**
2 **implications for volcanic hazards**

3 Dario Pedrazzi^{1*}, Gerardo Aguirre Díaz², Stefania Bartolini¹, Joan Martí¹, Adelina
4 Geyer¹

5

6 ¹ *Institute of Earth Sciences Jaume Almera, ICTJA-CSIC, Group of Volcanology.*

7 *SIMGEO (UB-CSIC) Lluís Sole i Sabaris s/n, 08028 Barcelona, Spain*

8 ² *Centro de Geociencias, Universidad Nacional Autónoma de México, Campus*

9 *Juriquilla, Querétaro, Qro. 76230, Mexico*

10

11 **corresponding author: Dario Pedrazzi (dpedrazzi@ictja.csic.es)*

12

13

14 Submitted to: Journal of the Geological Society of London

15

16

17 **Abstract**

18 In 1970, a hydrovolcanic eruption took place in the northern part of Deception
19 Island (South Shetland Archipelago, Antarctic Peninsula group). The eruption occurred
20 in the same general area as the 1967 eruption, but with new, more widely distributed
21 vents. Two groups of craters were formed as a result of the 1970 eruption, which
22 suggests that different active fissures and eruptive dynamics were operating during the
23 same eruption. One group consists of maar-like craters, while the other group is made of
24 conical shape edifices. The 1970 eruption can be classified as a VEI 3 eruption, with
25 mainly phreatomagmatic episodes that generated a bulk volume of about 0.1 km³ of
26 pyroclastic material and an eruptive column of up to 10 km in height, from which
27 fallout deposits have been recognized at a distance of more than 100 km to the
28 northeast. The 1970 eruption was similar to that of 1967 and conjointly these two events
29 show how eruption dynamics can be controlled by the physical characteristics of the
30 vents (e.g. the uppermost part of the volcano's substrate and the width and orientation
31 of the eruptive fissure) and by changing magma/water interaction, which together
32 generate different eruptive phases and associated volcanic hazards.

33

34 **Keywords:** Deception Island, South Shetland Archipelago, Antarctica,
35 phreatomagmatism, 1970 eruption, volcanic hazard

36

37

38 **Introduction**

39 Hydrovolcanic eruptions are common in coastal environments where erupting
40 magma may interact with seawater in either subaquatic or subaerial settings depending
41 on the location of the eruption conduit and vent (Sheridan & Wohletz 1983). Near-shore
42 and shallow subaqueous activity may generate high-intensity explosions characterised
43 by ballistic blocks, ash-fall and pyroclastic density currents, which, in contrast with the
44 lesser impact typically associated with magmatic eruptions of the same size, may
45 severely affect surrounding areas.

46 The 1970 eruption on Deception Island, whose over 20 recognised eruptions
47 during the past two centuries make it the most active volcano in the South Shetland
48 Archipelago (Antarctic Peninsula group), is an excellent example of a monogenetic
49 hydrovolcanic eruption in a coastal environment (e.g. Sheridan & Wohletz 1983). This
50 eruption took place in the northern part of the Deception caldera and gave rise to the
51 formation of several vents and cones that differ significantly in the shape of their craters
52 (Baker & McReath 1971, 1975). Several preliminary accounts of the 1970 eruption that
53 include a general description in Baker & McReath (1975) have already been published
54 (e.g. Baker & McReath 1971; Gonzalez Ferran *et al.* 1971; Shultz 1972). However, a
55 detailed description of the succession of deposits, as well as an accurate reconstruction
56 of the eruptive activity, is still lacking.

57 In this paper we describe in detail the stratigraphy, lithology and sedimentology
58 of the deposits of the 1970 eruption and use this information to infer the eruption
59 dynamics and transport and depositional processes. We then compare these data with
60 those from the 1967 eruption and analyse the potential hazard implications of this type
61 of eruptive activity on Deception Island, which is becoming one of the main tourist
62 attractions on the Antarctica.

63 **Geological setting and general characteristics of Deception Island**

64 Deception Island is the southernmost island in the South Shetland Archipelago
65 and is located at the southwestern end of the Bransfield Strait. It consists of a young
66 (<1.4 Ma) back-arc basin (Fig. 1a), which was formed as a consequence of the Phoenix
67 plate subduction under the Antarctic plate during the upper Mesozoic–Cenozoic interval
68 (Dalziel 1984). The Bransfield basin, <60-km wide and 500-km long, separates the
69 South Shetland Islands from the Antarctic Peninsula (Fig. 1b) and has a characteristic
70 graben structure, with tilted blocks and rotational faults developed under a regime of
71 continental extension (Jeffers & Anderson 1990; Gràcia *et al.* 1996; Vuan *et al.* 2005).

72 Deception Island consists of a <0.75-Ma (Valencio *et al.* 1979; Smellie 1988)
73 horseshoe-shaped volcanic edifice, with a below-sea-level diameter of 25 km (Smellie
74 1988; Barclay *et al.* 2009) and an above-sea-level diameter of around 13 km (Fig. 1c).
75 A sea-flooded depression known as Port Foster occupies the central part of the island
76 (Smellie 2001; Martí *et al.*, 2013). Several periods of contrasting styles of volcanic
77 activity can be distinguished (Smellie *et al.* 2002). Over 20 eruptions have been
78 identified over the past two centuries (Roobol 1980; Pallàs *et al.* 2001; Smellie *et al.*
79 2002), the most recent of which occurred in 1967, 1969 and 1970 (see: Orheim 1971c;
80 Baker *et al.* 1975; Roobol 1980; Smellie 2002).

81 The construction of this composite volcanic complex, which rises up to 540 m
82 a.s.l. at Mount Pond and 460 m at Mount Kirkwood (Fig. 1c), was truncated by the
83 formation of a central caldera (Port Foster) resulting from an explosive eruption of
84 basaltic-to-andesitic magmas, mostly as pyroclastic density currents with a total bulk
85 volume in the order of 90 km³ (Martí *et al.* 2013). The basement of the island is not
86 exposed but probably corresponds to Cretaceous–Tertiary consolidated sedimentary and
87 volcanic rocks and/or unconsolidated and poorly consolidated pre-Quaternary marine

88 sediments deposited on the submerged South Shetland Islands platform (Ashcroft 1972;
89 Grad *et al.* 1992; Smellie 2001). The pre-caldera units (BSF-Fig. 2) correspond mostly
90 to volcanic shield deposits, in which different eruptive cycles and vents can be
91 distinguished (Smellie 2001). Most of these units correspond to lava flows and
92 Strombolian deposits, as well as to palagonitised hyaloclastitic breccias. The shield-
93 related units are overlaid unconformably by a thick sequence of massive ignimbrites
94 and minor pyroclastic surge deposits of basaltic-to-andesitic composition, which
95 represent the syn-caldera deposits (Martí *et al.* 2013) (OCTF-Fig. 2). This succession is
96 overlaid unconformably by discontinuous sequences of post-caldera deposits originating
97 from different vents (PCD-Fig. 2), most located inside or around the caldera depression
98 itself (Smellie 2001).

99 **Methods**

100 A photointerpretation of ortophotos at a scale of 1:5,000 was necessary to
101 identify the potentially most interesting outcrops in the area. Fieldwork was conducted
102 during the austral summer of 2012–2013 in an area of about 5 km² around the cones of
103 the 1970 and 1967 eruptions. A total of six detailed stratigraphic logs were established
104 but due to the difficult access to some zones, it was not possible to cover the whole of
105 the area covered by the deposits from these eruptions. Nevertheless, these stratigraphic
106 logs are representative of the resulting successions of deposits.

107 The geometry and lithology of the deposits were documented in each outcrop
108 following lithostratigraphic and stratigraphic criteria; the colour, nature and relative
109 content of components, grain size variations, texture and sedimentary structures were
110 analysed. Maximum clasts (scoriae and lithics) of each identified layer were established
111 based on the geometric mean average of the three axes of the five largest clasts sampled
112 from a horizontal area of 0.5 m².

113 All data were managed using Surfer 7 and an open-source Geographic
114 Information System (GIS) framework (QGIS, www.qgis.org). The location of relevant
115 sites and the position of the stratigraphic logs were recorded using a portable GPS with
116 a precision of about 3 m. The reference zone used was the UTM projection Datum:
117 D_WGS_1984, zone 20 South.

118 Grain-size analyses employing dry-sieving techniques and componentry analysis
119 were performed by weighing/counting 42 representative samples. Samples were sieved
120 at 1 using sieves with mesh sizes in the range 32–1/32 mm (-5ϕ to 5ϕ). Clast
121 compositions were initially characterised in the field via hand-sample observations and
122 then later in the laboratory under a binocular microscope. Component analysis was
123 carried out on the -5ϕ -4ϕ , -3ϕ , -2ϕ and -1ϕ fractions of the deposits. Clasts were
124 separated into juvenile and accidental lithics, the latter belonging to the island basement
125 and to the syn- and post-caldera phase. Further analysis of the samples finer than -1ϕ is
126 not provided here since the original content and grain size distribution of the fine
127 fraction are significantly affected by the sieving process itself.

128 The physical parameters of the eruption were obtained: the erupted volume was
129 calculated with an isopach map using Pyle's method (1989), while the plume height was
130 determined by applying the method described by Carey & Sparks (1986) to an isopleth
131 map of clasts.

132 **Characteristics of the 1970 craters**

133 The 1970 craters are located in the northern part of Deception Island, between
134 Goddard Hill and Cross Hill, at the foot of the caldera wall and close to the beach (Fig.
135 3a). At least 13 vents from this eruption were identified and can be separated into two
136 main groups – the eastern and western – based on the location and shape of the craters.

137 The former group is located at the foot of Goddard Hill and consists of seven conical
138 shape edifices (a-g; Fig. 3b) that are aligned roughly in a NW-SW direction (Fig. 3b).
139 These steep-sided craters reach a maximum depth of 60 m. Crater g, described by Baker
140 & McReath (1975), has been eroded away by the island's glacier. The western group,
141 with maar-like shapes, is located at the foot of the exposed part of the caldera wall (Fig.
142 3b); its craters have almost vertical sides and rims that only reach about 15 m above sea
143 level. The first crater (h,i; Fig. 3b) is a composite structure consisting of two major
144 craters whose southernmost points are connected to Telefon Bay by a narrow, around
145 10-m-wide isthmus. The second crater (j; Fig. 3b), a depression located in the
146 northwestern part of the complex originating from the 1967 eruption, is partially filled
147 by a lake and seems to represent the remains of another eruptive centre. The last three
148 craters (k-m; Fig. 3b) are connected to each other by narrow channels and to Port Foster
149 by a 150-m-wide channel located in the eastern part. As reported by Baker & McReath
150 (1975), the isolated area of relatively large bombs with no traces of a source crater that
151 lies south of Cross Hill (Fig. 3b) might indicate another eruptive vent, supposedly
152 located near the shore.

153 **Characteristics of the pyroclastic succession**

154 We carried out a detailed characterisation of six stratigraphic logs in order to
155 reconstruct the succession of deposits. Although limited exposure only allowed us to
156 obtain one representative stratigraphic log from the Eastern Craters (1; Fig. 4), five
157 stratigraphic logs were obtained from the Western Craters (Lago Escondido Edifice) (2-
158 6; Fig. 4).

159 *Eastern Craters*

160 Stratigraphic log 1 has a total thickness of about 40 m with a visible
161 unconformity in the middle (Figs. 4 and 5a,b), which marks the important change

162 between the two parts of the succession (22-41 m). The base of the succession is not
163 exposed (Figs. 4 and 5e). The first part of the stratigraphic log (0–1 m) shows a
164 continuous change from laminated poorly sorted vesiculated, fine-to-coarse lapilli-sized
165 clasts with accidental lithics (syn-caldera ignimbrites and lava flows) that suddenly
166 change to a massive, poorly sorted, lithic-rich breccia deposit (1–4 m) with poorly
167 vesiculated bombs (Fig. 4). The succession continues from 4–11 m with a sequence of
168 bomb-rich deposits (Figs. 4 and 5c), alternating with massive, poorly sorted, lithic-rich
169 deposits (Figs. 4 and 5d). The next deposit is about 0.5 m thick, has an erosive base, and
170 is made up of coarse lapilli and bombs with a peculiar yellow colour. The rest of the
171 first half of the succession (11–22 m) consists of thick, massive, poorly sorted, lithic-
172 rich (lava and ignimbrite clasts) breccia deposits without any visible depositional
173 structures (Fig. 4). A marked unconformity indicates a change in the type of deposits in
174 the second half of the succession (Figs. 4 and 5a,b), which is characterised by a
175 continuous alternation of thick, coarse well sorted lapilli-sized breccia layers with
176 accidental lithics and non-vesiculated (juvenile) scoria and fine and coarse lapilli layers
177 with planar stratification (Fig. 4).

178 *Western Craters*

179 Stratigraphic logs 2–6 were taken around the crater of Lago Escondido, the
180 easternmost edifice of the Western Craters (h,i Figs. 3b and 5f). All stratigraphic logs
181 show a similar succession, mainly characterised by thick, massive, poorly sorted, lithic-
182 rich (ignimbrites and lava clasts) breccia with some levels of poorly sorted coarse lapilli
183 with weak lamination (Figs. 4 and 5g,h). The thickness of the sequence varies from
184 about 6 m in stratigraphic log 2 to less than 15 m in stratigraphic log 6 (Fig. 4). A little
185 stratification can be identified in some of the deposits (stratigraphic log 2; Fig. 4), as
186 well as enrichment by scoria bombs (Fig. 5i). A general increase in the content of lithic

187 clasts and grain size is observed in the uppermost deposits (Figs. 4 and 5j).

188 *Distribution of ash-fall deposits*

189 All vents were located in the northern part of the island and the ejecta were
190 mostly carried northwards. Ash-fall was restricted to the northern sector of the island
191 between the central part of Kendall Terrace and Pendulum Cove (Fig. 2a). No evidence
192 of ash was found on Mont Kirkwood. A considerable amount of the ash fell beyond
193 Deception Island, as shown in Figure 2b. Approximately 4 mm of fine ash fell on
194 Arturo Prat station, Greenwich Island, and about 1 mm on Bellingshausen station, King
195 George Island (Baker & McReath 1975). As shown in Figure 2b, variations in thickness
196 and distribution are consistent with a northeastward pattern of isopachs that extends
197 along the axis of the South Shetland Islands under the influence of a southwesterly
198 wind, which carried part of the material into the Bransfield Strait (Baker & McReath
199 1971, 1975).

200 *Grain size, modal variation and clast distribution*

201 Vertical variations in the grain size distribution and modal variations were
202 analysed by selecting representative samples from both the coarse- and fine-grained
203 layers (Fig. 4 and Supp. Material). The vertical variation of maximum clast sizes
204 (bombs and blocks) is shown in Figure 4. At stratigraphic log 1 there is a dominance of
205 coarse deposits in the lower part with a general decrease in grain size throughout the
206 succession. The Median Diameter ($Md\phi$) values of all samples range from -2.9 to -0.15,
207 while Sorting ($\sigma\phi$) values range from 1.08 to 3.76 (Fig. 6a). Deposits from the lowest
208 part of the succession are poorly sorted compared to the deposits from the upper part,
209 which are generally finer grained. Skewness ($\alpha\phi$) varies from 0.27 to -0.75 (Fig. 6d). In
210 the general trend of the lithic clast distribution (Fig. 4), the lowest part of the succession
211 has the largest proportion of blocks, which can measure up to 60 cm.

212 Stratigraphic logs 2–6 have similar successions. A dominance of coarse deposits
213 is observable in all the stratigraphic logs, with just an occasional slight decrease in grain
214 size corresponding to coarse and fine lapilli layers. The Median Diameter ($Md\phi$) values
215 of the all samples range from -3.11 to -0.018, while Sorting ($\sigma\phi$) values range from 1.75
216 to 3.52 (Fig. 6a); the deposits are generally poorly sorted. Skewness ($\alpha\phi$) varies from
217 0.34 to -1.96 (Fig. 6d). Maximum clast size reaches 60 cm except in the upper part of
218 the succession, where a general increase of up to several decimetres is observed (Fig.
219 4).

220 Median Diameter and Sorting were used to compare the deposits with the
221 diagrams proposed by Walker (1971) (Fig. 6b) and Houghton *et al.* (2000) (Fig. 6c).
222 The former demonstrates how most of the deposits fell inside the fallout and surge
223 fields, while the latter show deposits that are scattered over the phreatomagmatic and
224 the magmatic/phreatomagmatic fields. The final two diagrams (Figs. 6d,e) illustrate the
225 grain size distribution of the samples shown in Figure 4 and highlight the fact that the
226 most representative classes range from 0ϕ to -3ϕ .

227 An isopleth map from close to the eruptive centres is given (Fig. 7). The size
228 values recorded on this map represent an average of the three axes of the largest clasts
229 from any given site. Clasts are made of juvenile fragments and accidental lithics (grey
230 aphyric lava, yellow and greenish tuff and reddish vesicular lava). Some of the lithic
231 clasts related to the western craters that are shown in Figure 7d might have been
232 affected by re-distribution by streams and mudflows resulting from the unusual seasonal
233 melt on Deception Island during the 1970–71 summer, as described in Baker &
234 McReath (1975). An isolated area of relatively large bombs between Cross Hill and
235 Wensleydale Beacon with no traces of a source crater was reported by Baker &
236 McReath (1975). These bombs were probably discharged from another eruptive vent, as

237 shown in Figure 7a. A preliminary isopleth map for the distal deposits (Fig. 7e) was
238 obtained from data reported in Pallàs *et al.* (2001), Fretzdorff & Smellie (2002) and
239 Geyer *et al.* (2006, 2008). Further data were taken from Hodgson *et al.* (1998), who
240 reported an ash layer in a core from Midge Lake (Livingstone Island). Hodgson *et al.*
241 (1998) suggest that this horizon might correspond to any of the documented eruptions
242 on Deception Island (1967, 1969 or 1970) or to the earlier eruptions that occurred in
243 1842 and 1912–17. However, the reported dispersal area of the 1967 and 1969 eruptions
244 (Baker & McReath 1975, Smellie 2002) and the shallow position in the core of this ash
245 layer suggest that this horizon belongs to the 1970 eruption, although the 1842 and
246 1912-1917 episodes, which are only mentioned briefly in Wilkes (1845), Orheim
247 (1971c) and Roobol (1973, 1980, 1982), cannot be ruled out as possible origins.

248 *Componentry analysis*

249 The products of the 1970 eruption consist of a mixture of dense, black or
250 vesicular scoria of basaltic andesitic composition with differing proportions of
251 accidental lithic clasts (older lava flows and yellow and greenish tuff) (Fig. 4).
252 Variations in the occurrence of the lithic fragments can be seen in the stratigraphic
253 succession, as well as in the different groups of craters. As observed in Fig. 4 and
254 supplementary materials, the lava clasts are the most abundant accessory components in
255 the successions in both groups of craters. In the Lago Escondido edifice, the lava clasts
256 are particularly dominant in the lower part of the succession (e.g. samples 4-A4, 4-A5,
257 4-B1, 4-C1, 4-E2, 4-E6; Fig. 4) and also characterise the whole succession in
258 stratigraphic log 1 (Fig. 4). Greenish and yellow tuff clasts are typically present in
259 smaller number and in general are found in the lower part of stratigraphic log 1 (e.g.
260 samples 3-A1; Fig. 4) and in the upper part of the sequence from Lago Escondido (e.g.
261 samples 4-E7, 4-F5; Fig. 4).

262 Generally, accidental lithic clasts increase in percentage in the size range -4 to
263 -3 (Fig. 4). Small variations in the amount of juvenile components can be observed
264 throughout the first outcrop, where samples range around 90%. The second group of
265 craters shows a general decrease in the amount of juvenile components of up to 70–80%
266 (Fig. 4).

267 **Discussion**

268 Despite the limited number of exposures that we were able to study, we
269 managed to establish one stratigraphic log from the Eastern Craters (stratigraphic log 1;
270 Fig. 4) and five from the Western Craters from around the same vent area (Lago
271 Escondido Edifice) (stratigraphic logs 2-6; Fig. 4). We believe that all are representative
272 of the general succession of deposits formed by the 1970 eruption and its dynamics.

273 This eruption seems to have been continuous, as suggested by the absence of
274 discontinuities in the stratigraphic sequences, and was totally pyroclastic (magmatic and
275 hydrovolcanic) with no lava flow. The location of the craters along one of the main
276 structural limits of the caldera (see Martí *et al.* 2013) suggests that caldera faults fed the
277 eruption. Several vents opened during the eruption and generated different types of
278 craters and cones with contrasting eruptive styles.

279 The Eastern Craters near Goddard Hill contrast with the western group at
280 Telefon Bay that consist of maar-like craters. As suggested by Sohn (1996), the
281 morphology of edifices might be controlled by depositional processes; nevertheless,
282 morphology will also depend on the physical properties of the surrounding bedrock,
283 vent geometry and the water/magma ratio (Kokelaar 1986; Sohn 1996; Vespermann &
284 Schmincke 2000; White & Houghton 2000). The lithological and sedimentological
285 characteristics of the deposits forming the stratigraphic succession in the eastern cones
286 reveal that the lowest part corresponds to deposits formed from base-surge-type

287 explosions (e.g. Crowe & Fisher 1973; Fisher & Waters 1970; Druitt 1998). The high
288 degree of fragmentation of these deposits suggests a phreatomagmatic phase with
289 optimal magma–water energy transfer. The locus of the explosion was probably located
290 at the limit between the shield and the syn-caldera deposits (Fig. 8a-1) due to the
291 presence of both types of rocks as accessory lithic clasts in these deposits (sample 3-A1;
292 Fig. 4). This episode was followed by the deposition of poorly sorted fallout breccia
293 deposits. The nature of the lithic clasts in these breccia deposits, which mostly
294 correspond to shield-derived lava fragments and syn-caldera ignimbrites, suggest that at
295 this stage the locus of the eruption was located in a part of the shield structure that was
296 below the syn-caldera deposits (Fig. 8a2). A strong unconformity (Figs. 4 and 5a,b)
297 marks the transition towards the upper part of the succession dominated by alternating
298 thick, coarse, well-sorted lapilli-sized breccia layers with fine and coarse lapilli layers
299 with planar stratification, indicating the existence of continuous changes in the
300 efficiency of the hydromagmatic fragmentation. The presence of a strong unconformity
301 that also coincides with a change in the layer dip suggests a shift in the locus of the
302 explosions and a variation in the eruptive rate (e.g. Valentine and Fisher, 2000); the
303 lower part of the succession could belong to crater c and the upper part to crater d (Fig.
304 2). Water could have been drawn into the conduit due to a fractured aquifer and/or to
305 the melting of the surrounding ice-cap as a consequence of the eruption itself.

306 Unlike the craters near Goddard Hill, the activity in the western part started with
307 a very shallow submarine eruption (Fig. 8b1) (as deduced by the actual position of the
308 coast line compared to the 1969 coastline; see Shultz 1972; Baker & McReath 1975)
309 and then evolved into a subaerial phase (Fig. 8b2,b3), leading to the formation of a new
310 strip of land about 1,700-m long, 400-m wide and 12 m a.s.l. The 1970 activity caused
311 the partial destruction of the island that had formed in 1967 in Telefon Bay, which was

312 truncated at its northeastern and southwestern ends (Baker & McReath 1975). The
313 stratigraphic logs (2–6; Fig. 4) studied in this sector were all located around the same
314 vent area (Lago Escondido) whose morphology indicates the presence of two partially
315 coalesced craters. The succession of deposits observed in all of these craters is very
316 similar and is mainly characterised by breccia deposits with almost no evidence of
317 depositional structures. Stratigraphic logs 2 and 4 (Fig. 4) reveal the presence at the
318 base of the breccia deposits of a lithic-poor episode (Sample 4-A1; Fig. 4), which might
319 correspond to the first submarine and less explosive phase of the eruption (Fig. 8b1).
320 Stratigraphic log 6 (Fig. 4) has a uniform succession of breccia deposits and subordinate
321 fine lapilli deposits emplaced by pyroclastic surges, above all in the upper part of the
322 sequence (Fig. 4). The lithic content suggests an initial interaction with shallower lava
323 flows, probably emplaced from the post-caldera phase (e.g. samples A4, 4-A5, 4-B1, 4-
324 C1, 4-E2, 4-E6; Fig. 4) (Fig. 8b2), with a change in the upper part of the sequence
325 characterised by an increase in the number of yellow tuff lithic clasts (e.g. samples 4-
326 E7, 4-F5; Fig. 4) in both craters. A progressive lowering of the position of the
327 fragmentation level in the eruption conduit during the course of the eruption might have
328 led the magma to interact with a deeper part of the basement made of syn-caldera
329 yellow tuff (Fig. 8b3).

330 On the basis of the available field data, a preliminary quantitative evaluation of
331 the eruptive parameters can be attempted. Thickness and maximum lithic clast size
332 measurements enable us to obtain the isopach and isopleth maps for the 1970 eruption.
333 The minimum associated volume of the eruption was calculated using the isopach map
334 defined by Baker & McReath (1975) and Smellie (2002). Volume calculations were
335 carried out using the method proposed by Pyle (1989) that considers elliptical isopachs
336 and an exponential decay.

337 Violent mafic eruptions described in the literature produce volumes of 0.001 to
338 $>1 \text{ km}^3$ DRE and dispersal areas covering 10 to $>500 \text{ km}^2$ (see Wong & Larsen 2010).
339 The 1970 eruption is characterised by an estimated total bulk volume of less than 0.1
340 km^3 and a dispersal area of about $4 \times 10^3 \text{ km}^2$ (Fig. 2), calculated using the isopachs
341 extrapolated from the data collected at the Arturo Pratt and Bellingshausen stations and
342 data from sea-cores in the Central Bransfield Basin reported by Fretzdorff & Smellie
343 (2002). These authors found a correspondence for an ash layer with volcanic ash dating
344 from the 1970 eruption. Deposits from the 1970 eruptions have also been reported in
345 ice-cores from Livingston Island (Pallàs *et al.* 2001; Geyer *et al.* 2006, 2008).

346 Following the methods proposed by Carey and Sparks (1986) and in comparison
347 with the 1967 eruption, we can infer a column height of about 10 km. Wind velocities
348 for August 1970 were calculated using data from the Bellingshausen stations on King
349 George Island (http://www.antarctica.ac.uk/met/READER/upper_air/uawind.html) with
350 approximate values of 28–38 m/s at heights of 5,500 and 9,100 m, which confirms that
351 the deposits were strongly affected by wind during deposition.

352 The wide dispersion of deposits could also be explained by the height of the
353 tropopause above Antarctica, which is unusually low and in the range 8–10 km (Weyant
354 1966); additionally, the stratosphere here is much less stratified than in the tropics or at
355 mid-latitudes. This would allow for the rapid and widespread distribution of tephra in
356 the area (Kyle *et al.* 1981) and even permit small eruptions to inject material into the
357 stratosphere. This could also explain the generally coarse grain size character of
358 proximal deposits, which are probably fines depleted as shown in Figs. 4 and 6e,f.

359 The 1970 eruption was undoubtedly one of the most violent in the past century
360 on Deception Island and falls in the category of violent Strombolian (Wong & Larsen,
361 (2010) and corresponds to a VEI 3 of Newhall and Self (1982).

362 This eruption occurred in shallow seawater and at onshore ice-free locations, in
363 the same general area as the 1967 eruption but with more widely distributed vents. The
364 1967 episode was very similar in nature and size to the 1970 eruption and generated
365 submarine and land vents. Three overlapping pyroclastic cones (Fig. 3) with water-
366 filled craters were created in the northwestern corner of Telefon Bay, while a further
367 centre was located 2 km east of the new island on the shore of Port Foster between
368 Telefon Bay and Pendulum Cove (Fig. 3). The eruption has been reported in detail by
369 Roobol *et al.* (1975), who described a column height of about 2.5 km at the beginning
370 of the eruption, rising to 6 km and then reaching a maximum height of about 10 km.
371 The wind speed was less than 10 m/s (Valenzuela *et. al* 1968). As reported in Roobol *et*
372 *al.* (1975), a thin covering of ash was noted on Livingstone Island and probably on
373 Greenwich Island as well. An ash-coated iceberg was reported close to Elephant Island,
374 which is about 200 km to the northeast of Deception Island.

375 On Deception Island, eruptions of high explosivity due to magma/water
376 interaction are common and are characterised by shallow submarine vents or are located
377 on waterlogged shorelines or beneath the ice caps. The 1967 and 1970 eruptions
378 demonstrate that similar explosive events are controlled differentially by the physical
379 nature of the vent and the way in which the magma interacts with the surrounding
380 environment, leading to several closely spaced episodes with different characteristics
381 and associated hazards. Although there were 42 men in the British and Chilean stations
382 and more in the Argentinian station during the 1967 eruption, no lives were lost
383 (Roobol 1982), even though some of the installations were destroyed. Despite the lack
384 of witnesses to the 1970 eruption (Baker & McReath 1975), its characteristics, deduced
385 from the study of its deposits, suggest a similar or even larger event than that of 1967,
386 but with similar associated hazards.

387 The Bay of Port Foster has traditionally been used as a natural harbour by sailors
388 and, in particular, by whalers who installed the factory in Whaler's Bay that was
389 destroyed during the 1969 eruption (Smellie 2002). Scientific bases were built by
390 Argentina, UK and Chile around Port Foster, the latter two being destroyed by the 1967
391 and 1969 eruptions (Roobol 1982). Currently, a Spanish and an Argentinian base (Fig.
392 1) operate during the Antarctic summer seasons. The island has also become an
393 important tourist attraction and was visited by almost 50,000 people in 2004–2010, with
394 annual peaks of 10,000 visitors (IAATO, *International Association of Antarctica Tour*
395 *Operators*). Thus, the volcanic risk is increasing given the high probability of an
396 eruption in the near future. The characteristics of the 1970 and 1967 eruptions suggest
397 that a future eruption could have a considerable impact on the people and installations
398 on Deception Island, particularly if it occurs during the austral summer. Therefore, a
399 detailed reconstruction of past eruptions, as we have attempted in the present study, are
400 a necessary first step in a hazard assessment aimed at reducing the volcanic risk on
401 Deception Island.

402 **Conclusion**

403 The study of the stratigraphy, lithology and sedimentological features of the
404 eruption of 1970 on Deception Island enables us to reconstruct its eruptive dynamics
405 and main physical parameters. The eruption occurred close to the area of 1967 vents, in
406 shallow seawater and at onshore ice-free locations, and led to the formation of two
407 groups of craters – one with cone-shaped and the other with maar-like craters – that
408 reveal the differing nature of these two eruptions. The 1970 eruption alternated
409 magmatic and hydrovolcanic episodes that deposited fallout, ballistic blocks and bombs
410 and pyroclastic surges. A total bulk volume of less than 0.1 km³ has been estimated for
411 this eruption, and its tephra deposits dispersed northeastwards as far as King George

412 Island, >150 km away. This explosive episode is classified as violent Strombolian and
413 VEI 3, and produced a plume up to 10 km above sea level in height. The 1970 eruption
414 was similar to the 1967 episode and confirms how this type of post-caldera volcanism
415 on Deception Island is controlled by the location of the vents and magma interaction
416 with the surrounding environment. This could give rise to closely spaced eruptions or
417 even several episodes during the same eruptive event, with different characteristics and
418 associated hazards. A similar eruption occurring in the future on Deception Island might
419 represent a serious hazard to the increasing number of people that visit during certain
420 periods of the year and to the scientific installations that operate there.

421 **Acknowledgments**

422 This research was supported by the MICINN grant CTM2011-13578-E. AG is grateful
423 for her Juan de la Cierva Grant (JCI-2010-06092). We would like to thank all the
424 military staff from the Spanish Antarctic Base Gabriel de Castilla for their constant help
425 and for the logistic support, without which this research would not have been possible.
426 The English text was corrected by Michael Lockwood.

427 **References**

- 428 Ashcroft, W. 1972. Crustal structure of the South Shetland Islands and Bransfield Strait,
429 1st edn. *British Antarctic Survey, London*, 43 p., 41 fold. leaf p.
- 430 Baker, P., McReath, I., Harvey, M., Roobol, M. & Davies, T. 1975. The geology of the
431 South Shetland Islands: volcanic evolution of Deception Island. *British Antarctic Survey*
432 *Scientific Reports*, 78, 81 pp.
- 433 Baker, P.E. & McReath, I. 1971. Geological investigations on Deception Island.
434 *Antarctic Journal of the United States*, 6, 85-86.

435 Baker, P.E. & McReath, I. 1975. The 1970 eruption. In: *Baker P, McReath I, Harvey M,*
436 *Roobol M, Davies T (1975) The geology of the South Shetland Islands: volcanic*
437 *evolution of Deception Island*, British Antarctic Survey Scientific Reports 52-61.

438 Barclay, A.H., Wilcock, W.S.D. & Ibáñez, J.M. 2009. Bathymetric constraints on the
439 tectonic and volcanic evolution of Deception Island Volcano, South Shetland Islands.
440 *Antarctic Science*, 21, 153-167, doi: doi:10.1017/S0954102008001673.

441 Carey, S. & Sparks, R.S.J. 1986. Quantitative models of the fallout and dispersal of
442 tephra from volcanic eruption columns. *Bulletin of Volcanology*, 48, 109-125, doi:
443 10.1007/bf01046546.

444 Crowe, B.M. & Fisher, R.V. 1973. Sedimentary Structures in Base-Surge Deposits with
445 Special Reference to Cross-Bedding, Ubehebe Craters, Death Valley, California.
446 *Geological Society of America Bulletin*, 84, 663-682, doi: 10.1130/0016-
447 7606(1973)84<663:ssibdw>2.0.co;2.

448 Dalziel, I.W.D. 1984. Tectonic evolution of a forearc terrane, southern Scotia Ridge,
449 Antarctica. *Geological Society of America Special Papers*, 200, 1-32, doi:
450 10.1130/SPE200-p1.

451 Druitt, T.H. 1998. Pyroclastic density currents. In: *Gilbert, J.S., Sparks, R.S.J. (Eds.),*
452 *The Physics of Explosive Volcanic Eruptions. Geological Society, Spec. Publ.*, 145, 145-
453 182.

454 Fisher, R. & Waters, A. 1970. Base surge bed forms in maar volcanoes. *American*
455 *Journal of Science*, 268 157-180.

456 Fretzdorff, S. & Smellie, J.L. 2002. Electron microprobe characterization of ash layers
457 in sediments from the central Bransfield basin (Antarctic Peninsula): evidence for at
458 least two volcanic sources. *Antarctic Science*, 14, 412-421, doi:
459 doi:10.1017/S0954102002000214.

460 Geyer, A., Casas, J.M., Pallàs, R. & Gimeno, D. 2008. Chemical and physical
461 characterization of tephra layers from Livingston Island (Antarctica): ice drill data.
462 *Geotemas, VII Congreso Geológico de España*, vol 10, pp. 216.

463 Geyer, A., Casas, J.M., Pallàs, R., Gimeno, D. & Calvet, J. 2006. Chemical and physical
464 characterization of tephra layers from Livingston Island (Antarctica): ice drill data and
465 methodological considerations. *VII Simposio español de estudios polares*, Granada,
466 University of Granada

467 González-Ferrán, O., Munizafa, F. & Moreno, H. 1971. Síntesis de la evolución
468 volcánica de Isla Decepción y la erupción de 1970. *Instituto Antártico Chileno, Serie*
469 *Científicas*, 2, 1-14.

470 Gràcia, E., Canals, M., Lí Farràn, M., José Prieto, M., Sorribas, J. & Team, G. 1996.
471 Morphostructure and evolution of the central and Eastern Bransfield Basins (NW
472 Antarctic Peninsula). *Marine Geophysical Researches*, 18, 429-448, doi:
473 10.1007/bf00286088.

474 Grad, M., Guterch, A. & Sroda, P. 1992. Upper crustal structure of Deception Island
475 area, Bransfield Strait, West Antarctica. *Antarctic Science*, 4, 469-476, doi:
476 doi:10.1017/S0954102092000683.

477 Hodgson, A.D., Dyson, C.L., Jones, V.J. & Smellie, J.L. 1998. Tephra analysis of
478 sediments from Midge Lake (South Shetland Islands) and Sombre Lake (South Orkney
479 Islands), Antarctica. *Antarctic Science*, 10, 13-20.

480 Houghton, B.F., Wilson, C.J.N. & Pyle, D.L. 2000. Pyroclastic fall deposits. In:
481 *Sigurdsson, H., Houghton, B.F., McNutt, S.R., Rymer, H., Stix, J. (Eds.), Encyclopedia*
482 *of Volcanoes. Academic Press*, 555-570.

483 Ibáñez, J.M., Almendros, J., Carmona, E., Nuñez-Arévalo, C. & Abril, M. 2003. The
484 recent seismo-volcanic activity at Deception Island volcano. *Deep Sea Research Part II:*

485 *Topical Studies in Oceanography*, 50, 1611-1629, doi: <http://dx.doi.org/10.1016/S0967->
486 0645(03)00082-1.

487 Jeffers, J. & Anderson, J. 1990. Sequence stratigraphy of the Bransfield Basin,
488 Antarctica: implications for tectonic history and hydrocarbon potential. In: *St. John B*
489 *(ed) Antarctica as an exploration frontier: hydrocarbon potential, geology and hazards.*
490 *Am Ass Petrol Geol Stud Geol* 31:13–29.

491 Kokelaar, P. 1986. Magma-water interactions in subaqueous and emergent basaltic
492 volcanism. *Bulletin of Volcanology*, 48, 275-289.

493 Kyle, P.R., Jezek, P.A., Mosley-Thompson, E. & Thompson, L.G. 1981. Tephra layers
494 in the Byrd Station ice core and the Dome C ice core, Antarctica and their climatic
495 importance. *Journal of Volcanology and Geothermal Research*, 11, 29-39, doi:
496 [http://dx.doi.org/10.1016/0377-0273\(81\)90073-1](http://dx.doi.org/10.1016/0377-0273(81)90073-1).

497 Martí, J., Geyer, A. & Aguirre-Diaz, G. 2013. Origin and evolution of the Deception
498 Island caldera (South Shetland Islands, Antarctica). *Bulletin of Volcanology*, 75, 1-18,
499 doi: 10.1007/s00445-013-0732-3.

500 Newhall, C.G. & Self, S. 1982. The volcanic explosivity index (VEI) an estimate of
501 explosive magnitude for historical volcanism. *Journal of Geophysical Research:*
502 *Oceans*, 87, 1231-1238, doi: 10.1029/JC087iC02p01231.

503 Orheim, O. 1971c. Volcanic activity on Deception Island, South Shetland Islands. In:
504 *ADIE, R. J., ed. Antarctic geology and geophysics. Oslo, Universitetsforlaget*, 117-120.

505 Pallàs, R., Smellie, J.L., Casas, J.M. & Calvet, J. 2001. Using tephrochronology to date
506 temperate ice: correlation between ice tephra on Livingston Island and eruptive units
507 on Deception Island volcano (South Shetland Islands, Antarctica). *The Holocene*, 11,
508 149-160, doi: 10.1191/095968301669281809.

509 Pyle, D. 1989. The thickness, volume and grainsize of tephra fall deposits. *Bulletin of*
510 *Volcanology*, 51, 1-15, doi: 10.1007/bf01086757.

511 Roobol, M.J. 1973. Historic volcanic activity at Deception Island. *British Antarctic*
512 *Survey Bulletin*, 32, 23-30.

513 Roobol, M.J. 1980. A model for the eruptive mechanism of Deception Island from 1820
514 to 1970. *British Antarctic Survey Bulletin*, 49, 137-156.

515 Roobol, M.J. 1982. The volcanic hazard at Deception Island, South Shetland Islands.
516 *British Antarctic Survey Bulletin*, 51
517 , 237-245.

518 Roobol, M.J., Davies, T.G. & Baker, P.E. 1975. The 1967 eruption. In: *Baker P,*
519 *McReath I, Harvey M, Roobol M, Davies T (1975) The geology of the South Shetland*
520 *Islands: volcanic evolution of Deception Island*, pp. 16-37.

521 Sheridan, M.F. & Wohletz, K.H. 1983. Hydrovolcanism: Basic considerations and
522 review. *Journal of Volcanology and Geothermal Research*, 17, 1-29, doi: 10.1016/0377-
523 0273(83)90060-4.

524 Shultz, C.H. 1972. Eruption at Deception Island, Antarctica, August 1970. *Geological*
525 *Society of America Bulletin*, 83, 2837-2842, doi: 10.1130/0016-
526 7606(1972)83[2837:eadiaa]2.0.co;2.

527 Smellie, J., Thomson, J. & Thomson, M. 2002. Geology and geomorphology of
528 Deception Island. *British Antarctic Survey, Cambridge*, 77p. + 73 folded maps.

529 Smellie, J.L. 1988 Recent observations on the volcanic history of Deception Island,
530 South Shetland Islands. *British Antarctic Survey Bulletin*, 81.

531 Smellie, J.L. 2001. Lithostratigraphy and volcanic evolution of Deception Island, South
532 Shetland Islands. *Antarctic Science*, 13, 188-209, doi:
533 doi:10.1017/S0954102001000281.

534 Smellie, J.L. 2002. The 1969 subglacial eruption on Deception Island (Antarctica):
535 events and processes during an eruption beneath a thin glacier and implications for
536 volcanic hazards. In: SMELLIE, J.L. and CHAPMAN, M.G., eds. *Volcano-ice*
537 *interaction on Earth and Mars. Geological Society, London, Special Publication, 202,*
538 *59- 79.*

539 Sohn, Y.K. 1996. Hydrovolcanic processes forming basaltic tuff rings and cones on Jeju
540 Island, Korea. *Geological Society of America Bulletin*, 108, 1199-1211.

541 Valencio, D.A., Mendía, J. & Vilas, J.F. 1979. Palaeomagnetism and KAr age of
542 Mesozoic and Cenozoic igneous rocks from Antarctica. *Earth and Planetary Science*
543 *Letters*, 45, 61-68, doi: [http://dx.doi.org/10.1016/0012-821X\(79\)90107-9](http://dx.doi.org/10.1016/0012-821X(79)90107-9).

544 Valentine, G.A. & Fisher, R.V. 2000. Pyroclastic surges and blasts. In: *Sigurdsson, H.,*
545 *Houghton, B.F., McNutt, S.R., Rymer, H., Stix, J. (Eds.), Encyclopedia of Volcanoes.*
546 *Academic Press, 571–580.*

547 Valenzuela, E., Chavez, L. & Munizaga, F. 1968. Informe preliminar sobre la erupcion
548 de Isla Decepcion ocurrida en diciembre de 1967. *Boletín Instituto Antártico Chileno*, 3,
549 5-16.

550 Vespermann, D. & Schmincke, H.U. 2000. Scoria cones and tuff rings. In: *H.*
551 *Sigurdsson, B.F. Houghton, S.R. McNutt, H. Rymer and J. Stix (Editors), Encyclopedia*
552 *of Volcanoes. Academic Press, San Diego, 683-694.*

553 Vuan, A., Robertson Maurice, S.D., Wiens, D.A. & Panza, G.F. 2005. Crustal and upper
554 mantle S-wave velocity structure beneath the Bransfield Strait (West Antarctica) from
555 regional surface wave tomography. *Tectonophysics*, 397, 241-259, doi:
556 <http://dx.doi.org/10.1016/j.tecto.2004.12.011>.

557 Walker, G.P.L. 1971. Grain size characteristics of pyroclastic deposits. *Journal of*
558 *Geology*, 79, 696-714.

559 Weyant, W.S. 1966. The Antarctic atmosphere: climatology of the troposphere and
560 lower stratosphere. *American Geographical Society Antarctic Map Folio Series*, Folio
561 4.

562 White, J.D.L. & Houghton, B. 2000. Surtseyan and related phreatomagmatic eruptions.
563 In: *Sigurdsson, H., Houghton, B.F., McNutt, S.R., Rymer H., Stix J. (Editors),*
564 *Encyclopedia of Volcanoes. Academic Press, San Diego*, 495-511.

565 Wilkes, C. 1845. Narrative of the United States Exploring Expedition, during the years
566 1838, 1839, 1840, 1841, 1842. I-V, Atlas.

567 Wong, L. & Larsen, J. 2010. The Middle Scoria sequence: A Holocene violent
568 strombolian, subplinian and phreatomagmatic eruption of Okmok volcano, Alaska.
569 *Bulletin of Volcanology*, 72, 17-31, doi: 10.1007/s00445-009-0301-y.

570 **Figure captions**

571 **Fig. 1.** (a) Simplified regional tectonic map and location of the South Shetland Islands
572 Archipelago (modified from Ibañez *et al.* 2003). HFZ-Hero Fracture Zone, SFZ-
573 Shetland Fracture Zone; (b) South Shetland Islands Archipelago and location of
574 Deception Island (modified from Grad *et al.* 1992); (c) Orthophotomap of Deception
575 Island (http://lagc.uca.es/web_lagc/orto.jpg)

576 **Fig. 2.** (a) Simplified geological map of Deception Island (modified from Martí *et al.*
577 2013) showing the isopachs (black dashed lines) in cm of the 1967 eruption (modified
578 from Baker & McReath 1975); (b) Isopachs (red dashed lines) in cm of the 1970
579 eruption in the Shetlands Archipelago (modified from Baker & McReath 1975). 1-
580 Permanent ice, 2-alluvium, moraine, beach and undifferentiated deposits, 3-(PCD) Post-
581 Caldera Deposits, 4-(OCTF) Outer Coast Tuff Formation, 5-(BSF) Basaltic Shield
582 Formation, 6-Sites of 1970 eruption, 7-isopachs of 1970 eruption, 8-Spanish Base, 9-
583 Argentinian Base, 10-abandoned Chilean Base, 11-abandoned British base.

584 **Fig. 3.** (a) Geological map of the northern part of Deception Island (modified from
585 Martí *et al.* 2013); (b) orthophotomap of the same area showing the extent of the
586 proximal deposits, as well as an anomalous zone of bombs probably indicating a hidden
587 vent south of Cross Hill. 1-Permanent ice, 2-alluvium, moraine, beach and
588 undifferentiated deposits, 3-(PCD) post-caldera deposits, 4-(OCTF) Outer Coast Tuff
589 Formation, 5-(BSF) Basaltic Shield Formation, 6-locus of the eruption, 7-extent of the
590 proximal deposits, 8-crater rims, 9-inferred crater rims, 10-1967 eruption crater rims,
591 11-crater numbers, 12- Sites of stratigraphic logs.

592 **Fig. 4.** Composite stratigraphic logs of the deposits and componentry analysis of the
593 most representative samples. Stratigraphic log 1 refers to the Eastern Craters, whilst
594 stratigraphic logs 2-6 are located around Lago Escondido. Vertical variations in grain
595 size and the maximum diameter of lithic and scoria clasts are also indicated. 1: Massive,
596 poorly sorted, lithic-rich breccia, 2: massive, poorly sorted, lithic-rich breccia with large
597 lithic ballistic ejecta, 3: pyroclastic surge deposits, 4: scoriae, 5: debris deposits, 6: ice,
598 7: beach deposits, 8: unconformity, 9: no componentry, 10: juveniles, 11: lava, 12:)
599 yellow tuff.

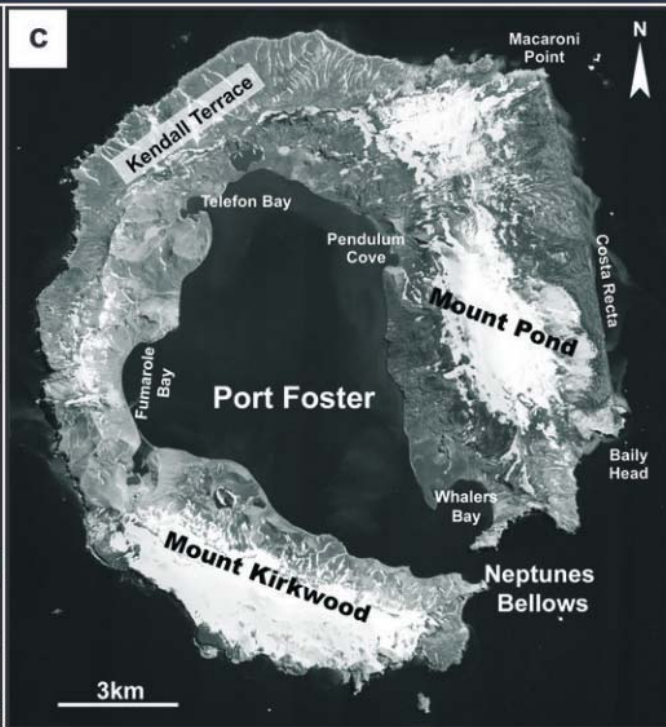
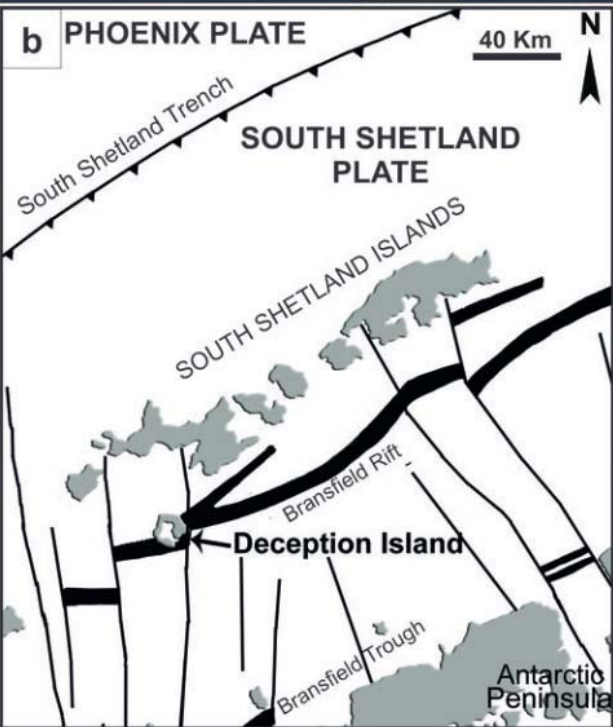
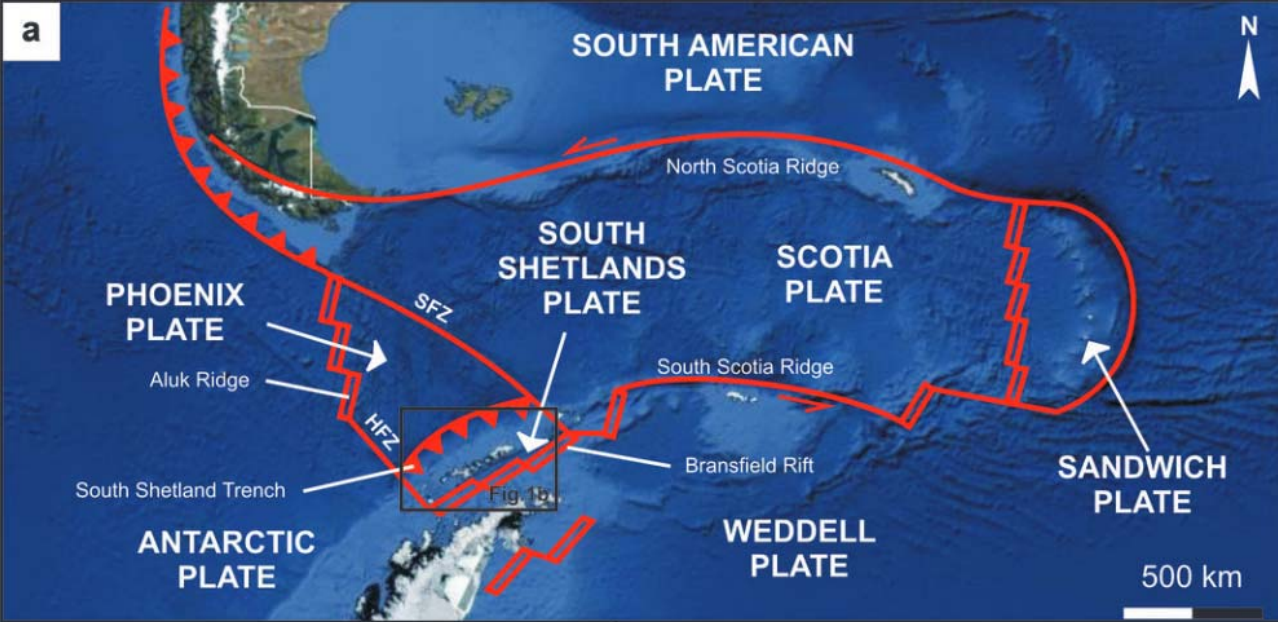
600 **Fig. 5.** Field photographs of the main stratigraphic logs: (a) general view of outcrop 1
601 showing the unconformity (dashed red line) in its highest part. Green and black dashed
602 lines indicate, respectively, the dip of the layers below and above the unconformity.
603 Yellow circle indicates the person used as a scale; (b) detailed view of outcrop 1. The
604 lower part is characterized mainly by massive deposits, whilst the upper part above the
605 unconformity (dashed red line) is constituted by alternating (black dashed lines) of
606 thick, coarse, lapilli-sized breccia layers and fine and coarse lapilli layers with planar
607 stratification; (c) example of bomb-enriched deposits; (d) typical massive lithic-rich
608 deposit; the scraper is about 15-cm long; (e) general view of the inner part of the

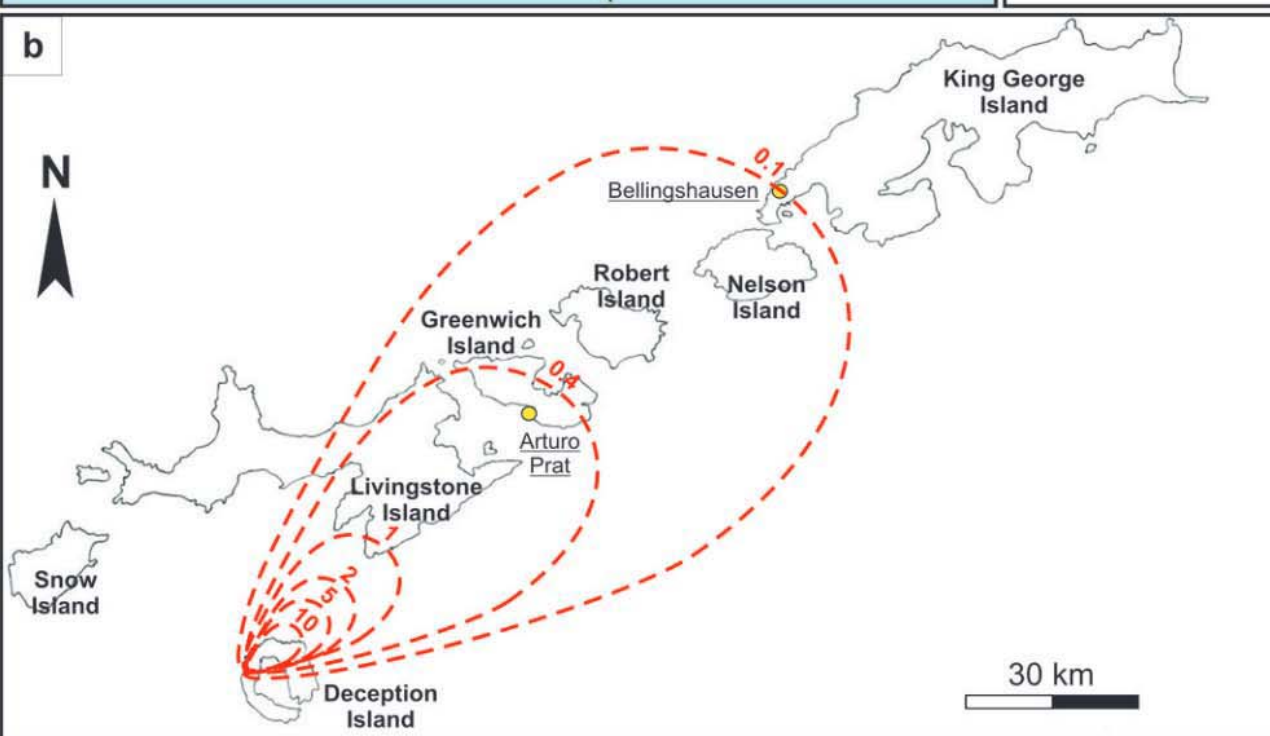
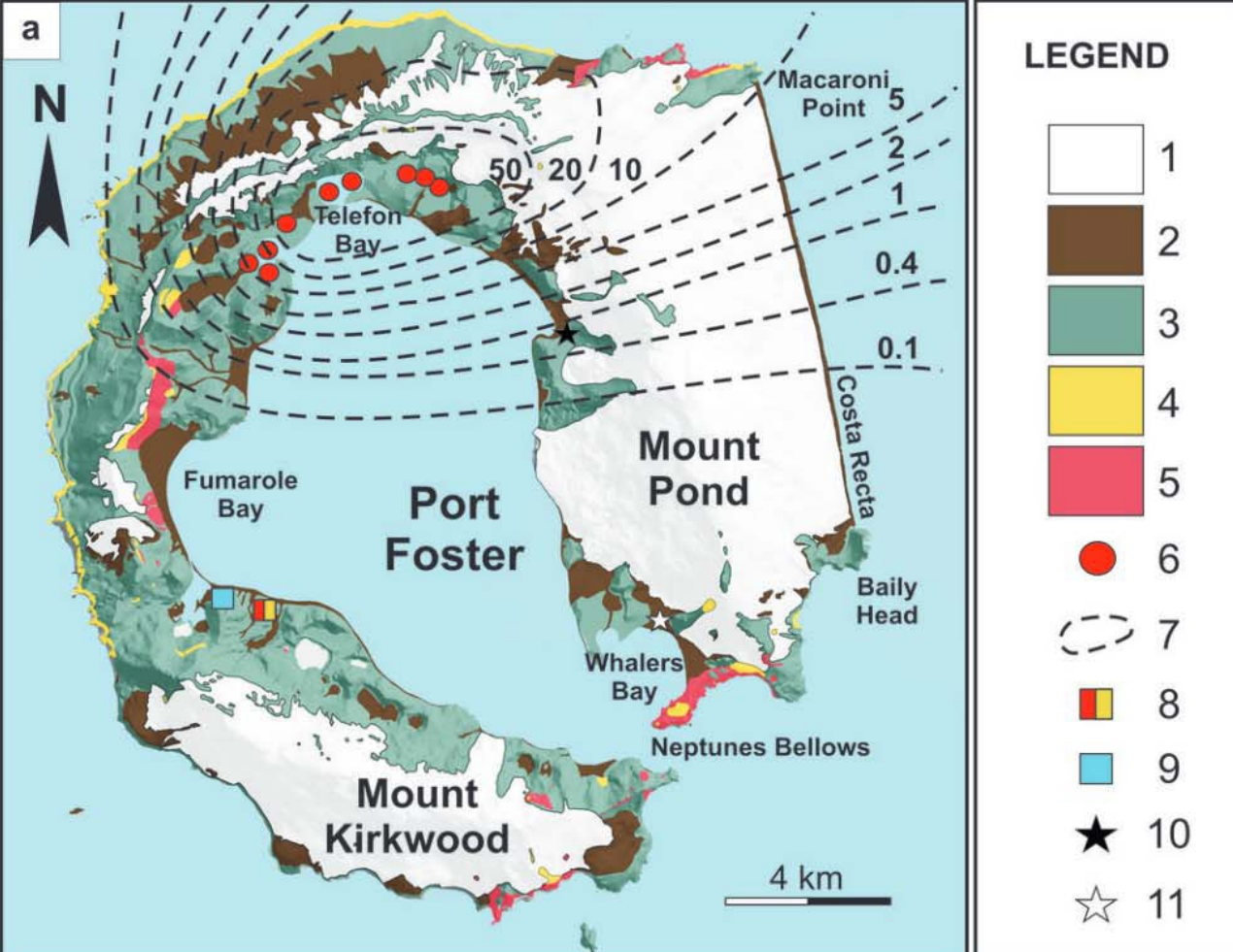
609 easternmost crater with a height of about 20 m in the background; (f) general view of
610 Lago Escondido; (g) typical outcrop consisting mainly of massive, unbedded and
611 subordinate fine lapilli deposits; the shovel is about 1-m long; (h) detail of a massive
612 deposits; the stick is 10-cm long; (i) bomb-rich deposit; (j) example of lithic close to
613 Lago Escondido Craters. L=lava, I=ignimbrite, S=scoria.

614 **Fig. 6.** Plot of grain-size data from the fall and surge deposits. (a) Sorting (σ) versus
615 Median Diameter (Md); (b) Sorting (σ) versus Median Diameter (Md) compared
616 with a Walker diagram (1971); (c) Houghton *et al.* (2000) diagram; (d) Sorting (σ)
617 versus Skewness (σ), granulometrical frequency distribution at (e) Eastern Craters and
618 (f) Western Craters.

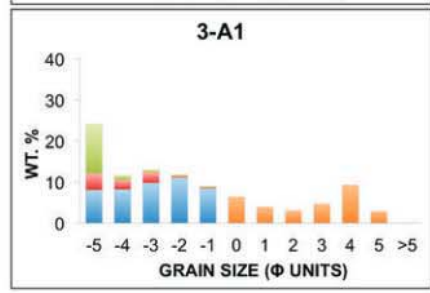
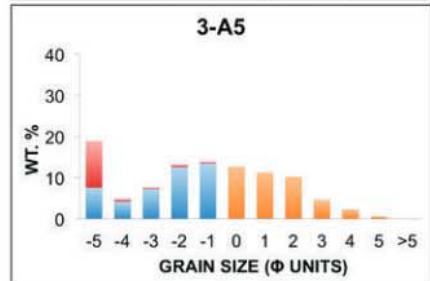
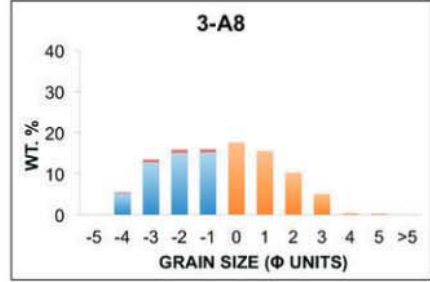
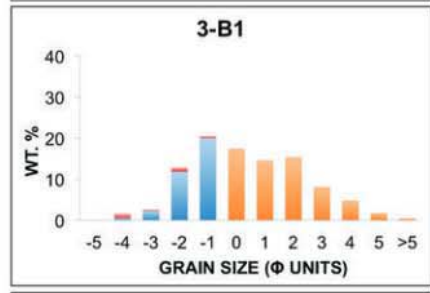
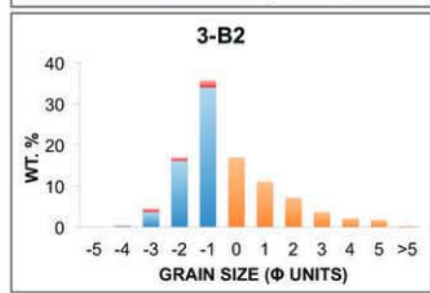
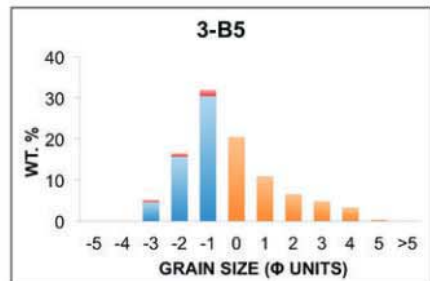
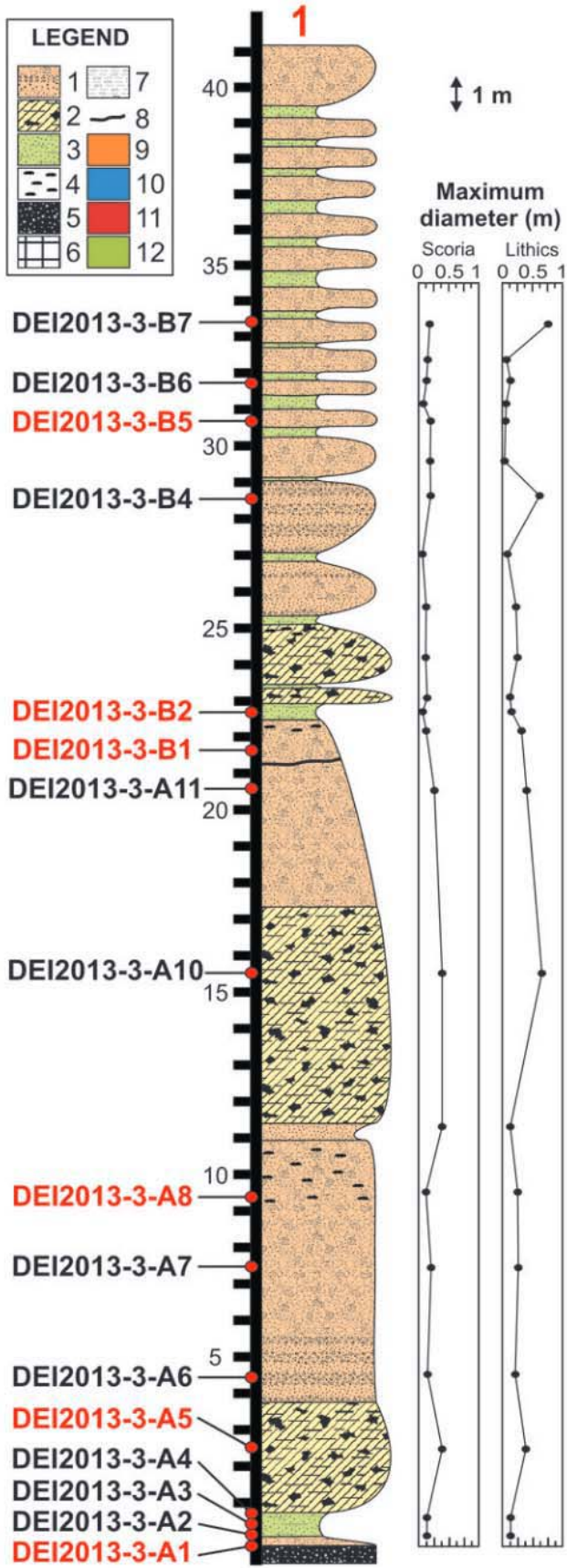
619 **Fig. 7** Proximal isopleth map in cm (white continuous line) showing the distribution of
620 lithics (a) south of Cross Hill; (b) Western Craters; (c) Western Craters-Lago
621 Escondido. The red continuous line represent the crater rims and the yellow continuous
622 lines the inferred crater rims; (d) Eastern Craters; (e) isopleth map in mm (red dashed
623 lines) in the Shetland Archipelago.

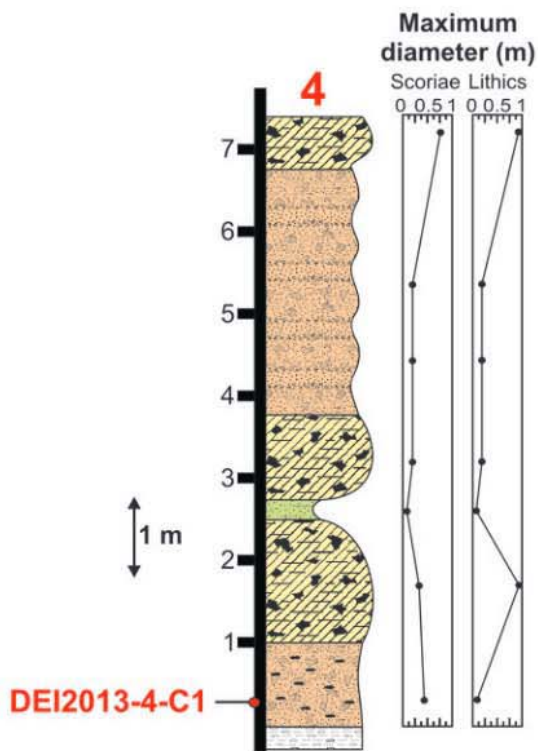
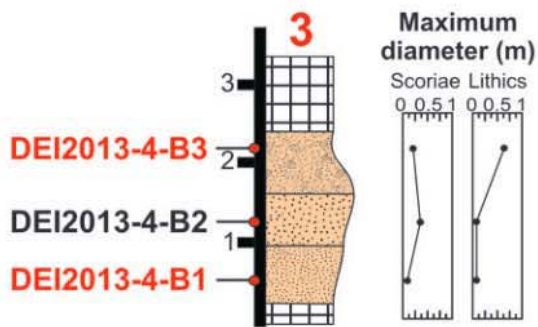
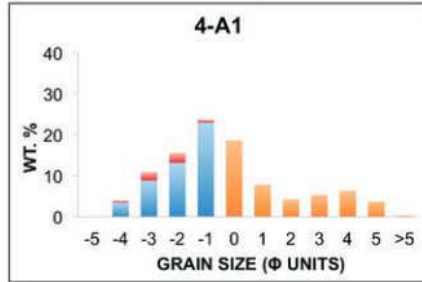
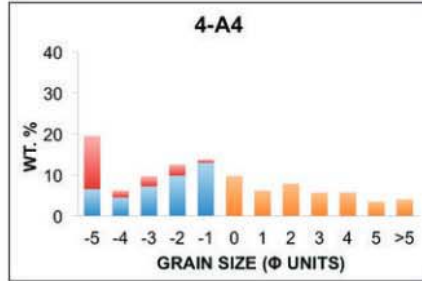
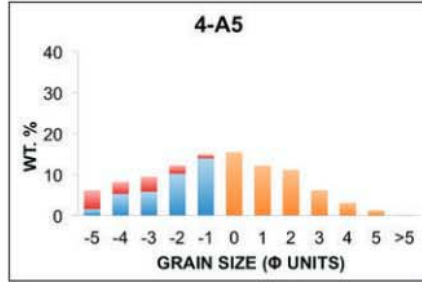
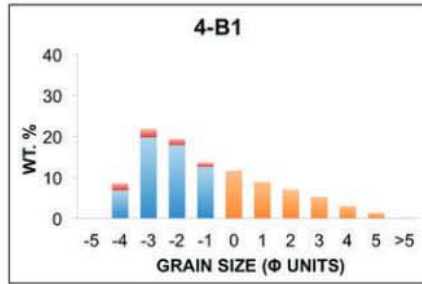
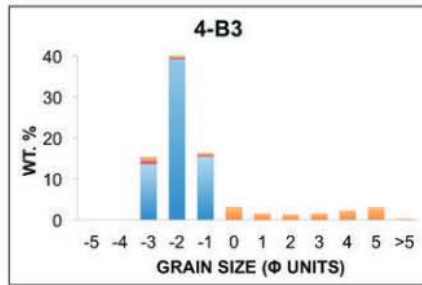
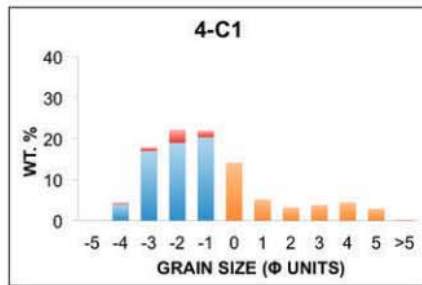
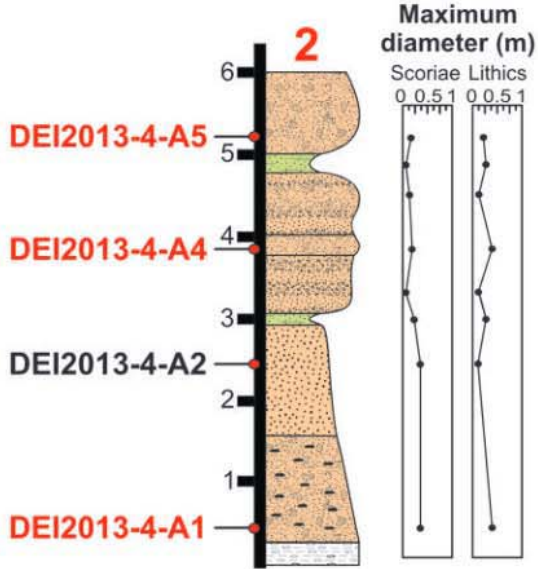
624 **Fig. 8** Sketch not to scale of the evolution of the 1970 eruption: Eastern Craters (a1) rise
625 of the magma and interaction with the syn-caldera deposits; (a2) decrease in the
626 fragmentation level and interaction with a deeper part of the pre-caldera deposits; Lago
627 Escondido (b1) interaction of the ascending magma with shallow marine water and
628 beginning of the eruption; (b2) hydrovolcanic activity due to the interaction with water
629 in the shallower post-caldera deposits; (b3) decrease in the fragmentation level in the
630 conduit and interaction with the basement made of syn-caldera deposits. 1) sea, 2)
631 breccia deposits, 3) volcanic deposits, 4) post-caldera deposits, 5) syn-caldera deposits,
632 6) pre-caldera deposits, 7) phreatomagmatic activity, 8) ballistic fallout, 9) fracture
633 zone, 10) infiltration area, 11) explosion locus, 12) dyke.

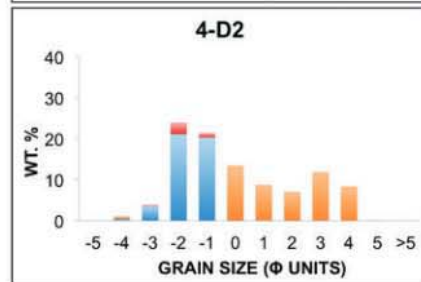
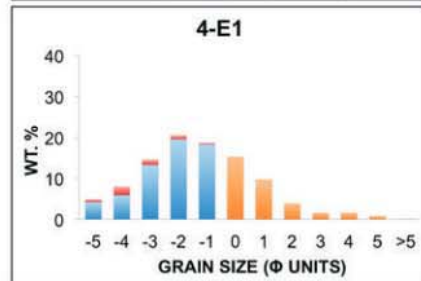
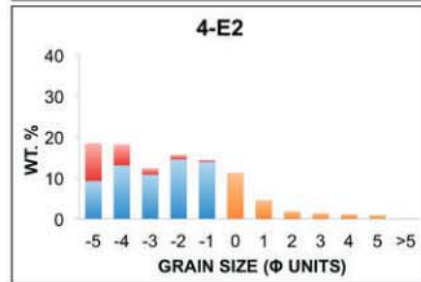
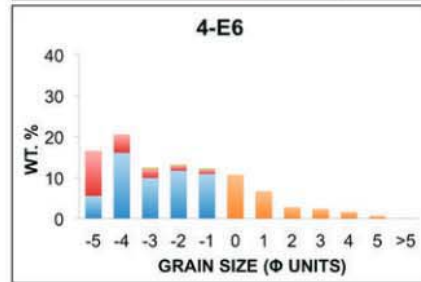
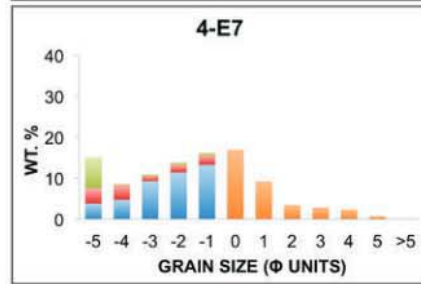
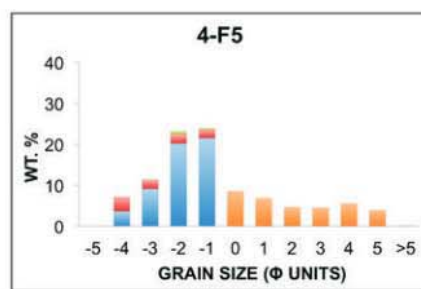
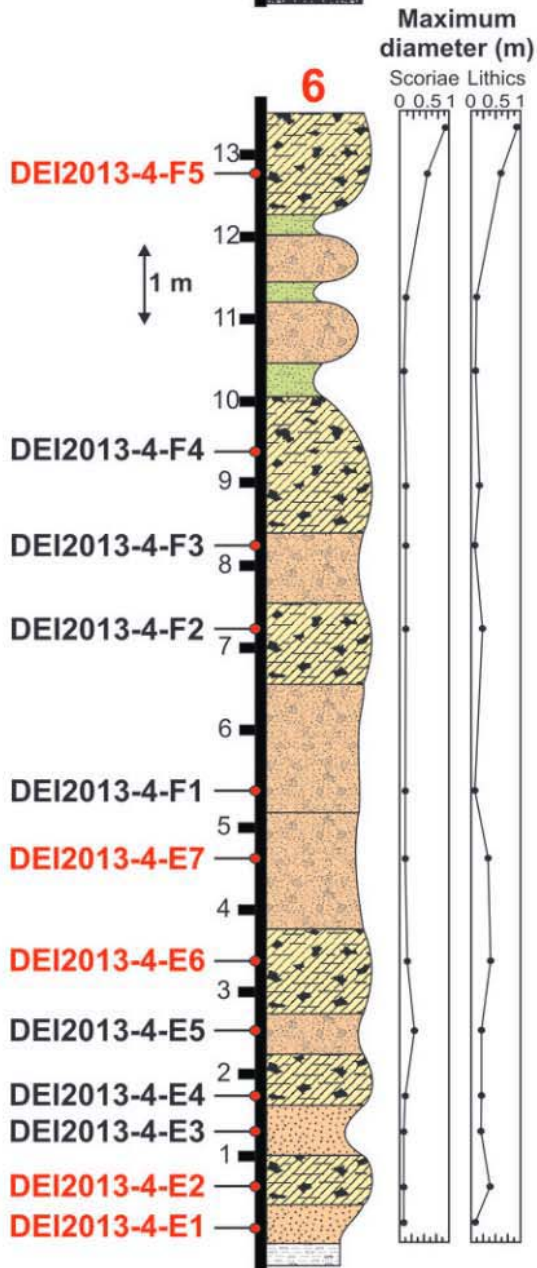
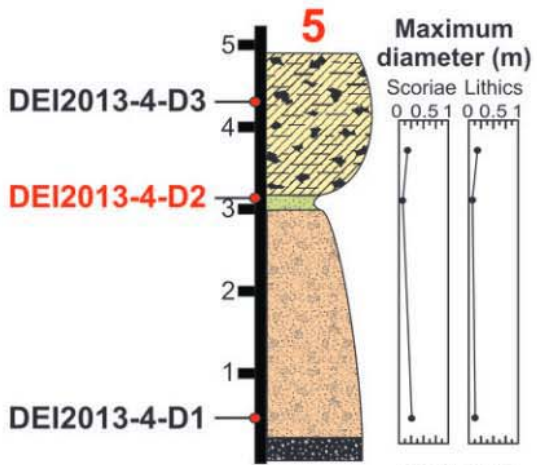


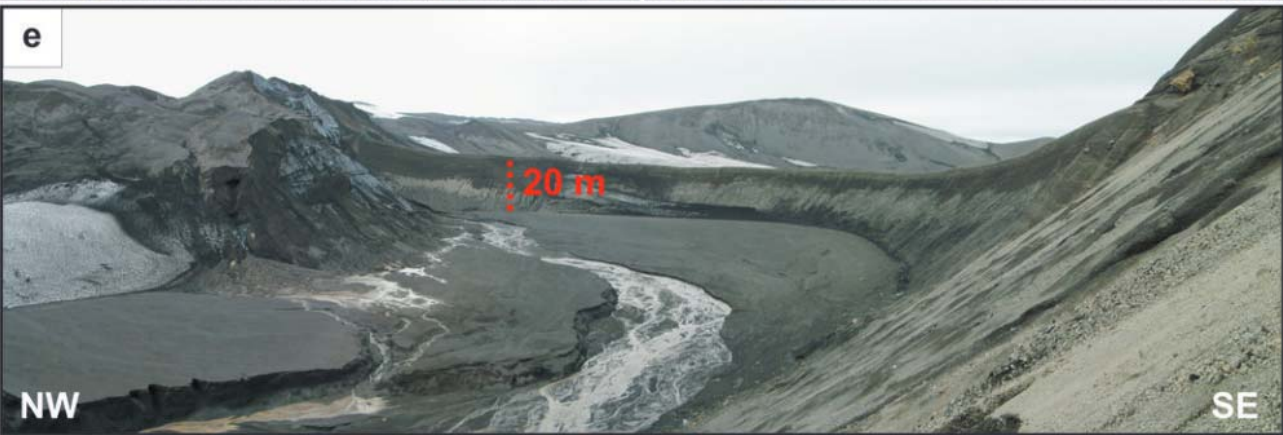
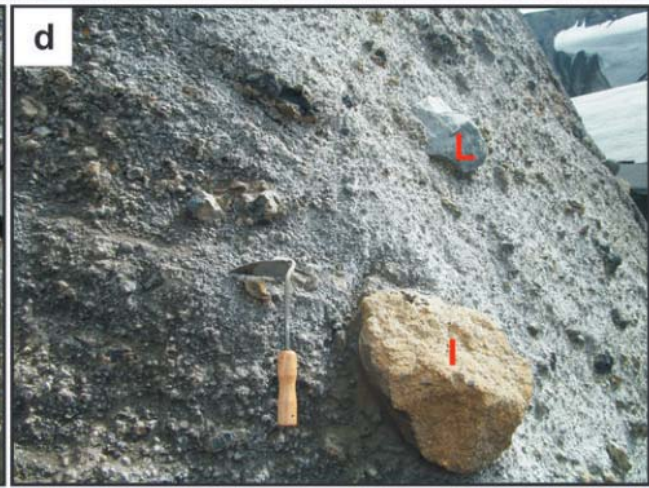


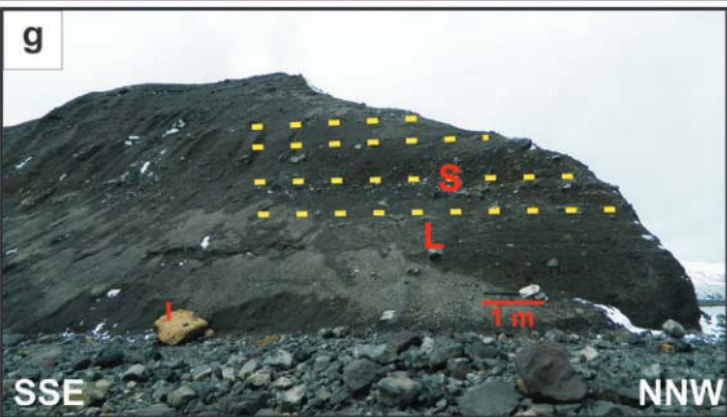
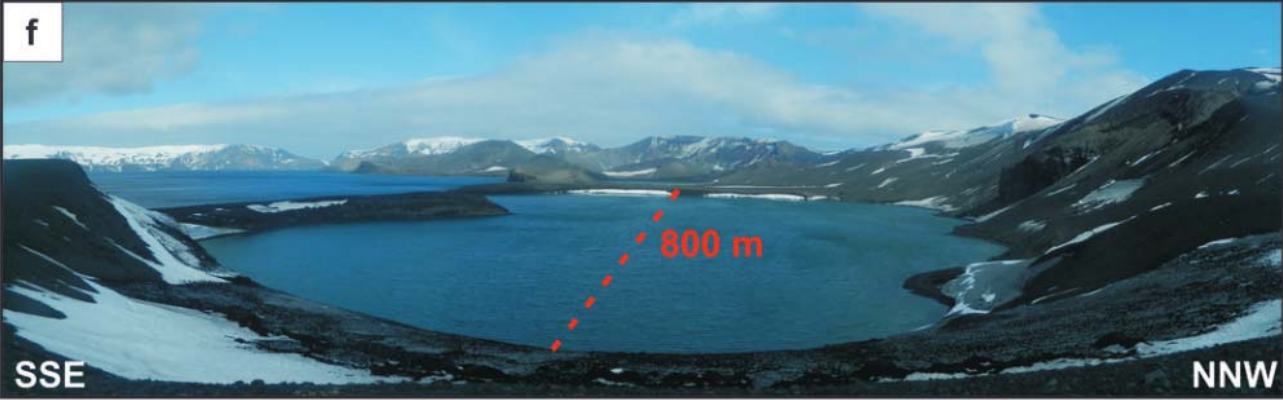


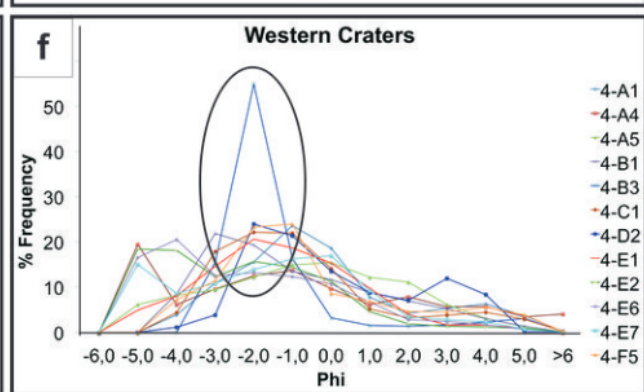
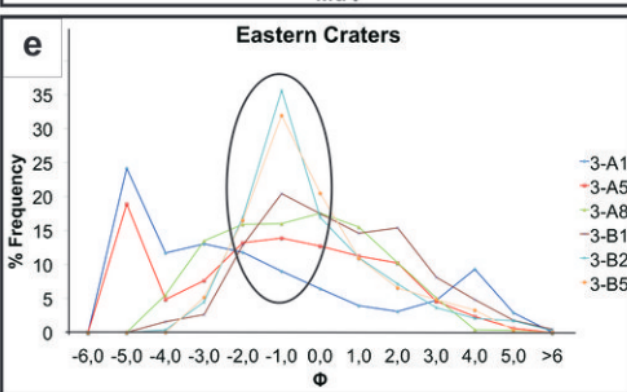
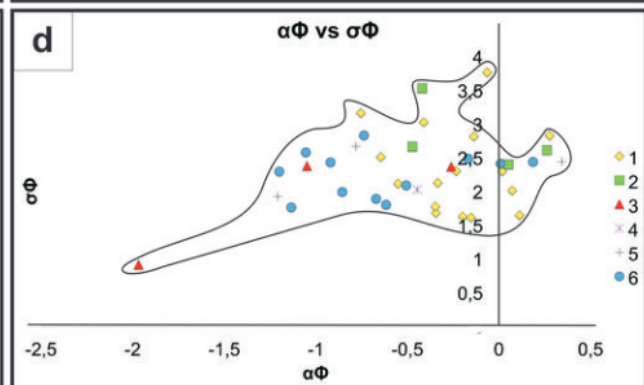
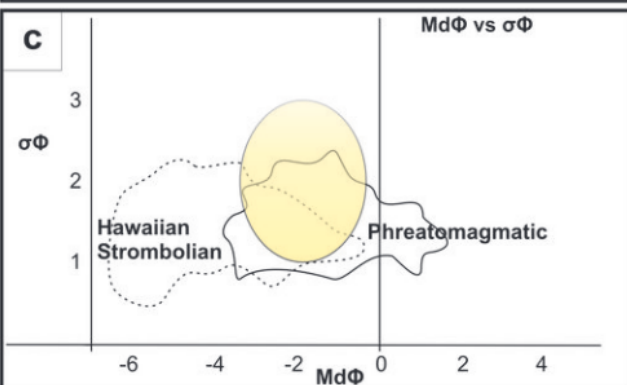
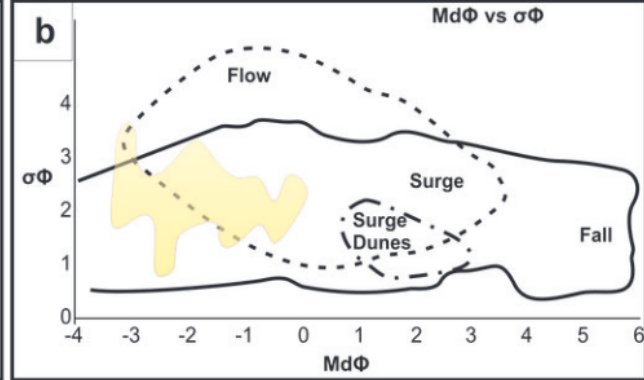
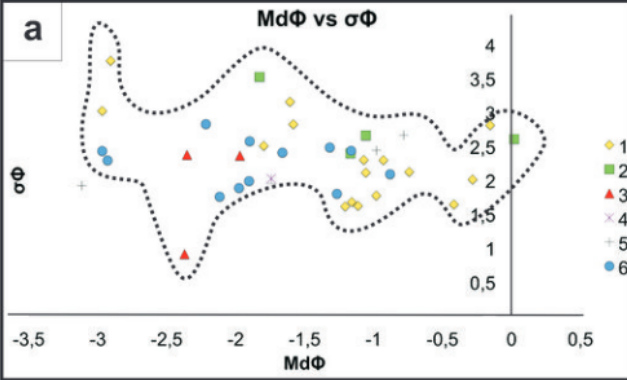


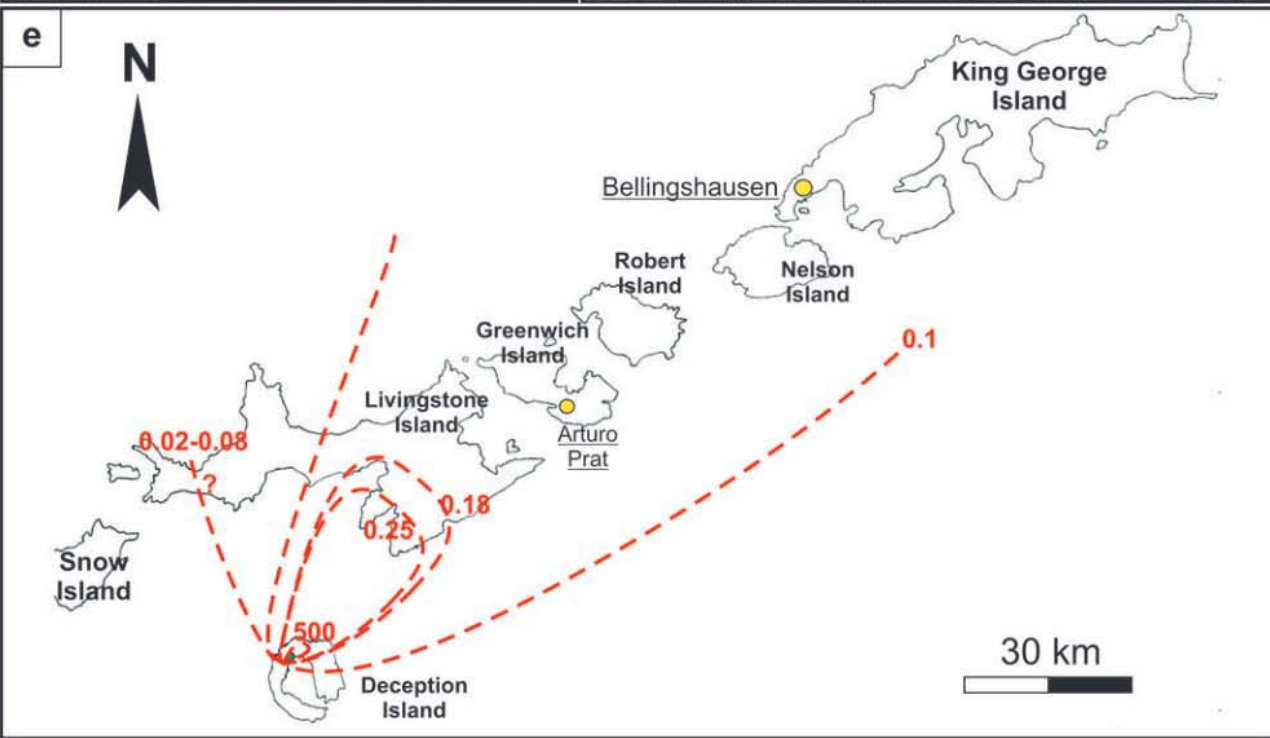
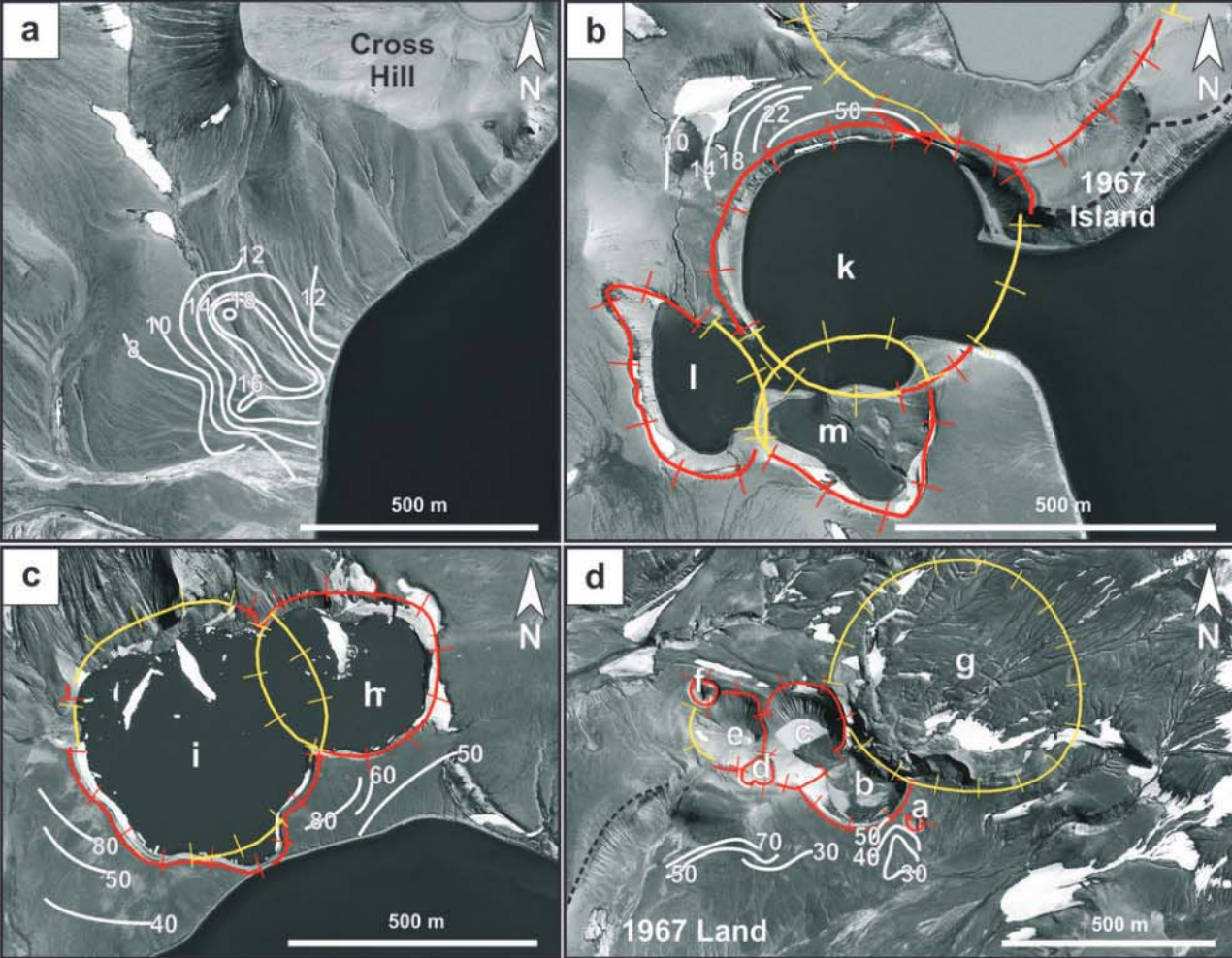


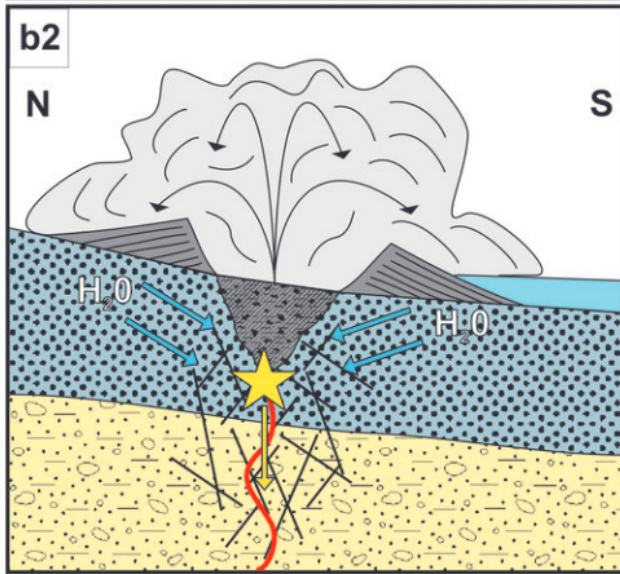
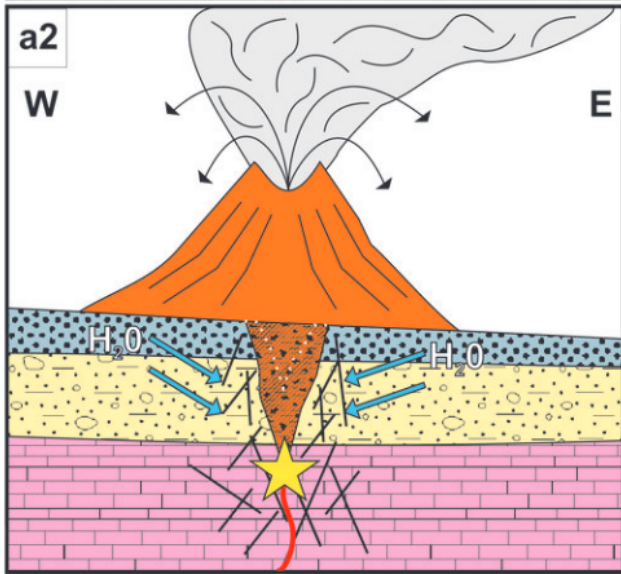
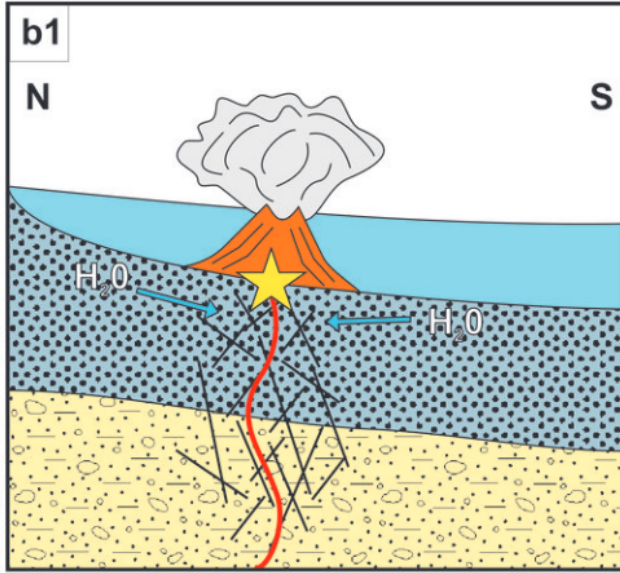
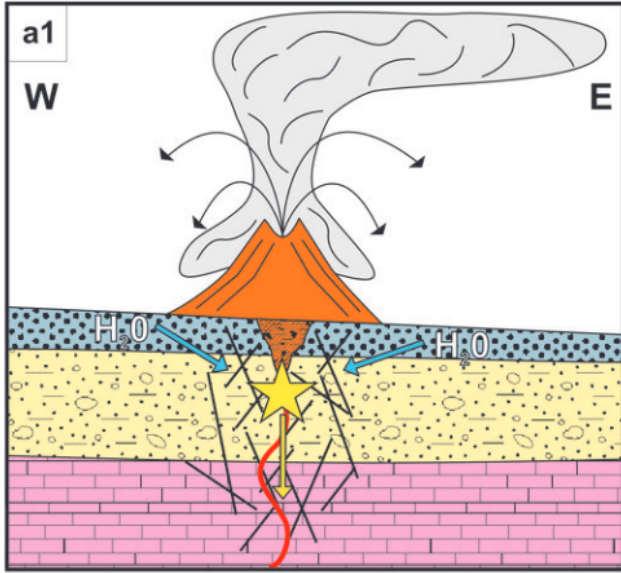


















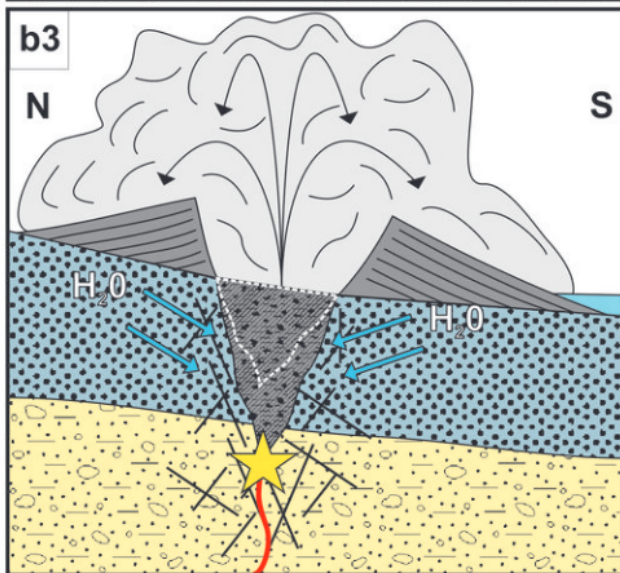






LEGEND

	1		7		11
	2		8		12
	3		9		
	4		10		
	5				
	6				



Appendix 5.1 Proof of delivery of the paper: “The 1970 eruption of Deception Island (Antarctica): eruptive dynamics and implication for volcanic hazard” in Journal of the Geological Society



[Home](#)

Manuscript #	2014-015
Current Revision #	0
Submission Date	29th Jan 14
Current Stage	Initial QC Started
Title	The 1970 eruption on Deception Island (Antarctica): eruptive dynamics and implications for volcanic hazards
Running Title	The 1970 eruption on Deception Island
Manuscript Type	Research Article
Special Section	N/A
Corresponding Author	Dario Pedrazzi (ICTJA-CSIC Jaume Almera)
Contributing Authors	Gerardo Aguirre-Díaz, Stefania Bartolini, Joan Molist, Adelina Traver
Abstract	In 1970, a hydrovolcanic eruption took place in the northern part of Deception Island (South Shetland Archipelago, Antarctic Peninsula group). The eruption occurred in the same general area as the 1967 eruption, but with new, more widely distributed vents. Two groups of craters were formed as a result of the 1970 eruption, which suggests that different active fissures and eruptive dynamics were operating during the same eruption. One group consists of maar-like craters, while the other group is made of conical shape edifices. The 1970 eruption can be classified as a VEI 3 eruption, with mainly phreatomagmatic episodes that generated a bulk volume of about 0.1 km ³ of pyroclastic material and an eruptive column of up to 10 km in height, from which fallout deposits have been recognized at a distance of more than 100 km to the northeast. The 1970 eruption was similar to that of 1967 and conjointly these two events show how eruption dynamics can be controlled by the physical characteristics of the vents (e.g. the uppermost part of the volcano's substrate and the width and orientation of the eruptive fissure) and by changing magma/water interaction, which together generate different eruptive phases and associated volcanic hazards.
	different eruptive phases and associated volcanic hazards.
Open Access	No I do not want to use this option

Manuscript Items

1. Author Cover Letter [PDF \(43KB\)](#) [Source File \(DOC\) 76KB](#)
2. Merged File containing manuscript text and 11 Figure files. [PDF \(6937KB\)](#)
 - a. Article File [PDF \(198KB\)](#) [Source File \(DOC\) 93KB](#)
 - b. Figure 1 [PDF \(684KB\)](#) [Source File \(TIF\) 5822KB](#)
 - c. Figure 2 [PDF \(477KB\)](#) [Source File \(TIF\) 3009KB](#)
 - d. Figure 3 [PDF \(823KB\)](#) [Source File \(TIF\) 8667KB](#)
 - e. Figure 4 [PDF \(458KB\)](#) [Source File \(TIF\) 1533KB](#)
 - f. Figure 4 [PDF \(373KB\)](#) [Source File \(TIF\) 1358KB](#)
 - g. Figure 4 [PDF \(390KB\)](#) [Source File \(TIF\) 1431KB](#)
 - h. Figure 5 [PDF \(1052KB\)](#) [Source File \(TIF\) 13745KB](#)
 - i. Figure 5 [PDF \(791KB\)](#) [Source File \(TIF\) 10649KB](#)
 - j. Figure 6 [PDF \(282KB\)](#) [Source File \(TIF\) 1000KB](#)
 - k. Figure 7 [PDF \(828KB\)](#) [Source File \(TIF\) 7955KB](#)
 - l. Figure 8 [PDF \(584KB\)](#) [Source File \(TIF\) 1409KB](#)
3. Supplemental_Material_a [Source File \(TIF\) 1297KB](#)
Granulometric and componentry histograms
4. Supplemental_Material_b [Source File \(TIF\) 1288KB](#)
Granulometric and componentry histograms

Manuscript Tasks

- [Send Manuscript Correspondence](#)
[Check Status](#)